2004-07-08

Investigation of CO Tolerance in Proton Exchange Membrane Fuel Cells

Jingxin Zhang
Worcester Polytechnic Institute

Investigation of CO Tolerance in Proton Exchange Membrane Fuel Cells

By

Jingxin Zhang

A Dissertation
Submitted to the Faculty

of the

WORCESTER POLYTECHNIC INSTITUTE

In partial fulfillment of the requirement for the

Degree of Doctor of Philosophy

In

Chemical Engineering

By

_____

June 2004

Approved:

_____
Prof. Ravindra Datta, Advisor
Head of Chemical Engineering Department

_____
Prof. Yi Hua Ma

_____
Prof. Nikolaos K. Kazantzis

_____
Prof. Joseph D. Fehribach

Abstract

The need for an efficient, low-polluting power source for vehicles in urban environments has resulted in increased attention to the option of fuel cell powered vehicles. Of the various fuel cell systems considered, the hydrogen fueled proton exchange membrane (PEM) fuel cell technology seems to be the most suitable one for the terrestrial transportation applications. This is thanks to low temperature of operation (hence, fast cold start), and a combination of high power density and high energy conversion efficiency. It is envisioned that before the problems associated with the storage and distribution of hydrogen are fully addressed, the hydrogen will be produced on-board via catalytic reforming of conventional fuels such as gasoline. However, this produces impure hydrogen containing CO_2 along with traces of CO which acts as a poison to PEM fuel cells.

Besides automobile, fuel cell is a promising candidate for stationary applications (distributed power for homes, office buildings, and as back-up for critical applications such as hospitals), and future consumer electronics. Although significant progress has been made on PEM fuel cells over the last twenty years, further progress in fuel cell research is still needed before the commercially viable fuel cell utilization in transportation, potable and stationary applications.

A chief current research goal is the design of PEM fuel cells that can operate with impure hydrogen containing traces of CO, which has been the objective of this research. Standard Pt and PtRu anode catalysts have been studied systematically under practical fuel cell conditions, in an attempt to understand the mechanism and kinetics of H_2/CO electrooxidation on these noble metal catalysts. In the study of Pt as anode catalyst, it was found, thus, that the fuel cell performance is strongly affected by the anode flow rate and cathode oxygen pressure. This was found to be due to the fact that there is finite CO electrooxidation even on Pt anode with H_2/CO as anode feed. Thus, anode overpotential and outlet CO concentration is a function of anode inlet flow rate at a constant current density. A CO electrooxidation kinetic model was developed taking into account the CO inventory in the anode, which could successfully simulate the experimental results. The on-line monitoring of CO concentration in PEM fuel cell anode exit proved that the

"ligand mechanism" and "bifunctional mechanism" coexist as the CO tolerance mechanisms for PtRu anode catalyst.

For PtRu anode catalyst, sustained potential oscillations were furthermore observed when the fuel cell was operated at constant current density with H_2/CO as anode feed. Temperature was found to be the key bifurcation parameter besides current density and the anode flow rate for the onset of potential oscillations. The anode kinetic model was further extended to the unsteady state which could reasonably reproduce and adequately explain the oscillatory phenomenon. The potential oscillations are due to the coupling of anode electrooxidation of H_2 and CO on PtRu alloy surface, on which OH_{ad} can be formed more facile, preferably on top of Ru atoms at lower overpotentials. One parameter bifurcation and local linear stability analysis showed that the bifurcation experienced during the variation of fuel cell temperature is a Hopf bifurcation, which leads to stable potential oscillations when the fuel cell is set at constant current density.

It was further found that a PEM fuel cell operated in an autonomous oscillatory state produces higher time-averaged cell voltage and power density as compared to the stable steady-state operation, which may be useful for developing an operational strategy for improved management of power output in PEM fuel cells in the presence of CO in anode feed. Finally, an Electrochemical Preferential Oxidation (ECPrOx) process is proposed to replace the conventional PrOx for cleaning CO from reformate gas, which can selectively oxidize CO electrochemically while generating supplemental electrical power without wasting hydrogen. The ECPrOx process exploits the strong adsorption of CO on the PtRu catalyst at low temperatures and the anode overpotential (in oscillatory state) to selectively electrooxidize CO over hydrogen.

Acknowledgement

I would like to thank my advisor, Professor Ravindra Datta, for his guidance and support over the past five years. I am deeply impressed by his breadth and depth of knowledge, his continuous devotion to reading and learning, and his sincerity and patience both as a teacher and a scholar. I especially enjoyed his style of mentoring students from which I have benefited tremendously in my personal and professional growth. I was given and fully enjoyed the maximum freedom in our field of scientific research. I also want to thank my committee for their time and suggestions for developing this thesis. Their comments and insightful suggestions have substantially improved the quality of my work. I would also like to express great appreciation to both my advisor and my committee for their continuous support and encouragement in my career development.

I would like to thank the dedicated staff of the Chemical Engineering Department at WPI for their help over the years. The hard work of Giacomo Ferraro and Douglas White has helped solve numerous technical problems emerging from our experiments such that this scientific investigation has become a more enjoyable experience. Joseph Kaupu, Sandra Natale and former staff members working in this department have made great contribution in making the department such a wonderful place to work and stay.

I would also like to thank all of my colleagues and friends, for their kind help in both my research and my personal life: Tony, Faisal, Manuela, Jinyi, Guanghui, Caitlin, Pyoungho, Nikhil, Hao, Xinrong and Li Wan. I also want to express my thanks to Dr. Ilie Fishtik for the many helpful and interesting discussions.

I want to thank my parents and parents-in-law for their support both financially and emotionally, which has made my decision to pursue the best education possible. I especially want to thank my dear wife, Ms. Wan Liu, for her understanding, patience, encouragement and unconditional love, without which I would not have succeeded this far.

Finally, I would like to thank the Dr. Chue-san Yoo Fellowship for financial support.

Table of Contents

List of Figures

List of Tables

Extensive Summary

The proton exchange membrane (PEM) fuel cell has attracted a great deal of attention as a potential power source for automobile and stationary applications due to its low temperature of operation, high power density and high energy conversion efficiency. Besides stationary and automobile applications, the PEM fuel cell is also a promising candidate as power supply for future consumer electronics. Great progress has been made over the past twenty years in the development of PEM fuel cell technology. However, there are still several technical challenges that need to be addressed before commercialization of PEM fuel cell.

Hydrogen is the most attractive fuel for PEM fuel cells, having excellent electrochemical reactivity, providing adequate levels of power density, as well as having zero emissions characteristics. Nevertheless, distribution and storage difficulties currently pose serious challenges to the use of pure hydrogen as a fuel for fuel cells. The infrastructure for its widespread distribution does not yet exist. Further, being the lightest element, its volumetric energy density is too low even in high pressure cylinders. Supplying liquid fuel such as methanol directly to the anode is another fuel choice (i.e., Direct Methanol Fuel Cell). In terms of simplicity and cost, the direct liquid fuel presents an attractive alternative to hydrogen fueled system. However, the power density of PEM fuel cell fueled directly with liquid fuel is too low to be used as power source in transportation and stationary applications. This is due to the sluggish anode kinetics and methanol crossover through the proton exchange membrane. Before the problems associated with using hydrogen or methanol directly as the anode feed are solved, a practical alternative is to use reformate as the anode feed, which is a H_2 rich gas obtained on demand from an on-board fuel processing system which converts a liquid hydrocarbon fuel, such as methanol or gasoline, into a H_2 rich gas.

However, regardless of which primary fuel and fuel processing system is used, traces of CO are present in the output reformate gas stream of a fuel processing system. Unfortunately, a CO concentration of 5 –10 ppm in the feed stream, which is still much lower than the CO concentration in the output stream of the most advanced fuel

processing system, can poison the state-of-the-art Pt anode catalyst used in the PEM fuel cell and limit its performance.

Thus, the objective of the present research is to investigate the CO tolerance issue in PEM fuel cells in order to eventually allow the use of reformate as the anode feed. Although the research for a CO tolerant anode catalyst system has been ongoing for more than two decades, the success, other than the state-of-the-art PtRu catalyst, is still limited. Other approaches in solving the CO poisoning problem, such as O_2 bleeding in the anode, increase system complexity and control issues due to safety concerns. Further, there is still disagreement on the mechanism of CO tolerance of PtRu catalyst. The elucidation of the reaction mechanisms and kinetics of H_2 and CO on the anode catalyst and the overall anode performance needs to be first accomplished before CO tolerance anode can be effectively designed.

A systematic approach has, thus, been adopted in this work. The standard Pt and PtRu anode catalysts were used to study the performance at practical fuel cell operating conditions with a fuel containing CO. From the performance data, the mechanism and kinetics of H_2/CO electrooxidation on Pt and PtRu catalysts were investigated in detail. Insights on the CO tolerance mechanism developed here will be useful in the design of better CO tolerant catalysts as well as the development of more practical operational and structural schemes to improve the CO tolerance of the PEM fuel cell. A summary of the chapters is provided below.

A general background of fuel cells, especially PEM fuel cells is provided in Chapter I. The selection of a fuel for a PEM fuel cell system is discussed. The research on improving the anode CO tolerance with reformate as anode fuel is described in considerable detail in order to present an complete picture of the state-of-the-art in this field. It should be pointed out that this is a very active area of research and some of the results reported in the very recent literature may have paralleled our work over the past five years. However, this does not diminish the originality of our research.

In Chapter II, an investigation of the fuel cell performance is described with Pt as the anode catalyst. It is found that the anode flow rate of a PEM fuel cell involving Pt anode electrocatalyst strongly influences the single cell performance when H_2 containing trace amounts of CO is used as the feed. The performance drops dramatically due to CO

poisoning as the anode flow rate increases. This effect of the flow rate on the extent of CO poisoning is determined to depend upon the actual concentration of CO in the anode chamber which in turn depends upon the feed content, the flow rate and CO electooxidation kinetics on Pt. Further, it is found that oxygen permeating across the PEM from the cathode side also appreciably affects the anode overpotential by providing another route for CO oxidation via a non-electrochemical pathway. A CO inventory model is developed that explains the observed phenomena in a PEM fuel cell operating with a H_2/CO mixture as the anode feed and a cathode feed with different oxygen partial pressures. Contents of this chapter have been published in *J. Electrochem. Soc*., **149**, A765 (2002).

To confirm our predictions described in Chapter II, Chapter III describes an experimental investigation in which the anode gas outlet CO concentration is measured by an on-line IR gas analyzer for a PEM fuel cell fed with H_2/100 ppm CO and with Pt or PtRu as anode catalyst. It is found that the anode outlet CO concentration increases with anode inlet flow rate at a given current density for Pt catalyst, which agrees well with our model predictions in chapter II. The outlet CO concentration with PtRu catalyst depends upon the current density at a cell temperature of 80 °C. The CO electrooxidation rate on Pt and PtRu is calculated using a CO material balance on the anode side. The results indicate that the enhanced tolerance of PtRu catalyst is due to the dual mechanisms of reduced CO affinity (ligand effect) and enhanced CO electrooxidation rates (bifunctional effect), with either mechanism dominating depending upon the anode overpotential. Contents of this chapter have been published in *Electrochem. Solid-State Lett*. **6**, A5 (2003).

Chapter IV describes the sustained potential oscillations experimentally observed in a PEM fuel cell with PtRu as the anode catalyst and with H_2/108 ppm CO as the anode feed when operating under a constant current density mode. These oscillations appear at fuel cell temperatures below 70 °C. A threshold value exists for both the current density and the anode flow rate at a given fuel cell temperature for the onset of anode potential oscillations. The potential oscillations are believed to be due to the coupling of anode electrooxidation of H_2 and CO on the PtRu catalyst surface, on which OH_{ad} is formed more readily, *i.e*., at lower overpotentials. A kinetic model is provided that can reproduce

the observed oscillatory phenomenon both qualitatively and quantitatively. Contents in this chapter have been published in *J. Electrochem. Soc*., **149**, A1423 (2002) and are the first detailed report on potential oscillations in fuel cells.

In order to understand further the mechanistic origin of the anode potential oscillation phenomenon in PEM fuel cells, a detailed mathematical analysis is performed in Chapter V. Temperature and anode flow rate are found to be key bifurcation parameters. The time-dependence of all key surface species must be taken into account for the model to predict the oscillatory behavior while the time-dependence of CO concentration in the anode chamber need not necessarily be considered. The bifurcation diagram of CO electrooxidation rate constant agrees very well with the effect of temperature on the oscillation pattern. The oscillator model is classified as a hidden negative differential resistance (HNDR) oscillator based on the dynamical response of the anodic current and surface species to a dynamic potential scan. A linear stability analysis indicates that the bifurcation experienced is a supercritical Hopf bifurcation. Contents in this chapter have been published in *J. Electrochem. Soc.,* **151**, A689 (2004).

The potential oscillation phenomenon observed in PEM fuel cells under constant current conditions was, in fact, found to be practically useful. In Chapter VI, the time-averaged cell voltage, efficiency and power density in an autonomous oscillatory state were found to be higher than in stable steady-state for a PEM fuel cell operating in the presence of CO in the anode feed. Thus, the average power density under such an oscillatory state at 55 °C was found to be twice that under a stable steady-state. The average cell voltage and power density gain is due to the decrease of the time-averaged anode overpotential in the oscillatory state. Thus Chapter VI provides experimental evidence that autonomous oscillatory operation of a fuel cell in the presence of CO can increase the power output as compared to that in stable steady-state operation. This observation may be useful for developing an operational strategy for improved management of power output of PEM fuel cells in the presence of CO. Contents in this chapter have been published in *Electrochem. and Solid-State Lett*., **7,** A37 (2004).

In addition to the power enhancement of PEM fuel cells at oscillatory state, it is found that the anode outlet CO concentration is significantly lower than that in the anode feed. Based upon these observations, an electrochemical preferential oxidation (ECPrOx)

process is developed in Chapter VII to cleanse CO from hydrogen rich gas mixture using a device similar in structure to a proton exchange membrane fuel cell. In this process, the selective CO electrooxidation is achieved at the anode by rendering the process electrochemical and by utilizing autonomous anode potential oscillations when operated at a constant current density. The oscillation period and amplitude of the ECPrOx device adjust automatically to the CO levels in the feed stream such that a self-controlled autonomous potential pulsing is achieved with a low level of CO in the cleansed reformate. Supplemental electrical power is produced from the ECPrOx device while CO is removed from the reformate gas, without H_2 or CO being wasted. The ECPrOx device can be operated near room temperature, high anode pressure, atmospheric air breathing, and without external humidification. The ECPrOx process is capable of recovering the energy associated with CO electrooxidation while delivering a high purity hydrogen stream to the fuel cell stack. Contents of this chapter will be submitted for publication in *J. Electrochem. Soc.* and a patent application has been filed.

Finally, Chapter VIII summarizes the conclusions of this investigation. Research following the current efforts is suggested that may deserve further investigations.

Chapter I

CO Tolerance in Proton Exchange Membrane (PEM) Fuel Cells-Literature Review

In this chapter, the general background of fuel cells, especially proton exchange membrane (PEM) fuel cells, is provided. The considerations in selecting a fuel for PEM fuel cell are discussed. The research in improving the anode CO tolerance to allow use of reformate as anode fuel is described in substantial detail in order to present an overall picture of work accomplished thus far in this active field of investigation.

1.1 About Fuel Cells

1.1.1 What is a Fuel Cell

Fuel cells are electrochemical devices that convert the chemical energy of a reaction directly into electrical energy. Although having components and characteristics similar to those of a typical battery, fuel cells differ in several respects. The battery is an energy storage device. The maximum energy available is determined by the amount of chemical reactant stored within the battery. The battery will cease to produce electrical energy when the limiting chemical reactants are consumed. The fuel cell, on the other hand, is an energy conversion device that theoretically has the capability of producing electrical energy for as long as the fuel and oxidant are supplied to the electrodes.

In 1839, William Grove, a British jurist and amateur physicist, reportedly first developed the principle of the fuel cell. Grove utilized four large cells, each containing hydrogen and oxygen, to produce electric power which was then used to split the water in the smaller upper cell into hydrogen and oxygen.[1]

Fuel cells were developed for and have long been used in the space program to provide electricity and drinking water for the astronauts. Undoubtedly, the “space race” in the fifties and sixties was one of the most significant events to influence the development of fuel cells.[2] The very first fuel cell used in a practical application was a proton exchange membrane (PEM) fuel cell, which is the same fuel cell type that is

currently the focus of many of the major development programs attempting to develop fuel cells for terrestrial applications, including transportation, stationary or portable power uses.

Fuel cells have many characteristics that make them favorable as energy conversion devices. Two of the most attractive features for terrestrial application are the combination of relatively high efficiency and low emissions. Some other characteristics that fuel cells offer are: no moving parts in the energy converter; quiet; modular installations to match load; good reliability; and remote and unattended operation.[3-5] "Distributed power" is a new approach that utility companies are beginning to implement, locating small, energy-saving power generators closer to where the need is. Fuel cells are becoming an alternative choice for rural energy needs where there are no existing power grids and power supply is often unreliable.

1.1.2 How a Fuel Cell Works

The basic structure of a fuel cell consists of an electrolyte layer in contact with a porous anode and cathode on either side. A schematic representation of a fuel cell with the reactant/product gases and the ion conduction flow directions through the cell is shown in Figure 1-1 (in this kind of fuel cell, the electrolyte is a proton exchange membrane). In a typical fuel cell, gaseous fuel containing, e.g., H_2, is fed continuously to the anode compartment and an oxidant (i.e., oxygen or air) is fed continuously to the cathode compartment. The electrochemical reactions take place at the electrodes to produce an electric current. The electrons released will flow through an outer circuit so that the electrical power produced can be utilized.

The functions of porous electrodes in fuel cells are: 1) To provide a surface site where gas/liquid ionization and de-ionization reactions can take place. 2) To conduct ions away from or into the three-phase interface once they are formed. An electrode must be made of materials that have good electrical conductance, and the electrode material should be catalytic as well as conductive, and porous rather than solid. The electrode should have a good electrolytic conductivity as well.

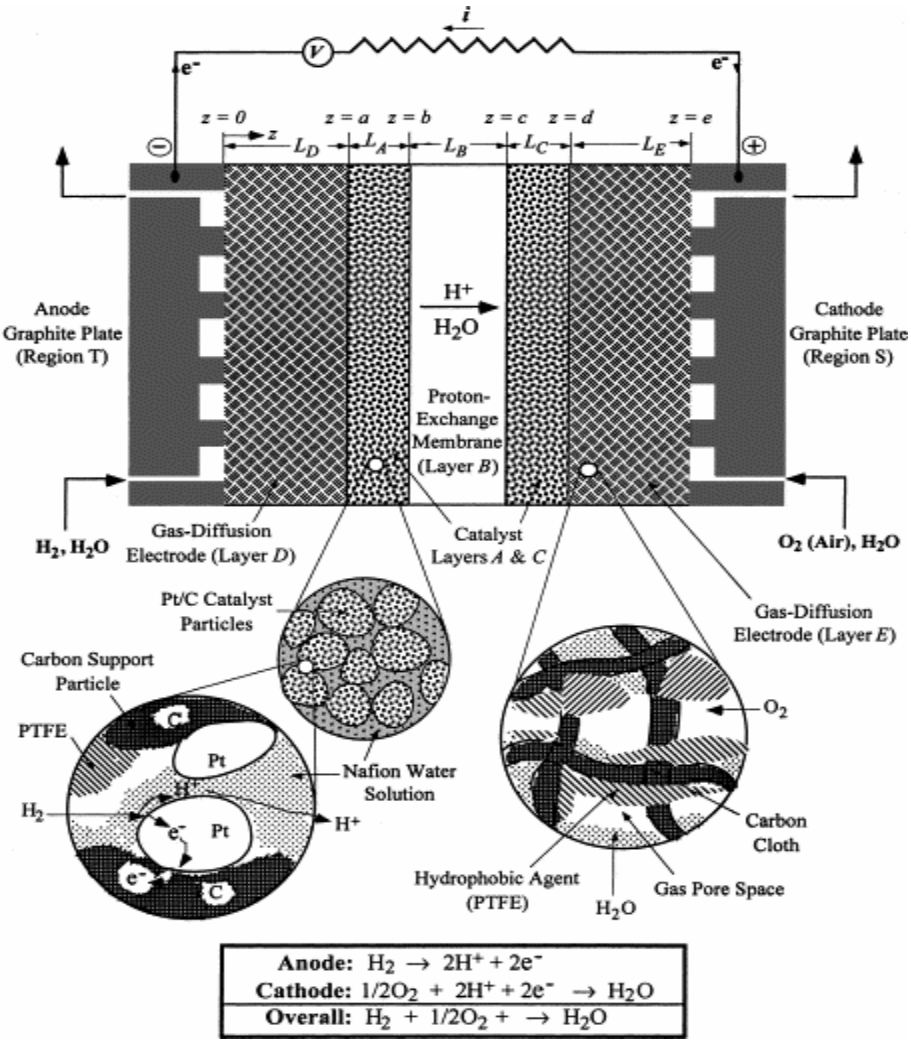

Figure 1-1. Schematic representation of the PEM fuel cell cross-section structure (ref. 87).

1.1.3 Fuel Cell Types and Potential Applications

A variety of fuel cells are in different stages of development.[3-5] Based on the type of electrolyte used, fuel cells can be classified as: 1) proton exchange membrane fuel cell (PEMFC); 2) alkaline fuel cell (AFC); 3) phosphoric acid fuel cell (PAFC); 4) molten carbonate fuel cell (MCFC); and 5) solid oxide fuel cell (SOFC). A comparison of the five kinds of fuel cell is listed in Table 1-1.

Proton exchange membrane fuel cell uses an ion-exchange membrane (fluorinated sulfuric acid polymer or other similar polymers) as electrolyte, which is an excellent proton conductor. The only liquid in this fuel cell is water; thus, corrosion problems are minimal. Water management in the membrane and electrode, however, is critical for efficient performance. The fuel cell must operate under conditions where the membrane is hydrated which, because of the limitation on the operating temperature imposed by the polymer, is usually less than 120 °C and, typically, 80 °C.

In alkaline fuel cell, the electrolyte is concentrated (85 wt %) KOH in fuel cells operated at high temperatures (~ 250 °C), or less concentrated (30-50 wt %) KOH for lower temperature (~ 120 °C) operation. The electrolyte is retained in a matrix and a wide range of electrocatalyst can be used (e.g., Ni, Ag, metal oxides, and noble metals). CO is a poison to the catalyst and CO_2 will react with KOH to form K_2CO_3, thus altering the electrolyte. Therefore, pure H_2, and preferably pure O_2 are required which limit the use of AFC except in niche applications (e.g., spacecraft).

Concentrated phosphoric acid (100%) is used in phosphoric acid fuel cell as electrolyte, which operates at 150 to 200 °C. At lower temperatures, phosphoric acid is poor ionic conductor, and CO poisoning of the Pt electrocatalyst in the anode becomes severe. The volatility of concentrated phosphoric acid is low compared to other common acids; consequently the PAFC is capable of operating at relatively high temperatures for extended periods. In addition, the high temperatures used result in low RH of water so that water management in the cell is not difficult.

Molten carbonate fuel cells typically use a combination of alkali carbonates or their combination (Na and K) as electrolyte, which is retained in a ceramic matrix of $LiAlO_2$. The fuel cell operates at 600-700 °C, where the alkali carbonates form a highly

Table 1-1 Comparison of Five Kinds of Fuel Cells

Fuel Cell	Electrolyte	Ionic Species	Operating temperature (°C)	Electrochemical Reactions
Polymer Electrolyte Membrane (PEM)	Solid organic polymer Poly-perfluorosulfonic acid	H^+	60-100	Anode : $H_2 \rightarrow 2H^+ + 2e$ Cathode: ½ O_2 +$2H^+$+ $2e \rightarrow H_2O$
Phosphoric Acid (PAFC)	Liquid phosphoric acid soaked in a matrix	H^+	175-200	Anode : $H_2 \rightarrow 2H^+ + 2e$ Cathode: ½ O_2 +$2H^+$+ $2e \rightarrow H_2O$
Alkaline (AFC)	Aqueous solution of potassium of hydroxide soaked in a matrix	OH^-	65-220	Anode : H_2+$2OH^- \rightarrow 2\ H_2O + 2e$ Cathode: ½ O_2 + H_2O + $2e \rightarrow 2OH^-$
Molten Carbonate (MCFC)	Liquid solution of lithium, sodium and/or potassium carbonates, soaked in a matrix	CO_3^{2-}	600-1000	Anode : H_2 +$CO_3^{2-} \rightarrow$ H_2O +CO_2+ 2e Cathode: ½ O_2 +CO_2+ $2e \rightarrow$ CO_3^{2-}
Solid Oxide (SOFC)	Solid zirconium oxide to which a small amount of ytrria is added	O_2^{2-}	600-1000	Anode : H_2 +$O^{2-} \rightarrow$ H_2O + 2e Cathode: ½ O_2 + $2e \rightarrow$ O^{2-}

conductive molten salt, with carbonate ions providing the ionic conduction. At the high operating temperature of a MCFC, Ni (anode) and nickel oxide (cathode) are adequate to promote catalytic reactions.

A solid, nonporous metal oxide, usually Y_2O_3-stabilized ZrO_2 is used as electrolyte in solid oxide fuel cells. The cell operates at 650-1000 °C, where ionic conduction by oxygen ions takes place. Typically, the anode is Co-ZrO_2 or Ni-ZrO_2, and the cathode is Sr-doped $LaMnO_3$.

1.1.4 Prospects of Proton Exchange Membrane Fuel Cell

The need for an efficient, non-polluting power source for vehicles in urban environments has resulted in increased attention to the option of fuel cell powered vehicles. Of various fuel cell systems considered, the PEM fuel cell technology seems to be the most suitable one for the terrestrial transportation applications.[1] This is due to its low temperature of operation (hence, faster cold start), excellent CO_2 tolerance and a combination of high power density and high energy conversion efficiency. Moreover, there is no free corrosive liquid in PEM fuel cells. They are able to withstand large pressure differentials. The material corrosion problems are minimal and they have demonstrated longevity.

Compared to internal combustion engines, fuel cell has a more efficient conversion process. The internal combustion engine is less efficient due to the conversion of chemical into thermal and then thermal to mechanical energy. If cars were powered by electricity generated from fuel cell, there would be no combustion involved. For a fuel cell powered electric vehicle, the fuel is stored in the vehicle's fuel tank and air is obtained from the atmosphere. As long as the vehicle's fuel tank contains fuel, the fuel cell will produce energy in the form of electricity and heat.

The introduction of fuel cells into the transportation sector will increase fuel efficiency and become an important strategy/technology to mitigate climate change. As fuel cell vehicles begin to operate on fuels from natural gas or gasoline, greenhouse gas emission will be reduced by 50%[1]. In the future, the combination of high efficiency fuel

cells and fuels from renewable energy sources such as ethanol would nearly eliminate greenhouse gas emissions.

PEM fuel cells, under consideration by vehicle manufacturers around the world as an alternative to the internal combustion engine, are the focus of this research.

1.2 Proton Exchange Membrane Fuel Cell

1.2.1 Single Cell Structure

The cross-section of a single polymer-electrolyte fuel cell is shown in Figure 1-1. The hardware involved is schematically shown in Figure 1-2. The cell typically consists of graphite bipolar plates, gaskets, two electrodes and an ion conducting membrane. The bipolar plates are pressed against the electrode with gaskets for sealing and collecting current.

The membrane-electrode assembly (MEA), which consists of the proton conducting membrane sandwiched between two electrodes (anode and cathode), is the heart of a PEM fuel cell. In each electrode, there is a catalyst layer and a gas-diffusion backing layer. The membrane is typically 50-175 μm thick.[6] The catalyst layer is about 5-50 microns thick containing dispersed Pt catalyst. The Pt/C powder has to be intimately intermixed with recast ionomer to provide sufficient ionic conductivity within the catalyst layer. This catalyst layer is in good contact with the membrane, which serves as the electrolyte and the gas separator in the cell. The gas-diffusion backing layer in immediate contact with the catalyst layer is made of hydrophobized porous carbon paper or carbon cloth. These layers are typically 100-300 μm thick[6] and are wet-proofed by treatment with polytetrafluoroethylene (PTFE). The role of backing layer is to enable direct and uniform access of the reactant gases to the catalyst layers as well as effective water supply and removal in either vapor or liquid form. The backing layer should also be of a material of high and stable electronic conductivity in a wet environment.

Hydrogen from the fuel gas stream is consumed on the anode catalyst, yielding electrons and protons. On the cathode catalyst, oxygen combines with electrons from the anode and hydrogen ions from the electrolyte to produce water. The half cell reactions for a H_2/O_2 PEM fuel cell are

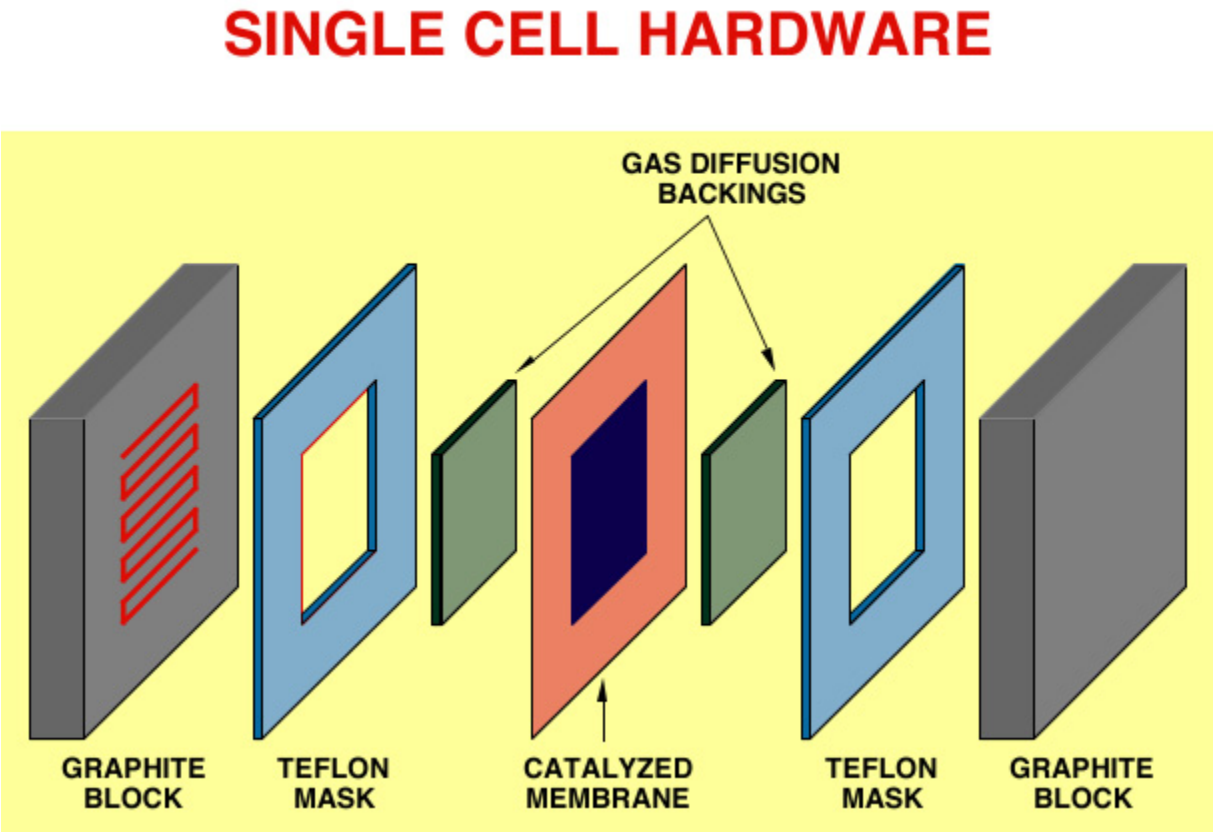

Figure 1-2. Single cell hardware in a PEM fuel cell (ref. 6).

Anode: $H_2 \leftrightarrows 2\ H^+ + 2\ e^-$ [1]

Cathode: $O_2 + 4\ H^+ + 4\ e^- \leftrightarrows 2\ H_2O$ [2]

The H_2 electrooxidation on Pt at PEM fuel cell operating temperatures is a very facile reaction. On the contrary, the reaction of oxygen molecules at the cathode is a four electron reduction process which occurs in a multi-step sequence and is exceedingly slow. Pt-based catalysts seem to be the only catalysts capable of generating high rates for the O_2 reduction reaction (ORR) at the relatively low overpotentials and temperatures (~ 80 °C) for polymer electrolyte membrane fuel cells. There is still substantial uncertainty regarding the mechanism of this complex process. The performance of the polymer electrolyte membrane fuel cells fed with H_2/O_2 is limited primarily by the slow rate of O_2 reduction, which is several orders of magnitude slower than the H_2 oxidation reaction (HOR).

The membrane functions are two fold. It acts as the electrolyte which provides ionic communication between the anode and cathode, while being an electronic insulator. It also serves as a separator for the two reactant gases. Optimized proton transport properties of the membrane and proper water management are crucial for efficient fuel cell operation. Dehydration of the membrane reduces proton conductivity and excess water can lead to flooding of the electrodes, thus, impeding gaseous reactant transport to catalyst. Both conditions result in poor fuel cell performance.

The hardware pressed against each backing layer serves the dual role of providing flow field for gases and as a current collector. The plates are made of a light-weight, strong, gas-impermeable, electron-conducting material. Graphite or metals are commonly used, although composite plates are now being developed.[6] The first task served by each plate is to provide a gas flow field while maintaining electronic contact with the gas-diffusion backing. The side of the plate next to the backing layer contains channels machined into the plate. The pattern of the flow field in the plate, as well as the width and depth of the channels, have a large impact on the effectiveness of the distribution of the reactant gases, and, hence, the current distribution across the active area of the MEA. Flow field design also affects the water supply to the membrane and water removal from the electrode. Consequently, it can affect the local membrane conductivity. The second role of the plate is as a current collector. Electrons produced by the oxidation of hydrogen

must be conducted through the anode, through the backing layer and through the plate before they can exit the cell, travel through the external circuit and re-enter the cell at the cathode plate. Thus, there must be a good electronic contact between the plates and the gas-diffusion backing.

The Teflon® masks shown are gaskets that confine the gas flow to the active area and provide, together with the periphery of the membrane, an effective seal to avoid leakage of reactant gases.

1.2.2 Major Milestones in PEM Fuel Cell Development

Historically, the first major application of a fuel cell system was in the Gemini space flights. For this purpose, the PEM fuel cell system developed by the General Electric Company was chosen.[2] The major improvement after the Gemini program was the development of perfluorosulfonic-acid membranes that are more stable than the hydrocarbon membranes used in the early PEM fuel cells.[3] These membranes, such as Nafion®, consist of a PTFE backbone, are essentially fully fluorinated and, therefore, they do not suffer from rapid degradation in a fuel cell, since C-F bonds are much more stable as compared to C-H bond in the electrochemical environment. DuPont originally developed perfluorosulfonic-acid membranes in the early 1960s for the use in the chlor-alkali industry. It was readily recognized that they are also well-suited for PEM fuel cells application[2].

Another significant milestone in the development of the PEM fuel cell is the early research work by Ballard Power Systems. Sponsored by the Canadian Department of National Defense and the National Research Council, Ballard began the PEM fuel cell work in 1984.[3] Their first objective was to design a cell which could run on air rather than on pure oxygen. Another objective was to use less expensive graphite as the material for the bipolar plate.

A very major improvement was the dramatic reduction of the Pt catalyst loadings in PEM fuel cells as first demonstrated by researchers at Los Alamos National Laboratory (LANL).[7] By impregnating the electrodes with perfluorinated ionomers in solution form, a dispersion of the polymer electrolyte could be accomplished within the electrocatalysts. The resulting electrode had much greater active interfacial area than the

previous method of simply hot-pressing the electrocatalysts to the membrane. In fact, it was demonstrated that an order of magnitude less catalyst loading than the conventional PEM fuel cell electrode was needed and yielded greatly improved performance. Researchers at LANL subsequently refined these electrode preparation techniques and developed the modern membrane electrode assembly (MEA), the heart of today's PEM fuel cells. The fuel cell research conducted at LANL during the mid-1980s and early 1990s laid the groundwork for the renaissance of PEM Fuel Cells.[2]

Significant performance improvement has been achieved through careful optimization of the MEA structure. The performance of the PEM fuel cell highly depends on the operating conditions (e.g., cell temperature, anode/cathode humidifications, anode/cathode total pressure, using O_2 or air as anode feed) and the properties of the MEA (e.g., anode/cathode catalyst loading, membrane thickness, ionomer loading in the catalyst layer, etc).

1.2.3 Fuel Options for PEM Fuel Cell

Hydrogen is the most attractive fuel for fuel cells. It has excellent electrochemical reactivity, provides high levels of power density, and has zero emission characteristics. Nevertheless, distribution and storage difficulties currently pose serious disadvantages to the use of pure hydrogen as the feed for fuel cells in automotive-propulsion.[8] Three forms of on-board hydrogen storage are usually considered: compressed gas, liquid hydrogen, and gas dissolved in metal hydrides or carbon nanotubes. Metal hydride systems are the safest of the three, but they have low mass and volumetric energy densities. Liquid hydrogen is complex, expensive, and bulky, and subject to considerable losses during and after refueling. Storage of practical amounts of H_2 as compressed gas requires very large high-pressure vessels. Distribution of hydrogen also poses difficulties as serious as storage. The infrastructure for its widespread distribution does not yet exist. Nevertheless, eventual cost effective delivery and dispensing of hydrogen can undoubtedly reduce the complexity and cost of fuel cell vehicles, thus enhancing the likelihood for success of the technology. Today, approximately 95% percent of all hydrogen is produced by "steam reforming" of natural gas, the most energy-efficient, large scale method of production. In

the long term, hydrogen generation could be based on photo-biological or photochemical methods.[1]

Another choice is to feed liquid fuel directly to the anode. Direct methanol fuel cell (DMFC) is one such possibility. The advantages of supplying methanol directly to the fuel cell are significant due to consumer acceptance of liquid fuels. Methanol distribution infrastructure exists to some extent already. More importantly, a direct methanol fuel cell system does not require a bulky and heavy hydrogen storage system. This advantage, in terms of simplicity and cost, means that DMFC presents an attractive alternative to hydrogen, in principle, fed system.

However, there are some inherent problems with DMFC: the slow anode kinetics (methanol electrooxidation) requires a large overpotential and severely decreases the cell voltage.[3] Furthermore, the perfluorsulforic-acid based membrane such as Nafion® is prone to the problem of methanol crossover, which poisons the cathode O_2 reduction catalyst and reduces the total fuel efficiency as well. Although composite membranes and membranes different from Nafion® are being actively pursued, the success so far is limited. The best performance with the most up to date DMFC technology is still too low to be used as a power source in transportation and stationary applications. The most probable near term success of DMFC is believed to be in portable electronics market, where relatively small power density is needed.[1]

In short, before the widespread use of direct hydrogen fuel cell or DMFC becomes a reality, a near term approach is to develop fuel cells fed with reformate, which is a H_2 rich gas obtained from a liquid hydrocarbon fuel processing system, fed with fuels such as methanol or gasoline. However, it is a multi-step complex process which, though well-developed for large-scale industrial production of hydrogen, presents serious challenges in scale down. A schematic of the overall fuel processing/fuel cell system is shown in Figure 1-3**.**

Currently, steam reforming of methanol to H_2 is the most developed technology,[8] however, partial oxidation of gasoline to H_2 is more attractive because of the huge gasoline infrastructure already in place. The steam reforming of methanol involves the reaction of steam and pre-vaporized methanol to 200 °C to produce a mixture of H_2, CO_2 and CO.[1] This mixture passes through another reactor, called a shift reactor, which uses

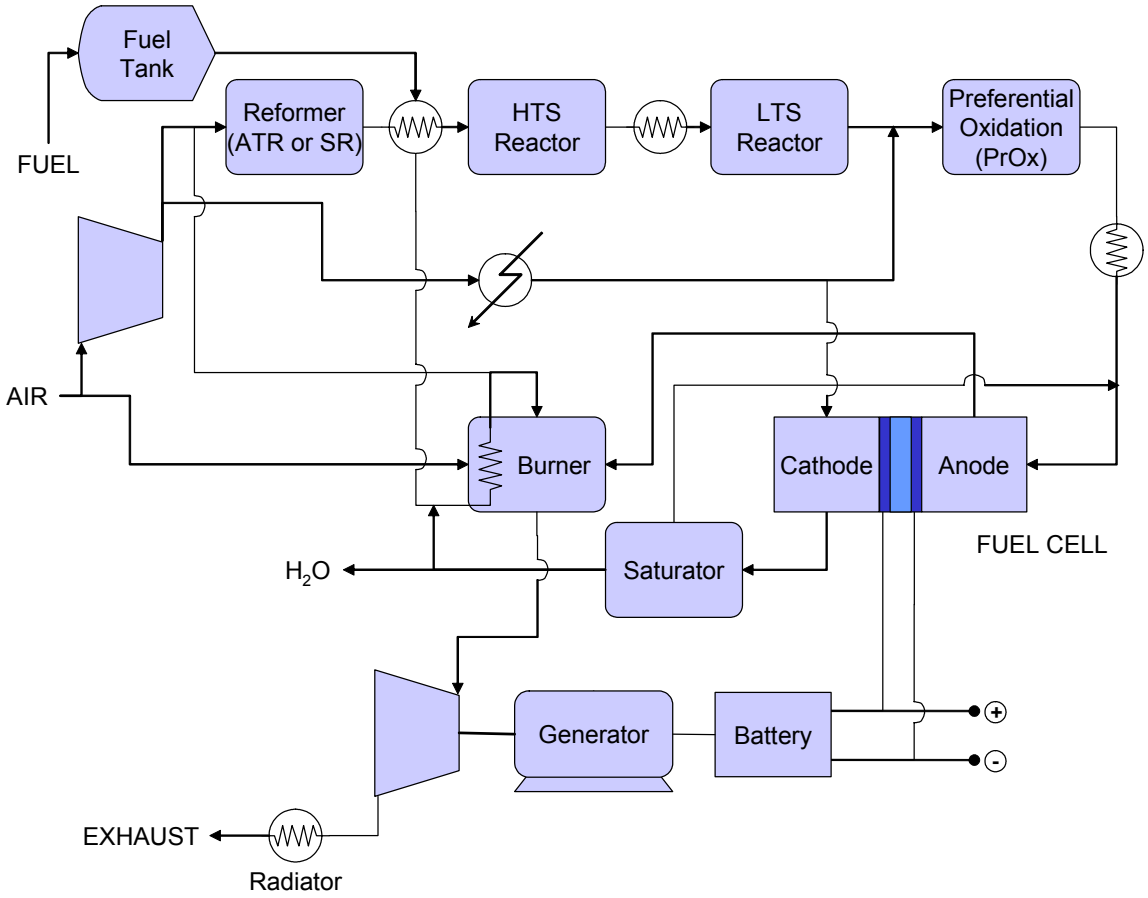

Figure 1-3. A schematic of fuel processing/fuel cell system (ref. 88).

catalysts and steam to convert nearly all of the CO to CO_2 as well as additional H_2. The final stage in which air is injected into the mixture, is called the preferential oxidation (PrOx) reactor. Oxygen in the air reacts with the remaining CO (~ 1%) over a Pt-containing catalyst to convert CO to CO_2. The final gas mixture contains about 70% H_2, 24% CO_2, 6% N_2, and traces of CO. A detailed review of the current technology of fuel processing is given by Chalk et al.[9]

The comparative study conducted by Brown[8] concluded that steam-reforming of methanol is currently the leading candidate for on-board generation of hydrogen for automotive propulsion. Research on other primary fuels is being extensively pursued in an attempt to find a practical system for on-board hydrogen generation. A gasoline powered PEM fuel cell vehicle is expected to have far lower emissions than those are allowable under the strictest California standards proposed,[1] although it is not zero emission, a goal met only with hydrogen fuel.

1.2.4 CO Poisoning Problem in Reformate-Fueled PEM Fuel Cell

Although on board fuel processing is currently the most practical option, unfortunately, regardless of the choice of the primary fuel and the fuel processing system, there are inevitably traces of CO present in the output gas stream of the fuel processing system. The level of CO impurities in the hydrogen produced via steam-reforming or partial oxidation is too high for PEM fuel cell applications. Even after the current PrOx reactor, the outlet CO concentration is about 50 ppm, and up to 100~500 ppm in startup and during transients.[9] LANL has developed the state-of-art PrOx catalyst and reaction system. It can achieve low concentrations of CO (10-20ppm) in a multistage reactor over a Pt/Al_2O_3 or Ru/Al_2O_3 catalyst.[10] In another study on low temperature PrOx reactors,[11] however, up to 100 ppm CO in the effluent was obtained with the best catalyst studied.

Unfortunately, even a concentration of CO of only about 5 –10 ppm in the feed stream can poison the Pt anode catalyst used in the PEM fuel cell (Figure1-4).[12] Therefore, overcoming the CO poisoning problem is of paramount interest and needs to be addressed in order to make reformate a viable fuel for PEM fuel cells.

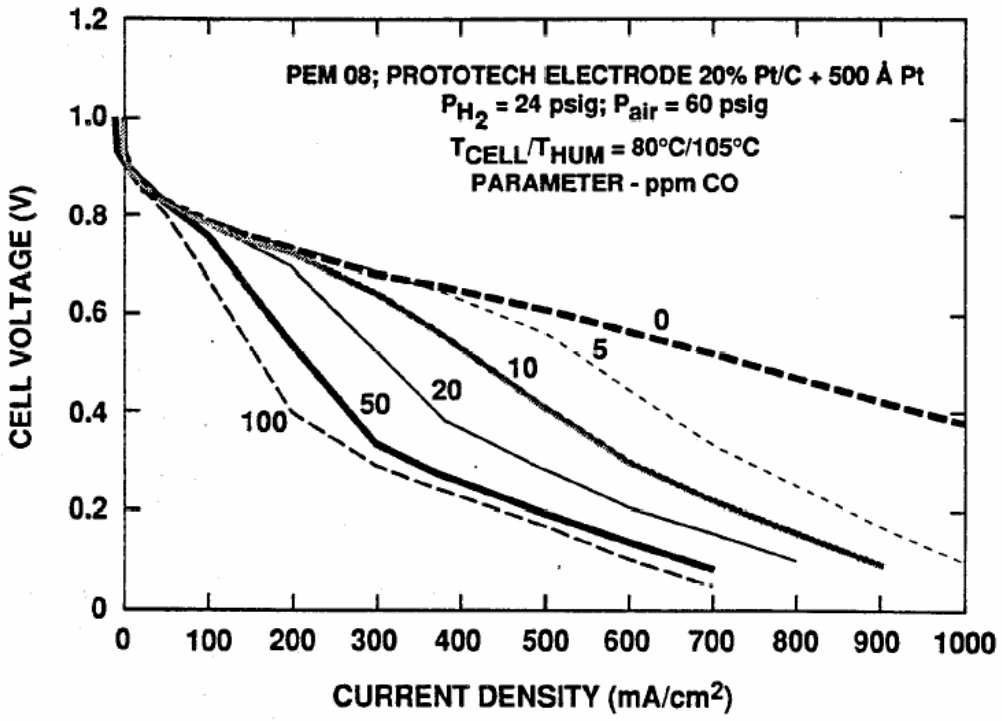

Figure 1-4. Polarization curves for a PEM fuel cell at 80 °C in the presence of low CO levels in the H_2 anode feed stream. The CO levels in ppm are specified next to each curve. Other experimental conditions are specified in the figure (ref. 12).

1.3 CO Tolerant PEM Fuel Cell

1.3.1 Effect of CO on the PEM Fuel Cell Performance

It is well known that CO binds strongly on Pt at low temperatures, thus, reducing Pt surface sites available for H_2 adsorption and oxidation. Although the electrochemical oxidation of CO with H_2O is thermodynamically favorable, the kinetics are slow, and in practice, a large overpotential is required before electrooxidation occurs. Surface coverage of CO on Pt at even the ppm gas concentrations is very high ($\theta_{co} \approx 0.98$-1.0) at typical PEM fuel cell operating temperatures.[13]

$$CO + H_2O \leftrightarrows CO_2 + 2H^+ + 2e^- \qquad [3]$$

Gottesfeld and Pafford[12] have shown that the fuel cell performance is highly dependent on the feed CO concentration (Figure 1-4). Even 5 ppm CO in hydrogen can cause a performance degradation when the current density is over about 400 mA/cm^2 and the voltage loss is over 300 mV at a current density of 1000 mA/cm^2. The voltage loss due to CO poisoning is more dramatic initially with an increase in the anode feed CO concentration (e.g., at a current density of 700 mA/cm^2, the voltage loss is over 400 mV for a CO concentration increase from 0 to 20 ppm, while the subsequent voltage loss is only about 100 mV for a further CO concentration increase from 20 to 100 ppm). A more detailed experimental work on the effect of CO concentration on PEM fuel cell performance is reported by Oetjen et al.[14] Both Pt and PtRu catalyst were evaluated using H_2/CO as anode feed with different CO concentration. The results show that with a 100 ppm CO in the anode feed, there is a 60% voltage loss as compared to pure H_2 feed on Pt anode catalyst. On the other hand, at identical experimental conditions, the PtRu (1:1 atomic ratio) anode catalyst provides only about 100 mV voltage loss at a current density of 500 mA/cm^2. Similar results are given by Acres et al,[15] for a 240 cm^2 Ballard Mark V cell. They investigated the impact of 10, 40, 100 ppm CO in the hydrogen fuel stream on the performance of a Pt-based anode at a platinum loading of 0.37 mg/cm^2.

Another parameter that determines how CO impacts PEM fuel cell performance is fuel cell temperature. The CO adsorption on Pt surface will become weaker as the temperature increases. Lee et al[16] showed the effect of temperature on fuel cell performance with a feed of H_2 containing 20 ppm CO. It is shown that the poisoning

effect is much more severe for low temperatures than at higher temperatures. For a cell voltage of 0.4 V, less than 100 mA/cm^2 could be sustained at 40 °C. However, a current density of 1500 mA/cm^2 could be sustained when the cell temperature was increased to 115 °C. This is an indication that operating PEM fuel cell at higher temperatures can improve the cell performance in the presence of CO, which will be discussed in more detail in a later section.

In more recent work, Qi et al[17] reported the effect of PtRu catalyst loading on the performance of a PEM fuel cell with an anode feed of 10 ppm CO/70% H_2/30 % CO_2. It was found that higher catalyst loading is beneficial to CO tolerance. For example, at a current density of 200 mA/cm^2, cell voltage is 0.69 V for a loading of 0.19 mg/cm^2 PtRu. When the catalyst loading is over 0.43 mg/cm^2, the cell voltage at the same current density can achieve 0.75 V. However, a still higher catalyst loading of 1.06 mg/cm^2 does not increase the cell voltage. This was ascribed to the higher conducting resistance and mass transport limitations caused by the thicker catalyst layer when the catalyst loading is increased.

Since the fuel processing reactor will experience start up, shut down or load change if used in the on-board generation of H_2, there would be concentration changes of CO superimposed on the steady-state CO concentration of 5-50 ppm.[18] Thus, the response of the fuel cell system to the transient change of CO concentration is also of practical interest. Bauman et al[18] reported the performance decay and recovery in PEM fuel cell in response to step changes in the level of CO in the feed stream. It was found that the transient time is primarily controlled by the CO inlet flux, which depends upon the CO concentration and anode inlet flow rate. Another important observation is that the transient time for a step change from 10 ppm to 200 ppm is much shorter than that for a step change from 0 to 200 ppm. The recovery by hydrogen purge was found to be sluggish and is a function of cell temperature. The rate is thought to be controlled by the rate of the thermal desorption of CO.

1.3.2 CO Tolerant Electrocatalyst Development

1.3.2.1 Electrocatalyst System

There has been a great deal of effort invested into overcoming the detrimental effect of CO on the fuel cell performance. The most successful approach to solving anode poisoning problem is the development of CO tolerant electrocatalysts capable of operating in the presence of, e.g., 100 ppm CO. Thus, much effort has been spent in modifying Pt by alloying with other metals to produce catalysts with improved CO tolerance. The most successful alloy thus far is the binary PtRu alloy catalyst. PtRu is also known to be a better catalyst for methanol electrooxidation based on the early work of Watanabe et al.[19] Later it was shown to have better CO tolerance as well by many other researchers[13] (Figure 1-5). Further improvement in the preparation and optimization of the PtRu catalyst is still a field of active research. Thus, Schmidt et al[20] and Paulus et al[21] tried to simplify the preparation procedure and improve the alloying of Pt with Ru. An organometallic preparation scheme was employed that can synthesize the colloid precursors for bimetallic catalyst. However, a recent result reported by Papageorgopoulos et al.[22] seems to challenge the effort in obtaining an alloyed PtRu catalyst. It was found that the nonalloyed PtRu was even better in the electrooxidation of H_2 containing 100 ppm CO. This positive effect was believed to stem from the higher H_2 oxidation activity of nonalloyed Pt compared to that of Pt alloyed with Ru, although Pt and Ru being in close proximity was still necessary for the CO electrooxidation**.** He et al.[23] introduced a third component (such as Os, Au, SnO_x, or WO_x) to the PtRu alloy in an attempt to further improve the H_2 electrooxidation activity in the presence of CO. It was found that the addition of SnO_x resulted in a very poor performance for H_2 oxidation. However, $Pt/Ru/WO_x$ was found to be twice as active as the PtRu catalyst at practical potentials for the electrooxidation of H_2 with 1% CO.

Despite the improvements in the CO tolerance of PtRu over Pt, complete tolerance to 100 ppm CO is not yet achievable at low catalyst loadings. Thus, other Pt based alloys have also been investigated as potential CO tolerant anode catalysts for PEM fuel cell. A non Pt-based alloy is reported by Schmidt et al.[24] Carbon supported PdAu catalyst was prepared via deposition of preformed bimetallic colloidal precursors. It was shown that in the overpotential range relevant to the fuel cell anode (0.1 V- 0.5 V), the performance of PdAu/C catalyst is better than the state-of-the-art PtRu (1:1 atomic ratio) catalyst at 60 °C in the lower current density range using both 250 ppm and 1000 ppm

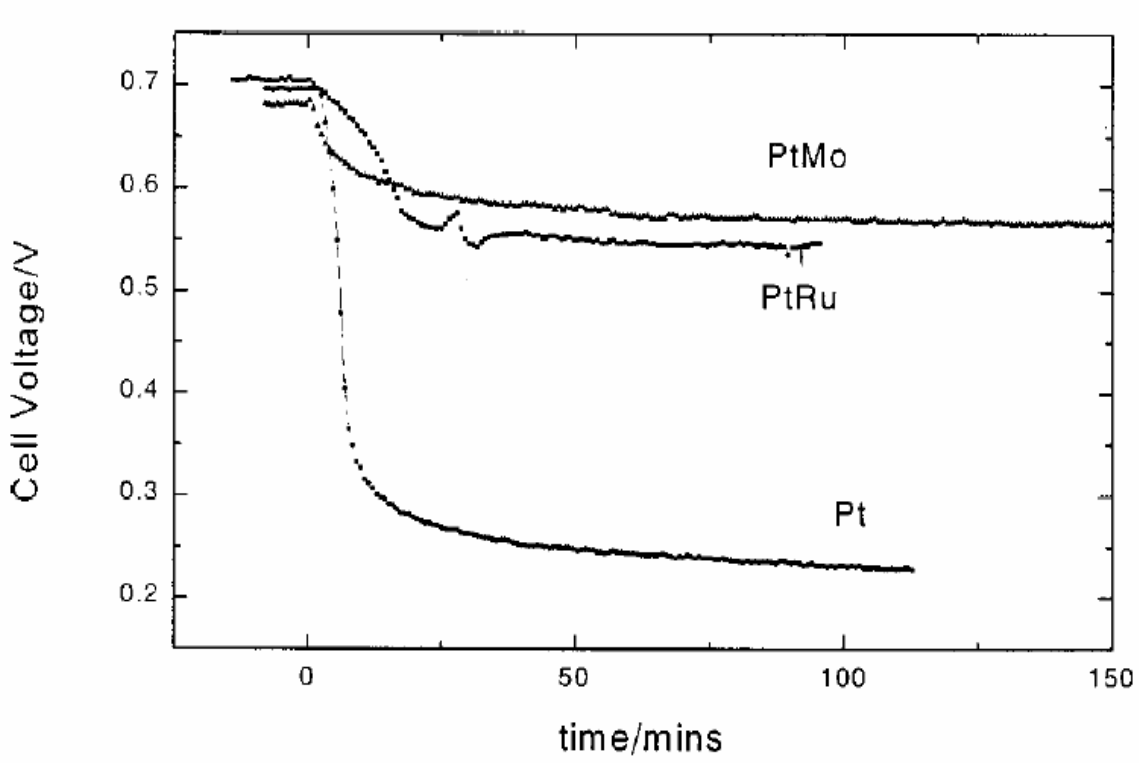

Figure 1-5. Change in cell voltage with time of MEAs containing Pt, PtRu, and PtMo anode electrodes upon switching between pure H_2 and 100 ppm CO in H_2 at t = 0, I =500 mA cm^{-2}, T = 80°C (ref. 33).

CO in H_2 as test gas (Figure 1-6). The experiments were conducted in an electrochemical cell with 0.5 M H_2SO_4 as the electrolyte. No data on the performance in PEM fuel cell was given.

A $PtRu/WO_3/C$ ternary system was studied by Chen et al.[25] The catalyst was prepared via a freeze drying method and was subsequently evaluated in 0.5 M H_2SO_4 at 80 °C. It was found that the CO tolerant properties were highly dependent on the heat treatment during the preparation. The performance of the catalyst using hydrogen reduction at 300 °C was much better than that obtained after thermal decomposition at 360 or 450 °C. When H_2/100 ppm CO was used as the fuel gas, a current density of over 500 mA/cm^2 could be achieved at an anode overpotential of 0.05 V for catalysts obtained from hydrogen reduction at 300 °C. However, the current density for the catalysts obtained at 360 or 450 °C was zero at identical experimental conditions. The greater Pt-Ru/WO_3 interface was believed to be responsible for the improved performance for samples reduced in hydrogen. However, no comparison was made to Pt or PtRu catalyst at the same loading under identical conditions.

Another binary combination of Pt-based catalyst is PtGe, which was prepared by a similar organometallic chemistry method.[26] A selective surface reaction was utilized between the reduced surface of Pt and an organometallic compound of Ge. Subsequent heat treatment under hydrogen lead to the deposition of Ge onto the crystal surface of Pt. Physicochemical characterization showed the presence of GeO_2 at Pt surface, which is believed to have changed the profile of strongly adsorbed CO, initiating the CO oxidation from 0.85 V to 0.68 V. PtSn binary catalyst was also prepared by the same group using the organometallic chemistry method.[27] Extensive characterization of the catalyst by Transmitting Electron Microscopy (TEM), Energy Dispersive X-ray analysis (EDX), X-ray Photoelectron Spectroscopy (XPS) and cyclic voltammetry (CV) showed that PtSn with 3-4 nm particle size was obtained. Pt and tin oxide exist on the catalyst surface once the catalyst was exposed to air. The onset potential of CO electrooxidation was shown to shift about 400 mV to a lower potential as compared to pure Pt. Ordered intermetallic phases of PtBi and PtPb were prepared and studied by Volpe et al.[28] as potential fuel cell electrocatalysts using formic acid as anode fuel. Both PtBi and PtPb exhibited high

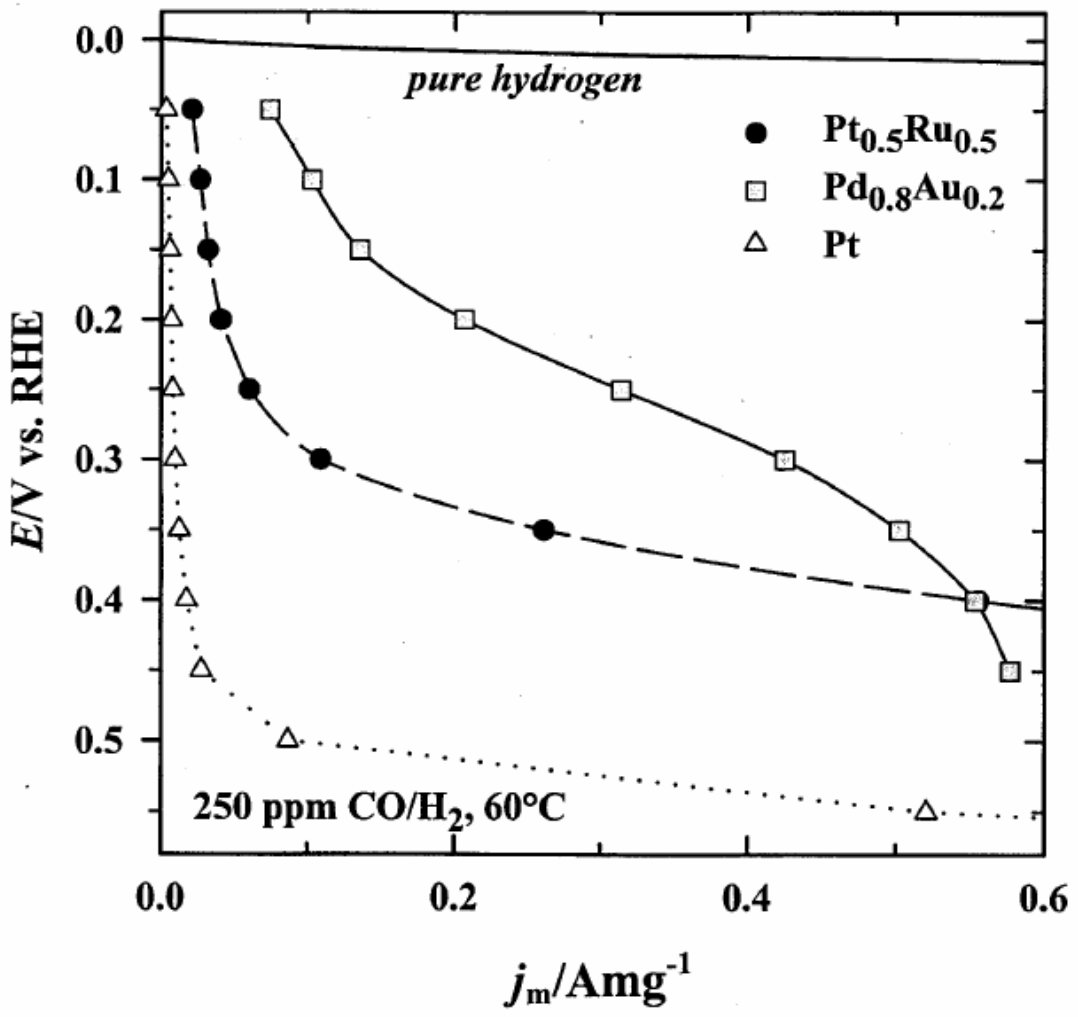

Figure 1-6. Potentiostatic oxidation of 250 ppm $CO:H_2$ on $Pd_{0.8}$ $Au_{0.2}$/Vulcan (□), PtRu/Vulcan (●), and Pt/Vulcan (Δ); 60°C, 2500 rpm, 0.5 M H_2SO_4 (ref. 24).

tolerance to CO poisoning by inhibiting CO adsorption. However, the stability of these catalysts remains to be improved.

The most widely studied alloy system other than PtRu is PtMo. Mukerjee et al[29] have studied PtMo catalyst using both cyclic voltammetry and a single fuel cell. The authors concluded that the performance of PtMo/C (with a atomic ratio of 4:1) is apparently better than that of the state-of-the-art PtRu catalyst. At a current density of 1000 mA/cm^2, the cell voltage using PtMo as the anode catalyst is about 200 mV higher than that with PtRu/C at 85 °C with 100 ppm CO in H_2 as the anode feed (Figure 1-7). The better performance of PtMo over PtRu is thought to be due to the lower potential at which CO electrooxidation begins to occur. Grgur et al[30] studied H_2/CO elctrooxidation on PtMo alloys using cyclic voltammetry. The performance was also compared against PtRu alloy with both 20 ppm CO and 100 ppm CO in H_2. The comparison of kinetic properties of supported catalysts with those of bulk alloys suggested that the alloying by Pt is incomplete, and the alloy nanocrystal surface are rich in Mo relative to the atomic ratios in the catalysts. Gouerec et al[31] developed a relatively simple preparation method for PtMo catalyst, the high energy ball-milling method. XRD and XPS characterization shows that Pt is in a metal state, but Mo (V or VI) is present in the catalyst. Although the final content of Mo in the catalyst is low (~ 5%), but the performance of this catalyst is similar to that of the commercial PtRu catalyst from Johnson-Matthey when exposed to H_2/ 100 ppm CO. Moreover, the prepared binary catalyst showed a stable performance of 80 hours at 0.5 V and 80 °C. Ioroi et al.[32] reported recently the investigation of the activity of Pt/MoO_x/C toward the oxidation of H_2/100 ppm CO. Under actual PEM fuel cell anode conditions, the anodic polarization of Pt/MoO_x/C depended upon the flow rate of H_2/CO mixture, thickness of the Nafion® membrane, and the cathode gas, indicating that permeated O_2 from the cathode side mitigated the CO poisoning of the Pt/MoO_x/C catalyst.

Although these results show that PtMo is a promising "CO tolerant" anode catalyst, a shortcoming of the PtMo catalyst prevents its practical application. As Ball et al.[33] showed recently, although PtMo had some advantage over PtRu in CO tolerance, in the presence of another major component of reformate feed, i.e., CO_2, the performance was significantly worse as compared with PtRu. The reason for the poor performance of

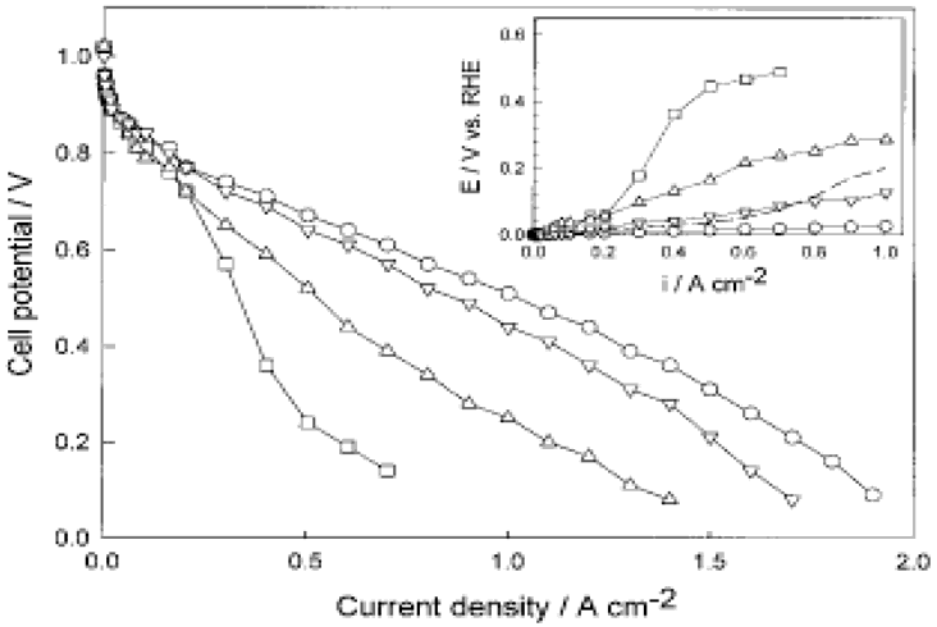

Figure 1-7**.** Performance of a 5 cm^2 cell with H_2/CO [100 ppm]//O_2 at 85°C, Nafion 115 membrane, respective anode/cathode pressures of 16/11 psig, and humidification temperature of 100/90°C. Cathode electrode: Pt/C (0.4 mg/cm^2). Anodes were Pt/C {□}, PtRu/C {Δ}, 4:1 PtMo/C {▽}; data for Pt/C (H_2/O_2) {○} are shown for comparison. Inset: Corresponding linearpolarization characteristics for the anodes showing the 4:1 PtMo/C polarization curve (- - -) projected from the RDE experiments (ref. 29).

PtMo in the presence of CO_2 was ascribed to the enhancement of the reverse water gas shift reaction catalyzed by PtMo.

$$CO_2 + H_2 \leftrightarrows H_2O + CO \quad [4]$$

The modification of Pt by metal macrocycle complexes was recently reported by Venkataraman et al.[34-35] to enhance the CO tolerance of Pt catalyst. Transition metal complexes of amines and macrocycle ligands such as cyclam, porphyrin, and phthalocyanine were used as co-catalysts of Pt for the electrochemical oxidation of H_2 containing CO. The complexes were believed to act as redox mediators in generating species that oxidize CO. The increase of the electroactive population of the complex and its proximity to Pt particles were suggested in order to further improve the CO tolerance of such catalysts.[34] The authors also observed that Pt catalysts synthesized using $Na_2S_2O_3$ could lead to a novel sulfur-containing Pt catalysts having high CO tolerance.[35] These catalysts showed inhibition of CO adsorption and a CO electrooxidation potential as low as 0.2 V.

1.3.2.2 Physicochemical Characterization of CO Adsorption and Electrooxidation

In order to understand the CO tolerance properties of Pt and other alloy catalysts, different physicochemical methods are employed in order to get a clear understanding of the mechanisms of CO adsorption and electrooxidation. This understanding is crutial in the design of better CO tolerant catalysts.

The most widely used method is the cyclic voltammetry technique, which is a common electrochemical methodology.[36] In these experiments, CO is either pre-adsorbed on the catalyst surface (which can be single crystal, polycrystalline or supported metal catalyst), or continuously bubbled through the liquid electrolyte solution. The electrode potential can be precisely controlled with the help of a reference electrode. The potential can be swept dynamically between two potential limits. Another advantage of this technique is that the mass transport of reactant gas can be controlled by the rotating disk electrode (RDE) technique. Thus, Gasteiger et al[37-39] have conducted extensive research on the H_2, CO and H_2/CO electrooxidation on different well-characterized metal and alloy electrode surfaces, particularly on Pt, Ru and PtRu alloy with different Pt:Ru atomic

ratios. It was found that the onset potential of CO electrooxidation is about 150-200 mV lower for PtRu than that for Pt (Figure 1-8). The ignition potential of significant current in the case of H_2/CO coincides with that of pure CO or CO in inert gases such as He. The observations support the hypothesis that H_2 electrooxidation is blocked by adsorbed CO. The comparison between Pt and PtRu shows that the introduction of Ru lowers the ignition potential of CO electrooxidation, thus vacating surface Pt sites for H_2 electrooxidation. The authors believe that the CO electrooxidation occurs via

$$CO_{ad} + OH_{ad} \rightarrow CO_2 + H^+ + e^- \qquad [5]$$

where OH is more readily formed on Ru surface at lower anode potentials as compared to Pt. This is the so-called "bifunctional" mechanism for CO tolerance.[37-38] However, it is not possible for the cyclic voltammetry technique to provide direct microscopic evidence on the nature of surface species on the electrode surface to corroborate the proposed mechanism. Schmidt et al.[40] further extended this cyclic voltammetry technique by using the thin-film RDE method to evaluate the reactivity of carbon supported Pt or PtRu catalyst. They showed that the conclusions extracted from these cyclic voltammetry results agreed well with the results obtained from PEM fuel cell tests.

A second technique is the FT-IR reflection-absorption spectroscopy. The CO adsorption and subsequent oxidation to CO_2 can be monitored *in-situ*. Kunimatsu et al.[41] showed that CO adsorption state on Pt depends on the potential at which it is adsorbed. The bridge-bonded CO can be oxidized as early as 0.2 V, but the linearly adsorbed CO begins at a higher potential of 0.35 V. Lin et al.[42] studied the CO electrooxidation on a model electrode prepared by electrochemical deposition of Ru on Pt(111). One conclusion of these researchers is that the electrooxidation of CO takes place preferentially at the Ru "islands", and CO adsorbed on Pt migrates toward Ru. In relevant work by the same authors,[43] CO stretch band frequencies are compared on Pt, Ru and PtRu electrode surface. The results indicate that relatively compact islands are formed on Pt or Ru, but a loose adlayer structure is formed on the PtRu alloy, which is believe to be beneficial to the CO electrooxidation. This technique is also adopted by Watanabe et al.[44] to study CO oxidation on Pt-Fe alloy, and by Rice et al.[45] to study CO adsorbed on carbon supported Pt catalyst.

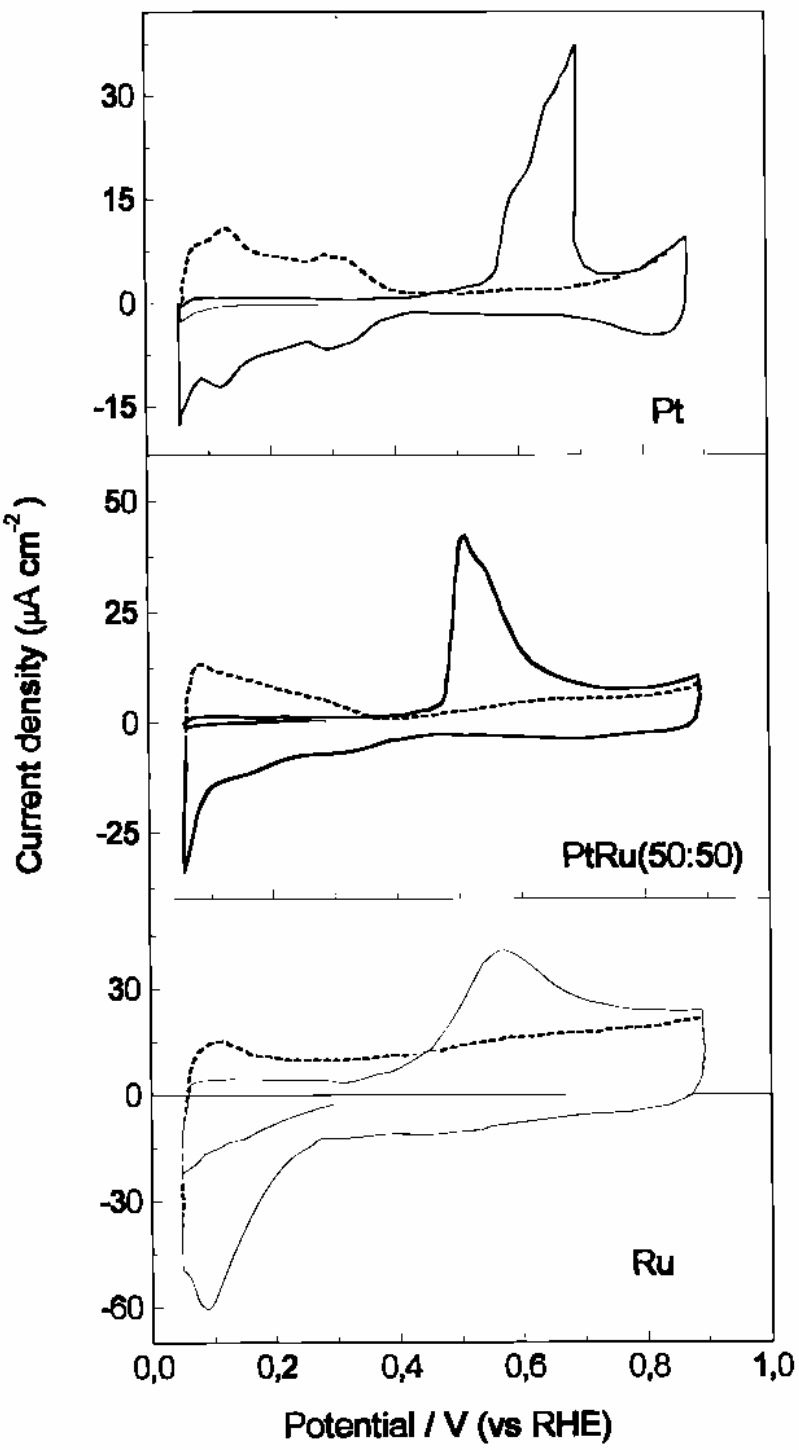

Figure 1-8**.** Cyclic voltammograms for the *oxidative stripping* of CO from Pt, PtRu(50:50) alloy, and Ru electrodes in 0.1 M $HClO_4$. The surface was saturated with CO at 0.3 V. After adsorption, CO was displaced from solution by 15 min of N_2 bubbling. Sweep rate 0.01 V/s (ref. 43).

Another technique that has been employed to study the CO oxidation on supported fuel cell catalyst is the extended X-ray absorption fine structure (EXAFS), which probes the changes to the short range atomic order (primarily, the first shell bond distance and coordination number). Lin et al.[46] studied the CO tolerance properties of two PtRu catalyst samples prepared in different ways. EXAFS was used together with half-cell and single cell measurement. The results showed that the catalyst with Pt-Ru bimetallic alloy interaction has better CO tolerance. On the other hand, the catalyst with mixed phases of Pt and RuO_x has a somewhat lower CO tolerance. The catalyst showing bimetallic alloy interactions was also found to have a weakened CO adsorption, which is believed to be the key mechanistic effect of the better CO tolerance. Maniguet et al.[47] use EXAFS technique to study the Pt/C electrocatalyst exposed to CO as a function of electrode potential. They found that, at potentials less than 0.5 V, adsorbed CO is clearly observed with a Pt-C distance of 1.85 Å. When the potential is over 1.05 V, an oxide layer is believed to be formed based on the presence of a Pt-O coordination shell at 2.0 Å. The X-ray adsorption technique was also utilized by Mukerjee et al.[48] and Viswanathan et al[49] to study carbon supported Pt and/or Pt-based alloy catalyst such as PtRu and PtMo.

Nuclear magnetic resonance spectroscopy (NMR) has also been used to study CO adsorption and oxidation on Pt/C or PtRu catalyst. Tong et al.[50] demonstrated that Ru weakens the Pt-CO bond in PtRu alloy catalyst by comparing the $2\pi^*$ Fermi level local density of states and the steady-state currents. These observations support another mechanism of CO tolerance, i.e., the so-called "ligand" mechanism. It is believed that the introduction of a second element changes the electronic structure of Pt, thus lowering the CO affinity on Pt surface. Rush et al.[51] used NMR in conjunction with voltammetry to investigate the mechanism for the electrocatalytic oxidation of CO on Pt/C electrocatalyst in H_2SO_4 at ambient temperature. The combined analysis of the results show that three distinct forms of CO_{ad} are identified, i.e., linear carbonyl, bridged carbonyl, and a reduced carbonyl. The relative populations of these three species are found to depend strongly on electrode potential and are independent of the surface coverage.

Mass spectroscopy (MS) has been used to study the CO and H_2/CO electrooxidation on Pt/C or PtRu/C as well. Jusys et al.[52] showed that, with their differential electrochemical mass spectroscopy, they could determine quantitatively the

individual reaction rates under controlled mass transport conditions as a function of electrode potential, paralleling to the Faraday current. One of the conclusions of these authors is that the hydrogen oxidation reaction on Pt surface proceeds in a way different from both a (1- θ_{co}) and (1- θ_{co})^2 dependence on free surface sites. The mass spectroscopy has also been coupled with cyclic voltammetry[53] or temperature-programmed desorption.[54]

Another classical electrochemical technique used in the study of H_2/CO electrooxidation is the electrochemical impedance spectroscopy. Ciureanu et al.[55-56] have systematically investigated the impedance pattern of H_2/CO electrooxidation on Pt/C and PtRu/C fuel cell catalysts. The advantage of this technique is that single fuel cell structure can be used directly in the experiment. The results show that the impedance pattern of Pt or PtRu electrode in the presence of H_2 and CO is highly dependent upon the electrode potential, from which the reaction information can be extracted. A critical value of electrode potential is observed where the diameter of two semicircles of the impedance pattern becomes equal. At this point, the electrode activity has been restored to the unpoisoned electrode. Leng et al.[57] and Wang et al.[58] utilized this for other alloys including PtSn and at different temperatures (Figure 1-9). They found that the potential where the 'pseudo-inductive' behavior appears differs for different catalysts and strongly depends on the temperature. Thus, it is proposed that the onset potential where 'pseudo-inductive' behavior appears can be used as a new criterion for the evaluation of the CO-tolerance for different anode catalysts at different operating temperatures.

1.3.2.3 First Principles Theoretical Analysis of CO Adsorption and Electrooxidation

As preliminary success has been achieved in the first-principles theoretical modeling of heterogeneous catalysis, density functional theory (DFT) and Monte Carlo simulation have also been used in electrocatalysis, especially on the state-of-the-art electrocatalysts such Pt or PtRu. Work of Norskov's group[59-60] is representative of the activity in this area. Thus, Christoffersen et al.[59] have discussed the effect of alloying Pt with other metals based on DFT. An extensive database of the effect of alloying on the CO oxidation reactivity that includes all binary combinations of the transition metal to the right in the periodic table is given. Liu and Norskov[60] have semi-empirically applied

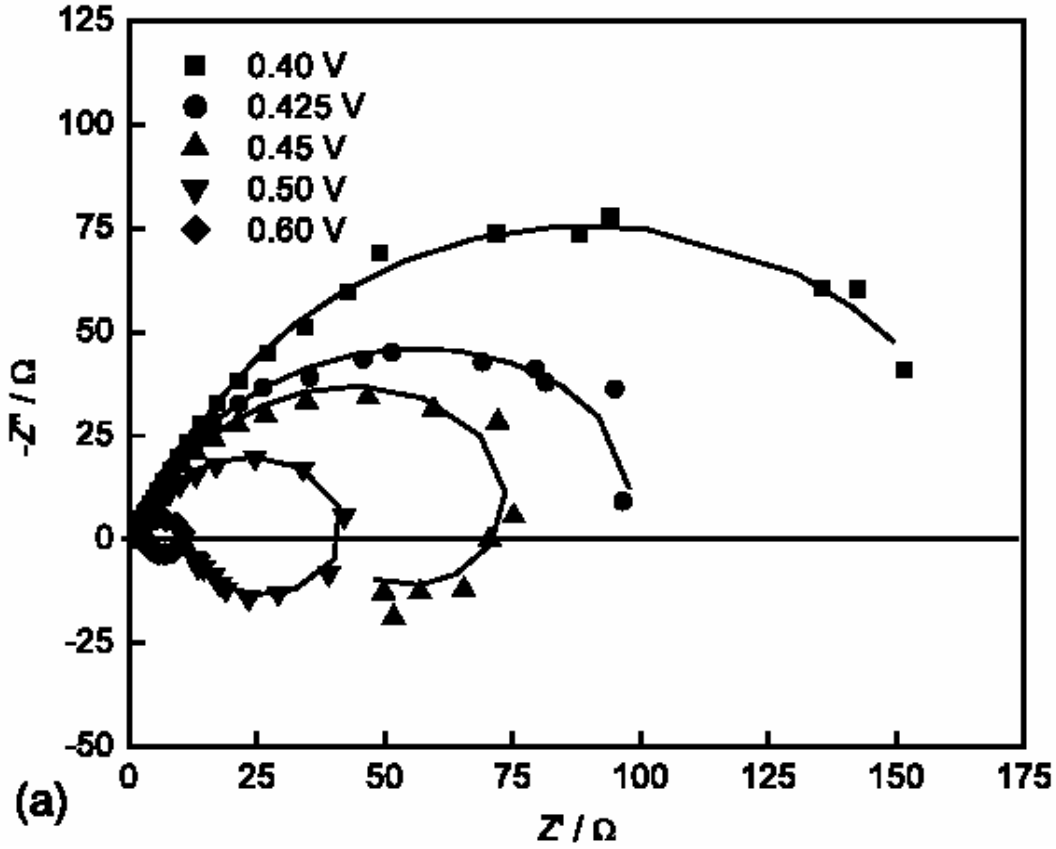

Figure 1-9. Complex impedance plots for a H_2/H_2 2 % CO cell with PtRu(1:1)/C anode (0.09 mg/cm^2 PtRu) at 50 °C as a function of the bias voltage (IR-uncorrected) (ref. 57).

the results calculated from density functional theory to the prediction of activity of Pt and PtRu toward H_2/CO electrooxidtion. Satisfactory results were obtained, although some of the key parameters were fitted rather than predicted.

Mitchell et al.[61] have applied the DFT to the calculations of adsorption and reaction of H_2, CO on the Pt-Pt, Pt-Ni, and Pt-Ru dimer surface. The calculation results showed that Pt-Pt binds CO much more strongly than Pt-Ni and Pt-Ru. Dynamic Monte Carlo simulation was used by Koper et al.[62] to study the CO electrocatalytic oxidation on Pt. With the mean-field approximation, the kinetics in the cyclic voltammetry experiments was simulated. Their studies showed that CO had a high surface mobility on Pt.

1.3.2.4 Phenomenological Modeling of Anode Kinetics in the Presence of CO

The CO poisoning of the anode has been an issue since the days of the investigation of phosphoric acid fuel cell. In addition to the physicochemical characterization in order to clarify the mechanism for the adsorption and electrooxidation of CO and H_2 on the catalyst surface, investigators also want to quantitatively evaluate the reaction mechanism and kinetics and to be able to predict the fuel cell performance in the presence of CO. The first attempt to quantify the effect of CO poisoning on hydrogen oxidation was that of Vogel et al.[63] The hydrogen electrooxidation was studied by cyclic voltammetry and steady-state polarization in acid solutions. The study showed that hydrogen dissociative adsorption (known as the Tafel step) is the rate controlling step when Pt surface is poisoned by CO. The electrochemical reaction rate parameters are the same for Pt catalysts in different states, i.e., smooth platinum, platinum black, or carbon supported platinum. A dual site mechanism was assumed to occur, i.e., the ratio of hydrogen oxidation current on CO poisoned Pt to the current on clean Pt was observed to be equal to $(1- \theta_{co})^2$. The surface coverage of CO is assumed to be in equilibrium with the CO in the liquid electrolyte. Dhar et al.[64-65] presented the results on CO poisoning of Pt catalyst in a porous fuel cell electrode in phosphoric acid solutions at different temperature. It was found that the CO poisoning loss is logarithmically dependent on the ratio of CO concentration to H_2 concentration, which is believed to be due to the replacement of H site by CO. Their results also support the dual site mechanism.

The first semi-quantitative analysis of the CO poisoning of the anode Pt catalyst in PEM fuel cell was reported by Bellows et al.[66] The idea of a CO_x inventory model was qualitatively presented and it was argued that CO tolerance is achieved when the rate of CO electrooxidation balances the combined adsorption rates from both CO and CO_2 present in the anode feed. In a subsequent publication,[67] the authors compared the polarization curve of PEM fuel cell using Pt or PtRu anode catalyst from different research groups and concluded that there exists a critical current where the anode potential becomes severely polarized. This critical current is related to catalyst loading, CO concentration, and fuel cell temperature. They also suggested that a Temkin isotherm might be appropriate for modeling the CO adsorption on PEM fuel cell catalyst.

A more complete analysis of the CO poisoning in PEM fuel cell was provided by Springer et al.[68]. Four chemical and electrochemical reaction steps were assumed to occur on PEM fuel cell anode catalyst exposed to hydrogen containing low levels of CO. In this model, the surface coverage of CO was treated as a steady-state, rather than an equilibrium species, as determined by the net adsorption rate and reaction rate. The simulation results show that the CO electrooxidation rate, on the order of nanoamperes/cm^2, could have a significant effect on the hydrogen electrooxidation current at low overpotentials (Figure 1-10). This anode kinetic model was later incorporated into an overall fuel cell model,[69] predicting the fuel cell performance including the dilution effect by CO_2 and N_2, which are present in the anode feed for a real reformate gas.

Most recently, Camara et al.[70] adopted the same modeling approach, in order to differentiate poisoning mechanisms of hydrogen oxidation on different anode catalysts, namely, Pt, PtRu and PtSn. In their model, linearly bonded and bridge bonded CO are treated separately, in terms of their kinetic parameters. Their simulation shows that onset of CO oxidation occurs via the bridge-bonded species, and the linearly adsorbed CO is oxidized at higher overpotentials, leading to an increase of the vacancies on the CO layers and thus of the rate of the hydrogen oxidation.

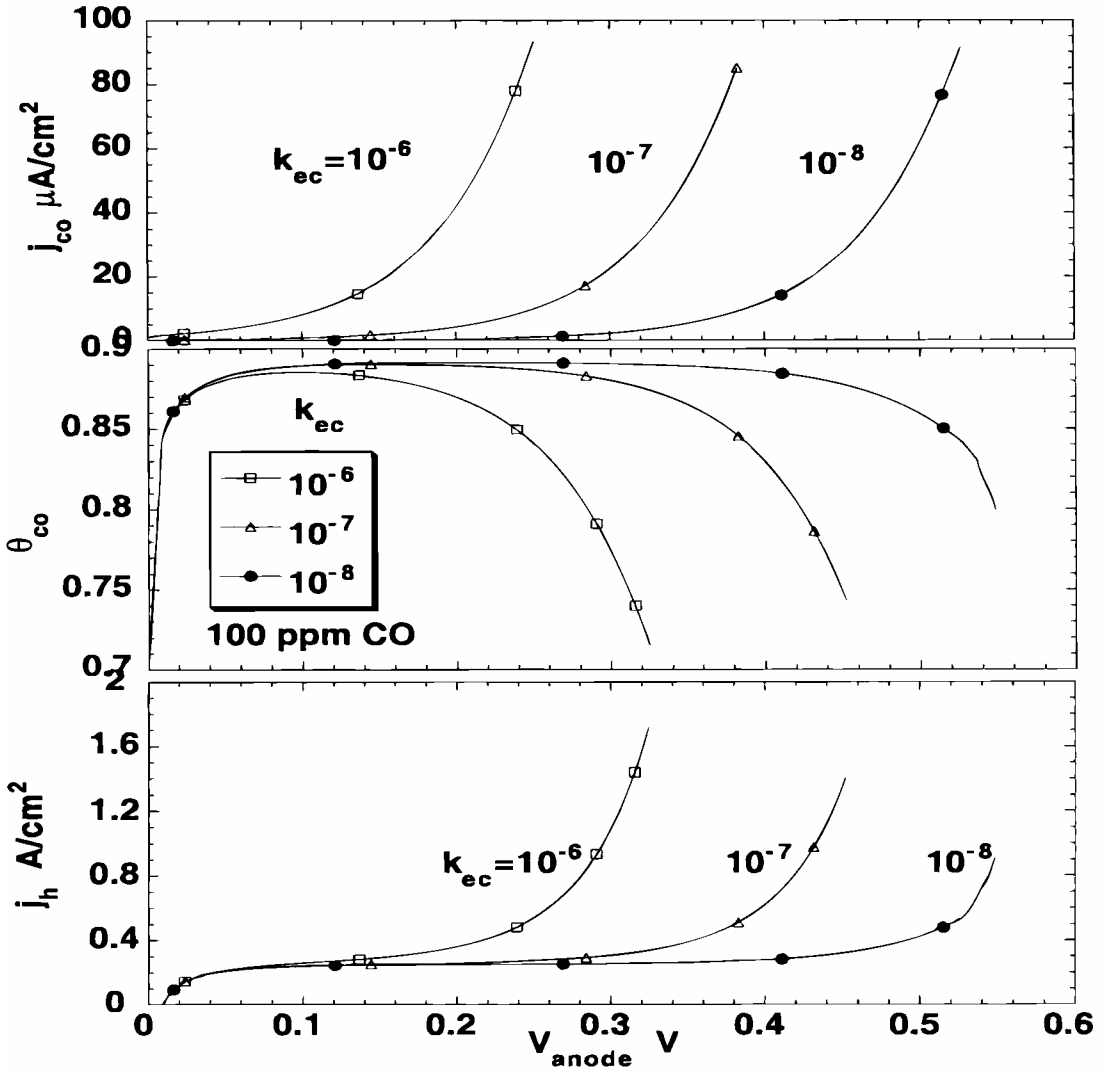

Figure 1-10**.** Effects of increase by factor of 10, or 100, in rate constant for CO electro-oxidation on CO electro-oxidation current (top), CO surface coverage (middle), and hydrogen electro-oxidation current (bottom). The abscissa shows anode overpotential *vs.* RHE (ref. 69).

1.3.3 Other Approaches in Improving CO Tolerance in PEM Fuel Cell

In addition to the search for CO tolerant anode catalysts, other approaches are also being actively pursued in order to improve the performance of the anode in the presence of low levels of CO. One of the most popular approaches is the oxygen (or air) bleeding in the anode. Thus, Gottesfeld et al.[12,71] found that the CO tolerance of anode could be significantly improved when low levels of oxygen or air are injected into the anode feed. This approach has proved to be very effective and it has been shown that with a 4.5% percent O_2 injection into a feed stream of H_2/100 ppm CO, the cell performance is completely recovered at 85 °C, i.e., the performance is identical to that of pure H_2 (Figure 1-11). It is believed that the injected O_2 reacts chemically with CO on the Pt catalyst, thus, reducing the surface coverage of CO and permitting the hydrogen oxidation reaction to proceed. Although the excess of O_2 reacts also with hydrogen, the cell voltage improvement can more than compensate the Columbic losses caused by the H_2 consumption. However, there are concerns of safety and hot-spot formation related to this technique.

Murthy et al.[72] studied the effect of air bleeding on the transient response of a PEM fuel cell exposed to relatively higher CO concentrations such as 500 and 3000 ppm. It was found that a 5% air bleeding could achieve a very good tolerance to 500 ppm CO, and the poisoning and recovery rate during the transient is also dependent upon the gas diffusion media. The interaction of CO kinetics and mass transfer through the gas diffusion media is assumed to account for this.

A slight variation of this method is the introduction of H_2O_2 into the anode humidifier.[73] In this method, dilute 5% H_2O_2 in the anode humidifier can successfully mitigate 100 ppm CO in H_2 feed. Furthermore, Bellows et al.[74] later showed that the mitigation effect depends on the slow decomposition of H_2O_2 into molecular O_2 within the humidifier itself, instead of H_2O_2 being carried by the gas stream to the catalyst surface and decomposing there, as originally believed.

A second approach is the modification of the anode structure. Thus, Rohland et al.[75] described the addition of a metal/graphite foam layer to the anode catalyst layer facing the gas stream. Metal catalyst such as Au or Pt is supported on the graphite foam, which improved the CO tolerance up to 750 ppm with very low levels of O_2 bleeding

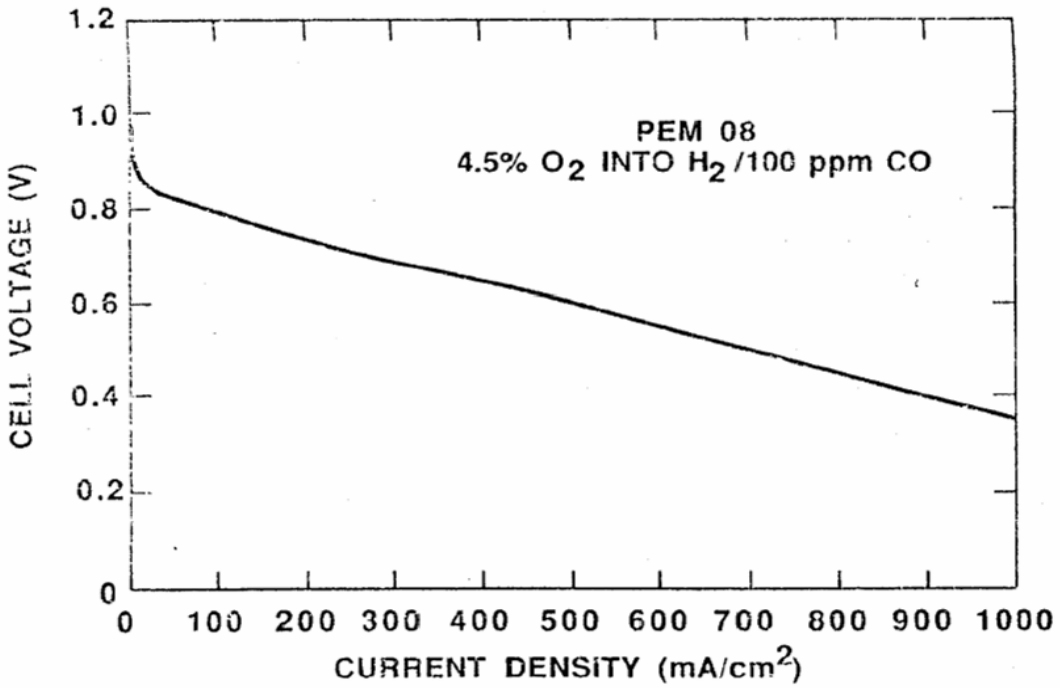

Figure 1-11. Polarization curve for the PEM fuel cell obtained when O_2 was injected at a level of 4.5% into the H_2 anode feed stream contaminated with 100 ppm CO. Other experimental conditions same as in Figure 1-4 (ref. 12).

(Figure 1-12). Yu et al.[76] proposed a composite electrode where an outer layer contains most of the amount of catalyst used, while the inner layer has a much lower catalyst loading (a thin film electrode). This has an apparent performance improvement over the conventional structure when hydrogen containing 50 ppm CO is used as the anode feed gas. In this case, no O_2 or air bleeding was used. Using a similar idea, Haug et al.[77-78] placed a Ru layer (it is termed as a "filter" by the authors) outside of the conventional anode catalyst layer facing the flow field. In the presence of 2 % of O_2 bleeding, the electrode with the Ru filter was shown to perform better than the electrode with catalyst layer only. The Ru filter is believed to preferentially promote the reaction of adsorbed CO with water, due to a low H_2 kinetics on Ru catalyst. More recently, researchers at Los Alamos National Laboratory[79-80] have presented results of a reconfigured anode, similar in concept to that described above. However, they use some metal oxide, such as Fe_3O_4 or Fe_2O_3, in the outer layer. This layer containing metal oxide replaces the precious metal and was shown to have the same or better CO tolerance effect when the O_2 bleed is used. Most recently, Santiago et al.[81] put Mo/C catalyst in the diffusion layer of the anode with the catalyst layer containing Pt/C, PtRu/C or PtMo/C. Enhanced activity for the H_2 electrooxidation reaction in the presence of CO was achieved with such an electrode structure. These results were attributed to a lowering of the CO concentration in the gas diffusion electrode promoted by a water gas shift (WGS) reaction taking place in the Mo/C layer. Thus, the authors believed that no direct contact between Pt and Mo was required to enhance the CO tolerance.

Another interesting way of improving the CO tolerance is reported by Carrette et al.,[82] who used a current pulsing technique to get a better overall performance using H_2 feed contaminated by different concentration of CO from 100 ppm to 1%. This method does not rely on any anode structure change or O_2 bleeding into the anode feed stream, but is rather based simply on an operational strategy of the fuel cell. By controlling the fuel cell current at a high value and then a lower value in a predetermined scheme, the cell voltage is polarized to high and lower values, alternately. Thus, the overall average cell performance is better than that at only one current value. It was shown that 70% of the performance with pure H_2 could be attained for the CO-contaminated PEM fuel cell using this operational scheme.

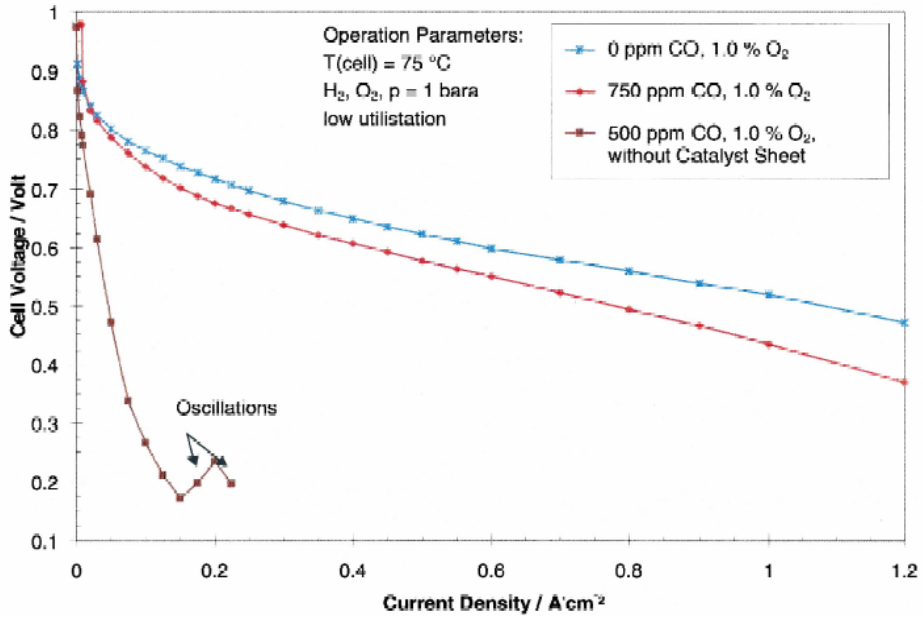

Figure 1-12. *V–i* plots of PEMFC with and without catalyst-sheet operated with CO-containing H_2 (ref. 75).

Operating the fuel cell at higher temperatures can obviously increase the CO tolerance of PEM fuel cells. This is due to the decreased surface coverage of CO on Pt-based electrocatalyst and higher electrooxidation rates at higher temperatures. It has been well demonstrated that the level of CO of about 1% can be tolerated in PAFC at 200 °C.[64-65] However, the state-of-the-art polymer electrolyte membrane does not work well above 100 °C due to the dehydration of the membrane and the ensuing loss of proton conductivity as well as the thermo-mechanical stability of the polymer. The CO poisoning effect in PEM fuel cells operated at temperatures up to 200 °C was evaluated recently by Li et al.[83] based on the use of phosphoric acid-doped PBI membranes. By defining the CO tolerance as a voltage loss less than 10 mV, it was observed that 3% CO in H_2 could be tolerated at current densities up to 0.8 A/cm^2 at 200 °C for a Pt catalyst while, at 125 °C, 0.1% CO in H_2 could only be tolerated at current densities lower than 0.3 A/cm^2. Research efforts are very extensive in developing new or modified proton conducting membranes for operation at temperatures over 120 °C,[84-86] the review of which is beyond the scope of this work.

References

1. S. Thomas, and M. Zalowitz, http:// education.lanl.gov/RESOURCES/fuelcells.
2. M. L. Perry, and T. F. Fuller, *J. Electrochem. Soc.,* **149**, S59 (2002).
3. K. Kordesch, and G. Simader, *Fuel Cells and Their Applications*, VCH, Weinheim (1996).
4. J. H. Hirschenhofer, D. B. Stauffer, R. R. Engleman, and M.G. Klett, *Fuel Cell Handbook*, for USDOE, Parsons Corp., Reading, PA (2002).
5. L. Blomen, and M.N. Mugerwa, *Fuel Cell Systems*, Plenum, New York (1993).
6. S. Gottesfeld, http:// education.lanl.gov/RESOURCES/H2/gottesfeld/education.html
7. I. D. Raistrick, in: R. E. White, K. Konishita, J. W. Van Zee, H. S. Burney (Eds.), *Proc. Symposium on Diapharms, Separators and Ion Exchange Membranes*, Vol. **86-13**, p.172 (1986).
8. L. F. Brown, *Int. J. Hydrogen Energy*, **26**, 381 (2001).
9. S. G. Chalk, J. F. Miller, and F. W. Wagner, *J. Power Sources*, **86**, 40 (2000).
10. I. H. Son, M. Shamsuzzoha, and A. M. Lane, *J. Catal*., **210**, 460 (2002).
11. C. He, H. R. Kunz, and J. M. Fenton, *J. Electrochem. Soc.*, **148**, A1116 (2001).
12. S. Gottesfeld, and J. Pafford, *J. Electrochem. Soc.*, **135**, 2651 (1988).
13. G. Hoogers, and D. Thompsett, *Cattech*, 3, 106 (2000).
14. H.-F. Oetjen, V. M. Schmidt, U. Stimming, and F. Trila, *J. Electrochem. Soc.*, **143**, 3838 (1996).
15. G. K. Acres, J. C. Frost, G. A. Hards, R. J. Potter, T. R. Rulph, D. Thompsett, G. T. Burstein, and G.J. Hutchings, *Catal. Today*, **38**, 393 (1997).
16. S. J. Lee, S. Mukerjee, E. A. Ticianelli, J. McBreen, *Electrchim. Acta*, **44**, 3283 (1999).
17. Z. Qi, C. He, and A. Kaufman, *J. Power Sources*, **111**, 239 (2002).
18. J. W. Bauman, T. A. Zawodzinski, Jr., and S. Gottesfeld, in *Proton Conducting Membrane Fuel Cells II*, S Gottesfeld and T. F. Fuller, Editors, PV 98-27, p. 136, The Electrochemical Society Proceedings Series, Pennington, NJ (1997).
19. M. Watanabe, and S. Motoo, *J. Electroanal. Chem.*, **60**, 275 (1975).

20. T. J. Schmidt, M. Noeske, H. A. Gasteiger, R. J. Behm, P. Britz, W. Brijoux, and H. Bonnemann, *Langmuir*, **13**, 2591 (1997).
21. U. A. Paulus, U. Endruschat, G. J. Feldmeyer, T. J. Schmidt, H. Bonnemann, and R. J. Behm, *J. Catal*., **195**, 383 (2000).
22. D. C. Papageorgopoulos, M. P. de Heer, M. Keijzer, J. A. Pieterse, and F. A. De Bruijn, *J. Electrochem. Soc.*, **151**, A763 (2004).
23. C. He, H. R. Kunz, and J. M. Fenton, *J. Electrochem. Soc.*, **150**, A1017 (2003).
24. T. J. Schmidt, Z. Jusys, H. A. Gasteiger, R. J. Behm, U. Endruschat, and H. Boennemann, *J. Electroanal. Chem.*, **501**, 132 (2001).
25. K. Y. Chen, Z. Sun, and A.C.Tseung, *Electrochem. Solid-State Lett*., **3**,10 (2000).
26. E. M. Crabb, and M. K. Ravikumar, *Electrochim. Acta*, **46**, 1033 (2001).
27. E. M. Crabb, R. Marshall, and D. Thompsett, *J. Electrochem. Soc*., **147**, 4440 (2000).
28. D. Volpe, E. Casado-Rivera, L. Alden, C. Lind, K. Hagerdon, C. Downie, C. Korzeniewski, F. J. DiSalvo, and H. D. Abruna, *J. Electrochem. Soc.*, **151**, A971 (2004).
29. S. Mukerjee, S.J. Lee, E. A. Ticianelli, J. McBreen, B. N. Grgur, N. M. Markovic, P. N. Ross, J. R. Giallombardo, and E. S. De Castro, *Electrochem. Solid-State Lett*., **2**, 12 (1999).
30. B.N. Grgur, N. M. Markovic, and P. N. Ross, *J. Electrochem. Soc*., **146**, 1613 (1999).
31. P. Gouerec, M.C. Denis, D. Guay, J. P. Dodelet, and R. Schulz, *J. Electrochem. Soc*., **147**, 3989 (2000).
32. T. Ioroi, K. Yasuda, Z. Siroma, N. Fujiwara, and Y. Miyazaki, *J. Electrochem. Soc.*, **150**, A1225 (2003).
33. S. Ball, A. Hodgkinson, G. Hoogers, S. Maniguet, D. Thompsett, and B. Wong, *Electrochem. Solid-State Lett*., **5**, A31 (2002).
34. R. Venkataraman, H. R. Kunz, and J. M. Fenton, *J. Electrochem. Soc.*, **151**, A703 (2004).
35. R. Venkataraman, H. R. Kunz, and J. M. Fenton, *J. Electrochem. Soc.*, **151**, A710 (2004).

36. A. J. Bard, L. R. Faulkner, *Electrochemical Methods, Fundamentals and Applications*, p. 213, John Wiley & Sons, New York (1980).
37. H. A. Gasteiger, N. M. Markovic, and P. N. Ross, *J. Phys. Chem*., **99**, 8290 (1995).
38. H. A. Gasteiger, N. M. Markovic, and P. N. Ross, *J. Phys. Chem*., **99**, 16757 (1995).
39. N. M. Markovic, C. A. Lucas, B. N. Grgur, and P. N. Ross, *J. Phys. Chem*., **103**, 9616 (1999).
40. T. J. Schmidt , H. A. Gasteiger, and R. J. Behm, *J. Electrochem. Soc*., **146**, 1296 (1999).
41. K. Kunumatsu, H. Seki, W. G. Golder, J. G. Gordon, and M. R. Philpott, *Langmuir*, **2**, 464 (1986).
42. W. Lin, M. Zei, M. Eiswirth, G. Ertl, T. Iwasita, and W. Veilstich, *J. Phys. Chem*., B, **103**, 6968 (1999).
43. W. Lin, T. Iwasita, and W. Veilstich, *J. Phys. Chem*., B, **103**, 3250 (1999).
44. M. Watanabe, Y. Zhu, and H. Uchida, *J. Phys. Chem*., B, **104**, 1762 (2000).
45. C. Rice, Y. Tong, E. Oldfield, A. Wieckowski, F. Hahn, F. Gloaguen, J. Leger, and C. Lamy, *J. Phys. Chem*., B, **104**, 5803 (2000).
46. S. Lin, T. Hsiao, J. Chang, and A. Lin, *J. Phys. Chem*. *B*, **103**, 97 (1999).
47. S. Maniguet, R. J. Mathew, and A. E. Russell, *J. Phys. Chem*., B, **104**, 1998 (2000).
48. S. Mukerjee, and R. C. Urian, *Electrochim. Acta*, **47**, 3219 (2002).
49. R. Viswanathan, G. Hou, R. Liu, S. Bare, F. Modica, G. Mickelson, C. U. Segre, N. Leyarovska, and E. S. Smotkin, *J. Phys. Chem*., B, **106**, 3458 (2002).
50. Y. Tong, H. Kim, P. K. Babu, P. Waszczuk, A. Wiechowski, and E. Oldfield, *J. Am. Chem. Soc.*, **124**, 468 (2002).
51. B. M. Rush, J. A. Reimer, and E. J. Cairns, *J. Electrochem. Soc.*, **148**, A137 (2001).
52. Z. Jusys, J. Kaiser, and R. J. Behm, *Phys. Chem. Chem. Phys*., **3**, 4650 (2001).
53. M. Krausa, and W. Vielstich, *J. Electroanal. Chem*., **379**, 307 (1994).
54. C. Lu, and R. Masel, *J. Phys. Chem. B*, **105**, 9793 (2001).

55. M. Ciureanu, and H. Wang, *J. Electrochem. Soc.*, **146**, 4031 (1999).
56. M. Ciureanu, H. Wang, and Z. Qi, *J. Phys. Chem*., B, **103**, 9645 (1999)
57. Y. Leng, X. Wang, I. Hsing, *J. Electroanal. Chem*., **528,** 145 (2002).
58. X. Wang, I. Hsing, Y. Leng, and P. Yue, *Electrochim. Acta*, **46,** 4397 (2001).
59. E. Christoffersen, P. Liu, A. Ruban, H. L. Skriver, and J. K. Norskov, *J. Catat*., **199**, 123 (2001).
60. P. Liu, and J. K. Norskov, *Fuel Cells*, **1**, 192 (2001).
61. P. C. Mitchell, P. Wolohan, D. Thompsett and S. Cooper, *J. Mol. Catal. A*, **119**, 223 (1997).
62. M. T. M. Koper, A. P. Jansen, R. A. Van Santen, J. J. Lukkien, and P. A. Hilbers, *J. Chem. Phys*., **109**, 6051 (1998).
63. W. Vogel, J. Lundquist, P. Ross and P. Stonehart, *Electrochim. Acta*, **20**, 79 (1975).
64. H. P. Dhar, L. G. Christner, A. K. Kush, and H. C. Maru, *J. Electrochem. Soc.*, **133**, 1574 (1986).
65. H. P. Dhar, L. G. Christner, and A. K. Kush, *J. Electrochem. Soc.*, **134**, 3021 (1987).
66. R. J. Bellows, E. P. Marucchi-Soos, and D. T. Buckley, *Ind. Eng. Chem. Res*., **35,** 1235 (1996).
67. R. J. Bellows, E. Marucchi-soos, in *Proton Conducting Membrane Fuel Cells II*, S Gottesfeld and T. F. Fuller, Editors, PV 98-27, p.218, The Electrochemical Society Proceedings Series, Pennington, NJ (1997).
68. T. Springer, T. Zawodzinski, and S. Gottesfeld, *in Electrode Materials and Processes for Energy Conversion and Storage IV*, J. McBreen, S. Mukerjee, S. Srinivasan, Editors, PV 97-13, p.139, The Electrochemical Society (1996).
69. T. E. Springer, T. Rockward, T. A. Zawodzinski, and S. Gottesfeld, *J. Electrochem. Soc.*, **148**, A11 (2001).
70. G. A. Camara, E. A. Ticianelli, S. Mukerjee, S. J. Lee, and J. McBreen, *J. Electrochem. Soc*., **149**, A748 (2002).
71. S. Gottesfeld, U. S. Pat. 4,910,099 (1990).

72. M. Murthy, M. Esayian, A. Hobson, S. MacKenzie, W. Lee, and J. W. Van Zee, *J. Electrochem. Soc.,* **148**, A1141 (2001).
73. V. M. Schmidt, H. F. Oetjen, and J. Divisek, *J. Electrochem. Soc*., **144**, L237 (1997).
74. R. J. Bellows, E. Marucchi-Soos, and R. P. Reynolds, *Electrochem. Solid-State Lett.*, **1**, 69 (1998).
75. B. Rohland, and V. Plzak, *J. Power sources*, **84**, 183 (1999).
76. H. Yu, Z. Hou, B. Yi, and Z. Lin, *J. Power Sources*, **105**, 52 (2002).
77. A. T. Haug, R. E. White, J. W. Weidner, W. Huang, S. Shi, N. Rana, S. Grunow, T. C. Stoner, and A. E. Kaloyeros, *J. Electrochem. Soc*., **149**, A868 (2002).
78. A. T. Haug, R. E. White, J. W. Weidner, W. Huang, *J. Electrochem. Soc*., **149**, A862 (2002).
79. P. A. Adcock, F. A. Uribe, J. A. Valerio, and T. A. Zawodzinski, in *Meeting Abstracts of 201th meeting of the Electrochemical Society*, Abstract No. 814, Volume 2002-1, May 12-17, 2002, Philadelphia, PA.
80. F. A. Uribe, and T. A. Zawodzinski, in *Meeting Abstracts of 201th meeting of the Electrochemical Society*, Abstract No. 806, Volume 2002-1, May 12-17, 2002, Philadelphia, PA.
81. E. I. Santiago, M. S. Batista, E. M. Assaf, and E. A. Ticianelli, *J. Electrochem. Soc.*, **151**, A944 (2004).
82. L. P. Carrette, K. A. Friedrich, M. Huber, and U. Stimming, *Phys. Chem. Chem. Phys.*, **3**, 320 (2001).
83. Q. Li, R. He, J. Gao, J. O. Jensen, and N. J. Bjerrum, *J. Electrochem. Soc.*, **150**, A1608 (2003).
84. S. Molhotra and R. Datta, *J. Electrochem. Soc*., **144**, L23 (1997).
85. C. Yang, P. Costamagna, S. Srinivasan, J. Benziger, and A.B. Bocarsly, *J. Power Sources*, **103**, 1 (2001).
86. K. T. Adjemian, S. J. Lee, J. Benziger, and A.B. Bocarsly, *J. Electrochem. Soc*., **149**, A256 (2002).
87. T. Thampan, S. Malhotra, J. Zhang, and R. Datta, *Catal. Today*, **67**, 15 (2001).
88. C. A. Callaghan, PhD proposal, Chemical Engineering Department, WPI (2004).

Chapter II

Influence of Anode Flow Rate and Cathode Oxygen Pressure on CO Poisoning of PEM Fuel Cells

In this Chapter, the anode flow rate of a proton exchange membrane (PEM) fuel cell involving Pt anode electrocatalyst is found to influence the single cell performance strongly when H_2 containing trace amounts of CO is used as feed. The performance drops dramatically due to CO poisoning as the anode flow rate increases until a large overpotential is reached when it levels off. This effect of the flow rate on extent of poisoning is found to be reversible and is explained to depend upon the actual concentration of CO in the anode chamber which in turn depends upon the feed content, the flow rate and CO oxidation kinetics on Pt. Further, it is found that oxygen permeating across PEM from the cathode side also appreciably affects the anode overpotential by providing another route for CO oxidation. A CO inventory model is provided that explains the observed phenomena in a PEM fuel cell operating with H_2/CO as anode feed and a cathode feed with different oxygen pressures. Contents of this chapter have been published in *J. Electrochem. Soc*..

2.1 Introduction

Proton exchange membrane (PEM) fuel cells power plants for stationary and mobile applications are planned to be operated on reformate gas feed that would inevitably contain trace amounts of CO.[1, 2] Extensive investigations have been performed to evaluate the CO tolerance of the PEM fuel cells with different electrocatalysts and under different conditions. It has been reported that the fuel cell temperature and CO content of the gas mixture are the key parameters that determine the performance for a given catalyst.[3-8] The poisoning effect of CO has also been investigated in electrochemical cells incorporating liquid electrolytes such as H_3PO_4 or H_2SO_4.[9-12] These investigations provide much insight into the effect of CO poisoning on the performance

of PEM fuel cell. The present work is motivated by our desire to study systematically the mechanisms and kinetics of standard fuel cell catalysts, such as Pt and PtRu, at real PEM fuel cell conditions. During the study of CO poisoning on PEM fuel cell performance with the Pt anode catalyst, we found the dramatic influence of certain operating parameters, namely the anode flow rate and cathode oxygen partial pressure, which have not so far been documented.

The performance of a single fuel cell is normally studied in the laboratory under a constant flow rate or stoichiometry. Though PEM fuel cell anode fed with pure H_2 is often operated near stoichiometry of one, reformate gas mixtures from catalytic reformers require higher flow rates, because considerable amounts of CO_2 and N_2 are also present in the gas mixtures, with H_2 concentration ranging from 40 to 75% depending upon the reforming system and specific process.[13] It is shown in this chapter that the anode flow rate and cathode oxygen partial pressure are very important operating parameters influencing the extent of CO poisoning when operating with a feed containing essentially pure H_2 along with trace amounts of CO. We report here for the first time, experimental results on the effect of the anode flow rate and cathode oxygen partial pressure on the performance of a single PEM fuel cell with Pt anode catalyst at different temperatures. These results are of significance both practically and fundamentally for a single cell as well as for stacks.

In modeling and experimental studies of H_2/CO oxidation on Pt anode in PEM fuel cells, it is often tacitly assumed that the CO concentration in the anode chamber is identical to that in the inlet feed. This, of course, is not true due to CO oxidation on Pt, especially when the anode inlet flow rate is small (low stoichiometry). Under these conditions, it is necessary to write an overall CO mass balance including terms for the rate of CO oxidation in addition to those for flow in and out so that the performance of Pt catalyst toward CO oxidation can be objectively evaluated. A preliminary CO_x inventory model has been put forth by Bellows *et al*.,[7] where the change of surface coverage of CO was attributed to the CO adsorption, CO electrooxidation, and CO_2 reduction (in a simulated refomate gas). They assumed CO adsorption onto Pt to be kinetically very rapid and approaching a complete monolayer coverage for concentration as low as 1 ppm.[7]

In the work reported here, the anode inlet flow rate and cathode oxygen partial pressure are found to dramatically influence the anode overpotential, and consequently the overall fuel cell performance. A more complete and quantitative inventory of CO in the anode side is, therefore, necessary, which is provided here to account for the effect of anode flow rate as well as cathode oxygen partial pressure on the PEM fuel cell performance.

2.2 Experimental

The 20% (w/o) Pt/C catalyst powder used to prepare the anode was purchased from E-TEK Inc. (Natick, MA). Gas diffusion electrodes already loaded with 20%(w/o) Pt/C at a metal loading of 0.4 mg/cm^2, were also purchased from E-TEK. Nafion® 115 and 117 proton-exchange membranes (Du Pont, Fayetteville, PA) were used after sequential treatment with 2% H_2O_2, deionized water, 0.5 M H_2SO_4 and again with deionized water in order to remove any inorganic and organic impurities. The membrane electrode assembly (MEA) was prepared by hot-pressing in a Model C Carver hot press at 130 °C and under a pressure of 4000 lbs for about 2 minutes. The MEA was then incorporated in a 5 cm^2 single cell from ElectroChem, Inc. (Woburn, MA), and tested in a test station with temperature, pressure, humidity and flow rate control. The current-voltage characteristics were recorded using a HP 6060B DC electronic load, interfaced with a PC using LabView software (National Instruments, Austin, TX).

The single fuel cell was tested at different temperatures, different anode flow rates, and different cathode oxygen pressures. Anode and cathode gases were first humidified through a stainless steel bottle containing water at a desired temperature before being fed into the fuel cell. The temperatures of the humidification bottles were set at 15 °C and 10 °C higher than that of the fuel cell for the anode and cathode side, respectively. The total pressure of both anode and cathode side was maintained at 30 psig. The experiment was conducted continuously, with some data being collected for as long as 20 hours to ensure a steady-state value. The flow rates reported in this study are all at the standard state (1 atm and 25 °C) and in units of standard cubic centimeter per min (scc/min). Pre-mixed H_2/108 ppm CO was purchased from MG Industries (Morrisville, PA). The CO concentration was certified by the supplier and was not

independently confirmed. The fuel cell performance results reported here are all with H_2/108 ppm CO; Pt loading, 0.4mg/cm^2 (20% Pt/C); 80°C; and Nafion® 115 membrane, unless otherwise noted.

2.3 Results

2.3.1 Effect of Anode Flow Rate

Figure 2-1 shows the steady state results of the change of cell voltage with the anode flow rate at 80 °C and a constant current density of 200 mA/cm^2. The data for pure H_2 (without any CO) under identical conditions are also plotted for comparison. The upper abscissa in Figure 2-1 shows the corresponding stoichiometry for the current density of 200 mA/cm^2. As expected, the cell voltage is not influenced by the flow rate for the case of pure H_2. However, it is dramatically influenced by the anode flow rate when operating with H_2/CO (108 ppm) mixture. At relatively small flow rates, the cell voltage deviation from that of pure H_2 is rather small. Thereafter, there is a region where the cell voltage drops precipitously with an increase of the anode flow rate. However, at relatively large flow rates, a plateau of the cell voltage is reached, and further increase of the anode flow rate does not significantly affect the cell voltage. These observations are explained below on the basis of the increasing CO content in the anode chamber to which the MEA is exposed with the flow rate, eventually approaching feed concentration at high flow rates. This is due to the mass balance accounting for CO entering and exiting anode chamber via flow as well as that consumed via the oxidation on Pt by water and oxygen diffusing through the PEM from the cathode.

In a study of transient CO poisoning by Bauman *et al*.,[14] the time it took to attain steady state current when switched from one CO content feed to another was found to be influenced by the anode flow rate. The higher the flow rate, the shorter the time it took for the cell to reach steady state. However, little difference was found in the steady state current for the flow rate of 1.5 stoichiometry versus 3.0 stoichiometry (Figure 4, ref. 14). Actually, this stoichiometry corresponds to the current *before* CO poisoning. Since after the introduction of CO, the cell current density drops from 960 mA/cm^2 to about

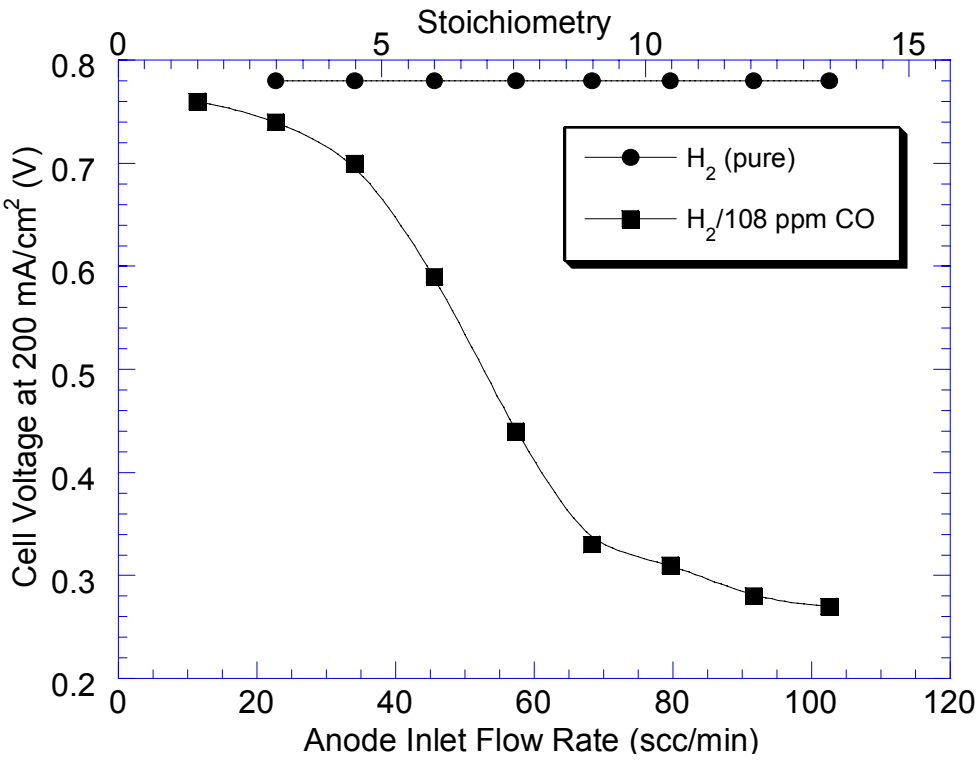

Figure 2-1. Effect of anode flow rate on cell voltage at constant current density for H_2 and H_2/ 108 ppm CO for 5 cm^2 PEM fuel cell at 80°C; Nafion® 115 membrane. Current density, 200 mA/cm^2.

120~140 mA/cm^2, the experimental stoichiometry for the current is nearly 10 rather than 1.5 which corresponds to the higher flow rate region of Figure 1, where the cell performance has low sensitivity to the change in the anode flow rate.

The cell voltage versus time data are shown in Figure 2-2 over a period of more than 3 hours with the fuel cell operating at 80 °C and a current density of 300 mA/cm^2 when several equal step changes were introduced in the flow rate. The cell voltage data were continuously collected for these step changes. After each adjustment, it is seen in Figure 2-2 that within a few minutes the fuel cell attains a steady state cell voltage corresponding to the new anode flow rate. The cell voltage remains fairly stable at various flow rates (± 20 mV). This figure also shows the dramatic cell voltage change in the initial step increase of anode inlet flow rate, with increasingly smaller changes for subsequent step changes of equivalent size. The scattered points between the different step changes are due to the rapid voltage recovery during the brief period of resetting of the anode flow rate from one value to another.

In order to investigate further the transient recovery behavior, the anode inlet feed valve was shut off after the cell reached a steady state corresponding to the given anode flow rate. The ensuing cell voltage recovery versus time is shown in Figure 2-3, followed by the cell repoisoning and voltage decline when the H_2/CO feed is reintroduced at the original flow rate. It should be pointed out that in this transient experiment, when the H_2/CO feed was stopped, the total pressure of anode chamber would drop gradually below 30 psig due to the consumption of H_2 to sustain a certain current density. It is seen from Figure 2-3 that the cell voltage recovers fully within a minute or two upon valve closure. After the anode gas is reintroduced, the cell voltage decreases rapidly to the value prior to valve closure. These results indicate that CO poisoning is highly reversible and rapid. It is also noteworthy that the time of poisoning to a steady-state voltage after the introducing of H_2/CO is dependent upon the anode inlet flow rate. The higher the inlet flow rate, the shorter the transient time to reach the steady state voltage. In Figure 2-3, the transient time decreased from about 110 s to about 50 s when the inlet flow rate was increased from 57.5 scc/min (Figure 2-3b) to 80 scc/min (Figure 2-3a). These results are in agreement with those of Bauman *et al.*,[14] who observed a transient period of less than 300 s. These periods are also of the order of the time constant for the anode chamber, the

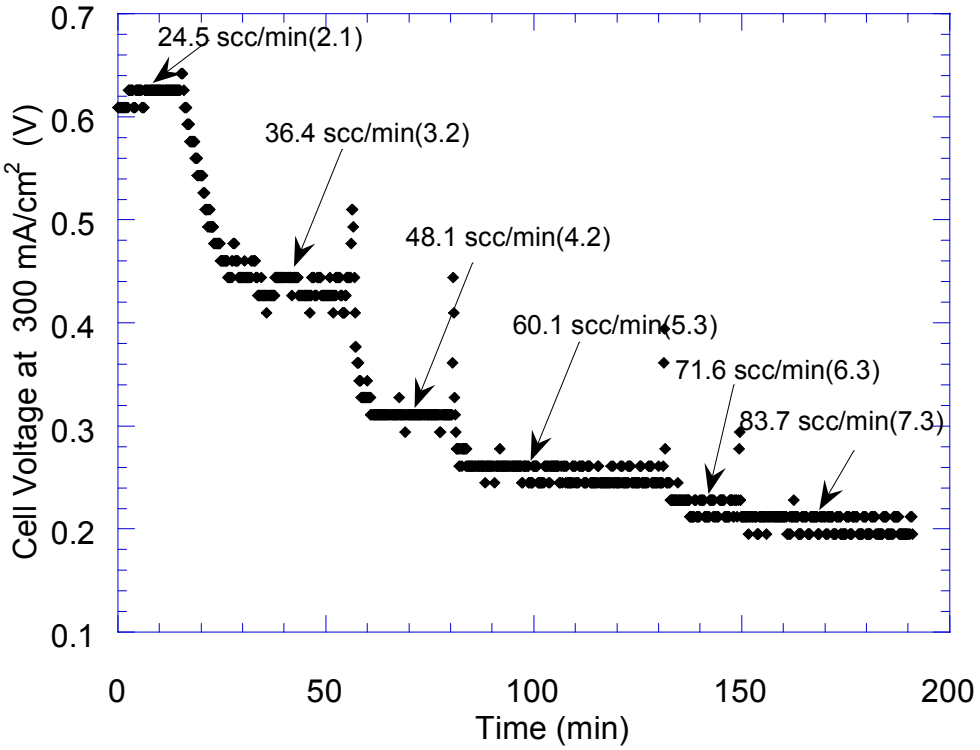

Figure2-2. Cell voltage profile at different anode inlet flow rates at 300 mA/cm^2 at 80°C; Nafion® 115 membrane. Numbers in the brackets are the corresponding stoichiometry.

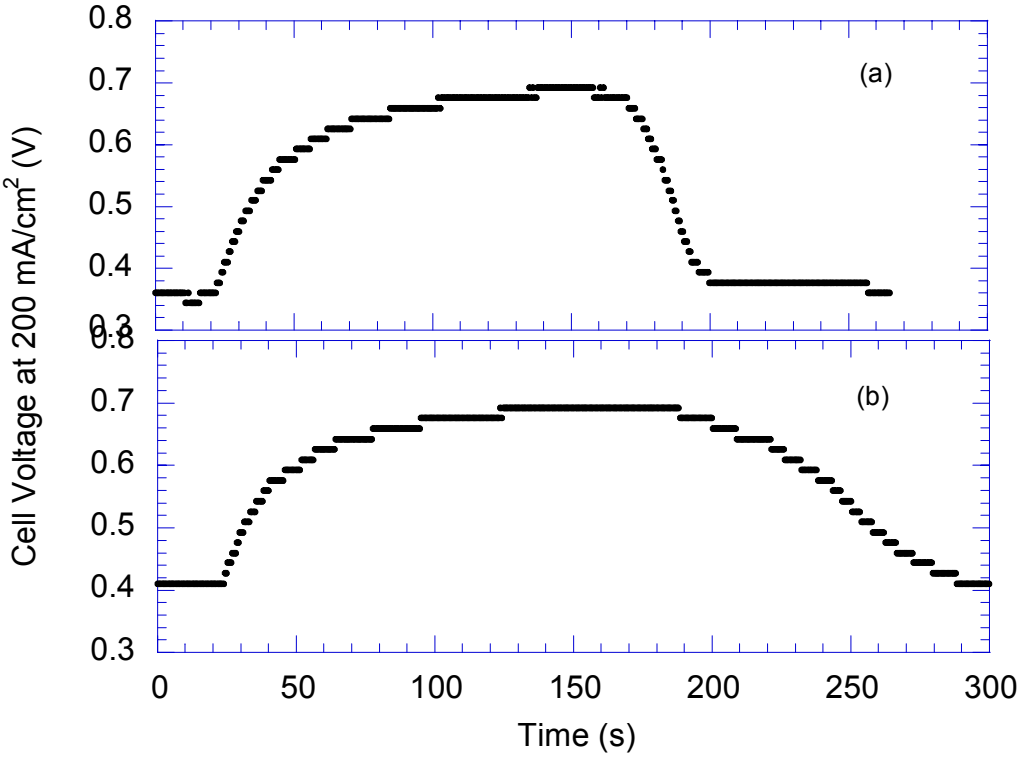

Figure 2-3. Recovery and poisoning transient for the cell operated at 200 mA/cm^2 at 80°C for different anode inlet flow rates. (a) 80 scc/min (b) 57.5 scc/min. Nafion® 115 membrane.

mass transfer and kinetics of the CO adsorption on Pt in the PEM fuel cell anode being much more rapid. This aspect is further discussed later on.

More detailed current–voltage characteristics for the PEM fuel cell at 80 °C are shown in Figure 2-4. The performance curve for pure H_2 is also plotted for comparison. We use the same protocol to get the performance curve for H_2/CO as we did with pure H_2. Namely, when the anode flow rate is set at a given value, the current is monitored at a cell voltage of 0.4 V until the current is stable. Then the current is measured for different cell voltages. At each cell voltage, the current is recorded in about 1 minute after the voltage settings. The curves shown in Figure 2-4 were obtained at different anode flow rates and clearly demonstrate the remarkable effect of the flow rate on the cell performance. Interestingly, the current-voltage curves exhibit trends that are qualitatively similar to those with H_2/CO gas mixtures of *different* CO contents.[3, 4] At low current densities, the difference between the cell voltage at different flow rates at a given current density is small. With an increase in current density, the deviation becomes increasingly large. Furthermore, it may be noticed that there are three regions with different slopes in the current–voltage curves. The slope at low current densities is smaller than that at relatively higher current densities. But below about 0.2 V for the high current density region, the slope of curves at different flow rates becomes smaller again. The similarity between the effect of flow rate for a given CO content and that of the CO content at a constant flow rate is not coincidental, as explained later. The CO content to which the MEA is exposed is, in fact, dependent upon the flow rate.

We further note that the performance reported here at low flow rates is better than that reported in the literature for similar CO contents.[3, 4, 8] Typically, the flow rates in these studies are larger and correspond to the large stoichoimetry flow rate region of this study. The performance reported in the literature is in good agreement with our data for the higher flow rates.[6, 8] Unfortunately, the flow rate values are often not reported in the literature.

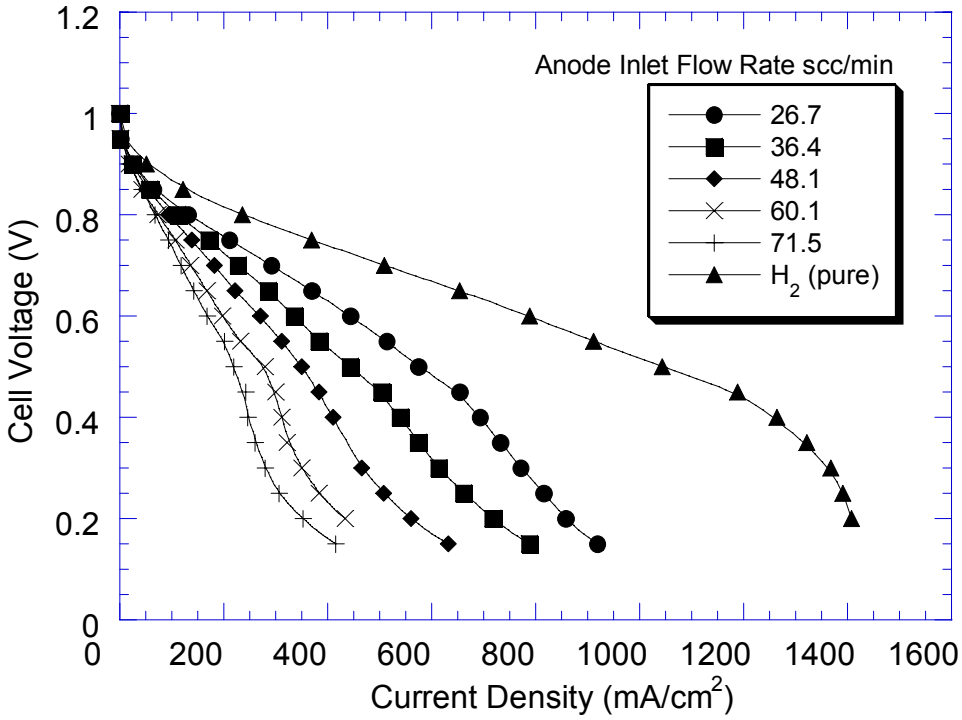

Figure 2-4. PEM fuel cell performance at different anode flow rates at 80 °C; Nafion® 115 membrane.

.

2.3.2 Anode Overpotential

The overall fuel cell voltage is given by the following expression[15]

$$V = V_0 - \eta_A - \eta_C - i\left(\frac{L}{\sigma}\right) - i(R_I) \qquad [1]$$

where V_0 is the open circuit potential, i is the current density, η_A and η_C are the anode and cathode overpotentials, respectively, L and σ are the thickness and conductivity of the proton-exchange membrane, respectively, while R_I is any interfacial resistance. Thus, at a constant current density, the difference in the polarization of the anode between the cases of the presence ($\eta_{H_2/CO}$) and the absence of CO (η_{H_2}) in the anode feed can be obtained by making measurements of the cell voltage under otherwise identical experimental conditions except for the anode feed gas composition:

$$\eta_{H_2/CO} - \eta_{H_2} = V_{H_2} - V_{H_2/CO} \qquad [2]$$

where V_{H_2} and $V_{H_2/CO}$ are the cell voltages with H_2 and H_2/CO, respectively. Further, since the overpotential for pure H_2 is small,[6, 15] it may be neglected without substantial error. Thus, the anode overpotential in the presence of CO is assumed to be simply the cell voltage difference between the two cases, *i.e.*,

$$\eta_{H_2/CO} \approx V_{H_2} - V_{H_2/CO} \qquad [3]$$

Figure 2-5 shows the hence calculated anode overpotential versus the flow rate at 80 °C and at different but constant values of the current density. It is noteworthy that there are three relatively distinct regions in the anode overpotential curve. Below about 25 scc/min, the anode overpotential rises slowly with the flow rate. In this range, only small current densities can be sustained. Above about 70 scc/min , the anode overpotential also increases only gradually with the anode flow rate for all current densities. In the

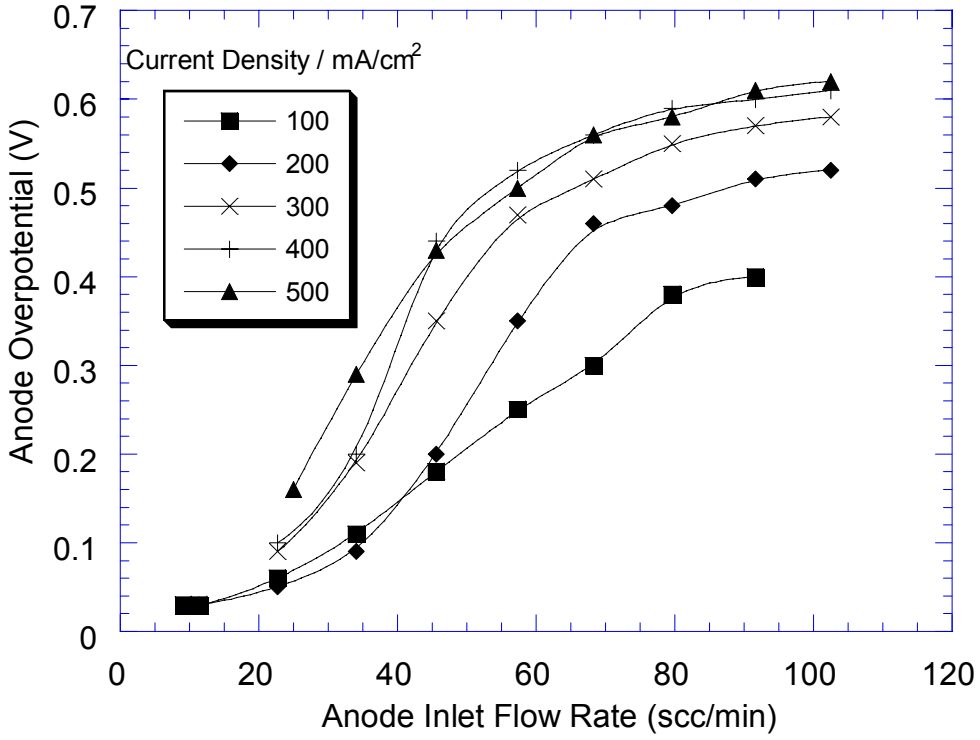

Figure 2-5. Anode overpotential versus flow rate at different current density at 80°C; Nafion® 115 membrane.

intermediate region between these values, the anode overpotential increases dramatically with flow rate. In this region at a given flow rate, the lower the current density, the smaller is the anode overpotential.

The change of anode overpotential with the anode inlet flow rate at three different temperatures is compared in Figure 2-6. It is clear that with the increase of the cell temperature, the maximum overpotential at relatively large flow rates decreases from about 0.7 V at 55 °C to about 0.5 V at 80 °C. Further, the transition of the anode overpotential from a low value to a high value (the intermediate range) takes place at lower flow rates as temperature decreases. For example, threshold values of roughly 40 scc/min at 80 °C, 25 scc/min at 70 °C, and 15 scc/min at 55 °C are observed at 200 mA/cm^2.

2.3.3 Effect of Oxygen Pressure

Experiments were also conducted under different cathode pressures using pure oxygen feed. The anode overpotential as a function of anode flow rate is thus plotted in Figure 2-7 for three different cathode oxygen pressures. It is clear that the anode overpotential is substantially influenced by O_2 pressure and it decreases as the cathode O_2 pressure increases. It should be pointed out that the cathode overpotential η_C is, of course, also a function of O_2 pressure.[15] In calculating anode overpotential, thus, the cell voltages V_{H_2} and $V_{H_2/CO}$ were both measured at the same O_2 pressures and subtracted according to equation 3.

It can be inferred from the above results that there must be some oxygen diffusing through the Nafion® membrane to the anode side and contributing to the CO oxidation in addition to that by water. In order to further confirm this, Nafion® 117 membrane was used in place of Nafion® 115. Further, air was used in the cathode instead of pure O_2, with all the other components of the MEA and the operating conditions remaining unchanged. The results are shown in Figures 2-8 and 2-9, respectively. As apparent in Figure 2-8, the cathode pressure for the case of the thicker Nafion® 117 membrane is less influential as compared with the case of Nafion® 115 membrane, with O_2 pressure

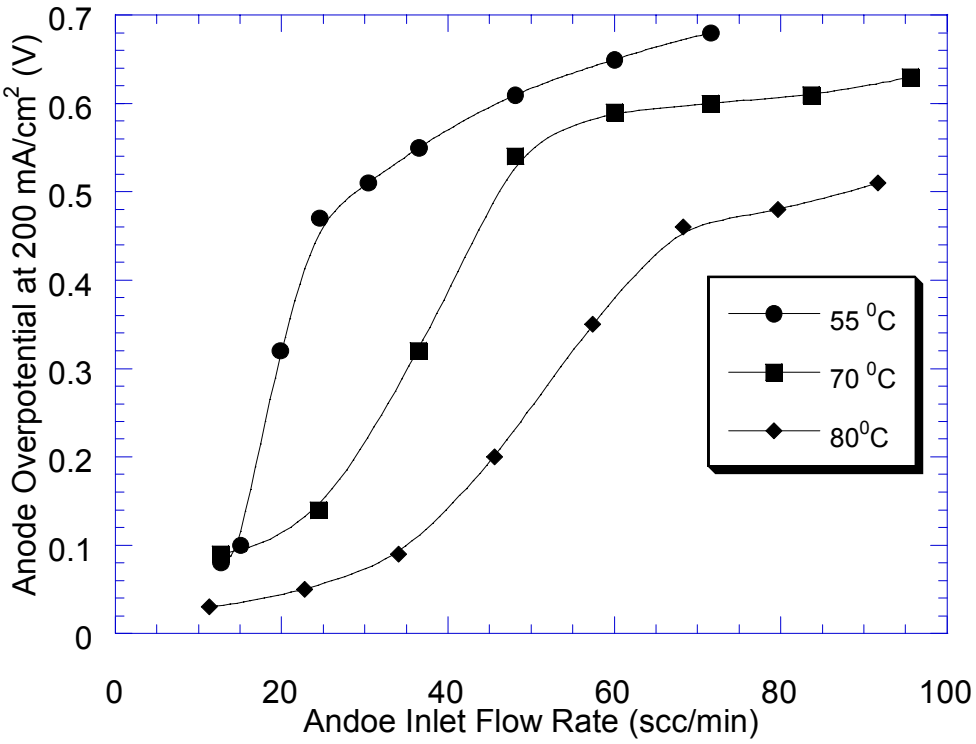

Figure 2-6. Anode overpotential versus flow rate at 200 mA/cm^2 at different temperatures; Nafion® 115 membrane.

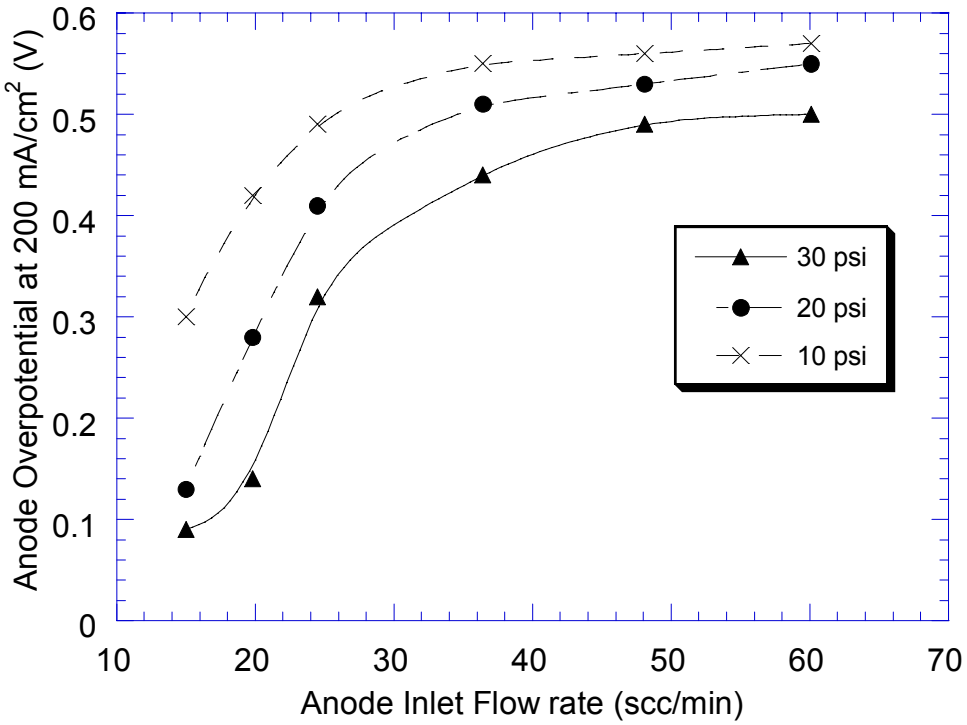

Figure 2-7. Anode overpotential versus flow rate at 200 mA/cm^2 at different cathode O_2 pressures; 80 °C ; Nafion® 115 membrane.

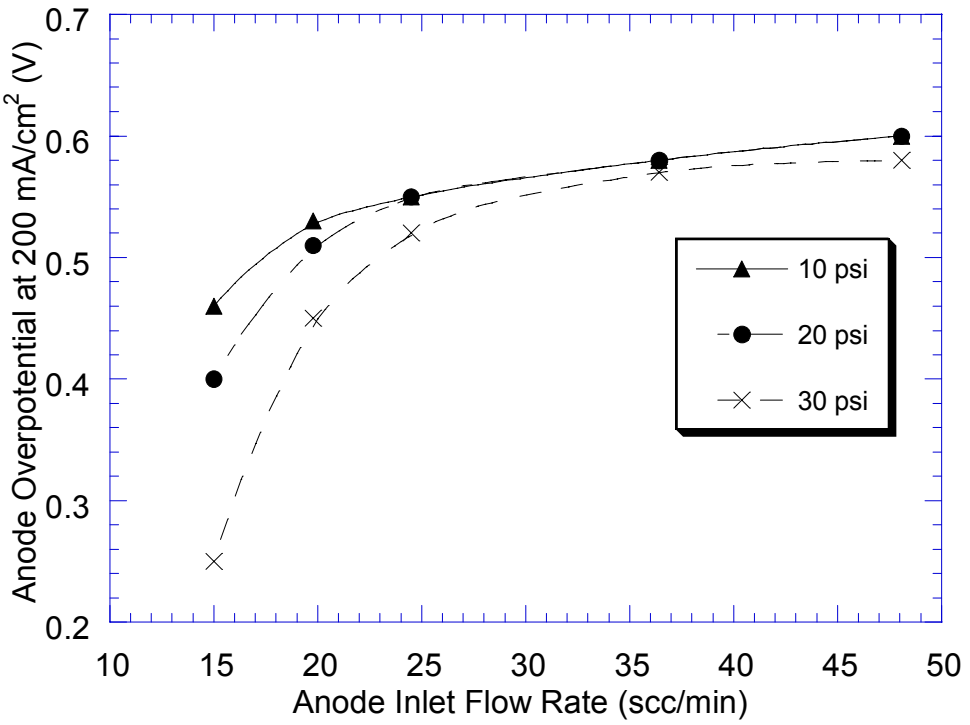

Figure 2-8. Anode overpotential versus flow rate at 200 mA/cm^2 at different cathode O_2 pressures; 80 °C ; Nafion® 117 membrane.

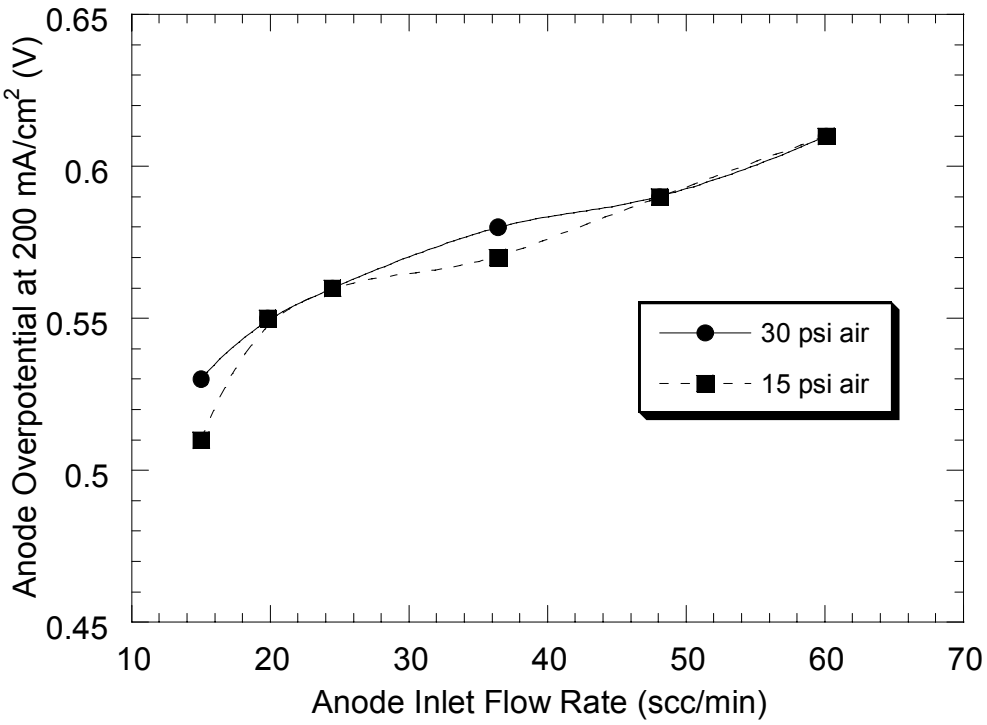

Figure 2-9. Anode overpotential versus flow rate at 200 mA/cm^2 at different cathode air pressures; 80 °C ; Nafion® 115 membrane.

affecting the overpotential mainly in the low flow rate region. When the anode overpotential is over 0.5 V, there is not any significant difference in the overpotential versus the flow rate at different O_2 pressures. When air is used in the cathode feed, the overpotential versus the flow rate curve is virtually independent of the cathode pressure (Figure 2-9). Further, the overpotential change with the anode flow rate is over a narrower range as compared with the case of pure O_2, with the overpotential being high throughout ranging from 0.5 V to 0.6 V for all flow rates. Thus, when air is used, only a small amount of oxygen permeates and the electrooxidation of CO via water is likely the dominant cleaning mechanism.

From these observations, it is virtually certain that any O_2 that permeates from cathode to anode plays an important role in the oxidative removal of CO and hence the observed anode flow rate effect. However, it is also apparent that O_2 is not the only agent of this CO removal. It is, thus, likely that the diffusing O_2 contributes to CO oxidation at lower anode overpotentials while water contributes to its electrooxidation at higher anode overpotentials. For practical applications involving use of air at low pressures, the role of O_2 is less significant.

2.4 Modeling

2.4.1 Mass Balance

The material balance for species *i* in the anode chamber maybe written as[15]

$$V\frac{dc_i}{dt} = v_0 c_{i,0} - vc_i - N_i A \qquad [4]$$

where V is the volume of the electrode chamber, assumed here to be well-mixed, which is not an unreasonable assumption for a small (5 cm^2) single cell. v_0 and v are the volumetric inlet and outlet anode flow rates, respectively. $c_{i,0}$ and c_i are the concentrations of species i in the inlet and outlet streams, respectively, N_i is the flux of species i into the MEA, and A is the geometric area of the MEA in the fuel cell. The flux N_i of H_2, CO or any other species is, in principle, affected by mass transfer limitations through the gas

diffusion backing layer and catalyst layer as well as by the kinetics of the electrode reactions.[15] Bauman *et al.*[14] found that mass transport barriers for CO are negligible. Our transient CO poisoning results further support this observation. Thus, mass transport limitations for CO are precluded as are those for H_2. In other words, the fluxes of CO as well as H_2 are assumed to be determined solely by the anode kinetics on Pt. Further, it is clear from the above described experiments that the CO oxidation on Pt results from both H_2O and O_2 permeating from the cathode. These are discussed next.

2.4.2 CO Oxidation Mechanism and Kinetics

There is still considerable controversy concerning the CO oxidation mechanism in fuel cells. It is commonly accepted, however, that the electrochemical CO oxidation in acidic solutions involves a surface reaction between adsorbed CO molecules and an oxygen-containing species,[16] the exact nature of which is as yet unclear. Markovic *et al.*[17, 18] and Gasteiger *et al*.,[9, 10] based on their extensive work on the CO electrooxidation in liquid electrolytes in the absence of molecular oxygen, suggest that CO_{ad} oxidation on Pt follows the same mechanism both in the pre-ignition region and ignition potential region in cyclic voltammetry, and involves the reaction with OH_{ad},[17] *i.e.*,

$$\text{Pt-OH} + \text{Pt-CO} \rightarrow 2\,\text{Pt} + CO_2 + H^+ + e^- \qquad [5]$$

Cyclic voltammetry and spectroscopic studies reveal that both the formation of oxygen-containing species and the CO oxidation reaction are potential dependent, and the reversible adsorption of OH_{ad} occurs in the potential range 0.7~0.8 V vs. reversible hydrogen electrode(RHE) in liquid sulfuric acid electrolyte.[17, 19] In a FTIR study by Iwasita *et al*.,[19] the lowest potential where the 3270 cm^{-1} peak appears, which is characteristic of OH_{ad}, is 0.7 V, although they proposed that the water dissociation to form OH_{ad} might begin at around 0.5 V. The cyclic voltammetry studies with PEM fuel cell at 80 ^oC also indicated that the ignition potential of the CO oxidation peak was in the range of 0.6~0.7 V,[20, 21] believed to be due to the appreciable formation of surface OH_{ad} species. However, Markovic *et al.*[17] argue that OH_{ad} can also be formed at low

overpotentials on the step/defect sites, such as those on Pt (100) surface. The nominal value of this defect concentration is on the order of 10^{12}-10^{13} per cm^2, which is less than 1% of the total number density of surface sites.[18] Thus, although the occurrence of OH_{ad} on Pt surface at low overpotentials is also possible, it is apparent that appreciable surface coverage of OH_{ad} occurs only at higher overpotentials. So there is the possibility that in the low potential region the oxygen containing species maybe other than OH_{ad}. Similar conclusion is reached by other researchers such as Ciureanu *et al*.[20] and Bush *et al*.[22] Despite this controversy, it is evident that there is a marginal CO electrooxidation on the Pt surface even before the significant CO electrooxidation occurs at higher overpotential.

Based on above discussions as well as the modeling work of Springer *et al*.[23, 24] and Ticianelli *et al*.,[25] we adopt the following reduced mechanism solely for the purpose of writing kinetics of H_2 and CO electrooxidation on Pt surface:

$$CO + Pt \leftrightarrows Pt\text{–}CO \qquad k_{ac}, K_C \qquad [6]$$

$$H_2 + 2\,Pt \leftrightarrows 2Pt\text{–}H \qquad k_{ah}, K_H \qquad [7]$$

$$Pt\text{-}H \rightarrow Pt + H^+ + e^- \qquad k_{oh} \qquad [8]$$

$$Pt\text{–}CO + H_2O \rightarrow Pt + CO_2 + 2H^+ + 2e^- \qquad k_{oc} \qquad [9]$$

where k_{ac} and k_{ah} are the adsorption rate constants of CO and H_2, respectively , K_C and K_H are the corresponding equilibrium constant for desorption of CO and H_2 (the reciprocal of the adsorption equilibrium constant). Similarly, k_{oc} and k_{oh} are the rate constants of the electrooxidation of CO and H_2, respectively. Reaction 9 is clearly not an elementary step, but is rather the overall reaction of CO electrooxidation via water.

It is also evident from the experimental results of this study that oxygen diffusing from the cathode to the anode is partly responsible for the CO oxidation in the anode side. This is in agreement with literature results that bleeding small amount of O_2 or air into the anode feed stream is effective in mitigating the CO poisoning of the PEM fuel cell anode.[3,14] One explanation for this is that CO is oxidized by O_2 via a non-electrochemical surface reaction, for instance

$$O_2 + 2\,Pt \leftrightarrows 2\,Pt\text{-}O \qquad [10]$$

$$\text{Pt-O} + \text{Pt-CO} \rightarrow 2\ \text{Pt} + \text{CO}_2 \qquad [11]$$

which is similar, in principle, to the preferential oxidation (PrOx) process[26]. Another possibility is that the adsorbed O reacts first with the adsorbed H to form OH_{ad} that further reacts with the surface CO electrochemically as per reaction 5.

$$\text{Pt-O} + \text{Pt-H} \leftrightarrows \text{Pt-OH} \qquad [12]$$

In summary, the mechanism of CO oxidation by molecular O_2 on Pt/C anode catalyst at temperatures below 100 °C is also not clear.[27, 28]

Of course, there is little doubt that the adsorbed oxygen reacts with the adsorbed hydrogen to form water as well. Therefore, only part of the oxygen diffusing across the membrane to anode would participate in the CO oxidation. This is accounted for simply by β, the selectivity parameter for the CO oxidation in our model.

The model provided by Springer *et al*.[24] is adopted here for the anode kinetics which is based on the mechanism described by equations 6 to 9. The rate expression for H_2 oxidation, which is also the overall fuel cell current density, is obtained from equation 8 and assumed to obey the Butler-Volmer equation

$$i = 2k_{\text{oh}}\theta_{\text{H}}\sinh\left(\frac{\alpha_{\text{H}}F\eta_{\text{A}}}{RT}\right) \qquad [13]$$

while the CO electrooxidation current based on equation 9 is expressed in a Tafel form[24]

$$i_{\text{CO}} = k_{\text{oc}}\theta_{\text{CO}}\exp\left(\frac{\alpha_{\text{CO}}F\eta_{\text{A}}}{RT}\right) \qquad [14]$$

In this expression, Springer *et al*.[24] assumed the concentration of the oxidizing species to be constant and included in rate constant k_{oc}. Here α_{CO} is the effective transfer coefficient for CO electrooxidation, and i_{CO} denotes the CO electrooxidation current density. Both k_{oc} and α_{CO} are treated here as fitted parameters. Further, equation 13 and 14 imply absence of mass transfer limitations.

The hydrogen adsorption as per equation 7 is assumed to be second order in vacant sites coverage, $\theta_0 = 1 - \theta_{CO} - \theta_H$. Detailed discussion of this can be found in Springer *et al.*'s work.[24] The surface coverages of CO and H_2 are determined by their adsorption, desorption and electrooxidation rates. Thus at steady state, the surface coverages of CO and H do not change with time, *i.e.*,

$$\rho \frac{d\theta_{CO}}{dt} = k_{ac} P_{H_2} x_{CO} (1 - \theta_{CO} - \theta_H) - K_C k_{ac} \theta_{CO} - k_{oc} \theta_{CO} \exp\left(\frac{\alpha_{CO} F \eta_A}{RT} \right) = 0 \qquad [15]$$

$$\rho \frac{d\theta_H}{dt} = k_{ah} P_{H_2} (1 - \theta_{CO} - \theta_H)^2 - K_H k_{ah} \theta_H^{\,2} - 2 k_{oh} \theta_H \sinh\left(\frac{\alpha_H F \eta_A}{RT} \right) = 0 \qquad [16]$$

where ρ is a constant, which equals to the moles of Pt per cm^2 electrode times the Faraday constant. All the values of model parameters are adopted from Springer *et al.*'s work[24] except α_{CO} and k_{oc} are fitted (see Table 2-1). For k_{ah} and K_C, their values corresponding to high CO surface coverage are used here.

2.4.3 Oxygen Permeation

It is assumed that the oxidation of CO by permeating O_2 from the cathode is controlled by the rate of the permeation of O_2 through the membrane, the oxidation kinetics themselves being rapid. Further, we use a parameter β, which accounts for the selectivity of the oxygen for the oxidation of CO, the balance fraction being utilized for oxidation of hydrogen. This parameter is comparable to the selectivity of O_2 in PrOx of CO in a hydrogen-rich gas.[26]

Oxygen permeation in proton-exchange membranes is relatively well studied.[29-32] Pathasarasy *et al.*[29] determined the permeability of O_2 in Nafion® at 80 °C to be 3.85×10^{-11} mol cm^{-1} s^{-1}. Gottesfeld *et al.*[30] reported an O_2 concentration (solubility) of 3.1×10^{-6} mol cm^{-3} and a diffusion coefficient of 4.0×10^{-6} cm^2 s^{-1} at 25 °C. Ogumi *et al.*[31, 32] used a transient method to measure the O_2 permeation in different membranes. Their result

shows that the O_2 solubility in Nafion at 50 °C is 5.9×10^{-6} mol cm^{-3}, and the diffusion coefficient is 5.2×10^{-7} cm^2 s^{-1}.

At steady state, we assume that the partial pressure of oxygen approaches zero at the anode-membrane interface due to rapid kinetics and rate limitations by the mass transfer through the proton-exchange membrane. Under steady state diffusion conditions, the flux of O_2 can thus be expressed as

$$N_{O_2} = \frac{KDP_{O_2}}{L} \qquad [17]$$

where D is the diffusion coefficient of O_2 in the Nafion membrane, L is the thickness of the membrane under operation, K is the Henry's law constant for O_2 dissolution in the Nafion membrane at 80 °C, P_{O_2} is the partial pressure of O_2 at the proton-exchange membrane surface at the cathode side. For simplicity, it is further assumed here that this corresponds to cathode chamber partial pressure of O_2, any difference being accounted for by β.

2.4.4 CO Inventory Model

Since CO is in trace amounts, it does not contribute materially to the flow rate at the anode inlet or outlet. At a constant current density, a definite amount of H_2 is consumed at the anode. The H_2 in excess of the stoichiometry flows out at the anode outlet. Since the CO electroxidation rate is inherently small compared to H_2 electrooxidation, its contribution to the overall current density is negligible as well. Furthermore, the CO and H_2 diffusion limitations through the diffusion layer and catalyst layer are also assumed to be negligible, as discussed earlier. In other words, the CO and H_2 partial pressures at the Pt surface are the same as that in the anode chamber.

Equation 4 as applied to H_2 in the anode chamber at steady state provides

$$\frac{P_0 v_0}{RT_0} - \frac{P_0 v}{RT_0} = \frac{i}{2F} A \qquad [18]$$

here, F is the Faraday constant and i is given by equation 13. Note that the volumetric flow rates are measured at 1atm and 298K, so that P_0 is 1 atm and T_0 is 298K, and not the fuel cell operating pressure or temperature.

Utilizing equation 4 for the CO inventory in the anode

$$\frac{P_0 v_0}{RT_0} x^0{}_{\mathrm{CO}} - \frac{P_0 v}{RT_0} x_{\mathrm{CO}} = \left(\frac{i_{\mathrm{CO}}}{2F} + 2\beta N_{\mathrm{O_2}} \right) A \qquad [19]$$

where $x^0{}_{\mathrm{CO}}$ and x_{CO} are the CO mole fractions in the anode feed and the anode compartment outlet, respectively. β is assumed here to be a fitted constant. The right-hand side of equation 19 accounts for the CO oxidized both electrochemically via water (equation 9) and non-electrochemically via permeating O_2 (equation 11).

The input parameters for the model are the given anode inlet flow rate v_0 and the constant current density i. The corresponding value of $\theta_{\mathrm{CO}}, \theta_{\mathrm{H_2}}, x_{\mathrm{CO}}, \eta_{\mathrm{A}}$ are then solved from the set of non-linear equations 13-19 using Berkley-Madonna software, and plotted as a function of the anode inlet flow rate v_0.

2.4.5 Modeling Results and Discussion

Figure 2-10 shows modeling results of the surface coverage of H and CO, θ_{H} and θ_{CO}, anode overpotential, η_{A}, and anode CO content, x_{CO} as a function of the anode inlet flow rate v_0 at i = 200 mA/cm^2 and 80 °C. It is seen from these results that for the set of assumed parameters (Table 2-1), the surface coverage of CO increases rapidly to an equilibrium value and does not change appreciably with further increase of the anode flow rate and the corresponding increase in x_{CO}. As expected, the surface is largely covered by CO, being nearly monolayer, which is consistent with literature.[7] This feature is due to the large CO adsorption equilibrium constant on Pt. The hydrogen surface coverage decreases with the flow rate, while the anode overpotential increases as indicated in the figure, so the current density i can remain constant at the desired value (equation 13). It is also seen that the hydrogen surface coverage can be several orders of

Table 2-1. Model Parameters

K_{CO}	2×10^{-6} atm	CO desorption equilibrium constant[a]
K_H	0.5 atm	H_2 desortion equilibrium constant[a]
α_H	1.0	transfer coefficient for H_2[a]
α_{CO}	0.12	transfer coefficient for CO[c]
k_{ah}	40.21 A cm^{-2} atm^{-1}	adsorption rate constant of H_2[a]
k_{ac}	10 A cm^{-2} atm^{-1}	adsorption rate constant of CO[a]
T	353 K	fuel cell temperature
k_{oh}	4.0 A cm^{-2}	electrooxidation rate constant for H_2[a]
k_{oc}	7×10^{-6} A cm^{-2}	electrooxidation rate constant for CO[c]
A	5 cm^2	electrode active area
P_{H_2}	2.53 atm	hydrogen partial pressure
$x_{CO}^{\ 0}$	108×10^{-6}	CO mole fraction in anode feed stream
D	8.7×10^{-6} cm^2 s^{-1}	O_2 diffusion coefficient in Nafion at 80 °C[b]
K	8.86×10^{-7} mol cm^{-3} atm^{-1}	Henry's law constant for O_2 dissolution in Nafion at 80 °C[b]
β	0.04	O_2 selectivity[c]
L	0.01 cm	thickness of Nafion® 115 membrane in MEA under fuel cell operation conditions

[a] From or calculated from ref. 24.

[b] From or calculated from ref. 29.

[c] Fitted parameters.

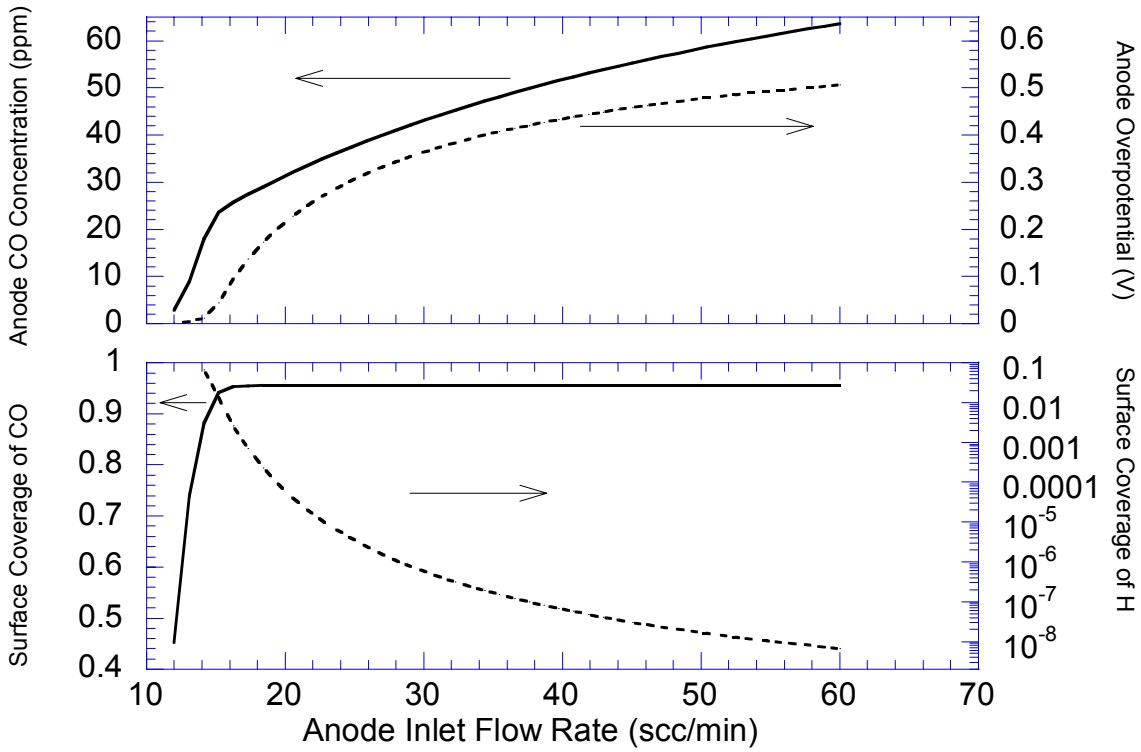

Figure 2-10. Model prediction of the steady state CO and H surface coverage, CO content in anode chamber and the anode overpotential as function of anode inlet flow rate at 80°C and 200 mA/cm^2; Model parameters have values given in Table 2-1.

magnitude lower than the CO coverage. However, even this exceedingly small surface coverage can sustain a large current density due to the very large H electrooxidation rate constant. The increase in anode overpotential η_A with the anode flow rate is qualitatively similar to the experimental results. The simulation also shows that the CO content x_{CO} in the anode chamber increases with the inlet flow rate as expected, and is the key reason for increased poisoning at higher flow rate. This simple inventory model here, thus reproduces the essential features of the experimental observations. The simulation confirms the observed form of dependency of the anode overpotential on the flow rate.

Figure 2-11 shows the simulation results for the anode overpotential change as a result of the change of anode inlet flow rate at different current densities. At larger current densities, the overpotential is higher. The maximum overpotential change from about 0.4 V at 100 mA/cm^2 to 0.60 V at 500 mA/cm^2 is similar to the experimental results (see Figure 2-5). Further, the modeling results qualitatively reproduce the S-shaped curve at smaller current densities, *e.g.*, at 200 mA/cm^2.

The simulation results for different cathode oxygen pressures are shown in Figure 2-12, which demonstrates that the anode overpotential increases with the decrease of the cathode oxygen pressure at a certain anode flow rate. The predicted trend of the polarization curve is in good quantitative agreement with the experimental results for different cathode O_2 pressure (Figure 2-7). The value of the selectivity β used in this simulation is 0.04, which is in the range indicated in the literature. Gottesfeld *et al.*[3] found that by injecting 2-5% O_2 into the anode stream, a complete performance recovery could be achieved for anode feed with H_2 containing 100-500 ppm CO. This indicates a selectivity on the order of 0.01.

The given CO inventory model, thus, adequately justifies the observed experimental phenomena of the effects of the flow rate and oxygen permeation even though there is not an exact correspondence between theory and experiments. At small anode flow rates, the CO content in the anode compartment is low as it is consumed by the electro and non-electrooxidaton. The slow increase of the anode overpotential is due to the fact that the marginal oxidation or electrooxidation of CO at low flow rates creates adequate bare Pt sites to sustain the desired current. As the inlet flow rate further increases, the anode chamber CO content becomes higher and the surface coverage of CO

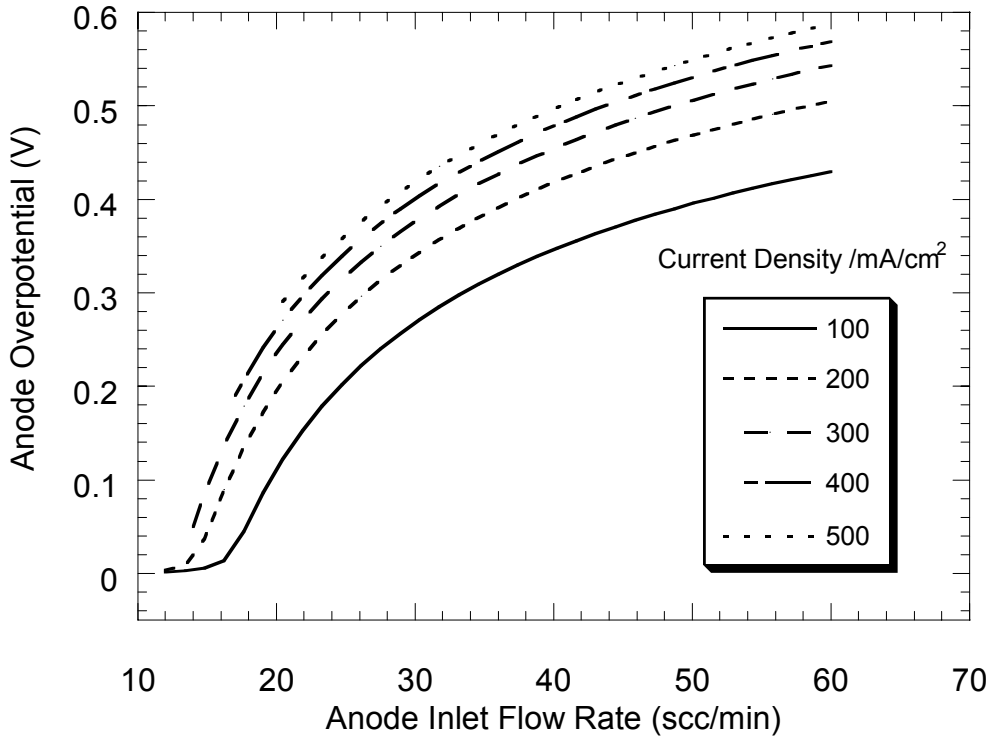

Figure 2-11. Model calculations of the steady state anode overpotential as a function of anode inlet flow rate at 80 °C and different current densities. Model parameters have values given in Table 2-1.

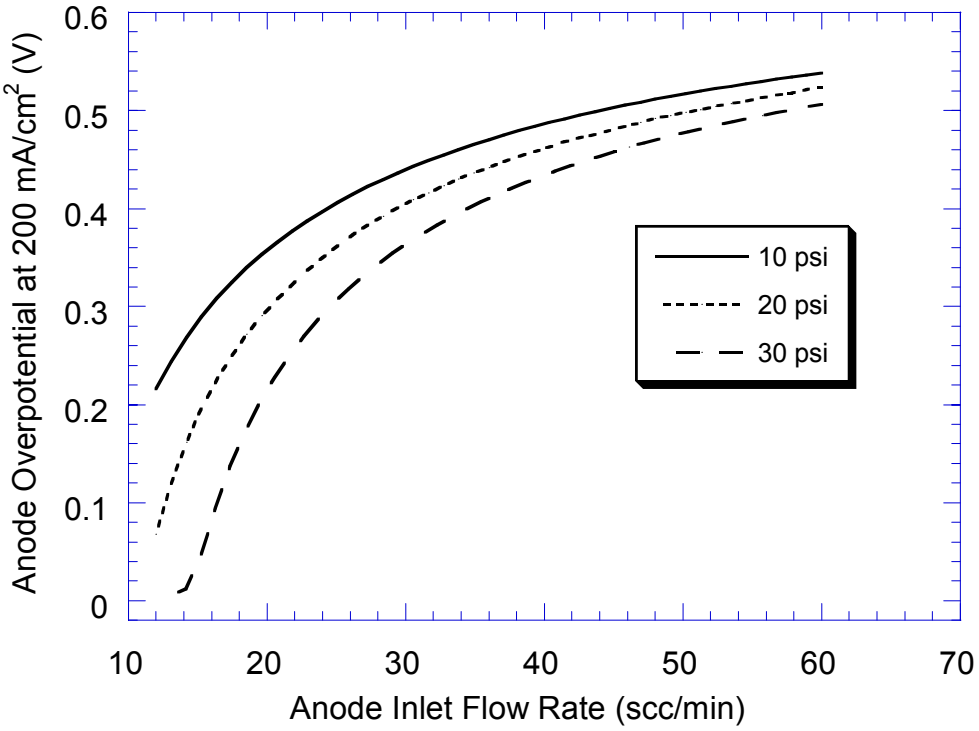

Figure 2-12. Model calculations of the steady state anode overpotential as a function of anode inlet flow rate for different cathode O_2 pressures at 80 °C and 200 mA/cm^2. Model parameters have values given in Table 2-1.

tends to increase as kinetics are unable to oxidize all CO coming in, unless the anode overpotential is increased correspondingly to accelerate the CO electrooxidation rate and sustain the current density. When the overpotential is high enough, the CO electrooxidation rate is fairly large compared to the inlet flow rate of CO, so that a plateau is reached and further increase of the anode overpotential is not necessary.

Even though the simple model described here is able to qualitatively explain the experimental observations, further work is needed to confirm the kinetics and the parameter values so as to obtain quantitative agreement with experiments.

2.5 Conclusions

The anode flow rate and cathode oxygen partial pressure are important operational parameters that strongly influence the performance of a PEM fuel cell involving a Pt anode when operating with H_2/CO feed. Cell voltage decreases dramatically with increasing anode flow rate at a constant current density due to increasing CO content in the anode chamber, requiring a higher anode overpotential to oxidize the adsorbed CO so as to sustain the desired current density. The influence of the flow rate was found to be rapid and reversible. Oxygen diffusing through the membrane is partly responsible for the removal of CO on the anode catalyst surface. A CO inventory model is proposed which provides an adequate explanation of the observed effects of the anode flow rate and cathode oxygen pressure. The CO oxidation hence needs to be included in the modeling of the overall fuel cell performance when reformate is used as the anode feed. More detailed study of the mechanism and kinetics at the PEM fuel cell operating conditions for H_2/CO is necessary to obtain better quantitative agreement between the theory and experiments.

References

1. T. R. Ralph, *Platinum Metals Rev.*, **41**, 102 (1997).
2. T. R. Ralph, G. A. Hards, J. E. Keating, S. A. Campell, D. P. Wilkinson, M. Davis, J. St-Pierre and M. C. Johnson, *J. Electrochem. Soc.*, **144**, 3845 (1997).
3. S. Gottesfeld, and J. Pafford, *J. Electrochem. Soc.*, **135**, 2651 (1988).
4. H.-F. Oetjen, V. M. Schmidt, U. Stimming, and F. Trila, *J. Electrochem. Soc.*, **143**, 3838 (1996).
5. S. J. Lee, S. Mukerjee, E. A. Ticianelli, J. McBreen, *Electrchim. Acta*, **44**, 3283 (1999).
6. G. K. Acres, J. C. Frost, G. A. Hards, R. J. Potter, T. R. Rulph, D. Thompsett, G. T. Burstein, and G.J. Hutchings, *Catal. Today*, **38**, 393 (1997).
7. R. J. Bellows, E. P. Marucchi-Soos, and D. T. Buckley, *Ind. Eng. Chem. Res.*, **35,** 1235 (1996).
8. R. J. Bellows, E. Marucchi-soos, in *Proton Conducting Membrane Fuel Cells II*, S Gottesfeld and T. F. Fuller, Editors, PV 98-27, p.218, The Electrochemical Society Proceedings Series, Pennington, NJ (1997).
9. H. A. Gasteiger, N. M. Markovic, and P. N. Ross, *J. Phys. Chem.*, **99**, 8290 (1995).
10. H. A. Gasteiger, N. M. Markovic, and P. N. Ross, *J. Phys. Chem.*, **99**, 16757 (1995).
11. H. P. Dhar, L. G. Christner, and A. K. Kush, *J. Electrochem. Soc.*, **134**, 3021 (1987).
12. H. P. Dhar, L. G. Christner, A. K. Kush, and H. C. Maru, *J. Electrochem. Soc.*, **133**, 1574 (1986).
13. J. K. Hong, L. A. Zook, M. Inbody, J. Tafoya, and N. E. Vanderborgh, in *Meeting Abstracts of 195th meeting of the Electrochemical Society* , Abstract No. 570 ,Volume 99-I, May 2-6, 1999, Seattle, Washington.
14. J. W. Bauman, T. A. Zawodzinski, Jr., and S. Gottesfeld, in *Proton Conducting Membrane Fuel Cells II*, S Gottesfeld and T. F. Fuller, Editors, PV 98-27, p. 136, The Electrochemical Society Proceedings Series, Pennington, NJ (1997).
15. T. Thampan, S. Malhotra, J. Zhang, and R. Datta, *Catal. Today*, **67**, 15 (2001).
16. S. Gilman, *J. Phys. Chem.*, **68**, 70 (1964).
17. N. M. Markovic, C. A. Lucas, B. N. Grgur, and P. N. Ross*, J. Phys. Chem.*, **103**, 9616 (1999).

18. N. M. Markovic, T. J. Schmidt, B. N. Grgur, H. A. Gasteiger, R. J. Belm, and P. N. Ross, *J. Phys. Chem .B*, **103**, 8568 (1999).
19. T. Iwasita, X. Xia, *J. Electroanal. Chem.*, **411,** 95 (1996).
20. M. Ciureanu, and H. Wang, *J. Electrochem. Soc.*, **146**, 4031 (1999).
21. T. Zawodzinski, C. Karuppaiah, Y. Wu, S. Savett, F. Uribe and S. Gattesfeld, Abstract 1098, The Electrochemical Society Meeting Abstract, Vol. 98-2, Boston, MA, Nov. 1-6, 1998.
22. B. M. Bush, J. A. Reimer, and E. J. Cairns, *J. Electrochem. Soc.*, **148**, A137 (2001).
23. T. Springer, T. Zawodzinski, and S. Gottesfeld, *in Electrode Materials and Processes for Energy Conversion and Storage IV*, J. McBreen, S. Mukerjee, S. Srinivasan, Editors, PV 97-13, p.139, The Electrochemical Society.
24. T. E. Springer, T. Rockward, T. A. Zawodzinski, and S. Gottesfeld, *J. Electrochem. Soc.*, **148**, A11 (2001).
25. E. A. Ticianelli, S. Mukerjee, S. J. Lee, and J. McBreen, in *Proton Conducting Membrane Fuel Cells II*, S. Gottesfeld and T. F. Fuller, Editors, PV 98-27, p.162, The Electrochemical Society Proceedings Series, Pennington, NJ (1997).
26. M. J. Kahlich, H. A. Gasteiger, and R. J. Behm*, J. Catal.*, **171**, 93 (1997).
27. R. J. Bellows, E. Marucchi-Soos, and R. P. Reynolds, *Electrochem. Solid-State Lett.*, **1**, 69 (1998).
28. V. M. Schmidt, J. L. Rodriguez, and E. Pastor, *J. Electrochem. Soc.*, **148**, A293 (2001).
29. A. Parthasarathy, S. Srinivasan, and A. J. Appleby, *J. Electrochem. Soc.*, **139**, 2530 (1992).
30. S. Gottesfeld, I. D. Raistrick, and S. Srinivasan, *J. Electrochem. Soc.*, **134**, 1455 (1987).
31. Z. Ogumi, Z. Takehara, and S. Yoshizawa, *J. Electrochem. Soc.*, **131**, 769 (1984).
32. Z. Ogumi, T. Kuroe, Z. Takehara, *J. Electrochem. Soc.*, **132**, 2601 (1985).

Chapter III

Online Monitoring of Anode Outlet CO Concentration in PEM Fuel Cells

In this chapter, the anode gas outlet CO concentration is measured by an on-line IR gas analyzer for a PEM fuel cell fed with H_2/100 ppm CO and with Pt or PtRu as anode catalyst. It is found that the anode outlet CO concentration increases with anode inlet flow rate at a given current density for Pt catalyst, which agrees well with our predictions in chapter II. The CO outlet concentration with PtRu catalyst depends upon the current density at a cell temperature of 80 °C. The anode outlet CO concentration is observed to decrease with the increase of anode inlet flow rate at low current densities, while at higher current densities, the outlet CO concentration follows a trend similar to that observed with Pt. The CO electrooxidation rate on Pt and PtRu is thus calculated using CO material balance on the anode side. The results indicate that the enhanced tolerance of PtRu catalyst is due to the dual mechanisms of reduced CO affinity (ligand effect) and enhanced CO electrooxidation rates (bifunctional effect), with either mechanism dominating depending upon the anode overpotential. Contents of this chapter have been published in *Electrochem. Solid-State Lett*..

3.1 Introduction

Reformed gas produced from conventional fuels such as gasoline, methanol, or natural gas will likely be used in electric vehicle or stationary applications of proton exchange membrane (PEM) fuel cells. Regardless of the reforming processes employed, e.g., steam reforming (SR), or autothermal reforming (ATR), the reformate gas largely consists of H_2, N_2, CO_2, CO, and H_2O. The strong poisoning effect of CO present in the reformate gas on Pt-based anode catalyst has long been known[1,2] and addressed especially frequently in recent literatures[3-12]. However, the attention in these studies has

been paid almost exclusively to the voltage-current characteristics of the PEM fuel cell under different operating conditions with Pt or different Pt-based alloy catalysts and with simulated reformate as anode feed.

In chapter II, we reported a significant effect of the anode flow rate on PEM fuel cell performance with H_2/108 ppm CO feed and Pt as anode catalyst[11]. The results were explained on the basis of a CO inventory model which simulates the effect of flow rate on the anode overpotential via CO material balance in the anode chamber including terms for flow in, flow out, as well as electrocatalytic oxidation. The model thus predicts that the anode CO concentration is a function of anode flow rate, which had not been previously reported.

The present work was motivated by our desire to confirm the earlier model predictions[11] by direct on-line measurement of the CO concentration in PEM fuel cell anode outlet gas. In this chapter, we provide such results based on using an IR analyzer to monitor the anode outlet CO concentration of PEM fuel cell. Results are provided using both Pt and PtRu as anode catalyst at conventional PEM fuel cell operating conditions. The experimental data on the anode CO concentration as a function of anode flow rate for Pt catalyst agrees well with our previous model predictions. Based on the CO material balance in the anode, the CO electrooxidation rate is calculated for both Pt and PtRu catalyst. These results provide the first direct experimental evidence from *in-situ* fuel cell experiments that both the "bifunctional electrooxidation mechanism" and the "ligand effect" resulting in reduced CO affinity for the surface proposed in the literature coexist for PtRu catalyst.

3.2 Experimental

The complete experimental details are provided in chapter II[11], and thus, only a summary is given here. Gas diffusion electrodes loaded with 20%(w/o) Pt/C or PtRu/C, at a metal loading of 0.4 and 0.35 mg/cm^2, respectively, were purchased from E-TEK. Nafion® 115 proton-exchange membranes (Du Pont, Fayetteville, PA) were used after treatment. The membrane electrode assembly (MEA) was prepared by hot-pressing in a Model C Carver hot press at 130 °C and under a pressure of 4000 lbs for about 2 minutes. The MEA was then incorporated in a 5 cm^2 single cell from ElectroChem, Inc. (Woburn,

MA), and tested in a test station with temperature, pressure, humidity and flow rate control. The current-voltage characteristics were recorded using a HP 6060B DC electronic load, interfaced with a PC using LabView software (National Instruments, Austin, TX).

Anode and cathode gases were humidified in stainless steel bottles containing water at the desired temperature before being fed into the fuel cell. The total pressure of both anode and cathode was maintained at 30 psig. The volumetric flow rates reported in this study are all at the standard state (1 atm and 25 °C) in units of standard cubic centimeters per min (scc/min). Pre-mixed H_2/100ppm CO was purchased from MG Industries (Morrisville, PA) and used as anode feed. The anode exit gas stream after the back pressure regulator first passes through a stainless steel filter (Model 85, Parker Hannifin, Tewksbury, MA), to eliminate any particulates and water droplets. The gas stream then passes through a membrane gas dryer (MD series, Perma Pure Inc., Toms River, NJ) which further lowers the dew point of the gas stream to below 2 °C before admission to the gas analyzer. A Model 200 IR gas analyzer (California Analytical Instruments, Orange, CA) was used after calibration to monitor the exit CO concentration.

3.3 Results and Discussions

Our experiments show that the IR gas analyzer is very suitable for on-line monitoring of CO concentration in the fuel cell anode outlet gas, especially in the 0 to 100 ppm range, which may be outside of the accurate detection limit of gas chromatography. The sensitivity, reproducibility, and stability proved to be excellent.

3.3.1 Anode Outlet CO Concentration Transient

A typical CO outlet concentration response following the switching between a H_2 and a H_2/100 ppm CO feed is shown in Figure 3-1. The corresponding cell voltage response at a constant current density of 200 mA/cm^2 and fuel cell temperature of 80 °C is also shown in the same figure. The anode inlet flow rate was constant at 48.1 scc/min. It was noticed that the cell voltage responds to CO introduction in the feed more quickly than the anode outlet CO concentration does. There is no significant CO concentration

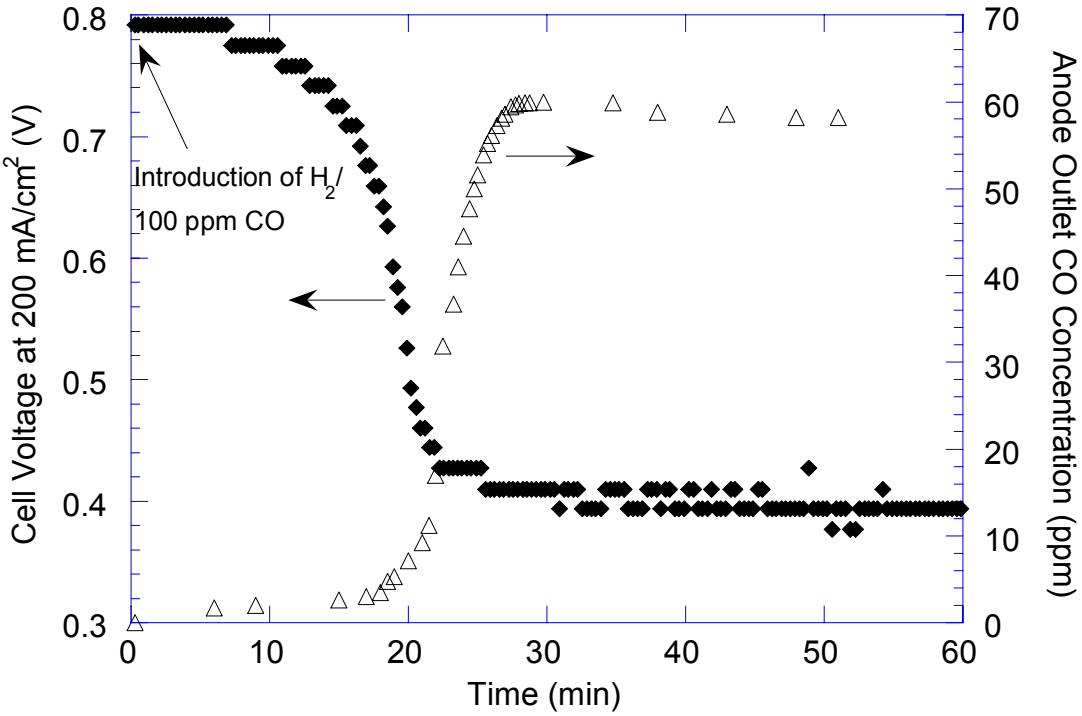

Figure 3-1. The transient of cell voltage and anode outlet CO concentration when the anode feed is switched from H_2 to H_2/ 100 ppm CO. Fuel cell temperature: 80 °C; Nafion 115 membrane; Current density, 200 mA/cm^2; Anode catalyst, Pt.

increase in the outlet during the initial rapid decrease of the cell voltage. The outlet CO concentration begins to increase only after there has been a significant decrease in the cell voltage. After this very slow initial increase, the CO concentration rapidly rises and finally stabilizes at about 60 ppm, which is 40 ppm lower than the inlet CO concentration, despite the fact that the outlet H_2 flow rate is lower than the inlet H_2 flow rate by 7.6 scc/min due to consumption of H_2 in the production of the current. These results indicate that there is an initial CO accumulation on the anode catalyst surface and in the anode chamber and tubing, such that the significant increase of outlet CO concentration lags the decrease of the cell voltage by roughly 10 minutes. The overpotential under steady state conditions is roughly 0.4 V. Another conclusion evident from these results is that at steady state, there is a finite rate of CO electrooxidation even on Pt at practical operating conditions. This lends credence to our earlier explanation of the anode flow rate effect[11], and also to other researchers' expectations on possible CO electrooxidation on Pt in the PEM fuel cell anode[4,8]. Such real-time monitoring of the anode outlet CO concentration is planned to be used to determine in-situ anode adsorption and kinetics in our future work.

3.3.2 Anode Outlet CO Concentration at Different Flow Rates for Pt Catalyst

Experiments were further conducted at different anode inlet flow rates and at a constant current density as previously described [11], with the results shown in Figure 3-2. The fuel cell is operated at 80 °C and a constant current density of 200 mA/cm^2 with Pt anode catalyst. It is seen that the anode outlet CO concentration is indeed a function of the anode inlet flow rate, as predicted[11]. The CO concentration increases from about 20 ppm to 60 ppm when the anode inlet flow rate is increased from 14 scc/min to 60 scc/min. Furthermore, the data also follow the model predictions reasonably well. A quantitative explanation to this phenomenon can be found in ref. 11. Qualitatively, the results may be explained as follows. When anode feed bearing CO is introduced, CO builds up on the catalyst surface. During this process, the increase in CO concentration in anode chamber and outlet is small (Figure 3-1). In order to sustain the given current density, thus, the anode potential is polarized to higher values, which concomitantly also

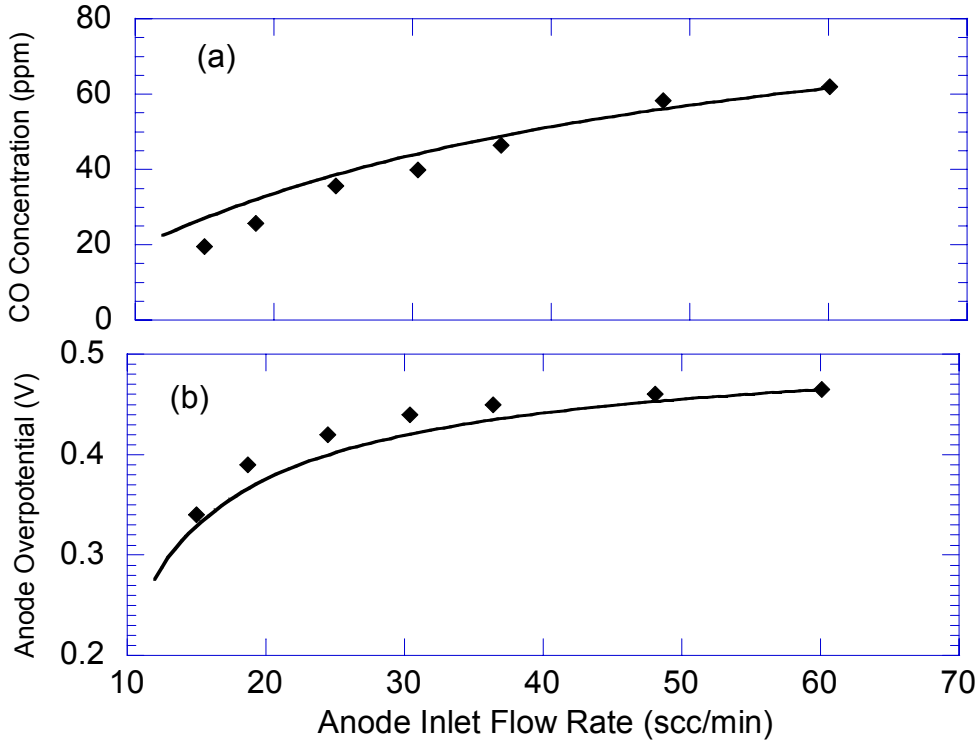

Figure 3-2. (a) Anode outlet CO concentration as a function of anode inlet flow rate. (b) Anode overpotential as a function of anode inlet flow rate. The dots are experimental data and the line is the prediction by our previous model for both cases. Fuel cell temperature: 80 °C; Nafion 115 membrane; Current density, 200 mA/cm^2; Anode catalyst, Pt. The fitting parameters used are α_{co}=0.34, k_{oc}=2.9 × 10^{-7} A/cm^2, β=0.03

promotes the electrooxidation of CO. Thus, eventually, a steady state is reached for both overpotential and CO concentration reflecting a balance between the rate of CO in and the rate of CO out plus the rate of its electrooxidation. Were there no electrooxidation, the CO outlet concentration would actually be higher than inlet, since some H_2 is getting consumed. An increase of the anode inlet flow rate introduces more CO into the anode chamber, which would increase the anode CO concentration and, consequently, the CO surface coverage of Pt catalyst. Thus, the anode potential is polarized to an even higher value, which further accelerates the CO oxidation rate. Thus, a new steady state with new values of anode overpotential and anode CO concentration is reached (Fig. 7 and Fig. 10 of ref. 11).

3.3.3 CO Oxidation by O_2 Permeating Through the Proton Exchange Membrane

We have previously reported that O_2 permeating through the membrane from the cathode contributes partly to the CO clean up in the anode chamber[11]. In order to determine the amount of CO thus oxidized via the non-electrochemical oxidation, experiments were conducted with the fuel cell simply as a catalytic membrane reactor, *i.e*., with all the electronic connections between the cathode and anode disconnected, *e.g*., the electronic load or the multimeter used to monitor the cell voltage. All the other experimental conditions were identical to that employed in the fuel cell performance test. Thus, the fuel cell was acting as a membrane reactor, with O_2 diffusing through the proton exchange membrane from the cathode and then reacting with CO and H_2 at the anode. The CO mass balance does directly prove our previous hypothesis that CO is oxidized by permeating O_2. A typical result is shown in Figure 3-3. In this experiment, the fuel cell temperature is set at 80 °C and the anode inlet flow rate is 15 scc/min, while the cathode total pressure is set at 30, 20, and 10 psi, respectively. The CO oxidation rate (normalized to the electrode geometric area) is plotted against the cathode O_2 partial pressure (the water vapor partial pressure is subtracted from the cathode total pressure, assuming that the cathode chamber is saturated by water vapor at 80 °C). It is evident from Figure 3-3 that there is a finite CO oxidation due to the non-electrochemical catalytic reaction between CO and permeating O_2.

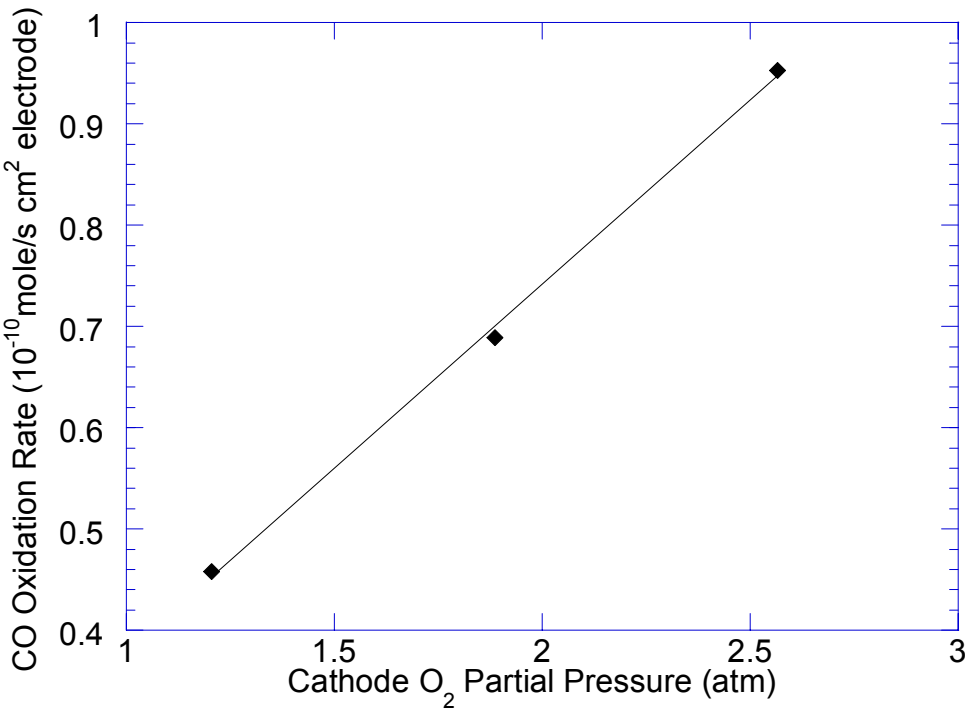

Figure 3-3. CO oxidation rate versus cathode O_2 partial pressure in the non-electrochemical reation. Fuel cell temperature: 80 °C; Nafion 115 membrane; Anode inlet flow rate, 15 scc/min; Anode catalyst, Pt

Furthermore, it may be noted that the CO oxidation rate is linearly dependent on the cathode O_2 partial pressure. This can be justified by the model mentioned in our previous work[11], where it is assumed that cathode O_2 dissolves in the swollen Nafion membrane and then diffuses to the anode. It is further assumed that the oxidation of CO by permeating O_2 from cathode is controlled by the rate of permeation of O_2 through the membrane.

3.3.4 CO Electrooxidation Rate on Pt Anode Catalyst

Since we have directly determined the contribution of CO oxidation in the non-electrochemical reaction by the permeating O_2, the CO electrooxidation rate can be calculated based on CO material balance, and subtracting the rate of the non-electrochemical oxidation. The results are shown in Figure 3-4, in which the hence calculated CO electrooxidation rate normalized to the electrode geometric area is plotted as a function of anode overpotential, determined as described in ref. 11. The CO electrooxidation rate is calculated at different anode flow rates, which vary from 14 scc/min to about 60 scc/min**.** It is shown that the electrooxidation rate is on the order of 10^{-10} mole/s cm^2 electrode at the fuel cell operation conditions used in this study, *i.e.*, fuel cell temperature 80 °C, a total pressure of 30 psi for both anode and cathode, and an anode feed containing H_2/ 100ppm CO. The electrooxidation rate increases with the anode overpotential exponentially, as expected per the Butler-Volmer equation. This is apparently the first *in-situ* experimental evaluation of CO electrooxidation rate on Pt catalyst in an operating PEM fuel cell.

3.3.5 Anode Outlet CO Concentration at Different Flow Rates for PtRu Catalyst

In order to compare the response of different anode catalysts towards CO impurity in the feed stream, PtRu was also used as the anode catalyst. Figure 3-5 shows the anode outlet CO concentration of a PEM fuel cell at 80 °C as a function of anode flow rate for various constant current densities ranging from 200 mA/cm^2 to 700 mA/cm^2. The feed stream contains 100 ppm CO, as indicated by the horizontal line in the middle of the

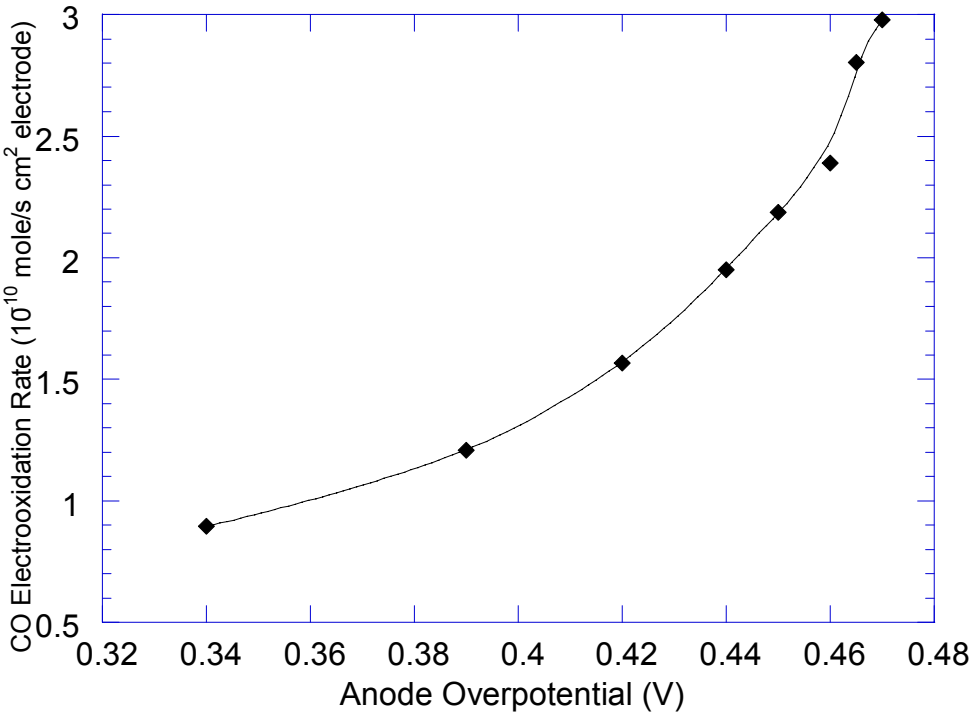

Figure 3-4. CO electrooxidation rate as a function of anode overpotential. Fuel cell temperature: 80 °C; Nafion 115 membrane; Anode catalyst, Pt.

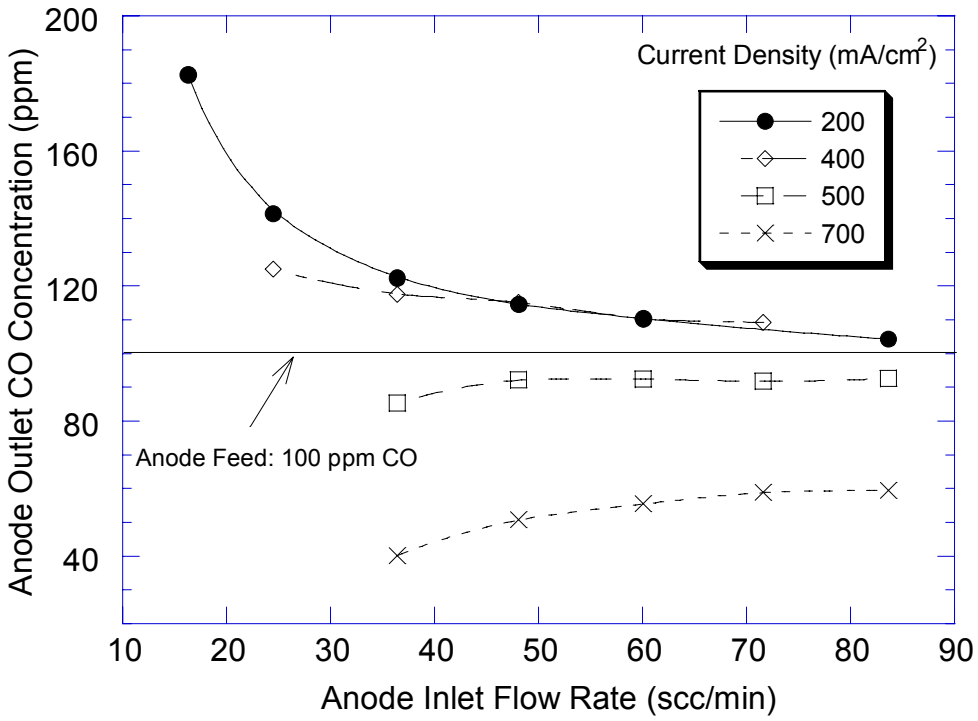

Figure 3-5. Anode outlet CO concentration as a function of anode inlet flow rate at various constant current densities. Fuel cell temperature: 80 °C; Nafion 115 membrane; Anode catalyst, PtRu.

figure. It was observed that at current density larger than 500 mA/cm^2, a trend similar to that with Pt anode catalyst is observed, *i.e.*, the anode CO concentration is below the feed concentration and increases with the anode inlet flow rate. However, when the current density is below 400 mA/cm^2, the CO concentration profile shifts to the region *above* the feed CO concentration. This distinctly different behavior is especially apparent for low current densities, *e.g.*, 200 mA/cm^2, for which at a flow rate of about 16 scc/min (corresponding to a stoichiometry of 2.1), the CO outlet concentration is nearly doubled! This means that at the current density of 200 mA/cm^2, there is no significant CO electrooxidation occurring at the anode. Thus, practically the CO entering the anode leaves the anode. Since at low anode inlet flow rates, a significant fraction of H_2 is consumed, the outlet CO becomes *more* concentrated than the feed. As the feed rate is increased, the outlet CO concentration declines asymptotically to the feed concentration at high flow rates, as a smaller fraction of H_2 feed is consumed. Thus, the observed trend of the outlet CO concentration variation with the anode inlet flow rate for PtRu is opposite to that observed with Pt. A material balance indicates that at 200 mA/cm^2 the difference between CO entering and exiting the fuel cell anode is only about 3 percent. It is, thus, clear that at the current density of 200 mA/cm^2 on PtRu anode catalyst, the CO electrooxidation rate is negligible. This clearly indicates that the adsorption of CO on PtRu is weaker as compared with Pt, and thus this current density can be sustained without significantly higher overpotential.

The effect of anode inlet flow rate on anode overpotential is less appreciable for PtRu, as compared to Pt catalyst. For example, the anode overpotenial is about 0.2 V at 200 mA/cm^2, and about 0.38 V at 700 mA/cm^2 for anode inelt flow rates between 15 scc/min to 84 scc/min.

3.3.6 Comparison of CO Electrooxidation Rate on Pt and PtRu at 80 °C

In order to compare the CO electrooxidation rate on Pt and PtRu catalyst, the CO electrooxidation rate is further normalized to the catalyst loading and plotted versus anode overpotential in Figure 3-6. It should be pointed out that contrary to the case of Pt catalyst, we did not observe experimentally that O_2 partial pressure has a significant

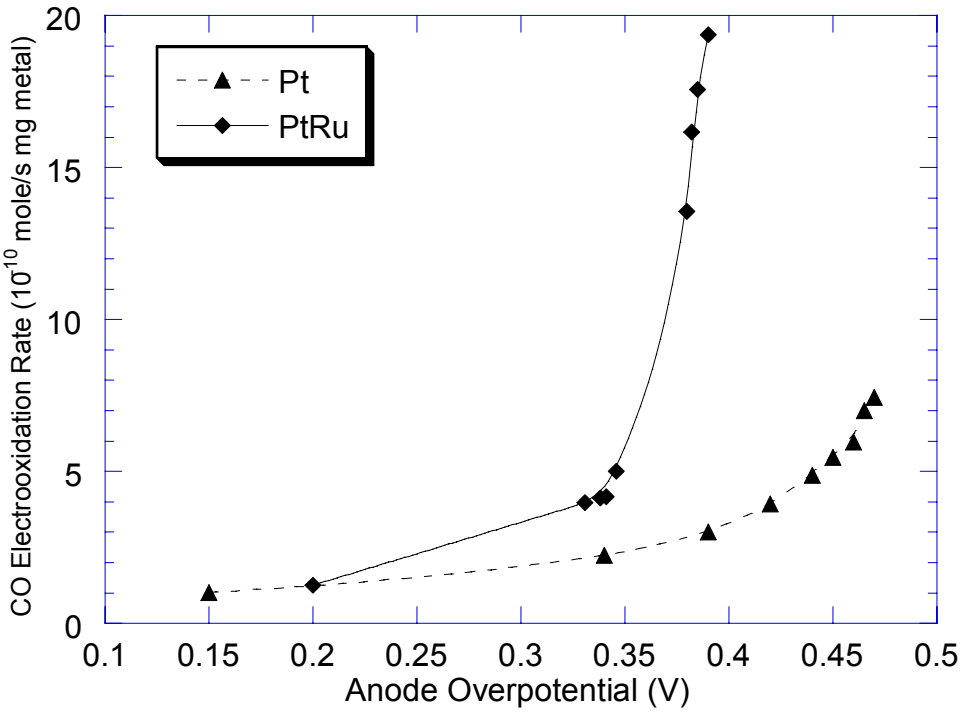

Figure 3-6. Comparison of CO electrooxidation rate on Pt and PtRu anode catalyst at 80 °C. Anode inlet flow rates are varied between 15 scc/min to 84 scc/min.

effect on the anode overpotential at a given current density for PtRu catalyst at 80 °C. It is seen from Figure 3-6 that the CO electrooxidation rate is small in lower overpotential range (*e.g.* < 0.3 V) for both Pt and PtRu catalyst. On the other hand, the electrooxidation rate increase dramatically in the anode overpotential range between 0.35~0.4 V for PtRu. On the contrary, the electrooxidation rate does not "ignite" until after the overpotential range of 0.45~0.5 V for Pt catalyst, a difference of roughly 0.1 V between the two catalysts. This figure looks qualitatively similar to the cyclic votammetry curve of H_2/CO electrooxidation on Pt and PtRu in liquid electrolyte, except the fact that the results in this work are obtained from steady state data in a functioning fuel cell. Moreover, the so called "ignition potential" for CO oxidation is quite comparable to the cyclic voltammetry results. (see Fig. 7 of ref. 3 and Fig. 7 of ref. 13). It can be noted that the CO electrooxidation rate is on the order of 10^{-10}~10^{-9} mole/s mg PtRu at 80 °C in the potential range shown in this study. In cyclic voltammetry studies, the kinetic information can not be easily obtained, especially in the relatively high overpotential region, due to the diffusion limitation of the reactant gas in the liquid electrolyte. In addition, it is very difficult to distinguish the CO electrooxidation current from that of hydrogen when H_2/CO mixture is studied. Thus, the experiment in this study offers a convenient and simple way to obtain *in-situ* kinetic information of CO electrooxidation in PEM fuel cell anode.

The results in this study also offer strong evidence for clarifying the CO tolerance mechanisms of PtRu catalyst. A well-accepted mechanism is the "bifunctional" mechanism[3, 14]. In this mechanism, it is believed that oxygen-containing species, *e.g.* OH, nucleate on Ru at lower electrode potentials than on Pt, so that CO is electrooxidized from the catalyst surface, generating additional free surface sites for H_2 oxidation. On the other hand, a recent EXAFS and adsorption study by Lin *et al.*[15] supports the "ligand" mechanism, *i.e.*, the interaction of CO with the alloyed PtRu catalyst is weakened as compared to Pt leading to lower surface coverage. Furthermore, the surface diffusion activation energy of CO on PtRu is also shown to decrease due to the Ru alloying effect, *i.e.*, by reducing the back donation of electrons from Pt, as demonstrated by an NMR study[16]. These results support the "ligand" mechanism [12, 17, 18], *i.e.*, the introduction of a second element such as Ru modifies the electronic structure of Pt by removing electron

density from Pt atoms, so that the Pt-CO bond is weakened and the equilibrium surface coverage of CO is reduced, making more free surface sites available for hydrogen electrooxidation.

The results here clearly indicate that in fact *both* these mechanisms discussed above are responsible for the enhanced tolerance of PtRu catalyst. At relatively lower overpotential (e.g. < 0.2 V), the "ligand" effect of reduced CO affinity dominates and PtRu catalyst is "CO tolerant" in a true sense at the lower current densities. This is supported by the fact that in this overpotential region the CO electrooxidation rate on PtRu is very small and is roughly the same as Pt catalyst. The anode CO content is strongly dependent on the anode inlet flow rate, and anode CO concentration well above that of the inlet is observed (Figure 3-5). At relatively high overpotentials (e.g., > 0.35 V), on the other hand, the "bifunctional" mechanism dominates. In this potential region, the CO electrooxidation rate is well above that of Pt catalyst, with CO oxidation igniting about 100-150 mV earlier than that on Pt catalyst. A recent study by Lu *et al.*[19] using temperature-programmed desorption coupled with mass spectroscopy also proposes that both mechanisms coexist for the CO tolerance of PtRu catalyst. They give a quantitative estimation of the contribution of both mechanisms, but the effect of electrode potential can not be explicitly evaluated in their non-electrochemical experiments. Liu and Norskov[20] also show that both mechanisms contribute to the CO tolerance of PtRu through DFT calculations, though the authors seem to favor the "ligand" effect as the dominating mechanism for the CO tolerance of PtRu in PEM fuel cell.

It is, thus, seen that the monitoring of anode outlet CO concentration is very useful in understanding the CO tolerance mechanism for different anode catalytic materials and in their direct evaluation and comparison. It is conceivable that the online monitoring of the outlet CO concentration may provide additional insights into the mechanism of CO poisoning as well as CO_2 poisoning of other alloy catalysts. Such studies are in progress.

3.4 Conclusions

In this work, we have shown that the direct on-line monitoring of the PEM fuel cell anode outlet CO concentration using an IR gas analyzer provides important insights

into the mechanistic study of CO electrooxidation. It is observed that the anode CO concentration is a function of anode flow rate at a constant current density, as earlier predicted theoretically by us. The fact that the CO concentration increases with anode inlet flow rate when Pt is used as anode catalyst agrees reasonably well with our previous model predictions. The CO outlet concentration behavior with PtRu catalyst is especially interesting and depends upon the current density at a cell temperature of 80 °C. The anode CO concentration is observed to decrease with the increase of anode inlet flow rate at low current densities, while at higher current densities; the outlet CO concentration follows the same trend as observed for Pt anode catalyst. The CO electrooxidation rate is calculated using CO material balance in the anode and compared as a function of anode overpotential for Pt and PtRu catalyst. The results indicate that the enhanced tolerance of PtRu catalyst is due to the dual action of reduced CO affinity (ligand effect) and enhanced electrooxidation rates (bifunctional effect).

References

1. W. Vogel, J. Lundquist, P. Ross and P. Stonehart, *Electrochim. Acta*, **20**, 79 (1975).
2. S. Gottesfeld, and J. Pafford, *J. Electrochem. Soc.*, **135**, 2651 (1988).
3. H. A. Gasteiger, N. M. Markovic, and P. N. Ross, *J. Phys. Chem*., **99**, 16757 (1995).
4. R. J. Bellows, E. P. Marucchi-Soos, and D. T. Buckley, *Ind. Eng. Chem. Res*., **35,** 1235 (1996).
5. H.-F. Oetjen, V. M. Schmidt, U. Stimming, and F. Trila, *J. Electrochem. Soc.*, **143**, 3838 (1996).
6. R. J. Bellows, E. Marucchi-soos, and R. P. Reynolds, *Electrochem. Solid-State Lett.*, **1**, 69 (1998).
7. S. J. Lee, S. Mukerjee, E. A. Ticianelli, J. McBreen, *Electrochim. Acta*, **44**, 3283 (1999).
8. T. E. Springer, T. Rockward, T. A. Zawodzinski, and S. Gottesfeld, *J. Electrochem. Soc.*, **148**, A11 (2001).
9. Z. Qi, C. He, and A. Kaufman, *Electrochem. Solid-State Lett.*, **4**, A204 (2001).
10. M. Murthy, M. Esayian, A. Hobson, S. MacKenzie, W. Lee, and J. W. Van Zee, *J. Electrochem. Soc.,* **148**, A1141 (2001).
11. J. Zhang, T. Thampan, and R. Datta, *J. Electrochem. Soc.*, **149,** A765 (2002).
12. S. Ball, A. Hodgkinson, G. Hoogers, S. Maniguet, D. Thompsett and B. Wong, *Electrochem. Solid-State Lett*., **5**, A31 (2002).
13. T. J. Schmidt , H. A. Gasteiger, and R. J. Behm, *J. Electrochem. Soc*., **146**, 1296 (1999)
14. M. Watanabe, and S. Motoo, *J. Electroanal. Chem*., **60**, 275 (1975)
15. S. Lin, T. Hsiao, J. Chang, and A. Lin, *J. Phys. Chem*. *B*, **103**, 97 (1999).
16. Y. Tong, H. Kim, P. K. Babu, P. Waszczuk, A. Wiechowski, and E. Oldfield, *J. Am. Chem. Soc.*, **124**, 468 (2002).
17. P. C. Mitchell, P. Wolohan, D. Thompsett and S. Cooper, *J. Mol. Catal. A*, **119**, 223 (1997).
18. M. Krausa, and W. Veilstich, *J. Electroanal. Chem*., **379**, 307 (1994).
19. C. Lu, and R. Masel, *J. Phys. Chem. B*, **105**, 9793 (2001).
20. P. Liu, and J.K. Norskov, *Fuel Cells*, **1**, 192 (2001).

Chapter IV

Sustained Potential Oscillations in PEM Fuel Cell with PtRu as Anode Catalyst

In this chapter, sustained potential oscillations are experimentally observed in a PEM fuel cell with PtRu as anode catalyst and with H_2/108 ppm CO as the anode feed when operating under a constant current density mode. These oscillations appear at fuel cell temperatures below 70 °C. A threshold value exists for both the current density and the anode flow rate at a given fuel cell temperature for their onset. The temperature dependence of the oscillation period shows an apparent activation energy around 60 kJ/mol. The potential oscillations are believed to be due to the coupling of anode electrooxidation of H_2 and CO on the PtRu catalyst surface, on which OH_{ad} is formed more readily, *i.e.*, at lower overpotentials. A simple kinetic model is provided that can reproduce the observed oscillatory phenomenon both qualitatively and quantitatively. Contents in this chapter have been published in *J. Electrochem. Soc*..

4.1 Introduction

The proton exchange membrane (PEM) fuel cell is emerging as a promising power source for both vehicular and stationary applications[1]. However, due to the difficulties associated with hydrogen storage and distribution, liquid fuels such as methanol and gasoline are planed to be processed on demand for generation of a hydrogen-rich gas as feed to PEM fuel cell anode. Such a feed stream will inevitably contain trace amounts of CO. Since the conventional Pt anode electrocatalysts are rendered ineffective with feeds containing even 5~10 ppm CO, PtRu anode catalysts have been developed that provide increased tolerance to CO poisoning. In our effort to investigate the performance and H_2/CO electrooxidation mechanism on PtRu electrocatalysts, we found sustained potential oscillations in a PEM fuel cell operated

under constant current density with a H_2/CO anode feed under practically relevant conditions.

Oscillatory phenomena are not uncommon in electrochemical systems[2]. Metal dissolution and deposition is reported to give potential oscillations in alkaline solutions[3-6]. It is also found that galvanostatic potential oscillations appear when some small organic molecules such as formic acid and formaldehyde are electrooxidized at the anode[7-13]. Okamoto *et al*. have reported the potential oscillations during the electrooxidation of formaldehyde in aqueous H_2SO_4 electrolyte[7-9]. Techniques such as electrochemical quartz crystal microbalance (EQCM)[10-11] and probe beam deflection (PBD)[12] have been used to follow the changes occurring on the electrode surface and the electrode/electrolyte interface during the potential oscillations in anodic oxidation of formic acid. Potential oscillations are also found in connection with the anodic oxidation of H_2 on platinum electrode when metal cations such as Cd^{2+}, Cu^{2+}, Sn^{2+}, Bi^{3+}, and Ag^{+} are present in the electrolyte solution[14-16]. These oscillations are believed to be due to the coupling of hydrogen oxidation and the electrosorption and/or electrodeposition and dissolution of the metal ions. Similar coupling effect was also observed when H_2 containing low concentrations of CO was oxidized on Pt electrode in an electrochemical cell with liquid electrolyte, resulting in potential oscillations at constant current density[17-19]. These oscillations were ascribed to a passivation-type polarization curve in the electrode reaction[19].

There are many reports in the literature on the modeling of oscillatory processes in electrochemical systems. Thus, Wolf *et al.*[20] provide a model for the galvanostatic oscillations that occur during the oxidation of hydrogen at a platinum electrode in the presence of electrosorbing metal ions and specifically adsorbing anion. The temporal change in the potential at the electrode was deduced by considering the total current density as a sum of the capacitive and charge transfer current densities, the latter comprising the charge passed during the oxidation of the hydrogen and the adsorption and desorption of the metal ions. Okamoto *et al.*[21] provide a model to reproduce the observed kinetic potential oscillations for the electrochemical oxidation of formic acid on Pt based on the assumptions that the water adsorption velocity is proportional to the surface coverage of CO, and that the saturation coverage of adsorbed CO is less than 1.

Another assumption is that both the forward and backward step of water adsorption depends upon potential, although it is considered as a non-electrochemical step. Yamazaki *et al*.[17] provide a model for hydrogen oxidation in H_2SO_4 solutions in the presence of metal ions such as silver, gold or gas impurities such as CO. A specific assumption in their model is that attractive interaction exists among CO_{ad}, which is necessary for the appearance of oscillation by the model. Detailed experimental and modeling work was reported by Strasser *et al*.[22] on the current oscillations during electrooxidation of formic acid on Pt under potentiostatic control. In this work, the scanned current/potential behavior as well as current oscillations were simulated successfully. Their model takes into account two possible reaction pathways for formic acid electrooxidation, and provides bifurcation analysis and mechanistic categorization of the oscillators.

Thus, although many reports exist on oscillatory phenomena in the electrochemical cell system, there is no systematic report on potential oscillations in PEM fuel cells so far in the literature. As far as we know, there is only one recent report that briefly mentions oscillations in a study of PEM fuel cell performance with feed containing CO[23]. This chapter, thus, reports for the first time, a systematic study of potential oscillations in a PEM fuel cell with PtRu as the anode catalyst. Sustained potential oscillations were observed when the fuel cell was operated at a constant current density with a H_2/CO anode feed under practically relevant fuel cell conditions. Experimental conditions that lead to such potential oscillations are presented here. Further, a realistic theoretical model is described based on a kinetic analysis of the reaction on PEM fuel cell anode in the presence of CO. This model uses few assumptions to reproduce satisfactorily the oscillatory pattern observed in the experimental work.

4.2 Experimental

Gas diffusion electrodes with 20%(w/o) Pt/C or PtRu/C catalyst were purchased from E-TEK, Inc (Somerset, NJ). A Pt electrode with a metal loading of 0.4 mg/cm^2 was used as the cathode. A PtRu (atomic ratio 1:1) electrode with a metal loading of 0.35 mg/cm^2 was used as the anode. Nafion® 115 proton exchange membrane (Du Pont, Fayetteville, PA) was used after sequential treatment with 2% H_2O_2, deionized water, 0.5

M H_2SO_4 and again with deionized water in order to remove any inorganic and organic impurities. The membrane electrode assembly (MEA) was prepared by hot-pressing in a Model C Carver hot press at 130 °C and under a pressure of 4000 lbs for about 2 minutes. The MEA was then assembled in a 5 cm^2 single cell from ElectroChem, Inc. (Woburn, MA), and tested in a test station with temperature, pressure, humidity and flow rate control. The fuel cell voltage was recorded using a HP 6060B DC electronic load, interfaced with a PC using LabVIEW software (National Instruments, Austin, TX) at a data sampling rate of 77 ms.

The single PEM fuel cell thus assembled was tested at different temperatures. Anode and cathode gases were first humidified through a stainless steel bottle containing water at the desired temperature before being fed into the fuel cell. The temperature of the humidification bottle was set at 15 °C and 10 °C higher than that of the fuel cell for the anode and cathode side, respectively, accounting for the heat losses and resulting condensations between the humidifier and the fuel cell. The total pressure of both the anode and the cathode was 30 psig unless otherwise indicated. The flow rates reported in this study are in units of standard (1 atm and 25 °C) cubic centimeter per minute (scc/min). Pre-mixed H_2/108 ppm CO was purchased from MG Industries (Morrisville, PA) and was used as the anode feed. The CO concentration was certified by the supplier and was not independently confirmed. Oxygen was used as the cathode feed.

4.3 Results

4.3.1 Onset of Potential Oscillations

The single PEM fuel cell was tested with pure hydrogen as well as H_2/108 ppm CO, using Pt and PtRu as anode catalyst, respectively. The results are shown in Figure 4-1. The cell voltage is plotted against time for the single cell operated under identical conditions (fuel cell temperature 42 °C, current density 300 mA/cm^2, anode flow rate 36.4 scc/min) except for those indicated inside the figure. It was found, as expected, that the cell voltage remained steady when pure hydrogen was used as the fuel for both Pt and PtRu anode catalysts. On the other hand, when the fuel was switched over to H_2/108 ppm

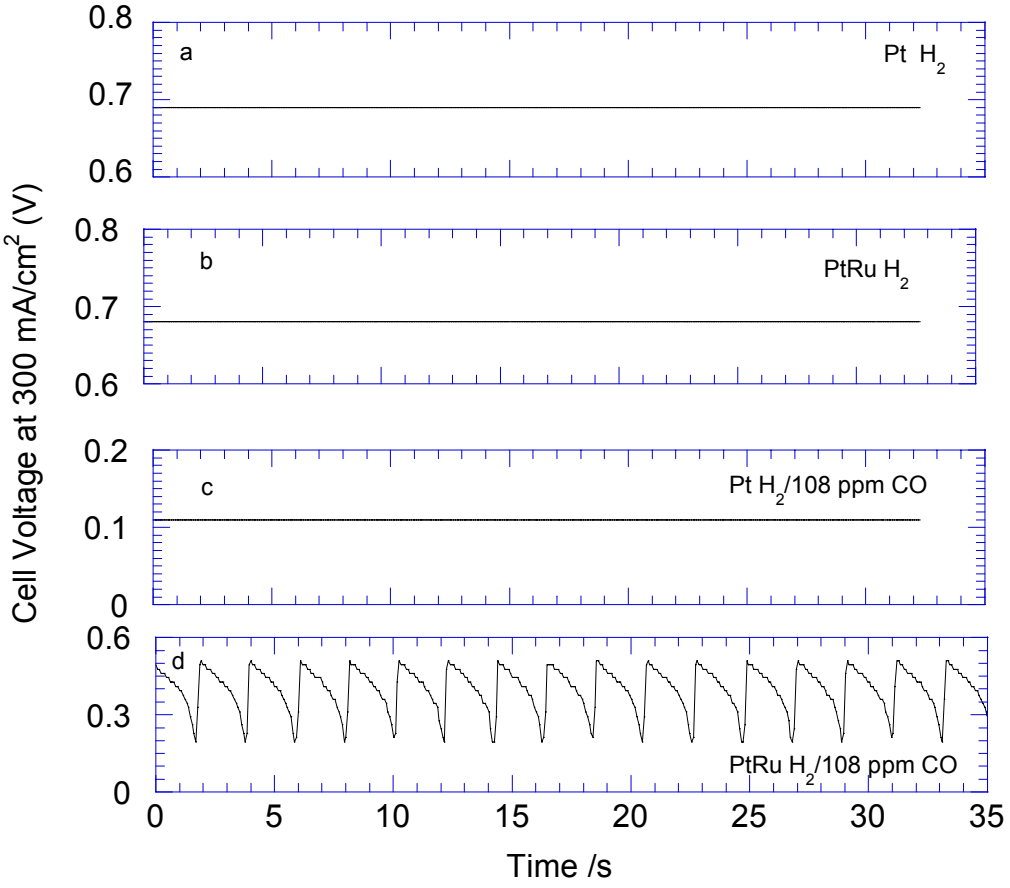

Figure 4-1. Fuel cell voltage pattern for (a) Pt with H_2 (b) PtRu with H_2 (c) Pt with H_2/108 ppm CO (d) PtRu with H_2/108 ppm CO. Other operation conditions are identical: cell temperature, 42 °C; current density, 300 mA/cm^2; anode inlet flow rate, 36.4 scc/min.

CO, periodic voltage oscillations appeared for the fuel cell with PtRu anode catalyst, but not for Pt. Such comparisons were conducted at all other experimental conditions where sustained potential oscillations were observed for the case of the H_2/CO and PtRu system. Based on these results, it is clear that the observed oscillations are unique to the H_2/CO feed and the PtRu anode in a PEM fuel cell under the conditions investigated.

The voltage oscillations appear only under certain operation conditions. It was observed that proper combination of fuel cell temperature, current density, and anode flow rate are crucial for the onset of the limit cycle. It was found that temperature is the most critical factor in determining the occurrence of voltage oscillations. No oscillations were observed when the cell temperature was above 80 °C, but commonly below 70 °C. Further, for a given temperature, potential oscillations were found to exist only in a certain range of current density and anode flow rate. Figure 4-2 shows roughly the current density – anode flow rate domains at different fuel cell temperatures where the potential oscillations appear. The domain becomes smaller at lower temperatures since only small current densities can be sustained at lower temperatures in the PtRu anode PEM fuel cell with a H_2/CO feed. It is evident that the domain boundary in Figure 4-2 should be smooth, but unfortunately, the experiments can only be performed in a discrete manner. It is a common observation that chemical oscillations typically appear only in a very narrow range of parameter values that are deducible, in principle, from the mathematical relations governing the dynamic system[24].

It is seen that the current density must be larger than a limiting value at a given anode flow rate, and vice versa, for the voltage oscillations to appear. The existence of a threshold current for the onset of potential oscillation has been reported in other works, such as in H_2 electrooxidation in the presence of metal cations (about 70 μA for a 20 cm^2 Pt wire)[16]or low concentration of CO in a liquid electrolyte (75 mA/cm^2 for a platinized porous carbon electrode)[19] .

The transition between steady conditions and a limit cycle with anode flow rate change is shown in Figure 4-3. Thus, when the anode flow rate is increased from 48.1 scc/min to 60.1 scc/min, sustained voltage oscillations appear. When the anode flow rate is changed back to the original lower flow rate, the voltage oscillations become damped and eventually disappear. The transition of cell voltage from a steady value to a periodic

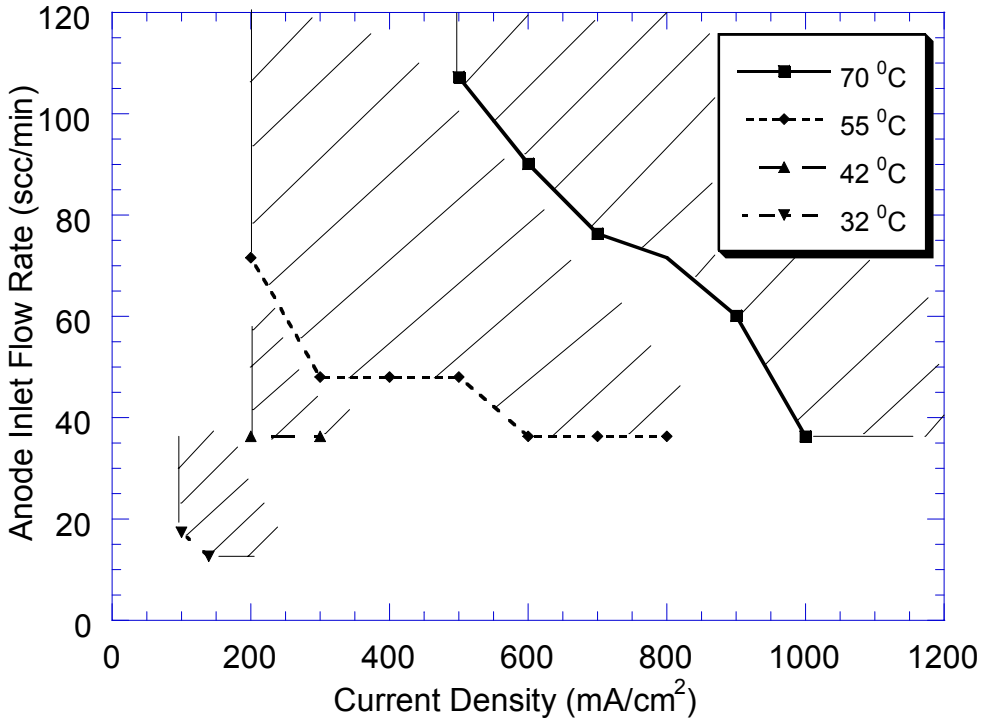

Figure 4-2. The current density – anode flow rate domain where anode overpotential oscillation appears at different temperatures.

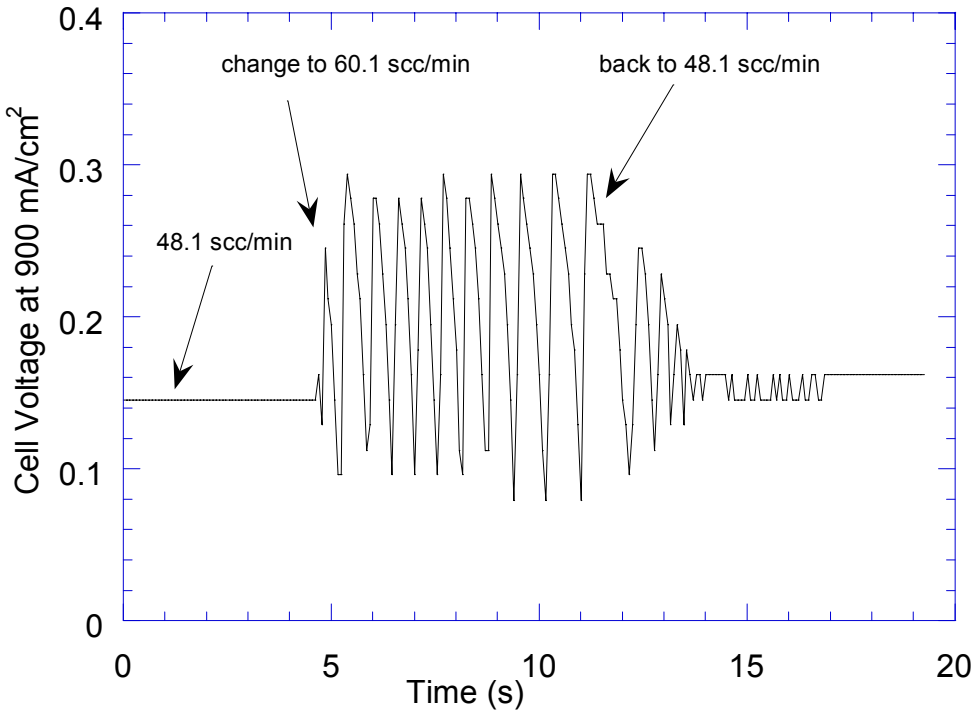

Figure 4-3. The transition of the fuel cell voltage between a steady value and oscillation with the variation of anode flow rate. Cell temperature, 70 °C; current density, 900 mA/cm^2.

oscillation was also observed when the current was crossed over from a value in the non-oscillating domain to one which leads to oscillations at a given flow rate.

4.3.2 Effect of Current Density

The cell voltage oscillations are clearly caused by periodicity in the anode overpotential. In order to single out the anode overpotential, the cell voltage for the case of pure H_2 was also measured at otherwise identical experimental conditions. The overall fuel cell voltage is[25-26],

$$V = V_0 - \eta_A + \eta_C - i\left(\frac{L}{\sigma}\right) - i(R_I) \qquad [1]$$

where V_0 is the open circuit potential, i is the current density, η_A and η_C are the anode and cathode overpotentials including any diffusional overpotential in the gas diffusion layer, respectively, L and σ are the thickness and conductivity of the proton-exchange membrane, respectively, while R_I is any interfacial resistance. Thus, at a constant current density, the difference in the polarization of the anode between the cases of the presence ($\eta_{H_2/CO}$) and the absence of CO (η_{H_2}) in anode feed may be obtained simply from the corresponding measurements of the cell voltage.

$$\eta_{H_2/CO} - \eta_{H_2} = V_{H_2} - V_{H_2/CO} \qquad [2]$$

where V_{H_2} and $V_{H_2/CO}$ are the cell voltages with H_2 and H_2/CO feed, respectively. Further, since the overpotential for pure H_2 is small, it may be neglected without substantial error. Thus, the anode overpotential in the presence of CO is assumed to be simply the cell voltage difference between the two cases, *i.e.*,

$$\eta_{H_2/CO} \approx V_{H_2} - V_{H_2/CO} \qquad [3]$$

Figure 4-4 shows a series of thus obtained anode overpotential oscillatory patterns at 55 °C and various current densities, while the anode flow rate was kept at a constant value of 48.1 scc/min. It is seen that the pattern of these oscillations is largely unaffected as the current density is increased from 300 mA/cm^2 to 700 mA/cm^2. One noteworthy feature of the oscillations at different current densities is that the minimum overpotential appears to be more uniform than the maximum. Further, the maximum and minimum potentials are not greatly dependent upon the current density, except for the fact that the amplitude of overpotential oscillations at 300 mA/cm^2 is about 50~60 mV lower than that at other current densities. The oscillation period of about 0.9 s also does not change very much with the applied current density. In the study of potential oscillations in H_2-CO oxidation on Pt electrode in an electrochemical cell, Deibert *et al.*[19] found that the oscillation frequency does not change for current density between 200 ~ 500 mA/cm^2, although they found that the frequency decreases slightly with the increase of current density in the range of 75~200 mA/cm^2. In the study of H_2 electrooxidation in the presence of Cu^{2+} by Krischer *et al.*[16] and formaldehyde oxidation in H_2SO_4 solution by Okamoto *et al.*[8], an oscillation pattern transition was found with current density and operation time. For example, period-doubling or tripling, or even aperiodicity, was observed accompanying the increase of the current density and the elapse of time. However, such transitions with current density and time were not found in this study.

4.3.3 Effect of Anode Flow Rate

The anode inlet flow rate is an important parameter for the onset of anode potential oscillations, as illustrated in Figure 4-2. Therefore, the effect of anode flow rate on the oscillations was further investigated as shown in Figure 4-5, where the anode overpotential is plotted versus time at 42 °C and 300 mA/cm^2 for different anode flow rates. Although the general shape and the period of oscillations do not change as the anode flow rate is changed from 36.4 scc/min to 71.6 scc/min, the amplitude is somewhat affected. This can be seen in Figure 4-6, where the maximum overpotential increases while the minimum overpotential decreases with increasing anode inlet flow rate. As discussed previously[26], the CO concentration in the anode compartment is a function of

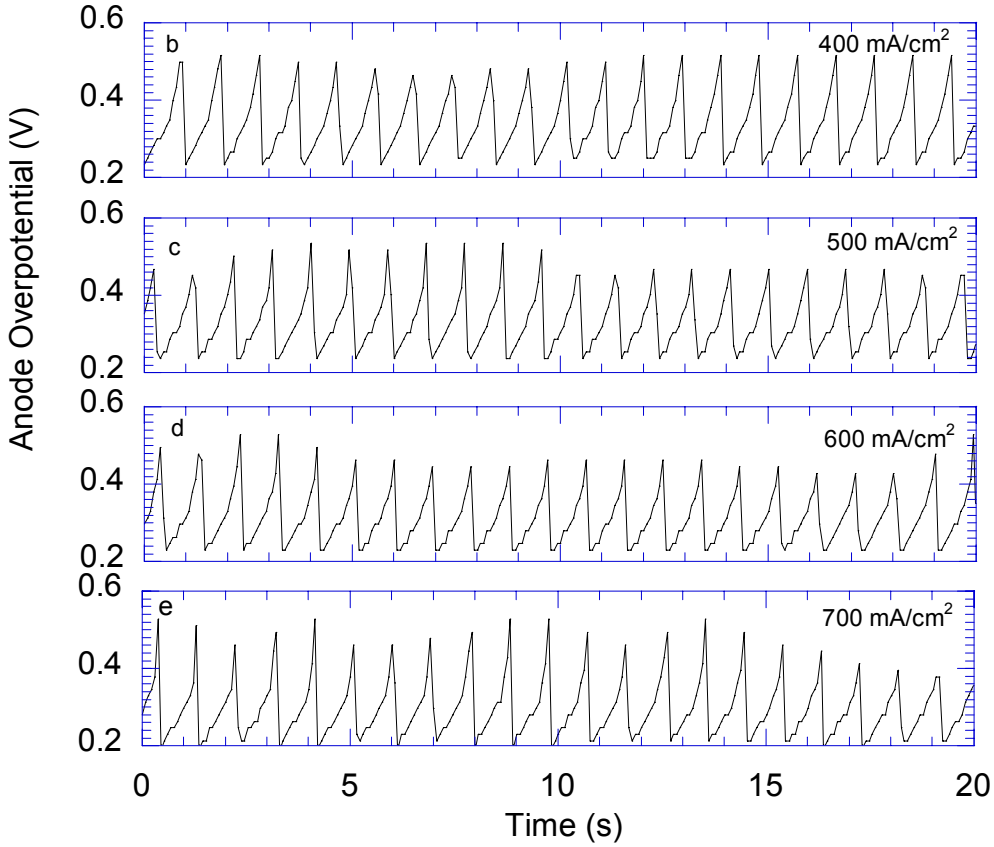

Figure 4-4. Potential oscillation of PEM fuel cell at 55 °C at different current densities. (a) 300 mA/cm^2 (b) 400 mA/cm^2 (c) 500 mA/cm^2 (d) 600 mA/cm^2 (e) 700 mA/cm^2. Anode flow rate is 48.1 scc/min for all cases.

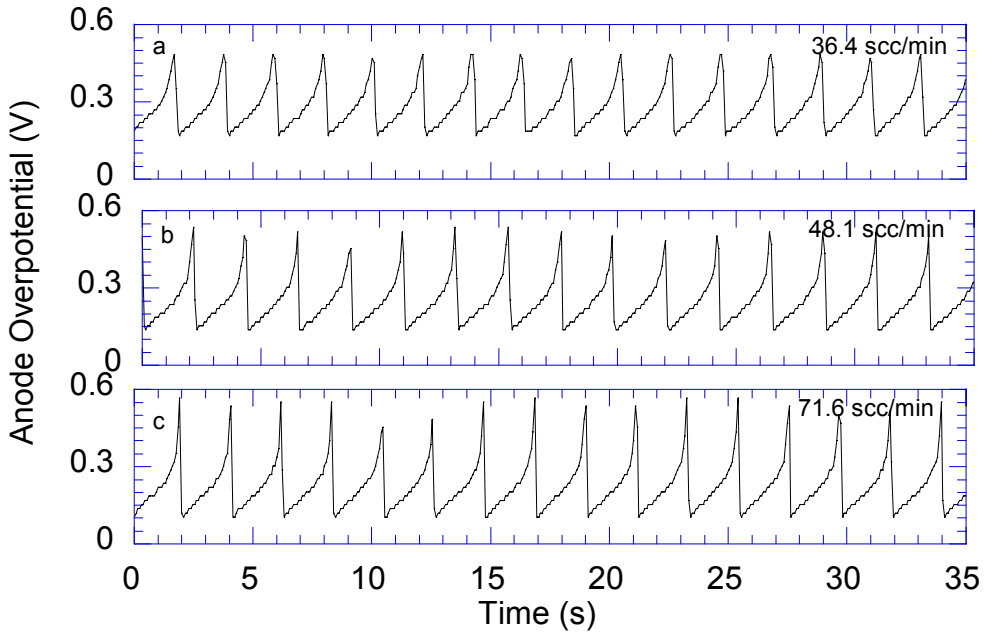

Figure 4-5. Potential oscillation of PEM fuel cell at 42 °C at different anode inlet flow rate. (a) 36.4 scc/min (b) 48.1 scc/min (c) 71.6 scc/min. The current density is 300 mA/cm^2 for all cases.

anode flow rate and, thus, the anode overpotential increases with anode flow rate. Therefore, the observed effect is likely due to the increasing CO concentration in the anode compartment with increasing anode flow rate. Similar trend in the maximum overpotential with the increase of CO bubbling rate was found by Yamazaki *et al.*[15] in their study of H_2-CO oxidation on Pt in aqueous electrolyte. Figure 4-6 also shows that the oscillation period does not change with increasing anode flow rate.

4.3.4 Effect of Fuel Cell Temperature

As discussed above, the oscillation period is relatively insensitive to the anode flow rate and the applied current density in the range investigated. However, it does change dramatically with temperature. Therefore, it is reasonable to compare the oscillation period at different temperatures, even though the corresponding current densities and the anode flow rates are different, as a result of the shifting of the limit cycle domain with temperature (Figure 4-2).

The oscillatory patterns at four different fuel cell temperatures are shown in Figure 4-7. The shape of anode overpotential change is similar, namely, a gradual increase to the maximum overpotential followed by a rapid drop to the minimum. However, the period decreases dramatically with an increase of fuel cell temperature, and the potential oscillations disappear altogether at temperatures higher than 70 °C. It may be noticed that the oscillation pattern is more pronounced and regular at lower temperatures. The peak value of anode overpotential is below 0.6 V in all cases. This feature may be essential for the occurrence of oscillations in PEM fuel cell systems. In the literature report of potential oscillations on Pt in the electrochemical cell, the maximum potential is in the range of 0.9~1.2 V[19], which is considerably higher than the cathode potential for appreciable O_2 oxidation current in PEM fuel cell. Actually, the cathode potential is polarized below 0.9 V for a current density of 100 mA/cm^2 at 80 °C. Thus, oscillations in a PEM fuel cell with Pt as anode electrocatalyst may not be observed for the H_2/CO feed. On the other hand, PtRu anode with its lower overpotential for CO electrooxidation, allows such periodic behavior to be observed in a PEM fuel cell.

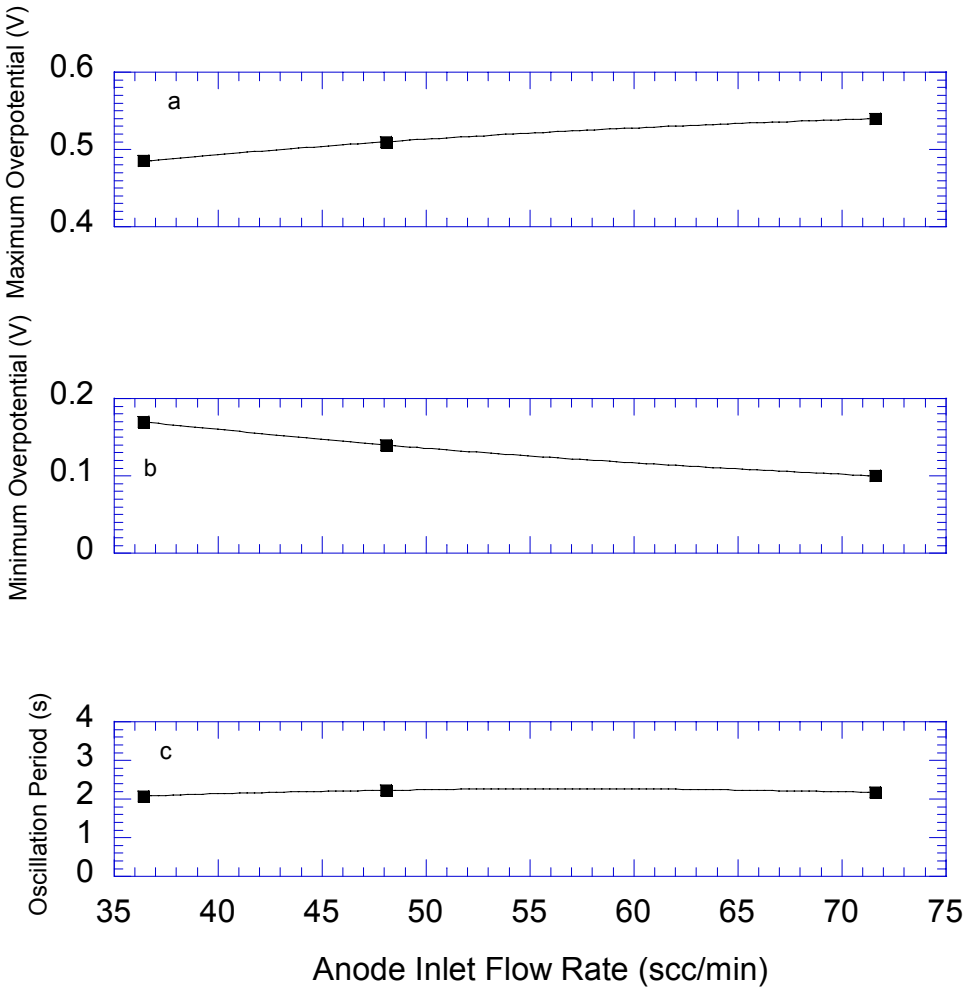

Figure 4-6. Dependence of (a) maximum overpotential (b) minimum overpotential (c) oscillation period on anode inlet flow rate for the potential oscillation shown in Figure 4-5.

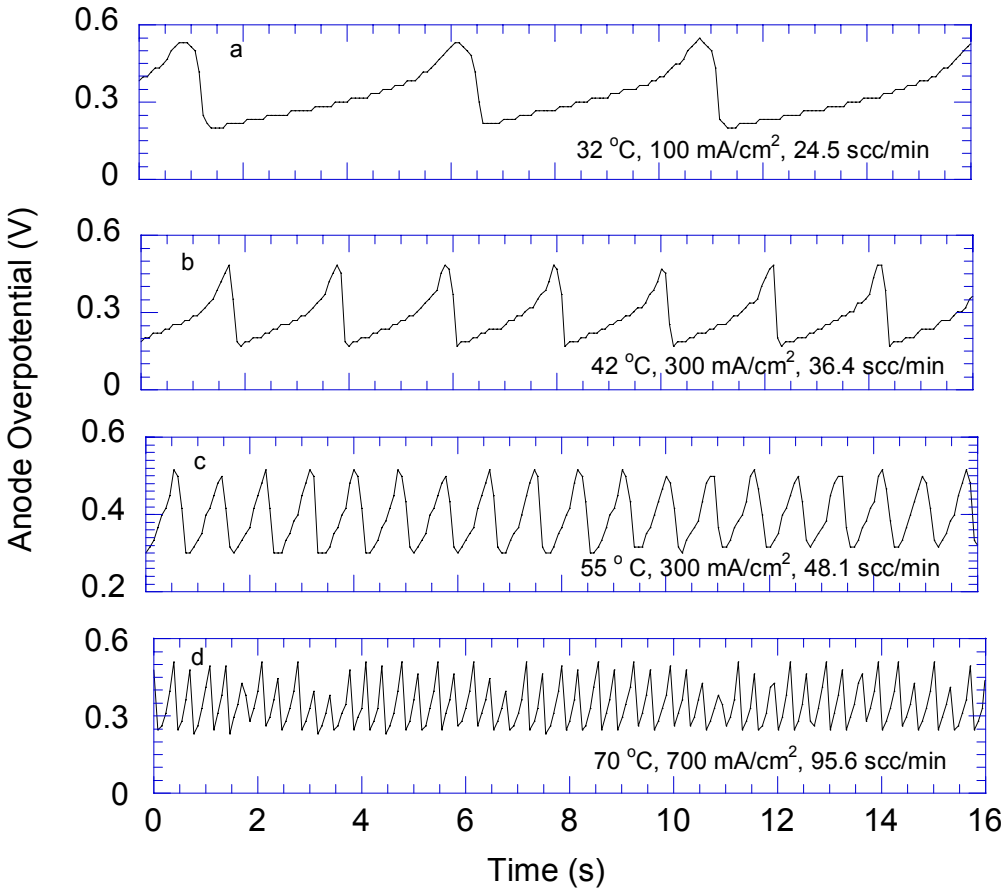

Figure 4-7. Potential Oscillation of PEM fuel cell at different temperatures. The fuel cell temperature, applied current density and anode inlet flow rate are as follows: (a) 32 °C, 100 mA/cm^2, 24.5 scc/min (b) 42 °C, 300 mA/cm^2, 36.4 scc/min (c) 55 °C, 300 mA/cm^2, 48.1 scc/min (d) 70 °C, 700 mA/cm^2, 95.6 scc/min.

In order to look more closely at the oscillation process, a magnified picture of the oscillation cycle is shown in Figure 4-8(a). It can be seen that two branches comprise a cycle. The fast overpotential decline is related to the surface reactivation; the relatively slow ascending branch is a result of the surface CO poisoning and the corresponding electrode polarization. It should be pointed out that the steps in the ascending branch are due to the discrete nature of the reading of the electronic load.

4.4 Discussion

The occurrence of the oscillatory behavior is evidently caused by the coupling of the kinetics of electrooxidation of H_2 and of CO on the anode catalyst. A qualitative explanation is discussed below followed by a theoretical model.

With the introduction of CO in the anode feed, the CO begins to build up on the surface until the catalyst surface is almost completely blocked ($\theta_{CO} \rightarrow 1$) due to the strong affinity of CO to the catalyst. In order to sustain the applied current, thus, the anode becomes increasingly polarized to a higher potential. This, in turn, accelerates the electrooxidation of CO_{ad} on the catalyst surface via the oxygen containing surface species such as OH_{ad}. At a certain overpotential, the CO electrooxidation rate exceeds the rate of CO adsorption and the surface coverage of CO declines. At this stage, H_2 oxidation reaction is no longer limited by the surface coverage of CO, due to the facile kinetics of H_2 electrooxidation. The anode overpotential, thus, drops quickly to a low value. This potential drop, however, recreates the situation where the rate of CO electrooxidation is exceeded by that of CO adsorption. Therefore, CO molecules begin to build up again on the catalyst surface and the electrode must again be polarized correspondingly to a higher overpotential. Thus the cycle is repeated. An explanation of the reason why the potential oscillations do not appear on Pt anode catalyst in PEM fuel cell is that the formation of OH_{ad} species is more facile on Ru surface than on Pt surface. Thus, Gasteiger *et al.*[27] have shown in their voltammetric study of H_2/CO electrooxidation that the ignition potential of CO oxidation on Pt is about 0.7~0.9 V at room temperature, when OH_{ad} is appreciably formed on the Pt electrode surface. Even at higher temparatures and lower CO concentrations (*e.g.*, at 60 °C and 250 ppm CO), the ignition potential is still above about 0.5 V[28]. On the other hand, the ignition potential of CO oxidation on PtRu alloy

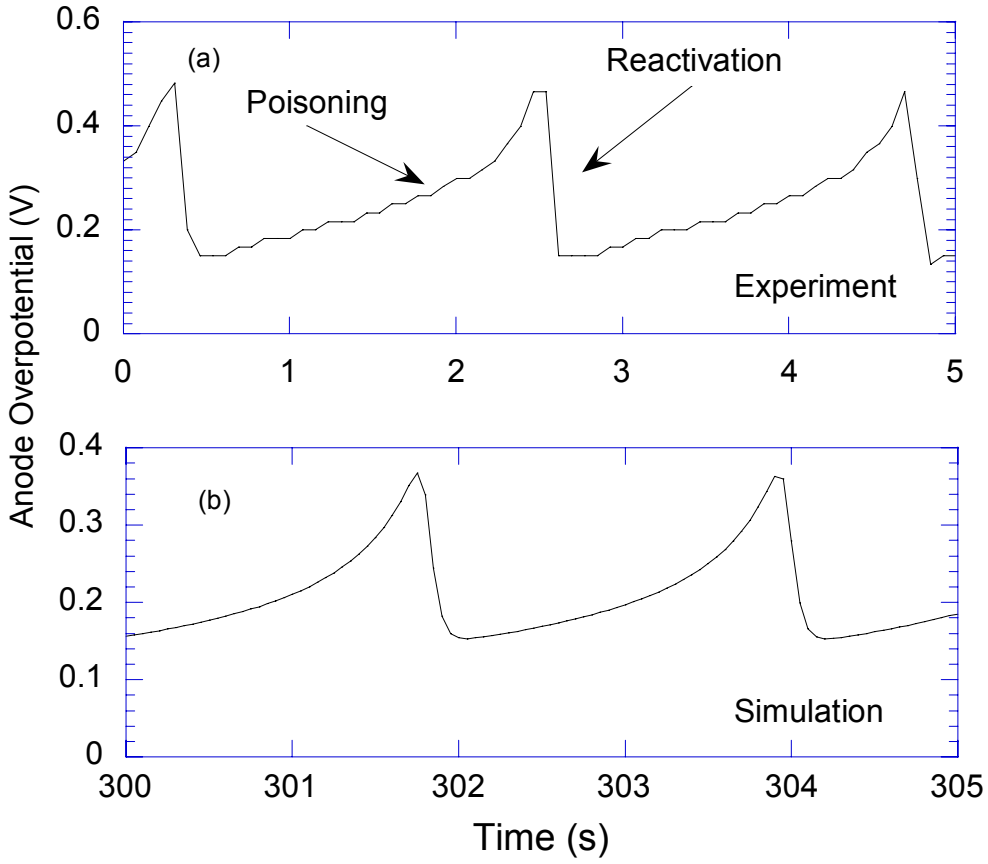

Figure 4-8. A magnified picture of the potential oscillation pattern from experiment (a) and simulation (b) at 42 °C. Current density, 300 mA/cm^2; anode inlet flow rate, 48.1 scc/min.

surface is shifted down to 0.3~0.45 V as per the CO stripping voltammetry[29], since the nucleation of OH_{ad} occurs on PtRu at a lower potential. Therefore, it is likely that in the overpotential range which is available in a PEM fuel cell under normal temperatures, conditions do not exist on Pt where CO electrooxidation rate exceeds that of CO adsorption so that periodic cleansing of the surface may be accomplished. However, on PtRu catalyst, there are periods when H_2 is oxidized on a less contaminated surface temporarily at lower overpotential until CO molecules build up again.

It was found in our previous study[26] that O_2 can also permeate through the proton exchange membrane from the cathode side to the anode and contribute to the CO oxidation on Pt catalyst via a non-electrocatalytic direct oxidation pathway. The anode overpotential was thus found to decrease for Pt at higher cathode O_2 pressures. Similar experiments were conducted here to check if O_2 permeation to the anode has any effect on the oscillatory phenomenon with PtRu catalyst. The oscillation pattern is, thus, compared for three different cathode O_2 pressures in Figure 4-9. It is apparent that the oscillations are not substantially affected as the cathode O_2 pressure is decreased from 30 psig to 10 psig except for a very small increase in oscillation amplitude. The oscillation period remains essentially constant. In comparison, there is a significant polarization drop of about 0.1 V for Pt anode catalyst when the cathode pressure is increased from 10 psig to 30 psig[26]. It, thus, appears that the direct CO oxidation via non electrocatalytic pathway with oxygen permeating from the cathode on PtRu is less significant as compared with the dominant route via OH_{ad} electro-oxidation. This demonstrates that H_2O is the major agent for CO oxidation on the PtRu catalyst.

As discussed above, the oscillation period decreases substantially with increasing temperature (Figure 4-7). If it is assumed that the oscillation period τ is inversely proportional to the rate constant of a kinetic step, *i.e.*,

$$\tau = \frac{C}{A_0 \exp\left(-\frac{E_a}{RT}\right)} \qquad [4]$$

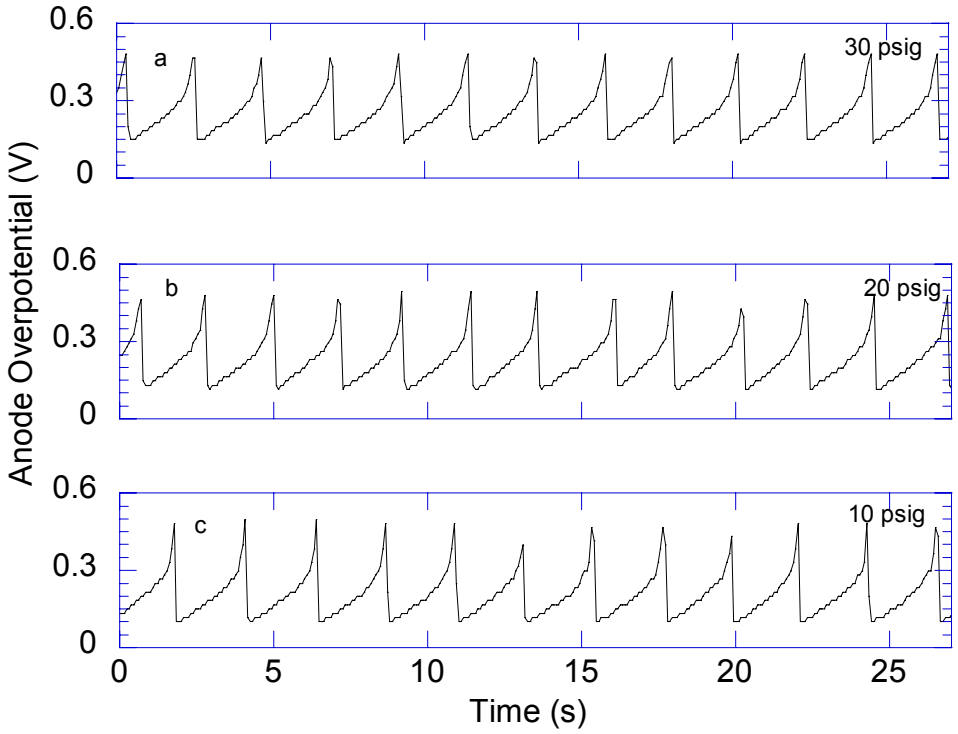

Figure 4-9. Potential oscillation of PEM fuel cell at 42 °C at different cathode O_2 pressure. (a) 30 psig (b) 20 psig (c) 10 psig. Current density, 300 mA/cm^2; anode inlet flow rate, 48.1 scc/min.

where τ is the oscillation period, C is a constant, A_0 is the preexponential factor, E_a is the activation energy. Then, we might expect the following temperature dependence of the oscillation period:

$$\ln\tau = \ln\left(\frac{C}{A_0}\right) + \frac{E_a}{RT} \qquad [5]$$

i.e., a plot of ln τ versus $1/T$ would yield a straight line with a slope equals to E_a/R. A plot of ln τ versus $1/T$ at four deferent temperatures is shown in Figure 4-10. It is seen that a very good linear relationship results with an activation energy of 60.9 kJ/mol. This could serve as a clue in determining which kinetic step might control the frequency of the oscillations.

Possible rate processes controlling the oscillatory behavior include bulk diffusion, adsorption onto catalyst surface, surface diffusion, and surface reaction of CO and/or H_2. It has been shown by others[30] as well as in our previous work[26] that there are no CO bulk diffusional limitations in fuel cell anode for the gas mixture of H_2 containing trace amounts of CO. Further, the adsorption of H_2 and CO on noble metal surface is a fast process, with low activation energies. Thus, the limiting process must be either a surface diffusion or a surface reaction step.

A quantitative estimation of the activation energy of the possible surface process was obtained using the unity bond index-quadratic exponential potential (UBI-QEP) method[31-32]. The calculation results together with some experimental data are listed in Table 4-1. It can be seen that the activation energy of the surface reaction between CO_{ad} and OH_{ad}, which is believed to be the elementary step in the electrooxidation of CO on PtRu surface by many researchers, is roughly between 40~ 50 kJ/mol. The dissociation of H_2O on the catalyst surface is an essential step in the formation of OH_{ad}. The activation energy for this step is calculated to be 78.6 kJ/mol on Pt surface and 59.8 kJ/mol on Ru. The experimental value for Pt is 104.5 ± 20.9 kJ/mol[34]. The theoretical prediction and experimental values of the surface diffusion activation energies are also listed in Table 4-1, and are unlikely to be rate limiting. Therefore, it is plausible that the oscillation is controlled by the surface reaction steps either of OH_{ad} formation or the reaction between OH_{ad} and CO_{ad}. However, due to the uncertainties in calculation of these values, this can not be determined unambiguously.

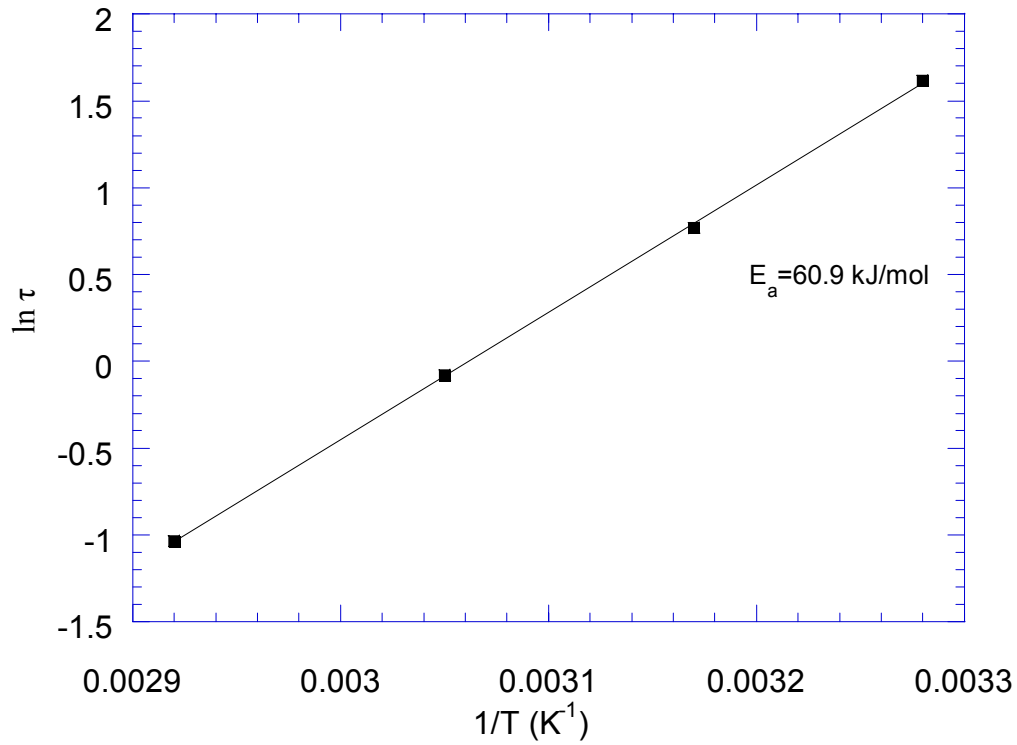

Figure 4-10. Plot of ln τ vs. $1/T$ as per equation [5].

Table 4-1. Estimation of the Activation Energy of Some Surface Steps using UBI-QEP Method

Surface Steps	Activation Energy E_a (kJ/mol)		
	UBI-QEP method		Experimental Data
	Pt	Ru	Pt
$CO_{ad} + OH_{ad} \rightarrow CO_{2,ad} + H_{ad}$	46.4[a]	46.0[a]	30~40[c]
$H_2O_{ad} \rightarrow OH_{ad} + H_{ad}$	78.6[a]	59.8[a]	105 ± 21[d]
OH_{ad} surface diffusion	23.0[b]	29.5[b]	
CO_{ad} surface diffusion	19[b]	17.3[b]	33.0 ± 8.4[e]

[a] ref. 31.
[b] ref. 32.
[c] ref. 33.
[d] ref. 34.
[e] ref. 35.

4.5 Modeling

An attempt is made here to model simply the experimentally observed potential oscillations of PEM fuel cell with PtRu as anode catalyst and with H_2/CO as anode feed. The fuel cell is operated in a constant current density mode and the CO concentration is 108 ppm, which is approximately the CO level in the reformate stream after Preferential Oxidation (PrOx) from a reformer.

The catalyst surface is assumed to be uniform in this model, with the surface site represented by S, *i.e.*, we do not consider a heterogeneous surface with two different metal sites, despite the fact that H_2 is likely to adsorb and dissociate on Pt preferentially, while H_2O is likely to adsorb and dissociate on Ru preferentially. However, in this model, the above mentioned difference in surface sites is neglected, assuming that alloying alters the energetics and kinetics of the surface reactions. It is also assumed that there is no interaction among surface species, which only interact indirectly via competition for the free surface sites.

At the reactor scale, the fuel cell temperature is at a fixed value, so that isothermal condition is assumed. The feed stream is always assumed to be saturated with water vapor. The anode chamber is assumed to be well-mixed, which is not an unreasonable assumption for a differential or small (5 cm^2) single cell[26].

The parameters used here are taken from the literature, with the exception of those not available, which were fitted to reproduce the experimental data. There are only two parameters that are fitted, as listed in Table 4-2. The resulting model presented here is able to explain adequately the potential oscillation found in the electrooxidation of H_2/CO on PtRu anode catalyst in PEM fuel cell.

4.5.1 Surface Chemistry

Tafel-Volmer mechanism is assumed for H_2 electrooxidation*, i.e.*, H_2 is dissociatively chemisorbed on surface sites represented by S, followed by the electrochemical oxidation of adsorbed hydrogen atoms,

$$H_2 + 2\,S \leftrightarrows 2\,S\text{–}H \qquad \vec{k}_{H_2,ad},\ K_H \qquad [6]$$

Table 4-2 Model Parameters Used in Simulation

K_{CO}	2×10^{-7} atm[a]	$\vec{k}_{OH}$	8×10^{-4} A cm^{-2} [e]
K_H	0.5 atm[a]	$\overleftarrow{k}_{OH}$	2760 A cm^{-2} [b]
α_H	1/2	x_{CO}^0	108×10^{-6}
α_{CO}	1/2	T	315 K
α_{OH}	1/2	C_{dl}	0.45 F[c]
$\vec{k}_{H,ox}$	4.0 A cm^{-2} [a]	γ	100[d]
$\vec{k}_{H_2,ad}$	402 A cm^{-2} atm^{-1} [a *]	C_t^*	2.2×10^{-9} mol/cm^2 [b]
$\vec{k}_{CO,ad}$	150 A cm^{-2} atm^{-1} [a*]	A	5 cm^2
$\vec{k}_{CO,ox}$	5.5×10^{-4} A cm^{-2} [e]	P_{H_2}	2.96 atm
i	0.3 A/cm^2	v_0	48.1 scc/min
V_A	2.63×10^{-7} m^3		

[a] ref. 36.
[b] ref. 37.
[c] ref. 19.
[d] Estimated by the specific surface area of 20%(w/o) E-TEK PtRu/C catalyst and an electrochemical efficiency(utilization) of the anode catalyst of about 30%.
[e] Fitted parameters.
These two values have been increased by a factor of 10 from the original value in order to match the simulated oscillation frequency with the experimental results.

$$S\text{–}H \leftrightarrows S + H^+ + e^- \qquad \vec{k}_{H,ox} \qquad [7]$$

The following mechanism is adapted for CO electrooxidation[27, 29]: CO molecules adsorb in a linear state, *i.e.*, one adsorption site per CO molecule,

$$CO + S \leftrightarrows S\text{–}CO \qquad \vec{k}_{CO,ad}\ ,\ K_C \qquad [8]$$

This process is assumed to be reversible.

Water is dissociated into surface hydroxyl group, OH ,

$$H_2O + S \leftrightarrows S\text{–}OH + H^+ + e^- \qquad \vec{k}_{OH}\ ,\ \overleftarrow{k}_{OH} \qquad [9]$$

Finally, adsorbed CO reacts with adsorbed hydroxyl group to form CO_2.

$$S\text{–}OH + S\text{–}CO \rightarrow 2\ S + CO_2 + H^+ + e^- \qquad \vec{k}_{CO,ox} \qquad [10]$$

This step is assumed to be irreversible.

4.5.2 Surface Kinetics

From equation [6], the net adsorption rate for H_2 is**,**

$$r_{H_2,ad} = \vec{k}_{H_2,ad} P_{H_2} \theta_0^2 - \vec{k}_{H_2,ad} K_H \theta_H^2 \qquad [11]$$

where θ_0 is the fraction of free surface sites, which is from the total site balance,

$$\theta_0 = 1 - \theta_{CO} - \theta_H - \theta_{OH} \qquad [12]$$

$\vec{k}_{H_2,ad}$ is the adsorption rate constant of H_2, and K_H is the equilibrium constant for H_2 desorption (the reciprocal of the adsorption equilibrium constant). θ_{CO}, θ_H, θ_{OH}, are the surface coverages of CO, H and OH, respectively. P_{H_2} is the partial pressure of hydrogen in the anode chamber.

The rate for hydrogen electrooxidation, reaction [7] is assumed to obey the Butler-Volmer equation,

$$r_H = 2\vec{k}_{H,ox} \theta_H \sinh\left(\frac{\alpha_H F \eta_A}{RT}\right) \qquad [13]$$

where $\vec{k}_{H,ox}$ is rate constant of H_2 electrooxidation, α_H is the transfer coefficient, assumed to be the same for the forward and reverse reaction, η_A is the anode overpotential. The other parameters have their usual meaning.

The net rate of CO adsorption is,

$$r_{CO,ad} = \vec{k}_{CO,ad} x_{CO} P_{H_2} \theta_0 - \vec{k}_{CO,ad} K_C \theta_{CO} \qquad [14]$$

where $\vec{k}_{CO,ad}$ is rate constant of CO adsorption, K_C is the equilibrium constant for CO desorption (the reciprocal of the adsorption equilibrium constant), and x_{co} is the mole fraction of CO in the dry (water free) anode gas.

The water dissociative adsorption is an electrochemical step (Equation 9), so that the rate will depend upon the anode potential. This process is assumed to be reversible and to obey the Butler-Volmer equation, namely,

$$r_{OH} = \vec{k}_{OH} \theta_0 \exp\left(\frac{\alpha_{OH} F \eta_A}{RT}\right) - \overleftarrow{k}_{OH} \theta_{OH} \exp\left(\frac{-(1-\alpha_{OH}) F \eta_A}{RT}\right) \qquad [15]$$

where $\vec{k}_{OH}$ and $\overleftarrow{k}_{OH}$ are the adsorption and desorption rate constants of water, and α_{OH} is the transfer coefficient for the reaction.

The CO oxidation step (equation [10]) is considered as an irreversible electrochemical step with charge transfer. Thus,

$$r_{CO} = \vec{k}_{CO,ox} \theta_{CO} \theta_{OH} \exp\left(\frac{\alpha_{CO} F \eta_A}{RT}\right) \qquad [16]$$

where $\vec{k}_{CO,ox}$ is the rate constant of CO electrooxidation, and α_{co} is the transfer coefficient for CO electrooxidation.

4.5.3 Mass Balance and Charge Conservation

With the above rate expressions, we can write the following unsteady-state site balance for the time evolution of the surface coverage of CO, H and OH,

$$(F\gamma C_t^*)\frac{\mathrm{d}\theta_{\mathrm{CO}}}{\mathrm{dt}} = r_{\mathrm{CO},ad} - r_{\mathrm{CO}} \qquad [17]$$

$$(F\gamma C_t^*)\frac{\mathrm{d}\theta_{\mathrm{H}}}{\mathrm{dt}} = r_{\mathrm{H_2},ad} - r_{\mathrm{H}} \qquad [18]$$

$$(F\gamma C_t^*)\frac{\mathrm{d}\theta_{\mathrm{OH}}}{\mathrm{dt}} = r_{\mathrm{OH}} - r_{\mathrm{CO}} \qquad [19]$$

where γ is roughness factor of the electrode (in the units of cm^2 PtRu/cm^2 electrode), C_t^* is the atom mole density per cm^2 PtRu surface.

The material balance for species *i* in the anode chamber is,

$$V_{\mathrm{A}}\frac{dc_i}{dt} = v_0 c_{i,0} - v c_i - N_i A \qquad [20]$$

where V_{A} is the volume of the electrode chamber, assumed here to be well-mixed. v_0 and v are the volumetric inlet and outlet anode flow rates, respectively. $c_{i,0}$ and c_i are the concentrations of species *i* in the inlet and outlet streams, respectively, N_i is the flux of species *i* into the MEA, and A is the geometric area of the MEA in the fuel cell. The flux N_i of H_2, CO or any other species is, in principle, affected by mass transfer limitations through the gas diffusion layer and catalyst layer, as well as by the kinetics of the electrode reactions[25]. But it is reasonable here to assume that the fluxes of CO as well as H_2 are determined solely by the anode kinetics, the limiting current densities being considerably higher than the current densities utilized in this study.

Applying equation [22] for the case of CO results in equation [23], which governs the time variation of the CO concentration in the anode chamber,

$$\frac{P_{\mathrm{H_2}}V_{\mathrm{A}}}{RT}\frac{dx_{\mathrm{CO}}}{dt} = \frac{P_0 v_0}{RT_0}x_{\mathrm{CO}}^0 - \frac{P_0 v}{RT_0}x_{\mathrm{CO}} - \frac{A}{F}r_{\mathrm{CO},ad} \qquad [21]$$

where T is the fuel cell temperature, V_{A} is the volume of the anode chamber, and x_{CO}^0 are the CO mole fractions in the anode feed and the anode compartment outlet, respectively.

Note that the volumetric flow rates are measured at 1atm and 298K, so that P_0 is 1 atm and T_0 is 298K, and not the fuel cell operating pressure and temperature.
Similarly, equation 22 as applied to H_2 in the anode chamber provides,

$$\frac{P_0 v}{RT_0} = \frac{P_0 v_0}{RT_0} - \frac{A}{2F} r_{H_2,ad} \qquad [22]$$

Considering capacitive and Faradaic currents and using the equation of charge conservation, equation for the time evolution of the electrode potential is obtained. The total current is the sum of the Faradaic current and the capacitive current (double layer charging and discharging current). The capacitive current is written as the product of the double layer capacity C_{dl} and the temporal change of the potential. The Faradaic current includes H and CO electrooxidation current and the net current of water dissociation,

$$C_{dl} \frac{d\eta_A}{dt} = A(i - r_H - r_{CO} - r_{OH}) \qquad [23]$$

The resulting system of coupled ODEs (equation 17-19, 21, 23) were solved with Berkeley-Madonna software (Kagi Shareware, Berkeley, CA) using a fourth order Runge-Kutta routine. The parameters used in the simulation are listed in Table 4-2.

4.5.4 Simulation Results

The simulation results are shown in Figure 4-11, together with experimental results under the same conditions, while a magnified simulation result is shown in Figure 4-8b to contrast with the experimental data. It is clear that the simulated oscillation curve captures all of the essential features of the anode potential oscillations. The simulation predicts that the anode overpotential increases gradually to a high value, and then drops to a lower value rapidly, as experimentally observed. The predicted oscillation frequency and the amplitude are also very close to the experiment value. The period is about 2.5 s, which is the same as in experiments. The simulated potential oscillation range is 0.14~0.38 V, with the maximum overpotential some 0.07V lower than the corresponding experimental value. This good agreement between experiment and simulation results

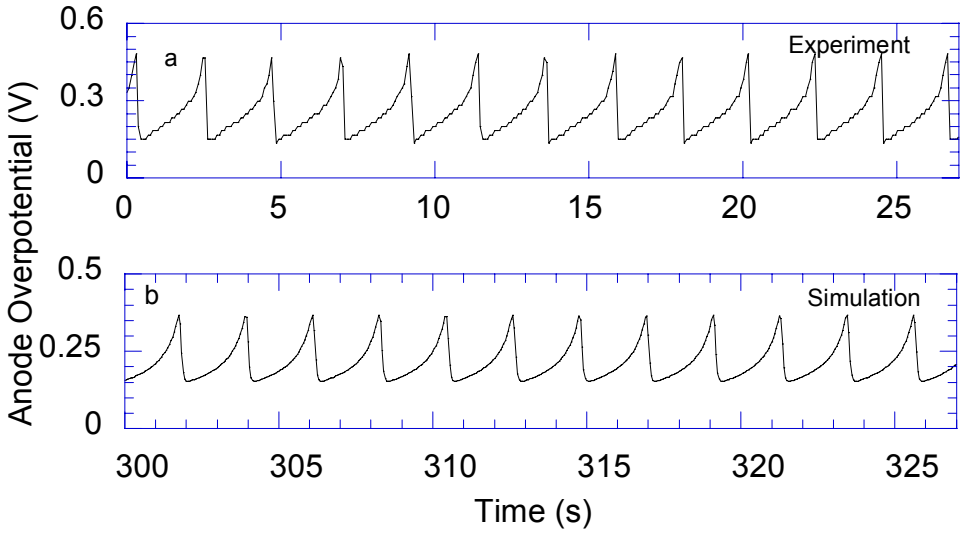

Figure 4-11. Comparison between experimental and simulation results. Fuel cell temperature, 42 °C; current density, 300 mA/cm^2; anode inlet flow rate, 48.1 scc/min. Parameter values used are listed in Table 4-2.

supports the qualitative interpretation of this oscillatory phenomenon described earlier in this chapter.

The computed time evolution of five system variables is shown in Figure 4-12. It is seen, as expected, that the surface coverages of CO, H and OH oscillate, together with the resulting periodic oscillation of CO mole fraction in the anode chamber and the anode overpotential. It may be noted that although the three surface species coverages oscillate simultaneously, the catalyst surface is dominated by CO. The gas phase CO concentration is also predicted to oscillate within a narrow range at the experimental conditions used. It is also interesting to note that these different variables assume different shapes in the time evolution. Figure 4-13 shows the locus of the limit cycle for some of the variables in phase diagram.

It is found in the simulation that the electrooxidation rate constant of CO, $\vec{k}_{\mathrm{CO},ox}$, is a key and a very sensitive parameter for the oscillations to appear. The oscillation patterns simulated with different values of the rate constant are shown in Figure 4-14. It is seen from the figure that with the increase of the rate constant, the oscillation frequency becomes larger and eventually, the oscillations extinguish at still larger values. This result looks qualitatively similar to the temperature effect on oscillation (Figure 4-7). The increase of the rate constant may be viewed as a result of the increase of fuel cell temperature. A rigorous simulation of the temperature effect will need the introduction of appropriate activation energies for the rate constants. Further, a detailed bifurcation analysis is needed to understand the parameter dependence of the oscillatory phenomenon.

In short, with this realistic but simple model, we have shown mechanistically and mathematically that the potential oscillations can exist with a H_2/CO feed to a PEM fuel cell anode. The agreement between experiment and simulation results lends credence to our explanation of the anode kinetics of H_2/CO electrooxidation on PtRu catalyst. This model can also be applied to predict the steady state performance of PtRu anode catalyst with CO impurities in anode feed. Further, it indicates that the parameter values used in this simulation are reasonable, but need to be further investigated.

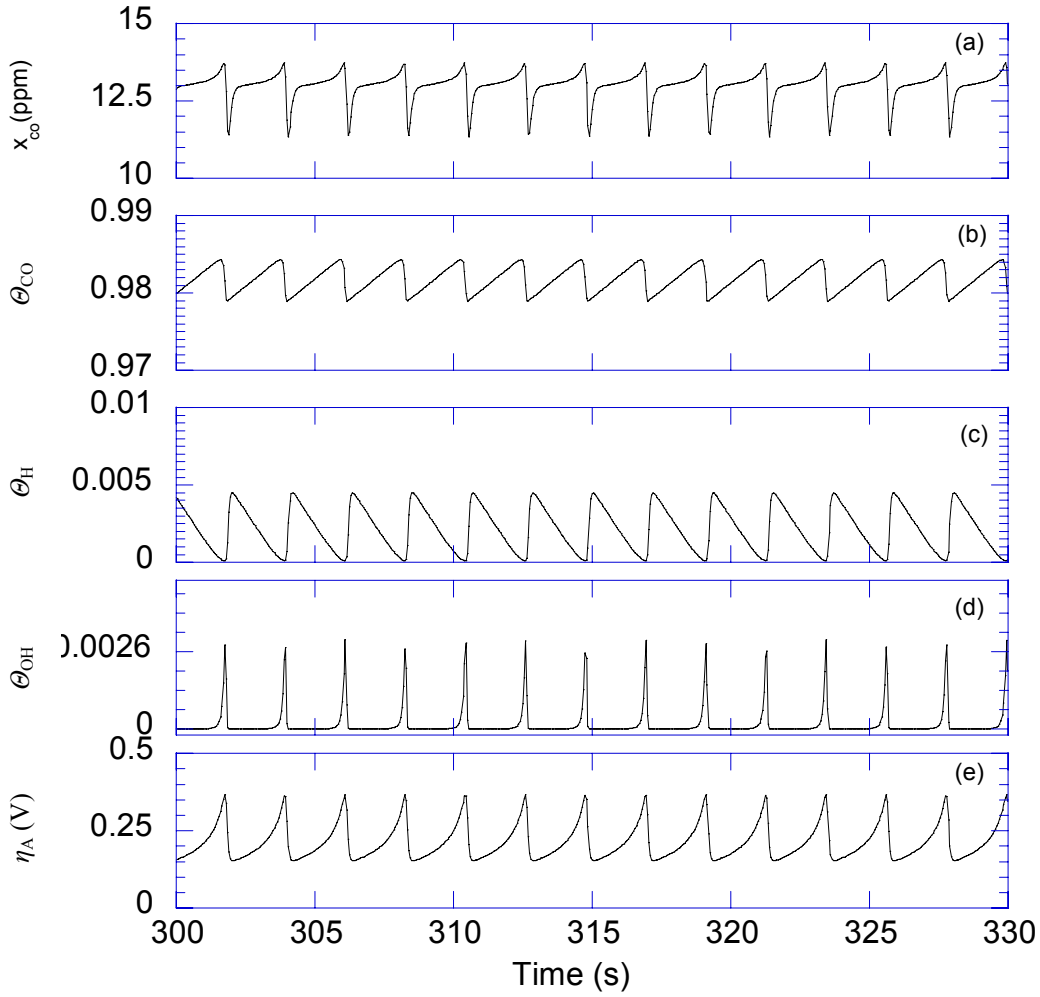

Figure 4-12. Time evolution of (a) anode CO mole fraction. (b) surface coverage of CO. (c) surface coverage of H. (d) surface coverage of OH. (e) anode overpotential for conditions of Figure 4-11. Parameter values used are listed in Table 4-2.

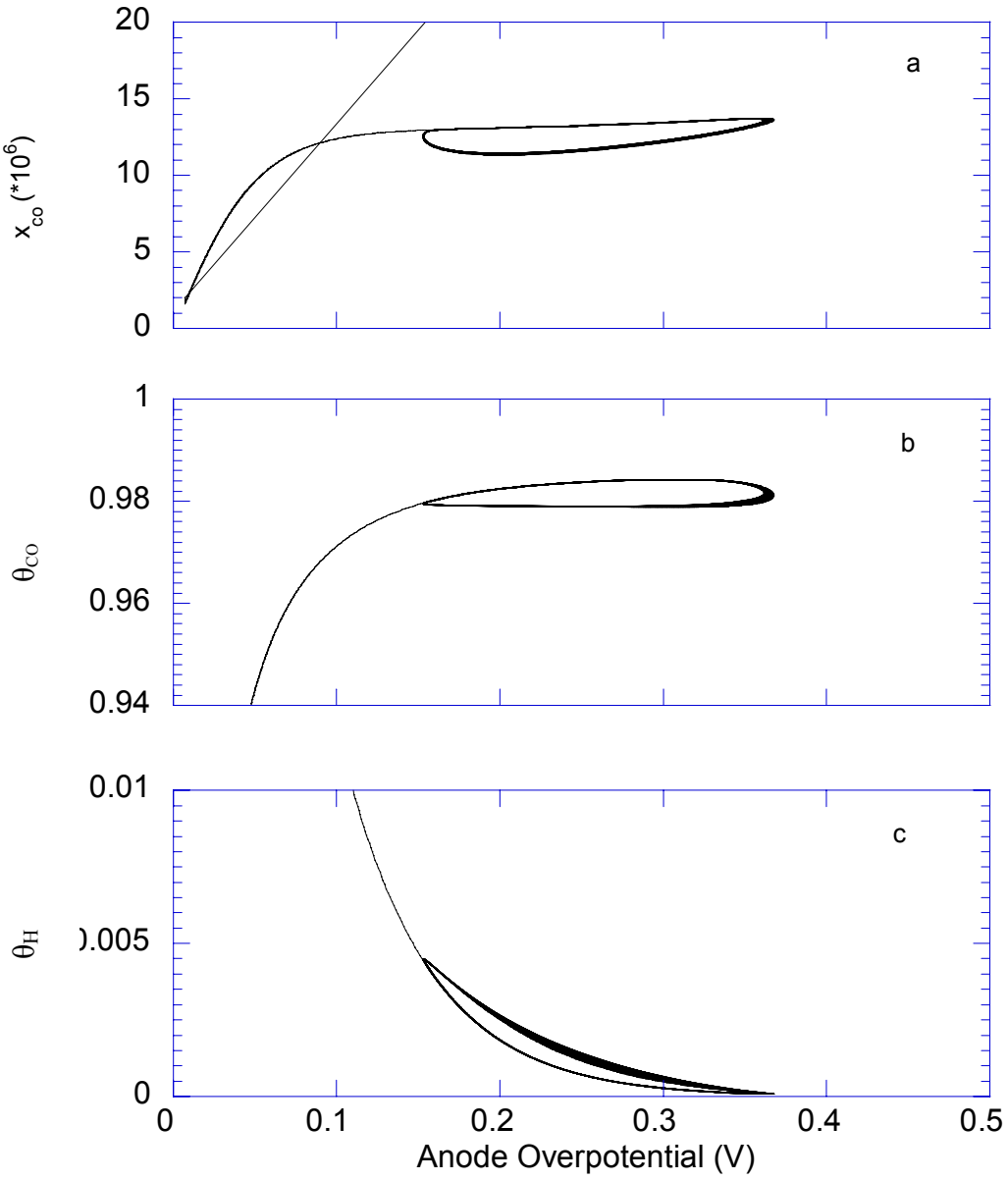

Figure 4-13. Computed phase diagram. (a) anode CO mole fraction. (b) surface coverage of CO. (c) surface coverage of H. versus anode overpotential.

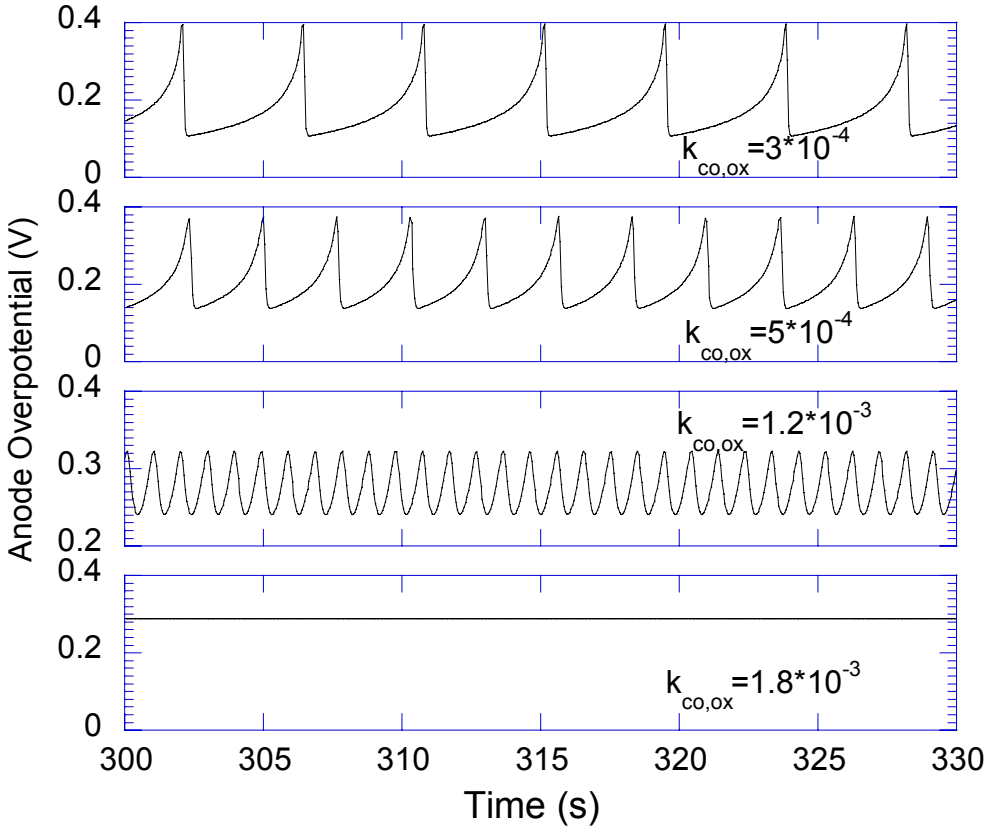

Figure 4-14. Simulated potential oscillation patterns with different values of the CO electrooxidation rate constant. All the other parameter values are the same as in Table 4-2.

4.6 Conclusions

Sustained potential oscillations are found experimentally in a PEM fuel cell operating at constant current density with PtRu as anode catalyst and a H_2/108 ppm CO as anode feed gas. The potential oscillations appear at certain operating conditions determined by fuel cell temperature, current density, and anode flow rate. A preliminary qualitative analysis indicates that these potential oscillations are due to the coupling of the electrooxidation of H_2 and CO on the binary PtRu alloy surface. Ru may be acting as the key component in the formation of OH_{ad} from water, which is the oxidation agent of CO_{ad}. The qualitative analysis also shows that a surface process may be controlling the potential oscillations, such as the dissociation of H_2O or the electrooxidation of CO. A simple but realistic kinetic model is proposed which reproduces the observed oscillatory phenomenon. The rate constant of CO oxidation is found to be a key parameter in the onset of oscillations.

References

1. T. R. Ralph, *Platinm Metals Rev*., **41**, 102 (1997).
2. B. E. Conway, and D. M. Novak, *J. Phys. Chem*., **81**, 1459(1977).
3. P. Russell and J. Newman, *J. Electrochem. Soc*., **133**, 59 (1986).
4. P. Russell and J. Newman, *J. Electrochem. Soc*., **134**, 1051 (1987).
5. J. St-Pierre, and D. L. Piron, *J. Electrochem. Soc*., **137**, 2491 (1990).
6. D. L. Piron, I. Nagatsugawa, and C. Fan, *J. Electrochem. Soc*., **138**, 3296 (1991).
7. H. Okamoto, N. Tanaka, and M. Naito, *J. Electrochem. Soc*., **147**, 2629 (2000).
8. H. Okamoto, N. Tanaka, and M. Naito, *J. Phys. Chem. A* , **102**, 7353 (1998).
9. H. Okamoto, N. Tanaka, and M. Naito, *J. Phys. Chem. A* , **102**, 7343 (1998).
10. G. Inzelt, and V. Kertesz, *Electrochim. Acta*., **40**, 221 (1995).
11. G. Inzelt, and V. Kertesz, *Electrochim. Acta*., **42**, 229 (1997).
12. V. Kertesz, G. Inzelt, C. Barbero, R. Kotz and O. Haas, *J. Electroanal. Chem*., **392**, 91 (1995).
13. H. Hunger, *J. Electrochem. Soc*., **115**, 492 (1968).
14. G. Horanyi, and C. Visy, *J. Electroanal. Chem*., **103**, 353 (1979).
15. T. Yamazaki, T. Kodera, R. Ohnishi and M. Masuda, *Electrochim. Acta.,* **35**, 431 (1990).
16. K. Krischer, M. Lubke, W. Wolf, M. Eiswirth, and G. Ertl, *Ber. Bunsenges. Phys. Chem.*, **95**, 820 (1991).
17. T. Yamazaki, and T. Kodera, *Electrochim. Acta*., **36**, 639 (1991).
18. S. Szpak, *J. Electrochem. Soc*., **117**, 1056 (1970).
19. M. C. Deibert, and D. L. Williams, *J. Electrochem. Soc*., **116**, 1291 (1969).
20. W. Wolf, K. Krischer, M. Lubke, M. Eiswirth and G. Ertl, *J. Electroanal. Chem*., **385**, 85 (1995).
21. H. Okamoto, N. Tanaka, M. Naito, *Chem. Phys. Lett*., **248**, 289 (1996).
22. P. Strasser, M. Eiswirth, and G. Ertl, *J. Chem. Phys*., **107**, 991 (1997).
23. M. Murthy, M. Esayian, A. Hobson, S. MacKenzie, W. Lee, and J. W. Van Zee, *J. Electrochem. Soc.,* **148**, A1141 (2001).
24. G. Ertl, *Science*, **254**, 1750 (1991).
25. T. Thampan, S. Malhotra, J. Zhang, and R. Datta, *Catal. Today*, **67**, 15 (2001).

26. J. Zhang, T. Thampan, and R. Datta, *J. Electrochem. Soc.*, **149**, A765 (2002).
27. H. A. Gasteiger, N. M. Markovic, and P. N. Ross, *J. Phys. Chem*., **99**, 8290 (1995).
28. T. J. Schmidt , H. A. Gasteiger, and R. J. Behm, *J. Electrochem. Soc*., **146**, 1296 (1999)
29. H. A. Gasteiger, N. M. Markovic, and P. N. Ross, *J. Phys. Chem*., **99**, 16757 (1995).
30. J. W. Bauman, T. A. Zawodzinski, Jr., and S. Gottesfeld, in *Proton Conducting Membrane Fuel Cells II*, S Gottesfeld and T. F. Fuller, Editors, PV 98-27, p. 136, The Electrochemical Society Proceedings Series, Pennington, NJ (1997).
31. A. V. Zeigarnik, R. E. Valdes-Perez, and J. Pesenti, *J. Phys. Chem. B*, **104**, 997 (2000).
32. E. Shustorovich, and H. Sellers, *Surf. Sci. Rep*., **31**, 1 (1998).
33. N. M. Markovic, T. J. Schmidt, B. N. Grgur, H. A. Gasteiger, R. J. Behm, and P. N. Ross, *J. Phys. Chem. B*, **103**, 8568 (1999).
34. A. B. Anton, and D. C. Cadogan, *Surf. Sci*., **239**, L548 (1990).
35. J. B. Day, P. Vuissoz, E. Oldfield, A. Weichowski, and J. Ansermet, *J. Am. Chem. Soc.*, **118**, 13046 (1996).
36. T. E. Springer, T. Rockward, T. A. Zawodzinski, and S. Gottesfeld, *J. Electrochem. Soc.*, **148**, A11 (2001).
37. M. T. Koper, T. J. Schmidt, N. M. Markovic, and P. N. Ross, *J. Phys. Chem. B*, **105**, 8381 (2001).

Chapter V

Mechanistic and Bifurcation Analysis of Anode Potential Oscillations in PEM Fuel Cells with CO in Anode Feed

In this chapter, a detailed mathematical analysis is performed to understand the anode potential oscillations observed experimentally in a PEM fuel cell with H_2/CO feed (ref. 9). Temperature and anode flow rate are found to be key bifurcation parameters. The time-dependence of all the key surface species must be accounted for in order for the model to predict the oscillatory behavior, while the time-dependence of CO concentration in the anode chamber need not necessarily be considered. The bifurcation diagram of CO electrooxidation rate constant agrees very well with the effect of temperature on the oscillation pattern. The oscillator model is classified as a hidden negative differential resistance (HNDR) oscillator based on the dynamical response of the anodic current and surface species to a dynamic potential scan. A linear stability analysis indicates that the bifurcation experienced is a supercritical Hopf bifurcation. Contents of this chapter have been published in *J. Electrochem. Soc.*.

5.1 Introduction

There is great interest in the development of cost effective and high performance proton exchange membrane (PEM) fuel cells for applications in the automotive and consumer electronics industries. [1] A stumbling block in the commercialization of PEM fuel cells, however, is the storage and distribution of H_2, which is the ideal fuel for a low temperature, high power density fuel cell. As an alternative, reformate gas containing CO_2 and traces of CO in addition to H_2 obtained from methanol or gasoline is also being investigated. [2] Furthermore, direct use of methanol, [3] propanol, [4] or formic acid[5] as the

anode feed is also being attempted for PEM fuel cells in order to reduce the system complexity and increase overall efficiency.

PEM fuel cells may be operated in a constant current, constant voltage or constant resistance mode. It is of course, theoretically conceivable that spontaneous periodic behavior may appear in this electrochemical reaction system due to the interplay of such factors as chemical and electrochemical reactions, mass transfer, current, and electrode potential. [6,7] The presence of CO, which is either a feed impurity (in reformate fuel) or a reaction intermediate (in direct fuel cells), increases the tendency of such a self-organized instability to appear. [8] Our earlier experiments indicated that periodic potential oscillations exist when the fuel cell is operating with H_2 containing CO and with PtRu as anode catalyst at a constant current density. [9] These spontaneous oscillations were observed over a practical operating temperature range (room temperature to about 80 °C) and current densities.

Although potential oscillations in PEM fuel cells have only recently been reported, the observation of spontaneous potential or current oscillations in other electrochemical systems is not uncommon. [6, 10-12] Nonlinear dynamics in electrochemical reactions has been reviewed by Hudson and Tsotsis.[10] Various examples of oscillatory behavior in electrochemical reaction systems can be found in this exhaustive review. Koper described the importance of negative differential resistance to the instability of an electrochemical system. [11] It was also shown rigorously that the frequency response method is very powerful in evaluating the stability of electrochemical systems. Examples of how the frequency response theory can be applied to such systems can be found in ref. 11. An experimental strategy was proposed by Strasser et al, [13] in an attempt to classify the known electrochemical oscillators based on mechanisms. Krischer recently reviewed the current understanding of basic principles governing temporal and spatial behavior in electrochemical systems exhibiting dynamic instability. [6] It is acknowledged that conditions far from thermodynamic equilibrium and appropriate feedback should be present for the occurrence of self-organized phenomena. The dynamic instability is linked to the interplay of the electrode kinetics, transport processes occurring in the electrolyte, and the external electrical circuit. Consequently, the differential equations governing the temporal evolution of these systems are derived from charge as well as mass balance.

Undoubtedly, the potential oscillations observed in PEM fuel cells serve as another interesting and important case for the study of electrochemical oscillators. Thus, an analysis on such oscillatory phenomenon is essential for its understanding and classification in the family of electrochemical oscillators. Moreover, although the phenomenological characterizations and modeling interpretation are abundant in the literature, [8, 14-17] a mathematical bifurcation analysis is still warranted. In a mechanistic analysis study by Strasser et al, [18] two simplified generic models describing electrochemical reaction systems have been discussed qualitatively in terms of the possible sign pattern of the Jacobian and nature of the eigenvalues. As far as we know, no quantitative demonstration of bifurcation analysis for a PEM fuel cell system has been presented so far. This chapter, thus, presents the first quantitative linear stability analysis on a realistic model describing the dynamic behavior of PEM fuel cell anode reaction system.

A detailed numerical analysis of mechanistic model is given here in terms of the existing theory of electrochemical oscillators. The essential components for describing the experimentally observed oscillation behavior are identified. The model is further classified as a hidden negative differential resistance (HNDR) oscillator based upon the dynamic response of the system. Finally, one parameter bifurcation diagrams are discussed, followed by a local linear stability analysis (details in appendix II). Thus, a Hopf bifurcation is quantitatively demonstrated in the fuel cell system.

5.2 Experimental

The experimental details can be found in our previous work.[19] A brief description is given here. Gas diffusion electrodes loaded with 20%(w/o) Pt/C or PtRu/C, at a metal loading of 0.4 and 0.35 mg/cm^2, respectively, were purchased from E-TEK. PtRu/C was used as anode catalyst, while the cathode catalyst was Pt/C. Nafion® 115 proton-exchange membranes (Du Pont, Fayetteville, PA) were used after treatment. The membrane electrode assembly (MEA) was prepared by hot-pressing in a Model C Carver hot press at 130 °C and under a pressure of 4000 lbs for about 2 minutes. The MEA was then incorporated in a 5 cm^2 single cell from ElectroChem, Inc. (Woburn, MA), and tested in a test station with temperature, pressure, humidity and flow rate control. The

anode feed is H_2/108 ppm CO and oxygen is used as cathode feed. The fuel cell voltage was recorded using a HP 6060B DC electronic load, interfaced with a PC using LabVIEW software (National Instruments, Austin, TX) at a data sampling rate of 77 ms.

In order to monitor the CO concentration in the fuel cell anode outlet gas, the exit gas stream after the back pressure regulator first passes through a stainless steel filter (Model 85, Parker Hannifin, Tewksbury, MA) to eliminate any particulates and water droplets. The gas stream then passes through a membrane gas dryer (MD series, Perma Pure Inc., Toms River, NJ) which further lowers the dew point of the gas stream to below 2 °C before admission to the gas analyzer. A Model 200 IR gas analyzer (California Analytical Instruments, Orange, CA) was used after calibration to monitor the exit CO concentration. The FP-AI-100 analog input module/FP-1000 network module (National Instruments, Austin, TX) is used to collect data from the gas analyzer with LabVIEW software.

5.3 Anode Dynamic Model

The anode kinetic model developed previously[9] is provided below. More details may be found in ref. 9. The symbols are listed separately**.** It should be noted that all the rates (and rate constants) in the model have been expressed as equivalent current densities (A/cm^2) based on the geometric area of the electrode.

5.3.1 Surface Kinetics

The model assumes uniform surface sites, represented by S. It is assumed that alloying between Pt and Ru only alters the energetics and kinetics of the surface reactions.

$$H_2 + 2S \leftrightarrows 2S\text{–}H \qquad \vec{k}_{H_2,ad},\ K_H \qquad [1]$$

$$S\text{–}H \leftrightarrows S + H^+ + e^- \qquad \vec{k}_{H,ox} \qquad [2]$$

$$CO + S \leftrightarrows S\text{–}CO \qquad \vec{k}_{CO,ad},\ K_C \qquad [3]$$

$$H_2O + S \leftrightarrows S\text{–}OH + H^+ + e^- \qquad \vec{k}_{OH},\ \overleftarrow{k}_{OH} \qquad [4]$$

$$S\text{–}OH + S\text{–}CO \rightarrow 2S + CO_2 + H^+ + e^- \qquad \vec{k}_{CO,ox} \qquad [5]$$

The net adsorption rate for H_2 is,

$$r_{\mathrm{H}_2,ad} = \vec{k}_{\mathrm{H}_2,ad} p_{\mathrm{H}_2} \theta_0^2 - \vec{k}_{\mathrm{H}_2,ad} K_{\mathrm{H}} \theta_{\mathrm{H}}^2 \quad [6]$$

where θ_0 is from the total site balance,

$$\theta_0 = 1 - \theta_{\mathrm{CO}} - \theta_{\mathrm{H}} - \theta_{\mathrm{OH}} \quad [7]$$

The rate for hydrogen electrooxidation is,

$$r_{\mathrm{H}} = 2\vec{k}_{\mathrm{H},ox} \theta_{\mathrm{H}} \sinh\left(\frac{\alpha_{\mathrm{H}} F \eta_{\mathrm{A}}}{RT}\right) \quad [8]$$

The net rate of CO adsorption is,

$$r_{\mathrm{CO},ad} = \vec{k}_{\mathrm{CO},ad} x_{\mathrm{CO}} p_{\mathrm{H}_2} \theta_0 - \vec{k}_{\mathrm{CO},ad} \mathrm{K}_{\mathrm{C}} \theta_{\mathrm{CO}} \quad [9]$$

The water dissociative adsorption rate is,

$$r_{\mathrm{OH}} = \vec{k}_{\mathrm{OH}} \theta_0 \exp\left(\frac{\alpha_{\mathrm{OH}} F \eta_A}{RT}\right) - \overleftarrow{k}_{\mathrm{OH}} \theta_{\mathrm{OH}} \exp\left(\frac{-(1-\alpha_{\mathrm{OH}}) F \eta_A}{RT}\right) \quad [10]$$

The CO oxidation rate is,

$$r_{\mathrm{CO}} = \vec{k}_{\mathrm{CO},ox} \theta_{\mathrm{CO}} \theta_{\mathrm{OH}} \exp\left(\frac{\alpha_{\mathrm{CO}} F \eta_{\mathrm{A}}}{RT}\right) \quad [11]$$

5.3.2 Mass and Charge Conservation

With the above rate expressions, we can write the following unsteady-state site balance for the time evolution of the surface coverage of CO, H and OH,

$$(F\gamma C_t^*) \frac{\mathrm{d}\theta_{\mathrm{CO}}}{\mathrm{dt}} = r_{\mathrm{CO},ad} - r_{\mathrm{CO}} \quad [12]$$

$$(F\gamma C_t^*) \frac{\mathrm{d}\theta_{\mathrm{H}}}{\mathrm{dt}} = r_{\mathrm{H}_2,ad} - r_{\mathrm{H}} \quad [13]$$

$$(F\gamma C_t^*) \frac{\mathrm{d}\theta_{\mathrm{OH}}}{\mathrm{dt}} = r_{\mathrm{OH}} - r_{\mathrm{CO}} \quad [14]$$

The following equations governs the time variation of the CO concentration in the anode chamber considered as well-mixed,

$$\frac{p_{H_2} V_A}{RT}\frac{dx_{CO}}{dt} = \frac{P_0 v_0}{RT_0} x_{CO}^0 - \frac{P_0 v}{RT_0} x_{CO} - \frac{A}{F} r_{CO,ad} \qquad [15]$$

Similarly, balance for H_2 in the anode chamber provides

$$\frac{P_0 v}{RT_0} = \frac{P_0 v_0}{RT_0} - \frac{A}{2F} r_{H_2,ad} \qquad [16]$$

Considering capacitive and Faradaic currents and using the equation of charge conservation, equation for the time evolution of the electrode potential is obtained. The total current is the sum of the Faradaic current and the capacitive current (double layer charging and discharging current).

$$C_{dl}\frac{d\eta_A}{dt} = A(i - r_H - r_{CO} - r_{OH}) \qquad [17]$$

The resulting system of coupled ODEs (equation 12-14, 15, 17) were solved with Berkeley-Madonna software (Kagi Shareware, Berkeley, CA) using a fourth order Runge-Kutta routine. The above model predicts that periodic potential oscillations exists under our experimental conditions, and also provides reasonable prediction of both the oscillation periods and magnitude. The computation results shown in the following section are obtained using parameters given in ref. 9 unless otherwise noted.

5.4 Results and Discussion

5.4.1 Temperature as an Experimental Bifurcation Parameter

Electrochemical systems, under certain conditions, lose stability upon the change of certain control parameters. Applied potential, applied current, and bulk concentration of reactants are often reported to be such parameters. [7, 20,21] However, literature reports on temperature as a bifurcation parameter are rare.[22] During our study of anode potential oscillations in PEM fuel cell with PtRu anode catalyst, we found that fuel cell

temperature is a very sensitive bifurcation parameter. The anode overpotential patterns at five different fuel cell temperatures are shown in Figure 5-1. It is seen that for fuel cell temperatures below 70 °C, sustained potential oscillations exist under the specified experimental conditions. However, the oscillations disappear at a fuel cell temperature of 80 °C, and a stable steady state is obtained. Clearly temperature is acting as a bifurcation parameter, upon the change of which the system behavior changes. However, temperature effect has rarely been investigated in oscillatory electrochemical systems in the previous literature, [22] possibly because of the use of liquid electrolytes.

Another feature worth mentioning is the change of oscillation period and magnitude with temperature. The oscillation period becomes longer as the temperature reduces from the bifurcation point (somewhere between 70 and 80 °C). Moreover, the magnitude of oscillation increases as temperature decreases. These characteristics are very typical for a Hopf bifurcation (discussed below).

5.4.2 Electrode Properties Essential for the Description of Nonlinear Behavior

There are two characteristic properties of fuel cell electrode which are important for the successful description of the dynamic behavior of the anode reaction system. The first one is the anode capacitance, which will directly affect the magnitude of the charging and discharging current. As shown in a recent study by Kim *et al*[23], the total specific capacitance of a porous carbon electrode is determined primarily by the real surface area of the electrode. It has been determined that for carbon power with BET surface area of 2408 m^2/g, the specific capacitance is 217 F/g. [23] The electrode used in this work is an E-TEK standard double sided electrode. The carbon power used is Vulcan XC-72 R carbon black with an average particle size of 30 nm and a specific surface area of 254 m^2/g. [24] If it is assumed that the capacitance of the carbon power is proportional to the surface area, then the porous carbon in this work can be estimated to have a specific capacitance of 22.9 F/g.

The carbon loading in the diffusion layer[24] is about $4mg/cm^2$, and the catalyst loading is 0.35 mg/cm^2. The metal loading (PtRu) in the supported catalyst is 20% (w/o). Then the total carbon loading in the anode is about 27 mg (20 mg in the diffusion layer

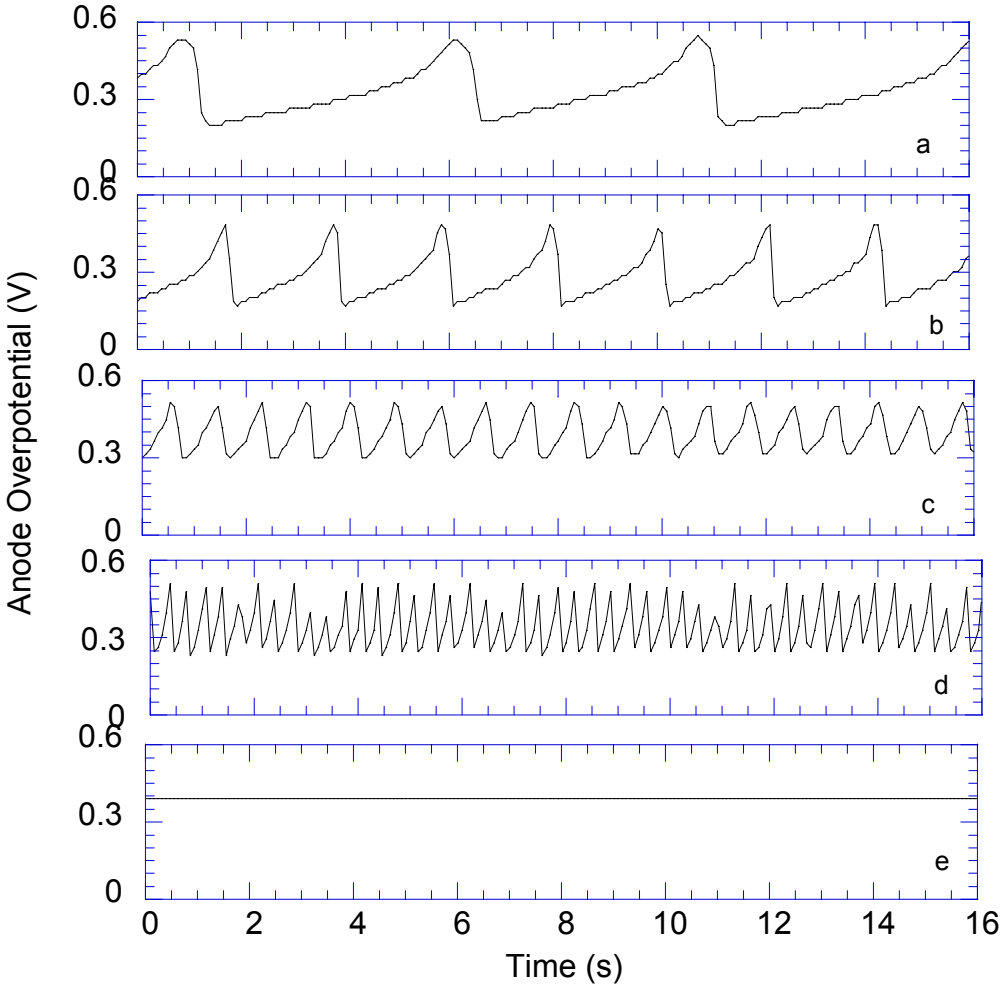

Figure 5-1. Anode potential patterns (periodic oscillations and stable steady state) in PEM fuel cell at different temperatures and a constant current density. The fuel cell temperature, current density and anode inlet flow rate are as follows: (a) 32 °C, 100 mA/cm^2, 24.5 sccm (b) 42 °C, 300 mA/cm^2, 36.4 sccm (c) 55 °C, 300 mA/cm^2, 48.1 sccm (d) 70 °C, 700 mA/cm^2, 95.6 sccm (e) 80 °C, 700 mA/cm^2, 83.7 sccm. Anode feed , H_2/108 ppm CO in all cases. The oscillation patterns are not affected appreciably by the current density and anode inlet flow rate (ref. 9).

and 7 mg in the catalyst layer). Thus, the total capacitance of the porous electrode in the PEM fuel cell anode in this study is estimated to be 0.62 F. This value agrees reasonably well with the value used previously in the simulation (0.45 F).[9]

The second electrode property of importance in discussing instability is the roughness factor of electrode, which is used to characterize the real catalyst surface area available per geometric electrode surface area. The reaction rates are directly related to catalytic sites available in the porous electrode. The roughness factor depends upon the catalyst loading, the metal particle size (dispersion) and ionomer and PTFE loading in the electrode. [25] Such dependence is due to the fact that electrochemically active catalyst site should be accessible by reactant gas, protons and electrons simultaneously. The roughness factor in this study was not independently measured, but estimated from literature result. It is reported by Adjemian et al[26] that an average roughness factor of 135 cm^2/cm^2 was found for an E-TEK Pt/C electrode with a Pt loading of 0.4 mg/cm^2 and an Nafion loading of 0.6 mg/cm^2. The electrode used in this study is also an E-TEK standard electrode, with the metal particle size and ionomer loading being the same. Thus, the roughness factor of the electrode in this study can be estimated based on actual metal loading. The result obtained (118 cm^2/cm^2) agrees well with the value used in the simulation (100 cm^2/cm^2).[9]

5.4.3 Current Carrier and Essential Variables

An individual electrochemical reaction step within a mechanism of multiple reactions can be considered the "current carrier" of the mechanism, if it provides the bulk portion of the total faradaic current at all times. The three contributions of the Faradaic current in this anode model, *i.e.,* H_2 electrooxidation current, CO electrooxidation current and H_2O dissociatively adsorption current, are shown in Figure 5-2a. It is evident that the contribution from CO electrooxidation and water dissociation is rather small as compared to that from H_2 oxidation, the difference being at least two orders of magnitude. Thus the hydrogen electrooxidation is the major current carrier. When the two minor current contributions are neglected in the overall charge conservation equation (Equation [17]),

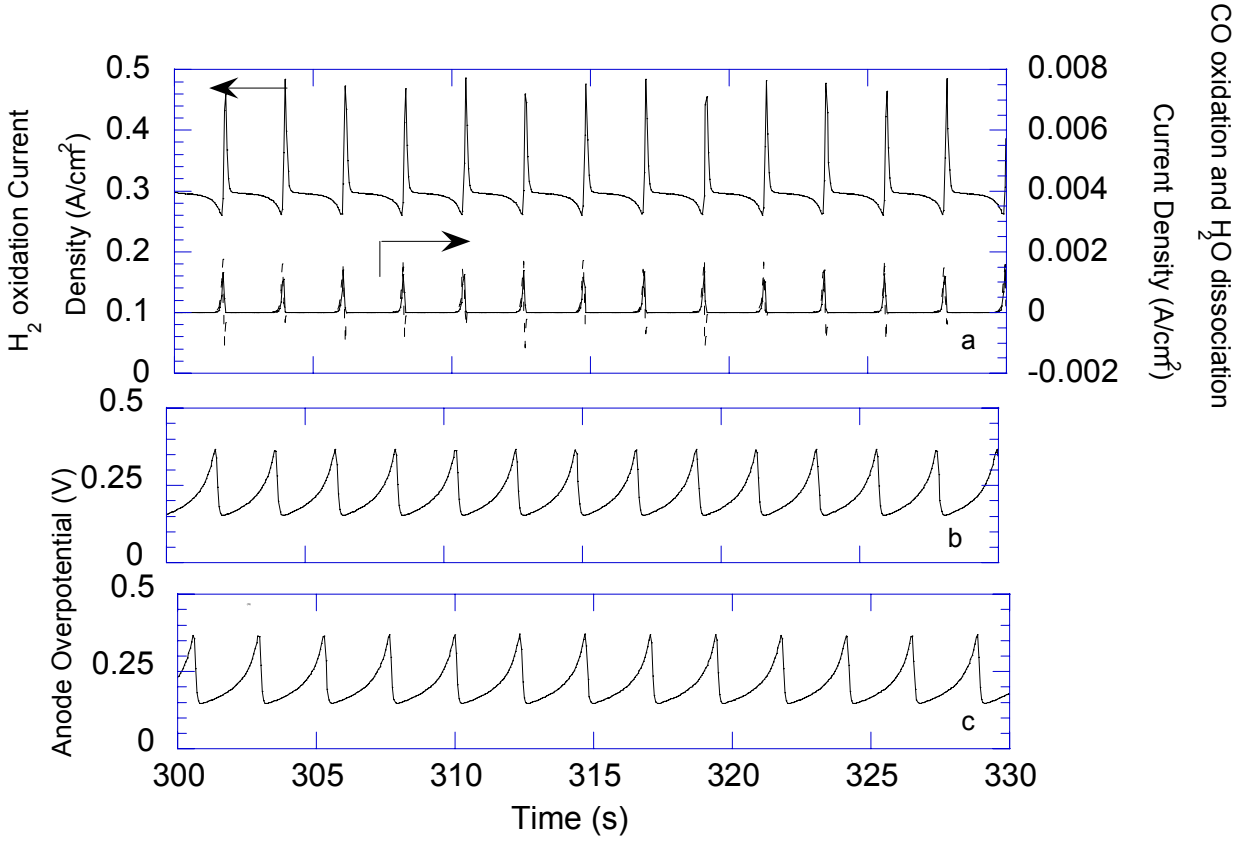

Figure 5-2. Comparison of the current providing reactions. (a) magnitude of H_2 oxidation current, CO oxidation current and H_2O dissociation current. For right y axis, solid line, CO oxidation current; dashed line, H_2O dissociation current. (b) oscillation pattern calculated with all the three current providing reactions. (c) oscillation pattern calculated with H_2 oxidation current only.

the model, as expected, can still reproduce the oscillation pattern, without appreciable change in the oscillatory behavior (Figure 5-2c).

It is found computationally that the three surface species (CO, H, OH) are all essential variables, *i.e.*, the time dependence of all these is indispensable for the overall reaction dynamics. No oscillations are obtained when any one of the three surface coverages is set to a constant value. However, the time dependence of anode CO concentration (x_{CO}) is found to be not essential for the model to predict oscillations. Figure 5-3 shows the simulated oscillation pattern with the complete model (Figure 5-3a) or with constant values of x_{CO} (Figures 5-3b and 5-3c). Consequently, when the five ODEs are reduced to four, the model still displays oscillatory behavior. However, it is found that the actual value of the constant anode CO concentration has very large effect on the shape of oscillation pattern. Thus, when the feed CO concentration (108 ppm) is used as the anode chamber CO concentration, the model predicts an oscillation with a much shorter period than that observed experimentally. However, reasonable agreement between experiment and simulation (Fig. 5-3c) is realized when the assumed constant anode chamber CO concentration is around the CO concentration predicted by the CO mass balance equation. It should also be noted that if the assumed CO concentration (x_{CO}) is less than about 8 ppm, no oscillation is predicted by the model. Therefore, although the CO concentration in the anode chamber need not necessarily be time-dependent for the system to demonstrate oscillatory behavior, the steady-state material balance of CO in the anode chamber (equation [15] with $dx_{CO}/dt = 0$) is absolutely necessary for the model to reflect the real anode CO concentration as measured experimentally with the CO analyzer, [19] and to reproduce the experimental potential oscillation pattern.

In order to check if the anode CO concentration in an operating fuel cell is oscillating simultaneously with anode overpotential, an on-line CO gas analyzer was used to monitor the anode exit gas steam. We were, however, unable to observe any CO concentration oscillations in the fuel cell anode outlet stream. However, a constant CO concentration of 10 ppm is observed for an inlet CO of 100 ppm, which is in good agreement with the model prediction of a CO concentration between 11~13 ppm.

Apart from the possibility that the anode CO concentration does not oscillate in reality, another reason for not observing CO concentration oscillation in our experiment

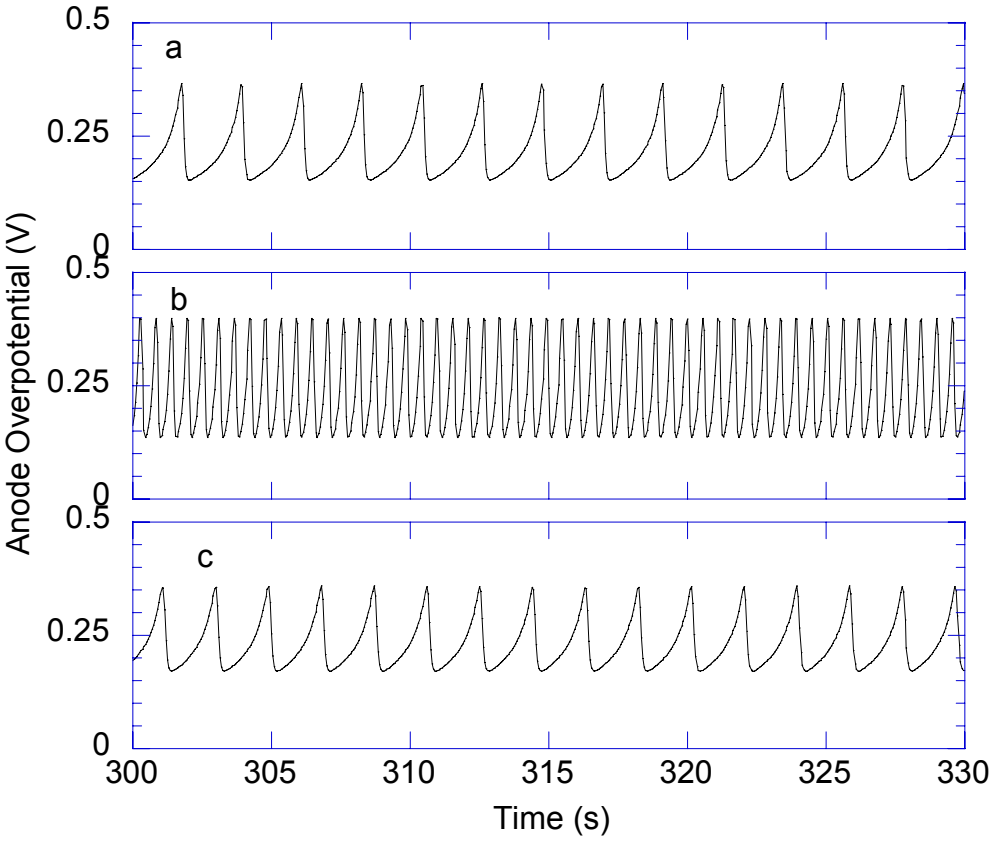

Figure 5-3. Simulation of oscillation pattern with and without anode CO concentration as a time-dependent variable. (a) CO concentration as a time-dependent variable in the model. (b) with a constant anode CO concentration x_{co}=108 ppm. (c) with a constant anode CO concentration x_{co}=12 ppm.

is that the oscillation has a period of only 0.3 to 5 seconds, while the response time of the analyzer is on the order of a second at designed flow rate (> 500 scc/min, while the flow rate used in this study is well below 100 scc/min). Thus, the response time of the analyzer is of the same order as the oscillation periods. In addition, the anode outlet gas has to pass a filter and a dryer before admitted to the IR gas analyzer, thus the dispersion effects may smear out any concentration variations during the travel of the gas stream between the anode and the analyzer.

5.4.4 Mechanistic Classification of the Anode Potential Oscillation

There are a large number of oscillatory systems in electrochemical processes. A systematic classification of such oscillators is useful in elucidating and simplifying the origin of the oscillatory behavior. The classification has been based on such factors as the operating conditions, the reaction chemistry, and most recently, on the mechanistic role of potential and chemical species.[13] In this section, the anode model is used to predict the system behavior in a potential scan, the response of which provides insight on the characterization of the oscillatory phenomenon[6]. The calculated cyclic voltammogram for a linear rate of 20 mV/s is shown in Figure 5-4 and Figure 5-5b. It should be pointed out that the hydrogen current is assumed to be not limited by hydrogen mass transport in the electrode, since the anode limiting current density is usually very large. [25] Thus, the hydrogen limiting current in the anode is not reflected in the computed cyclic voltammogram in Figure 5-4 and 5-5b.

In Figure 5-4, the overall anode current in the forward and reverse scan is plotted versus the anode overpotential at a scan rate of 20 mv/s. It indicates that the overall current density does not increase appreciably until an anode overpotential of about 0.35 V is reached in the anodic scan. The current increases dramatically after this “ignition potential”. However, the current decreases when a peak value is reached at about 0.4 V. In the reverse scan, the overall current density traces the anodic scan in the potential region higher than 0.4 V, but below that, the overall current density does not follow the forward scan. The current begins to drop precipitously only when the anode overpotential is lower by about 50 mV. Thus, a hysterisis is observed in the calculated cyclic

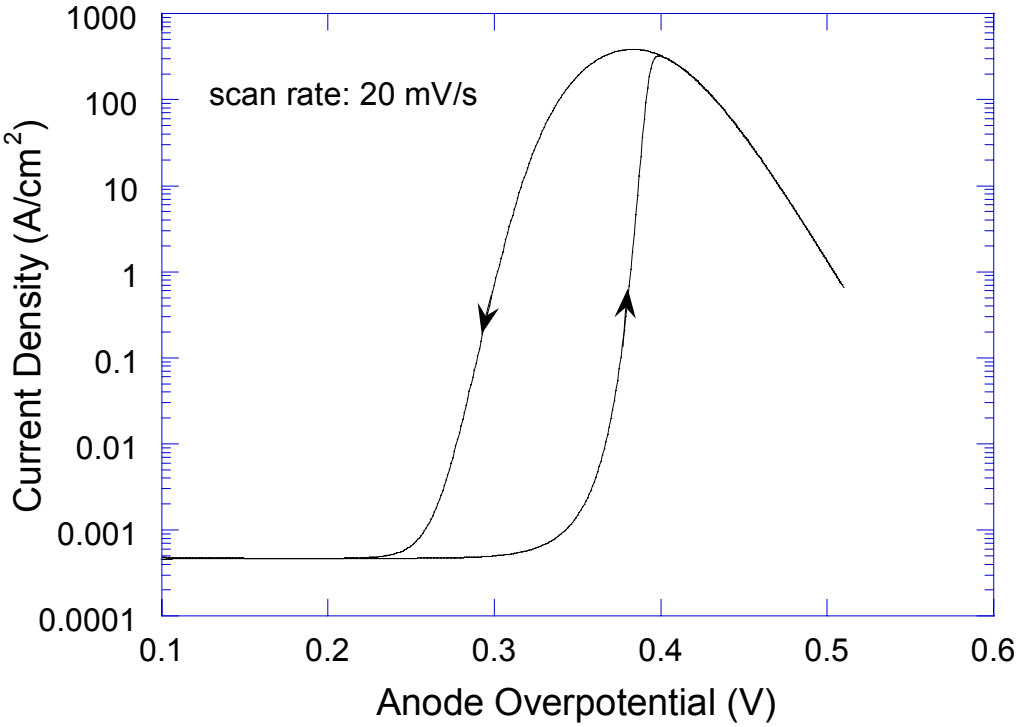

Figure 5-4. Calculated cyclic voltammogram of fuel cell anode at a scan rate of 20 mV/s.

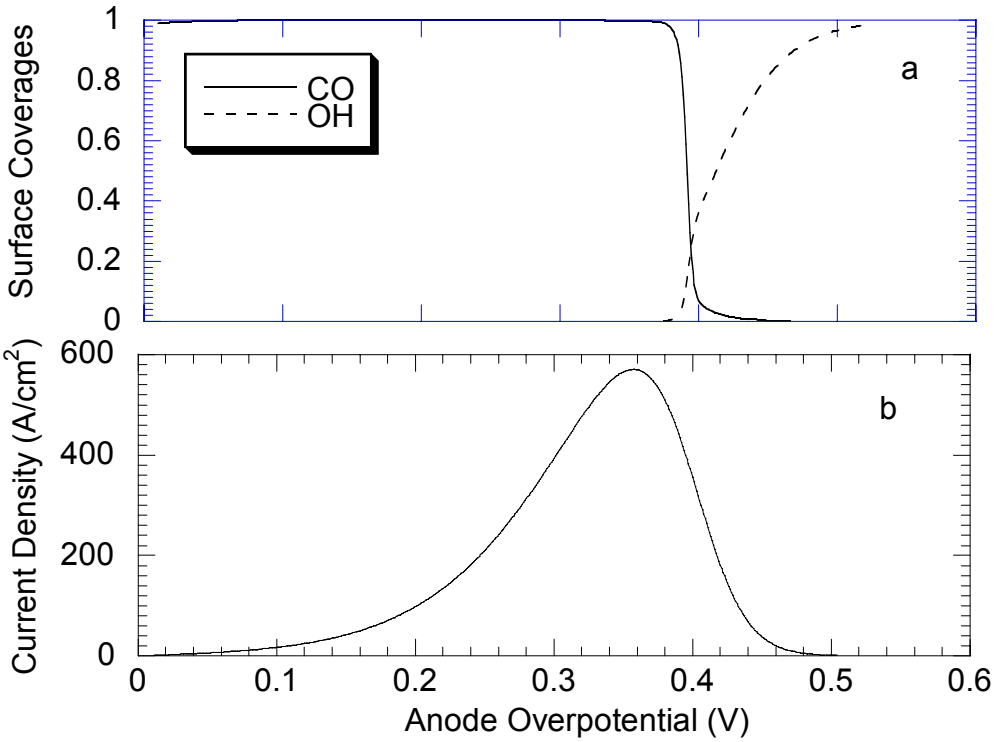

Figure 5-5. Calculated surface coverage of CO and OH (a) and H_2 oxidation current without the presence of CO (b) in the forward scan at 20 mV/s.

voltammogram. Hysterisis in cyclic voltammogram during a dynamic potential scan has been observed in the study of H_2/CO electrooxidation in the liquid electrolyte[27, 28]. This dynamic response is especially similar to the experimental cyclic voltammetry curve reported by Krischer et al[29] in H_2 electrooxidation when Cu^{2+} and Cl^- are present in the electrolyte solution (Figure 13c in ref. 29).

Hydrogen electrooxidation is an extremely fast reaction and the initial low current density in Figure 5-4 is due to the surface blockage by adsorbed CO. Thus the corresponding change of surface coverage of both CO and OH in the forward scan is shown in Figure 5-5a. It can be seen that the catalyst surface is dominated by CO when the anode overpotential is lower than about 0.38 V. In this potential region, hydrogen electrooxidation can barely proceed on the CO covered surface. When the anode overpotential is larger than 0.38 V, the surface coverage of CO decreases precipitously. But correspondingly, the surface coverage of OH gradually increases and approaches a saturation value as the anode overpotential further increases. Therefore, the catalyst surface will be dominated by OH groups, which leads to the eventual decrease of the overall current density, as shown in Figure 5-4. Thus, in this region of the stationary current-potential curve (Figure 5-4), a "negative differential resistance" appears, *i.e.*, the total current decreases with the increase of electrode potential. This negative differential resistance is known to be one of several features which are necessary for the existence of electrochemical instability. [7, 11] The surface coverage of H is not shown in Figure 5-5a, it follows the same trend as the current density in forward scan in Figure 5-4.

The negative differential resistance can be seen more clearly in the absence of CO both in the gas phase and on the catalyst surface. The anodic current without CO in the feed is shown in Figure 5-5b. It may be noted that the negative polarization slope now appears at a potential of 0.36 V, whereas in the presence of CO (Figure 5-4), the current is still increasing at this anode overpotential. Thus, a part of the negative resistance caused by OH nucleation becomes "hidden" via the reactive removal of CO from the catalyst surface with OH. Only after most of the CO has been removed does the effect of the negative Faradaic impedance become distinguishable. Moreover, galvanostatic oscillations are found both in our models and in the experiments. All these features are

the characteristics of a class of electrochemical oscillator termed as hidden negative differential resistance (HNDR) oscillator by Krischer[6] and Strasser *et al*[13].

A comparison between the PEM fuel cell anode reaction system in this work with examples of HNDR oscillators in the literature further supports the above classification. The oscillatory system in this study has the following essential components of a HNDR oscillator: (1) a current carrying process (H electrooxidation, which depends upon the anode overpotenital); (2) a process responsible for the occurrence of the negative differential resistance (potential-dependent adsorption and desorption of OH); and (3) a potential-dependent process in which potential has a positive effect on the reaction rate (reactive removal of CO). Another important feature for HNDR oscillator is the relative time scale of different processes. In this case, the OH adsorption, which is potential dependent, being a very fast process is of prime importance for the occurrence of potential oscillations.

Besides the essential components, the simultaneous presence of a fast positive destabilizing feed back loop and a slow negative stabilizing feedback loop have also been identified in our model, in a manner similar to that of Strasser *et al*. [17] The two feedback loops are depicted in Figure 5-6. The positive feedback loop operates as follows: since hydrogen electrooxidation is the main current carrying reaction, an increase of the number of free sites results in an increase of H surface coverage θ_H, which tends to increase the current (equation [8]). Since the total current is controlled at a constant value I, the system dynamics automatically lowers the anode overpotential, which in turn leads to a reduction of OH (equation [10]) and release of more free surface sites (equation [7]). The negative feedback loop is depicted in Figure 5-6a. The surface species θ_{CO} participates in this negative feedback loop, which is negatively impacted by θ_{OH}, but has a negative effect on θ_H as well. The potential dependent reduction of surface OH is crucial for the model to reproduce the oscillation phenomenon. If the water dissociation is assumed to be an irreversible step in the model, no oscillations are predicted. Thus, the reverse reaction in Equation 4 is an essential feedback for the appearance of oscillations. Moreover, the different time scales of CO and OH adsorption are of great importance in the feedback loops of potential oscillations.

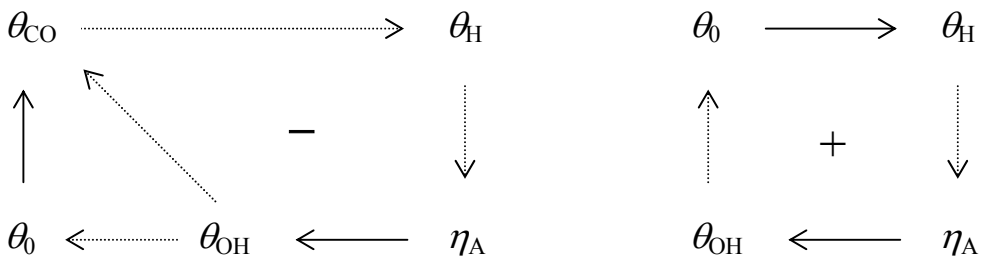

(a) Slow negative feedback loop (b) Fast positive feedback loop

Figure 5-6. Positive and negative feedback loops in the anode dynamic model. The solid (dashed) arrow indicates a positive (negative) influence. An even number of negative influences lead to positive effect, and an odd number of negative influences lead to negative feedback loop.

The phase angles of different variables are compared in Figure 5-7. It can be seen that the variables, though oscillating simultaneously, assume different phase angles. It is seen that the increase of the anode overpotential lags behind the increase of θ_{CO}, while the increase of anode overpotential η induces the increase of θ_{OH}. These two variables are almost in phase, and θ_{OH} follows the variations of η almost without delay. This is in agreement with the fact that the positive feedback loop is a fast one.

As a typical example of an HNDR oscillator, galvalnostatic potential oscillation is observed under practical fuel cell operating conditions. It is believed that a potentiostatic current oscillation is also possible for an HNDR oscillator. [6, 11] However, current oscillations were not observed when the fuel cell voltage was held constant. One possible reason may be that there is no serial resistance large enough to bring the current and anode potential down to the bifurcation region. It has been reported that current oscillation was observed only after a large serial resistance is introduced. [30] Another possible reason is the self-adjustment of fuel cell electrode potential. In fact, in our fuel cell experiments, it is the potential difference between the anode and cathode that is controlled when the fuel cell voltage is held constant. It was shown by Springer et al[31] that the anode and cathode potential has a self-adjustment mechanism in voltage control mode. Thus, the overall potential drop will redistribute along anode, membrane and cathode so as to generate a maximum current, which may be responsible for the disappearance of any current oscillations as well.

5.4.5 One Parameter Bifurcation Diagrams

It has been experimentally observed that the potential oscillations set in at certain operation conditions. [9] The fuel cell temperature, current density and anode flow rate are found to be the key operating parameters affecting the onset of potential oscillations. The one parameter bifurcation diagrams for the above parameters are computed with the anode dynamic model. The bifurcation diagram for the anode inlet flow rate is shown in Figure 5-8 for a temperature of 42 °C and a current density of 300 mA/cm^2. It can be seen that oscillation starts at a smaller flow rate, which is in agreement with the experimental observations. The oscillation amplitude is predicted to increase with the anode inlet flow

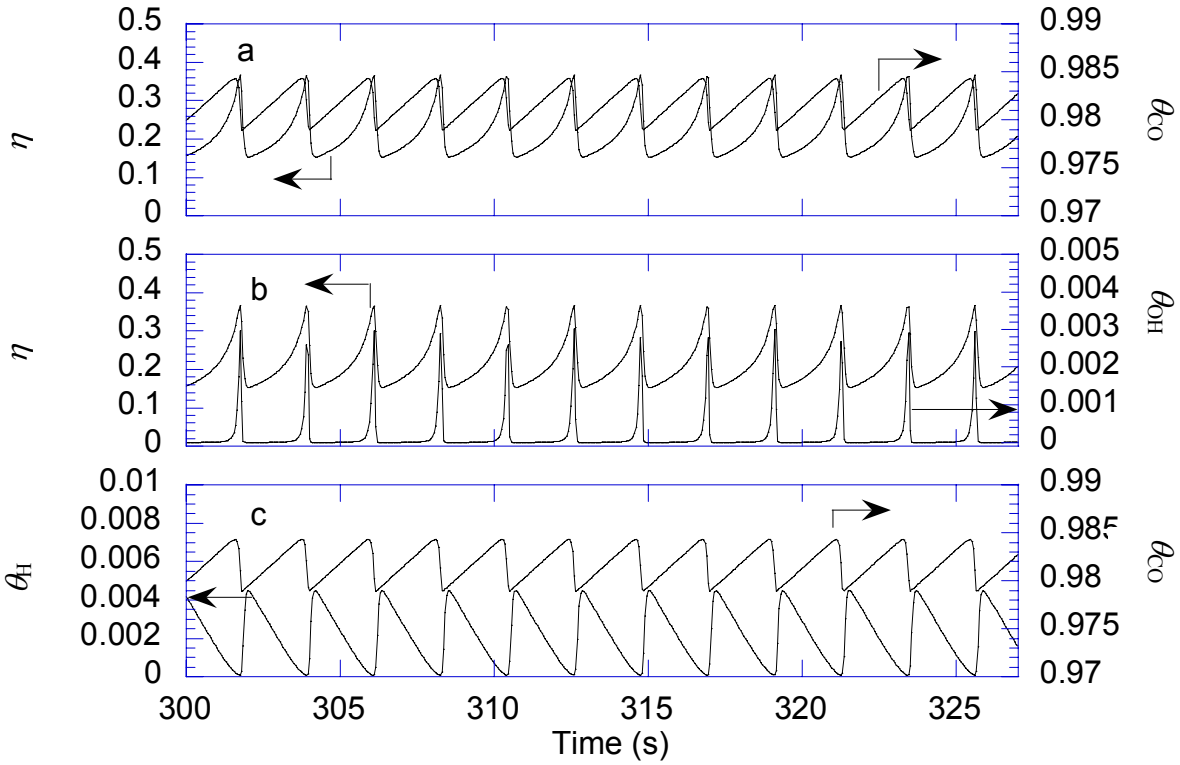

Figure 5-7. Comparison of the phase angle of the essential variables.

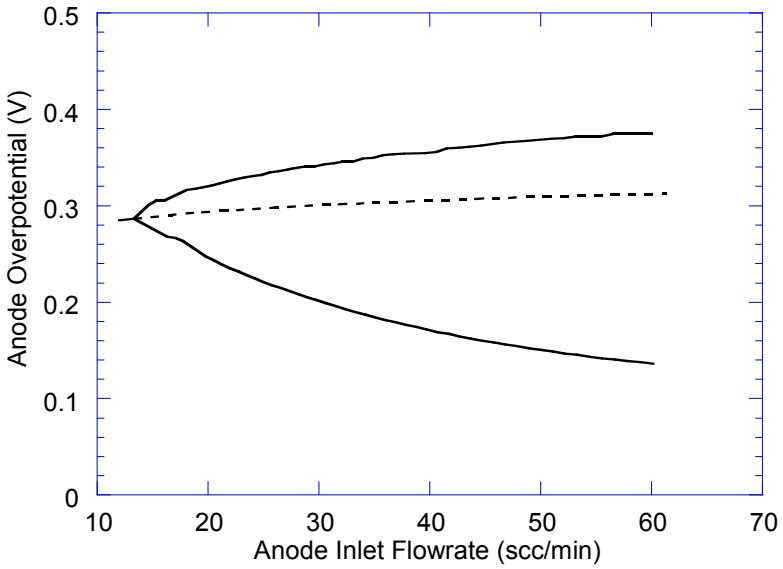

Figure 5-8. One parameter bifurcation diagram for the anode inlet flow rate. The dashed-line symbolizes the unstable steady state; the upper and lower branch of the solid line indicates the maximum and minimum overpotential in the oscillations. Temperature, 42 °C; Current density, 300 mA/cm^2.

rates, which is also observed experimentally. [9] Furthermore, it is predicted that the oscillation period does not change appreciably with the increase of anode inlet flow rate, especially within the flow rate range of the experiment. This is also in agreement with the experimental observations. [9]

As a reflection of the effect of temperature (Figure 5-1), the CO electrooxidation rate constant $\vec{k}_{\mathrm{CO},ox}$ turns out to be a crucial parameter for the shape of the calculated oscillation pattern. [9] The computed one parameter bifurcation diagram in terms $\vec{k}_{\mathrm{CO},ox}$ is illustrated in Figure 5-9. The other model parameters are kept unchanged. The rate constant is, of course, related to the fuel cell temperature through the Arrhenius equation. It is shown that for large $\vec{k}_{\mathrm{CO},ox}$ (high temperature), a stable steady state anode overpotential is observed. As $\vec{k}_{\mathrm{CO},ox}$ decreases (temperature lowers), the stable steady state loses its stability via a supercritical Hopf bifurcation (as discussed in next section). The dashed-line in the figure symbolized the unstable steady state, which appears as sustained potential oscillations, with the maximum and minimum overpotential indicated by the upper and lower branch of the solid line. It is shown that the oscillation amplitude is small near the bifurcation point, while the amplitude grows when $\vec{k}_{\mathrm{CO},ox}$ (temperature) is far from the bifurcation point. When $\vec{k}_{\mathrm{CO},ox}$ is small enough (e.g., 5.5×10^{-6}), no oscillatory solution is obtained. Instead, only a steady-state point is found. It should be pointed out that the non-smoothness in the curve near the bifurcation point in figure 5-8 and 5-9 is due to the discrete manner in the computation.

It has been shown that potential oscillations do not exist experimentally for PEM fuel cells with Pt anode under identical experimental conditions.[9] This observation may be justified mathematically by the model as well. It is computationally found that when the water adsorption rate constant $\vec{k}_{\mathrm{OH}}$ is lower than a certain value (e.g., $< 1\times10^{-5}$ A/cm^2 which corresponds to 4.71×10^{-4} s^{-1}, is similar to the value of 10^{-4} s^{-1} used for $\vec{k}_{\mathrm{OH}}$ of Pt in ref. 8), no oscillation is predicted by the dynamic model. The decreasing of water adsorption rate constant may simulate the change of the catalyst from PtRu to Pt. Therefore, the disappearance of oscillations at smaller value of water adsorption rate

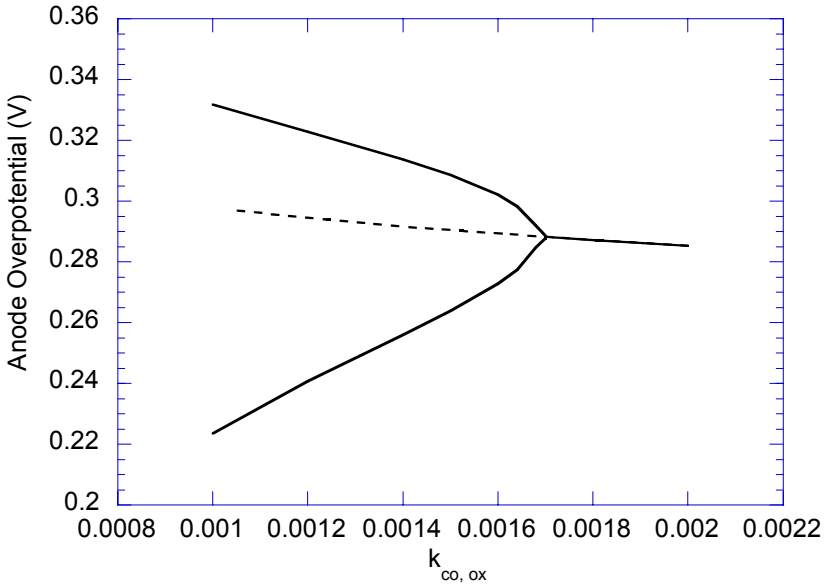

Figure 5-9. One parameter bifurcation diagram for the CO electrooxidation rate constant $\vec{k}_{\mathrm{CO},ox}$. Other conditions as in Figure 5-8.

constant in the simulation is reasonably consistent with the experimental fact that oscillation is not observed on Pt anode.

The bifurcation diagram for the applied current density was also computed. Unfortunately, the predicted bifurcation diagram using the parameter values in our previous work is not able to explain the experimentally observed effect. However, the predictions can be made to match the experimental results by increasing the H_2 electrooxidation rate constant. However, this improvement in the prediction of bifurcation analysis for current density compromises the excellent prediction of the other two bifurcation parameters discussed above. Thus, it seems that fine-tuning of the parameter values used in our simulation is still necessary in order to reproduce all the bifurcation behavior.

In a spatially extended system, self-organization in time is generally accompanied by pattern formation in space. [6, 32-33] Although the fuel cell anode chamber and anode surface may be assumed to be homogeneous in this work, a spatial pattern is possible for fuel cells with large electrode area, and in this case space as an additional variable must be taken into account. In fact, the steady state spatial profile of reactant concentration and current density is now attracting attention.[34, 35]

5.4.6 Local Linear Stability Analysis: A Hopf Bifurcation

Spontaneous oscillations in a physicochemical system are generally related to the fact that the stationary state is unstable. The stability of the stationary state may change under the influence of a control parameter and can be studied using bifurcation theory, which is an efficient mathematical tool to analyze a dynamic system. It can predict not only when a certain bifurcation will occur, but also the properties of a bifurcation in a set of differential equations modeling the electrochemical system. [7] For a local bifurcation (*e.g.*, saddle-node bifurcation, Hopf bifurcation), local linear stability analysis can be applied.[7]

The details of the local stability analysis are in Appendix II. The eigenvalues of the system as a function of the bifurcation parameter $\vec{k}_{\mathrm{CO},ox}$ are plotted in Figure 5-10a-c and Figure 5-11. It should be pointed out that Figure 5-11 are complex planes, with x and

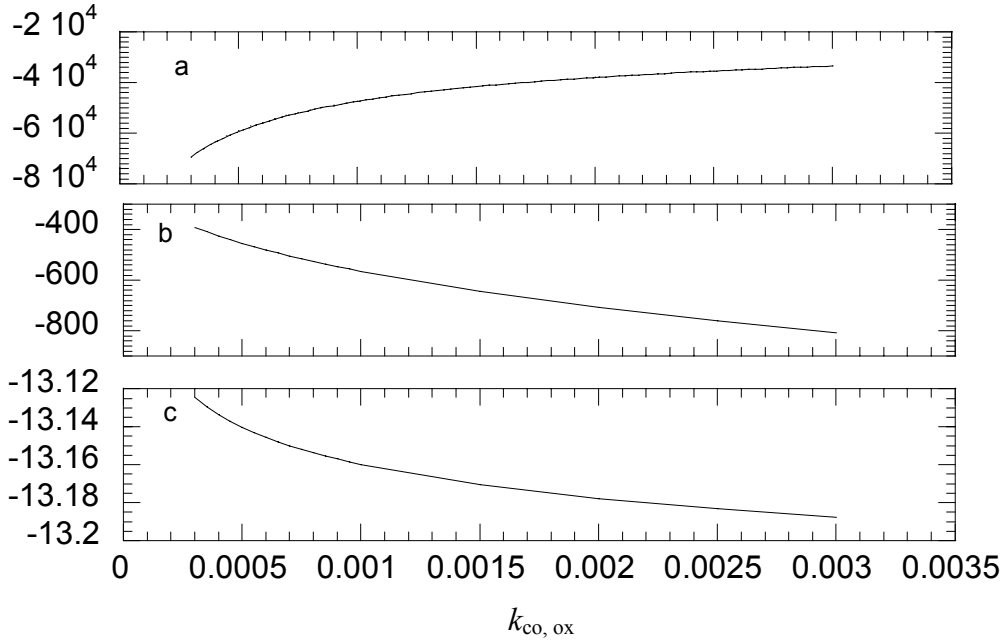

Figure 5-10. The three real eigenvalues of the dynamic model as a function of the CO electrooxidation rate constant $\vec{k}_{\mathrm{CO},ox}$.

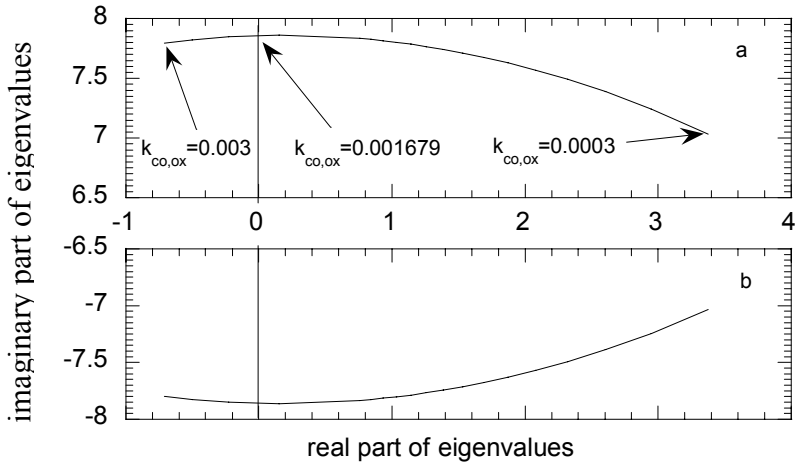

Figure 5-11. The two complex conjugate eigenvalues of the dynamic model as a function of the CO electrooxidation rate constant $\vec{k}_{\mathrm{CO},ox}$. This is a complex plain with x-axis being the real part, and y-axis the imaginary part of the two complex conjugate eigenvalues.

y axis being the real and imaginary parts of the eigenvalues. It is found that with the *decrease* of $\vec{k}_{\mathrm{CO},ox}$, the real parts of the two conjugate complex eigenvalues will change sign from negative to positive (detailed calculation indicates that the real part passes the imaginary axis at a critical $\vec{k}_{\mathrm{CO},ox}$ value of 0.001679). The equilibrium solution is stable when $\vec{k}_{\mathrm{CO},ox}$ is greater than 0.001679, but the equilibrium solution loses stability as $\vec{k}_{\mathrm{CO},ox}$ decreases below 0.001679. Since the imaginary parts are nonzero and all the other eigenvalues are negative, the Hopf bifurcation theorem[36] allows us to conclude that at least locally (i.e., for parameter values sufficiently close to the critical value), the system undergoes a Hopf bifurcation from which a periodic orbit or limit cycle is born. The periodic orbit emerging from this Hopf bifurcation can be stable or unstable. While it is difficult to prove how much $\vec{k}_{\mathrm{CO},ox}$ can decrease below the critical value before some other bifurcation occurs, numerical (computational) experiments indicate that the oscillatory solution is stable for reasonable values of $\vec{k}_{\mathrm{CO},ox}$ below the critical value.

From the characteristics of both the experiments (Figure 5-1) and the simulations (Figure 14 in ref. 9), i.e., the oscillations are small-amplitude close to the bifurcation point, and the amplitude grows and period increases as the bifurcation parameter move away from the critical value, the bifurcation in terms of fuel cell temperature is a supercritical Hopf bifurcation, which is further proved by the bifurcation diagram and local linear stability analysis. Thus, a coherent picture of Hopf bifurcation in this nonlinear reaction system emerges both experimentally and mathematically.

5.5 Conclusions

Temperature is found to be a key bifurcation parameter in anode potential oscillations in PEM fuel cells. Hydrogen electrooxidation is the major current-producing reaction, and all the surface species have to be time-dependent in order for the model to predict the oscillatory behavior. However, the CO concentration in the anode chamber need not necessarily be time dependent. The online CO concentration monitoring does not show any oscillation, but does confirm the model prediction on the average value of

CO concentration. It is possible that any small oscillations in this are smeared out or not measurable by the CO detector.

The oscillation model is classified as a Hidden Negative Differential Resistance (HNDR) oscillator based on the response of anodic current and coverage of surface species in a dynamic linear potential scan. Both the bifurcation diagram and a linear stability analysis in terms of the CO electrooxidation rate constant indicate that the bifurcation experienced during the variation of fuel cell temperature is a supercritical Hopf bifurcation, which leads to stable potential oscillations when the fuel cell is set at constant current density.

As a most promising power source, the unstable steady state (sustained oscillations) in PEM fuel cell operation will undoubtedly attract more attention, both in terms of the manipulation of the system stability (control method) and possible enhancement in total efficiency under self-sustained oscillation conditions.

List of Symbols

A	geometric area of the electrode in the fuel cell
C_{dl}	anode capacity
C_t^*	atom mole density per cm^2 PtRu surface
F	Faraday constant
i	fuel cell current density
K_C	equilibrium constant for CO desorption (the reciprocal of the adsorption equilibrium constant)
K_H	equilibrium constant for H_2 desorption (the reciprocal of the adsorption equilibrium constant)
$\vec{k}_{CO,ad}$	rate constant of CO adsorption
$\vec{k}_{CO,ox}$	rate constant of CO electrooxidation
$\vec{k}_{H_2,ad}$	rate constant of H_2 adsorption
$\vec{k}_{H,ox}$	rate constant of H_2 electrooxidation
$\vec{k}_{OH}$	rate constant of water adsorption
$\overleftarrow{k}_{OH}$	rate constant of water desorption
P_0	standard pressure, 1 atm
p_{H_2}	partial pressure of hydrogen in the anode chamber
R	gas constant
r_{CO}	rate of CO electrooxidation
$r_{CO,\,ad}$	net rate of CO adsorption
r_H	rate of H_2 electrooxidation
$r_{H_2,ad}$	net rate of H_2 adsorption
r_{OH}	net rate of water dissociation
T	fuel cell temperature
T_0	standard temperature, 298 K
V_A	volume of the anode chamber
v_0	anode inlet volumetric flow rate

v	anode outlet volumetric flow rate
x_{CO}^{0}	CO mole fraction in the anode feed
x_{CO}	CO mole fraction in the anode chamber
Greek	
α_{CO}	transfer coefficient of CO electrooxidation
α_{H}	transfer coefficient of hydrogen electrooxidation
α_{OH}	transfer coefficient of water oxidative dissociation
η_{A}	anode overpotential
γ	roughness factor of the anode (in the units of cm^2 PtRu/cm^2 electrode)
θ_0	fraction of free surface sites
θ_{CO}	surface coverage of CO
θ_{H}	surface coverage of H
θ_{OH}	surface coverage of OH

Appendix I

Model Parameters			
K_{CO}	2×10^{-7} atm[a]	$\vec{k}_{OH}$	8×10^{-4} A cm^{-2} [e]
K_H	0.5 atm[a]	$\overleftarrow{k}_{OH}$	2760 A cm^{-2} [b]
α_H	0.5	$x^0{}_{CO}$	108×10^{-6}
α_{CO}	0.5	T	315 K
α_{OH}	0.5	C_{dl}	0.45 F[c]
$\vec{k}_{H,ox}$	4.0 A cm^{-2} [a]	γ	100[d]
$\vec{k}_{H_2,ad}$	402 A cm^{-2} atm^{-1} [a *]	C_t^*	2.2×10^{-9} mol/cm^2 [b]
$\vec{k}_{CO,ad}$	150 A cm^{-2} atm^{-1} [a*]	A	5 cm^2
$\vec{k}_{CO,ox}$	5.5×10^{-4} A cm^{-2} [e]	P_{H_2}	2.958 atm
i	0.3 A/cm^2	v_0	48.1 scc/min
V_A	2.63×10^{-7} m^3		

[a] ref. 31.
[b] ref. 8.
[c] ref. 37.
[d] Estimated by the specific surface area of 20%(w/o) E-TEK PtRu/C catalyst and an electrochemical efficiency(utilization) of the anode catalyst of about 30%.
[e] Fitted parameters.
[*] These two values have been increased by a factor of 10 from the original value in order to match the simulated oscillation frequency with the experimental results.

Appendix II

The system of differential equations is linearized about the stationary state and the stability is defined in terms of recovering from a small perturbation. Solving the linearized equations amounts to calculating the eigenvalues of the associated Jacobian matrix. Stability is determined by the sign of these eigenvalues[7]. The mathematical analysis proves that the system experiences a Hopf bifurcation as the electrooxidation rate constant, $\vec{k}_{CO,ox}$, passes through a critical value.

The ODEs of the model is formulated into a single system in the six dependent variables (θ_O, θ_{CO}, θ_H, θ_{OH}, x_{CO}, η_A):

$$\frac{d\theta_{CO}}{dt} = A_1 x_{CO}\theta_0 - A_2\theta_{CO} - A_3\vec{k}_{CO,ox}\theta_{CO}\theta_{OH}\exp(\alpha_1\eta_A) \quad [18]$$

$$\frac{d\theta_H}{dt} = A_4\theta_0^2 - A_5\theta_H^2 - A_6\theta_H\sinh(\alpha_2\eta_A) \quad [19]$$

$$\frac{d\theta_{OH}}{dt} = A_7\theta_0\exp(\alpha_3\eta_A) - A_8\theta_{OH}\exp(-\alpha_4\eta_A) - A_3\vec{k}_{CO,ox}\theta_{CO}\theta_{OH}\exp(\alpha_1\eta_A) \quad [20]$$

$$\frac{d\eta_A}{dt} = A_9 - A_{10}\theta_H\sinh(\alpha_2\eta_A) - A_{11}\vec{k}_{CO,ox}\theta_{CO}\theta_{OH}\exp(\alpha_1\eta_A) - A_{12}\theta_0\exp(\alpha_3\eta_A) + A_{13}\theta_{OH}\exp(-\alpha_4\eta_A) \quad [21]$$

$$\frac{dx_{CO}}{dt} = A_{14} - A_{15}x_{CO} + A_{16}x_{CO}\theta_0^2 - A_{17}x_{CO}\theta_H^2 - A_{18}x_{CO}\theta_0 + A_{19}\theta_{CO} \quad [22]$$

where A_i and α_i are fixed lumped constants defined in terms of the physical constants but independent of $\vec{k}_{CO,ox}$. The lumped parameters and their corresponding numerical values are listed in Table 5-1. In addition to these five equations, the six dependent variables must also satisfy the additional constraint of site balance, namely $\theta_0 = 1 - \theta_{CO} - \theta_H - \theta_{OH}$.

The equilibrium solution (i.e., a solution that is constant in time) was found numerically for several values of $\vec{k}_{CO,ox}$. Then the Jacobian matrix for the above system [18-22] of differential equations was computed and evaluated at the equilibrium points. Finally, the eigenvalues of this matrix were calculated using Maple 7.

The eigenvalues of the system were calculated for various values of the bifurcation parameter $\vec{k}_{\mathrm{CO},ox}$. Three of the five eigenvalues are real and negative as $\vec{k}_{\mathrm{CO},ox}$ varies between 0.0003 and 0.003. The other two are complex conjugate eigenvalues.

Table 5-1. Lumped parameters and base case values in the ODE systems

A_1	$\frac{\vec{k}_{CO,ad}\, p_{H_2}}{F\gamma C_t^*}$	2.092×10^{4} s^{-1}	A_{13}	$\frac{A\overleftarrow{k}_{OH}}{C_{dl}}$	3.067×10^{4} V s^{-1}
A_2	$\frac{\vec{k}_{CO,ad} K_C}{F\gamma C_t^*}$	1.413×10^{-3} s^{-1}	A_{14}	$\frac{P_0 v_0 T}{p_{H_2} V_A T_0} x_{CO}^0$	1.176×10^{-4} s^{-1}
A_3	$\frac{1}{F\gamma C_t^*}$	47.11 C^{-1}cm^2	A_{15}	$\frac{P_0 v_0 T}{p_{H_2} V_A T_0}$	1.088 s^{-1}
A_4	$\frac{\vec{k}_{H_2,ad}\, p_{H_2}}{F\gamma C_t^*}$	5.606×10^{4} s^{-1}	A_{16}	$\frac{ART}{2FV_A}\vec{k}_{H_2,ad}$	1.024×10^{3} s^{-1}
A_5	$\frac{\vec{k}_{H_2,ad} K_H}{F\gamma C_t^*}$	9.469×10^{3} s^{-1}	A_{17}	$\frac{ARTK_H}{2Fp_{H_2}V_A}\vec{k}_{H_2,ad}$	1.729×10^{2} s^{-1}
A_6	$\frac{2\vec{k}_{H,ox}}{F\gamma C_t^*}$	3.769×10^{2} s^{-1}	A_{18}	$\frac{ART}{FV_A}\vec{k}_{CO,ad}$	7.639×10^{2} s^{-1}
A_7	$\frac{\vec{k}_{OH}}{F\gamma C_t^*}$	3.769×10^{-2} s^{-1}	A_{19}	$\frac{ARTK_C}{Fp_{H_2}V_A}\vec{k}_{CO,ad}$	5.162×10^{-5} s^{-1}
A_8	$\frac{\overleftarrow{k}_{OH}}{F\gamma C_t^*}$	1.300×10^{5} s^{-1}	α_1	$\frac{\alpha_{CO}F}{RT}$	18.42 V^{-1}
A_9	$\frac{Ai}{C_{dl}}$	3.333 V s^{-1}	α_2	$\frac{\alpha_H F}{RT}$	18.42 V^{-1}
A_{10}	$\frac{2A\vec{k}_{H,ox}}{C_{dl}}$	88.89 V s^{-1}	α_3	$\frac{\alpha_{OH}F}{RT}$	18.42 V^{-1}
A_{11}	$\frac{A}{C_{dl}}$	11.11 F^{-1}cm^2	α_4	$\frac{(1-\alpha_{OH})F}{RT}$	18.42 V^{-1}
A_{12}	$\frac{A\vec{k}_{OH}}{C_{dl}}$	8.889×10^{-3} V s^{-1}			

References

1. M. L. Perry and T. F. Fuller, *J. Electrochem. Soc.*, **149,** S59 (2002)**.**
2. L. F. Brown, *Int. J. Hydrogen Energy*, **26**, 381 (2001)**.**
3. C. Lamy, A. Lima, V. LeRhun, F. Delime, C. Coutanceau, and J. M. Leger, *J. Power Sources*, **105**, 283 (2002).
4. Z. G. Qi, M. Hollett, A. Attia, and A. Kaufman, *Electrochem. Solid-State Lett*., **5** A129 (2002).
5. C. Rice, S. Ha, R. I. Masel, P. Waszczuk, and T. Barnard, *J. Power Sources*, **111**, 83 (2002).
6. K. Krischer, In *Modern Aspects of Electrochemistry*; Vol. 32, J. O'M. Bockris, B. E. Conway, and R. E. White, Editors, p.1, Plenum, New York (1999).
7. M. T. M. Koper, *J. Chem. Soc., Faraday Trans.*, **94**, 1369 (1998).
8. M. T. M. Koper, T. J. Schmidt, N. M. Markovic, and P. N. Ross, *J. Phys. Chem. B* **105**, 8381 (2001).
9. J. X. Zhang, and R. Datta, *J. Electrochem. Soc.*, **149**, A1423 (2002).
10. J. L. Hudson, and T. T. Tsotsis, *Chem. Eng. Sci*., **49**, 1493 (1994).
11. M. T. M. Koper, *Adv. Chem. Phys*., **92**, 161 (1996).
12. P. Strasser, *Interface*, **9**, 46 (2000).
13. P. Strasser, M. Eiswirth, and M. T. M. Koper, *J. Electroanal. Chem*., **478**, 50 (1999).
14. S. Nakanishi, Y. Mukouyama, and Y. Nakato, *J. Electrochem. Soc.*, **148**, E405 (2001).
15. H. Okamoto, N. Tanaka, and M. Naito, *Chem. Phys. Lett*., **248**, 289 (1996).
16. W. Wolf, K. Krischer, M. Lubke, M. Eiswirth, and G. Ertl, *J. Electroanal. Chem*., **385**, 85 (1995).
17. P. Strasser, M. Eiswirth, and G. Ertl, *J. Chem. Phys.*, **107**, 991 (1997).
18. P. Strasser, M. Lubke, P. Parmanada, M. Eiswirth, and G. Ertl, *J. Phys. Chem.*, *B* **102**, 3227 (1998).
19. J. X. Zhang, R. Datta, *Electrochem. Solid-State Lett*., **6**, A5 (2003).
20. K. Krischer, M. Lubke, W. Wolf, M. Eiswirth, and G. Ertl, *Ber. Bunsenges. Phys. Chem.*, **95**, 820 (1991).

21. P. Strasser, M. Lubke, F. Raspel, M. Eiswirth, and G. Ertl, *J. Chem. Phys.*, **107**, 979 (1997).
22. T. J. Schmidt, B. N. Grgur, N. M. Markovic, and P. N. Ross, *J. Electroanal. Chem*., **500**, 36 (2001).
23. C. H. Kim, S. I. Pyun, and H. C. Shin, *J. Electrochem. Soc.*, **149**, A93 (2002).
24. E-TEK catalog, 2002.
25. T. Thampan, S. Malhotra, J. Zhang, and R. Datta, *Catal. Today*, **67**, 15 (2001).
26. K. T. Adjemian, S. J. Lee, S. Srinivasan, J. Benziger, and A. B. Bocarsly, *J. Electrochem. Soc.*, **149**, A256 (2002).
27. H. A. Gasteiger, N. M. Markovic, and P. N. Ross, *J. Phys. Chem.*, **99**, 16757 (1995).
28. N. M. Markovic, C. A. Lucas, B. N. Grgur, and P. N. Ross, *J. Phys. Chem. B*, **103**, 9616 (1999).
29. K. Krischer, M. Lubke, W. Wolf, M. Eiswirth, and G. Ertl, *Electrochim. Acta* , **40** 69 (1995).
30. W. Wolf, M. Lubke, M. T. M. Koper, K. Krischer, M. Eiswirth, and G. Ertl, *J. Electroanal. Chem*., **399**, 185 (1995).
31. T. E. Springer, T. Rockward, T. Zawodzinski, and S. Gottesfeld, *J. Electrochem. Soc.*, **148**, A11 (2001).
32. P. Strasser, J. Christoph, W. F. Lin, and M. Eiswirth, *J. Phys. Chem. A* , **104**, 1854 (2000).
33. J. Y.Lee, J. Christoph, P. Strasser, M. Eiswirth, and G. Ertl, *J. Chem. Phys.* **115**, 1485 (2001).
34. S. C. Cleghorn, C. R. Derouin, M. S. Wilson, and S. Gottesfeld, *J. Appl. Electrochem*., **28,** 663 (1998).
35. Y. Morimoto, T. Suzuki, and H. Yamada, Abstract 816, The Electrochemical Society Meeting Abstract, Vol. 2002-2, Salt Lake City, UT, 2002.
36. J. Guckenheimer, and P. Holmes, *Nonlinear Oscillations, Dynamical Systems, and Bifurcations of Vector Fields*, p. 151, Springer-Verlag, New York (1983).
37. M. C. Deibert, and D. L. Williams, *J. Electrochem. Soc*., 116, 1291 (1969).

Chapter VI

Higher Power Output in a PEM Fuel Cell Operating Under Autonomous Oscillatory Conditions in the Presence of CO

Time-averaged cell voltage, cell efficiency and power density in an autonomous oscillatory state was found to be higher than that in stable steady-state for a PEM fuel cell operating in the presence of CO in the anode feed reformate gas. The average power density under such an oscillatory state at 55 °C is found to be twice that under a stable steady-state. The average cell voltage and power density gain is due to the decrease of the time-averaged anode overpotential in the oscillatory state. This report thus provides experimental evidence that autonomous oscillatory operation of fuel cell in the presence of CO can increase the power output as compared to that in stable steady-state operation. Contents in this chapter have been published in *Electrochem. and Solid-State Lett*..

6.1 Introduction

Periodic or chaotic behavior has been observed in both homogeneous and heterogeneous reaction processes, and especially in electrochemical systems.[1] If such a system is well-mixed, only temporal periodic variation of the variables appears. Otherwise, spatio-temporal patterns may be observed, e.g., in the concentration of adsorbed species on an electrode surface.[2] The literature is replete with reports of oscillatory phenomenon in electrochemical systems, and the mechanistic understanding of the origin of such oscillations is being continually advanced.[3-6] Generally speaking, the periodic behavior of an electrochemical system is due to the interplay of nonlinear electrode kinetics, mass transport, and the external electrical circuitry. The mathematical models for these phenomena contain nonlinear differential equations for reactant concentrations, coverage of surface species, and current or voltage as variables.

Oscillations in reaction systems used to be considered puzzling and largely irrelevant. Later, there was an effort to search for ways to exploit nonlinear kinetics.[7-8] It has been found, for instance, that the reaction rate is increased in a forced oscillatory biochemical reaction.[9] Similar phenomenon was also observed in the conventional chemical reactions with nonlinear kinetics.[10] In these examples it was demonstrated that efficiency could be improved by operating in a forced oscillatory state. With the improved theoretical understanding of periodic behavior in electrochemical systems, the expectations of their practical utility are also increasing.[7-8]

We have found recently that sustained potential oscillations exist in proton exchange membrane (PEM) fuel cell fed with H_2 containing low levels of CO when operated under constant current conditions.[11] The oscillations were determined to be due to the nonlinear kinetics of the anode reactions coupled with the mass and charge conservation. Here we present our findings on increased power output of PEM fuel cells when operated under such oscillatory conditions.

6.2 Experimental

The experimental details can be found in our previous work.[11] In short, two pieces of electrode were bonded to either side of a solid polymer electrolyte membrane (Nafion® 115). An electrode containing 0.35 mg/cm^2 PtRu (atomic ratio 1:1, E-TEK) was used at the anode, exposed to a simulated reformate gas (H_2 containing low levels of CO, also containing 20% CO2 in some experiments). The cathode containing 0.4 mg/cm^2 Pt (E-TEK) was exposed to humidified O_2. A membrane-electrode-assembly (MEA) with 5 cm^2 effective electrode area was prepared by hot-pressing at 130 °C and under a pressure of 4000 lbs for about 2 minutes. The MEA was tested in a single cell (Electrochem, Inc.) in a test station with temperature, pressure and mass flow control. The total pressure at both anode and cathode chamber was 30 psig. The volumetric flow rates reported in this study are all in units of standard (1 atm and 25 °C) cubic centimeters per min (sccm). An electronic load (HP 6060B) interfaced with a PC was used to measure the current-voltage characteristics of the fuel cell.

6.3 Results

The performance of a fuel cell in the laboratory may be experimentally evaluated under constant voltage, constant current, or constant resistance modes with an electronic load. We observed sustained potential oscillations when a fuel cell fed with H_2/CO was operated under the constant current mode, with the anode catalyst being PtRu.[11] Since oscillations were not observed when the fuel cell was operated under the constant voltage or constant resistance modes, it is possible to directly compare the performance under an oscillatory state with that in a stable steady-state.

The fuel cell current-voltage relationship at room temperature obtained for a H_2 feed containing 100 ppm CO under constant voltage mode (stable steady-state) is shown in Figure 6-1, along with the corresponding power output (in the units of mW/cm^2). Even though the open circuit voltage is around 1.0 V, it is seen that the cell voltage drops precipitously to 0.4 V, even when only a small current (i.e., 30 mA/cm^2) is drawn. Such a large initial drop in cell voltage is due to the severe poisoning of even the PtRu catalyst by CO at room temperature. The peak power output is found to be only around 40 mW/cm^2, which occurs at a current density of about 200 mA/cm^2. When on the other hand, the fuel cell is operated in the constant current mode, the cell voltage begins to oscillate. The cell voltage pattern at three different constant current densities is shown in Figure 6-2. It is seen that the cell voltage oscillates over a wide range, and hence so does the power output, also shown in Figure 6-2. Of course, the temporal variation of voltage and wattage are identical, since current is constant. Furthermore, since voltage efficiency, $\varepsilon_v = V/V_0$, the ordinate in Figure 6-2 can also be viewed as being proportional to efficiency. The amplitude and period of the oscillations at room temperature are found to be larger than those at higher temperatures. This is consistent with our finding that the oscillatory behavior observed by varying the fuel cell temperature is due to a Hopf bifurcation.[12]

The time-averaged cell voltage and power density corresponding to Figure 6-2 are plotted in Figure 6-3. It can be seen that the time-averaged cell voltage does not change greatly as a function of current density. The time-averaged power output thus increases almost linearly with the current density in the range investigated. Further, the time-averaged cell voltage is substantially higher when compared to the stable steady-state

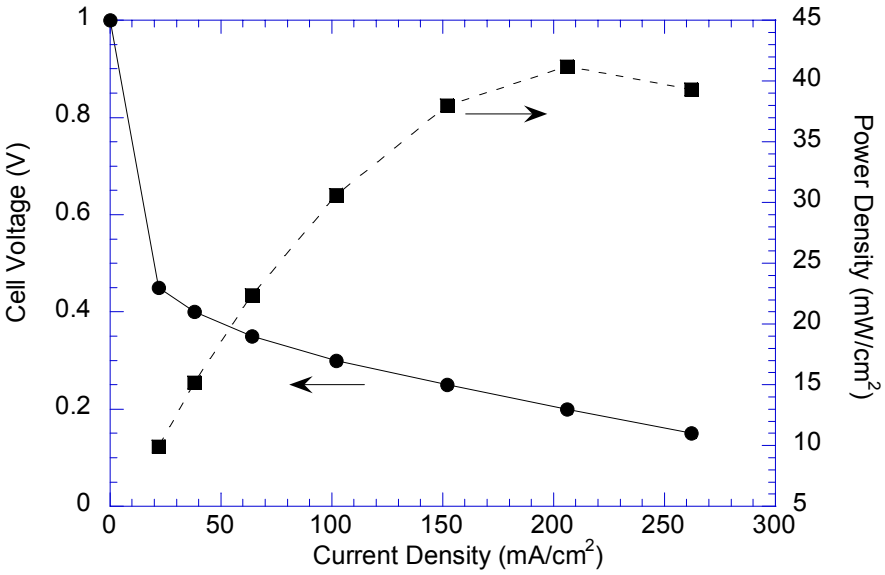

Figure 6-1. Cell voltage and power output at different current densities at stable steady-state (constant voltage mode) at room temperature. Anode feed: H_2/100 ppm CO; Anode inlet flow rate: 60.1 sccm; Cathode feed: O_2.

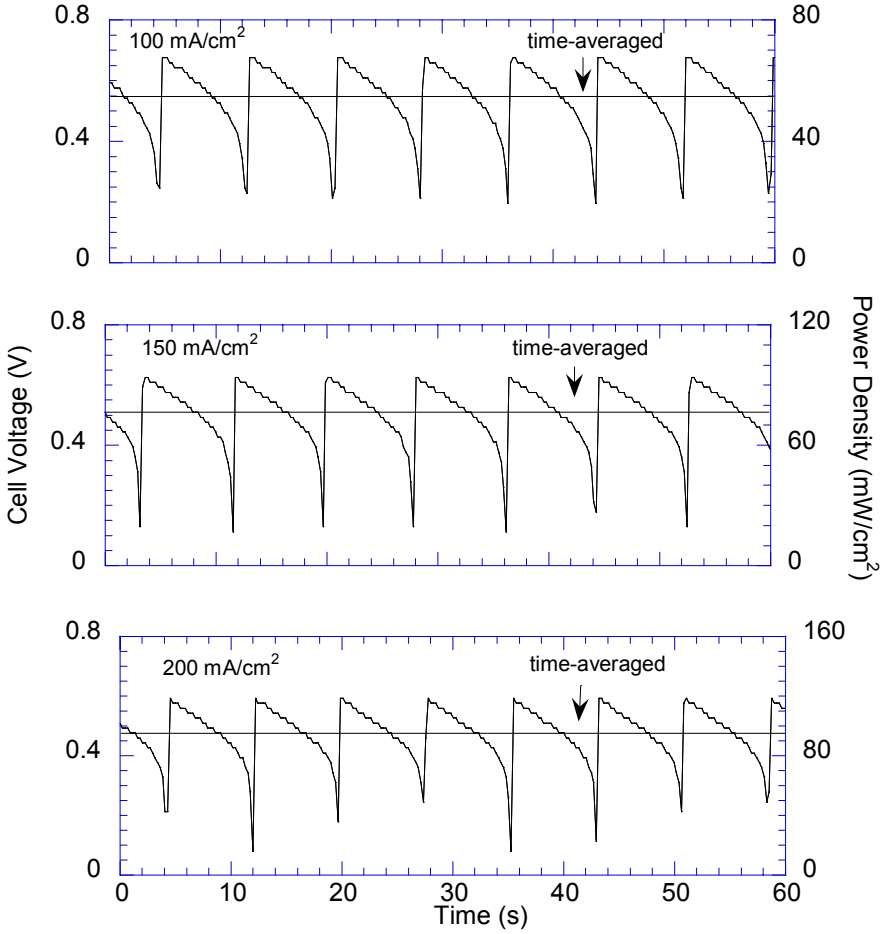

Figure 6-2. Cell voltage and power density at different current densities in autonomous oscillatory state (constant current mode). The solid straight line indicates the time-averaged value of both cell voltage and power density. The other conditions are the same as in Figure 6-1.

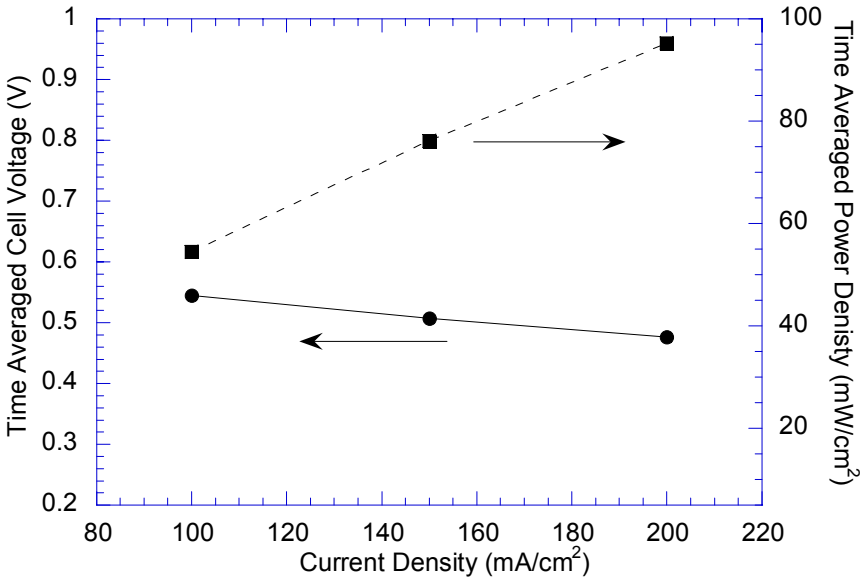

Figure 6-3. Time-averaged cell voltage and power output at different current density in autonomous oscillatory state (constant current mode) at room temperature. The other conditions are the same as in Figure 6-1.

value (Figure 6-1). For example, at a current density of 200 mA/cm^2, if the fuel cell were operated at stable steady state, *i.e.*, in the constant voltage mode, the cell voltage is only about 0.2 V, while under the oscillatory state, the time-averaged cell voltage is almost 0.5 V. It is, thus, evident from a comparison of Figures 6-3 and 6-1 that the time-averaged power output when operated under the oscillatory conditions is substantially higher than that under stable conditions. Similar results were obtained for a H_2 feed containing 100 ppm CO and 20% CO_2, as well as for a H_2 feed containing 200 ppm CO.

The performance of the fuel cell operated with a H_2/108 ppm CO anode feed under stable steady-state conditions (constant voltage mode) at different temperatures is summarized in Figure 6-4. It can be seen that the fuel cell performance is poor at low temperatures. Further, no limitation imposed by transport of reactant gases is evident from the polarization curves in the current density range investigated. The corresponding power density is plotted in Figure 6-5. The power output improves with the increase of fuel cell temperature, which is attributable to both reduced CO affinity for the catalyst surface, as well as enhanced H_2 and CO electro-oxidation rates.[11] The peak power output thus, at 55 °C is about 90 mW/cm^2, while the peak power density at 80 °C is about 180 mW/cm^2.

Figure 6-6 shows the time-averaged cell voltage and power density under the autonomous oscillatory state at a fuel cell temperature of 55 °C. It can be seen that the average cell voltage decreases gradually with the current density, and is higher than that in Figure 6-4 for the same current density. The time-averaged power density in the oscillatory state shown in Figure 6-6 is nearly double when compared to that in Figure 6-5 at 55 °C (*i.e.*,150-200 mW/cm^2 vs. about 90 mW/cm^2 maximum). This power output is even higher than the maximum at 80 °C for the stable steady-state. Moreover, the power output at 55 °C in the oscillatory state shown in Figure 6-6 may not have peaked yet.

6.4 Discussions

Autonomous oscillations were observed by us at temperatures below about 70 °C.[11] A quantitative mechanistic model and analysis has been given by us before.[11,12] Qualitatively, when CO builds up on the catalyst surface, *i.e.*, as θ_{CO} increases, the anode

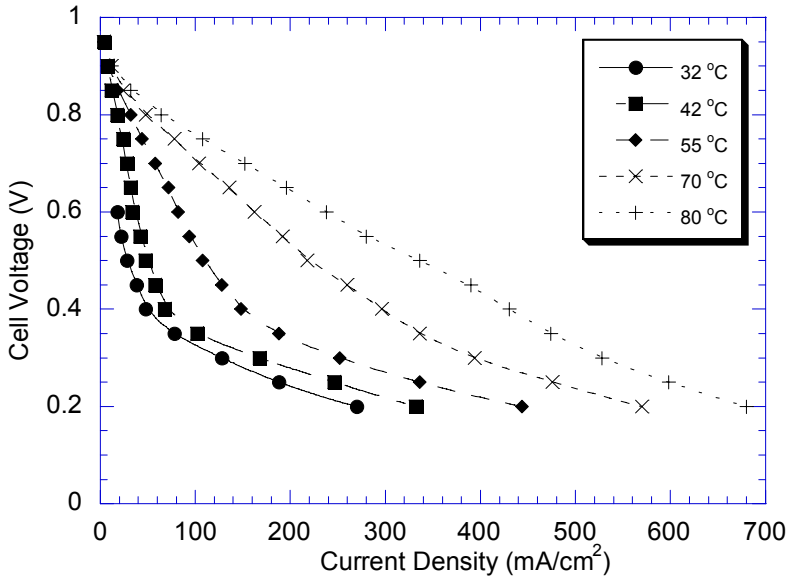

Figure 6-4. Polarization curves at stable steady-state (constant voltage mode) for various cell temperatures. (●) 32 °C (■) 42 °C (♦) 55 °C (×) 70 °C (+) 80 °C. Anode feed: H_2/108 ppm CO; Anode inlet flow rate: 48.1 sccm.

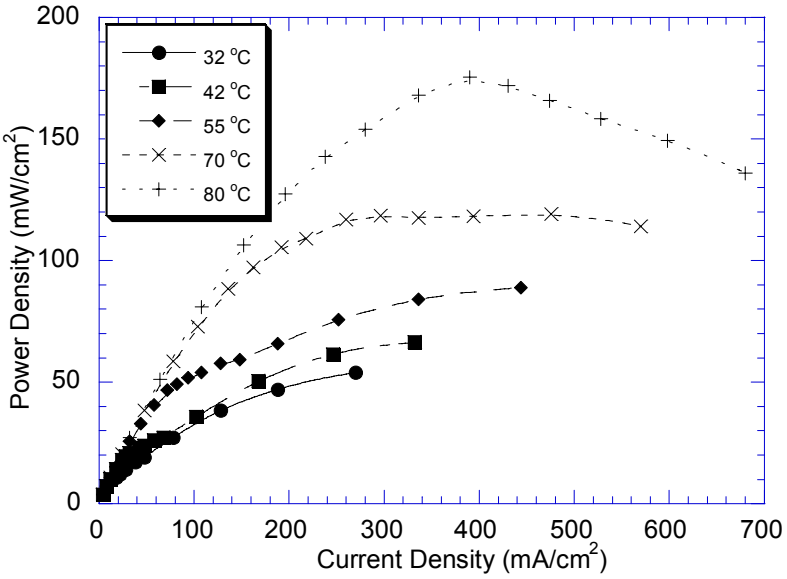

Figure 6-5. Power output of stable steady-states (constant voltage mode) for various cell temperatures shown in Figure 4.

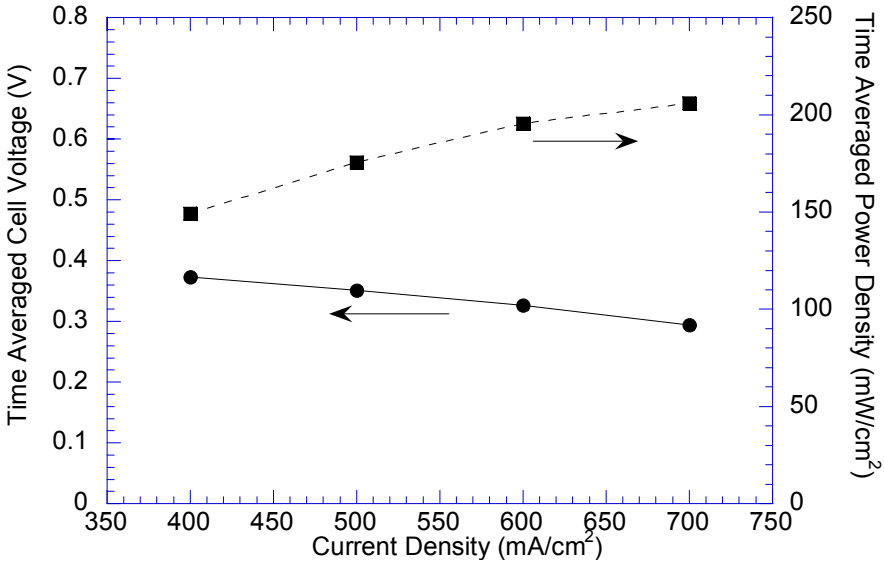

Figure 6-6. Time-averaged cell voltage and power output at different current densities in autonomous oscillatory state (constant current mode). T_{cell} = 55 °C; Anode feed: H_2/108 ppm CO; Anode inlet flow rate: 48.1 sccm.

becomes increasingly polarized to a higher potential in order to compensate for a smaller θ_H and to sustain the applied constant current. The anode overpotential increase accelerates the electrooxidation of CO_{ad} on the catalyst surface via the oxygen containing surface species such as OH_{ad}, which is formed more readily on catalyst surface at higher overpotentials. When the CO electrooxidation rate exceeds the rate of CO adsorption, the surface coverage of CO, θ_{CO} declines. This happens quickly beyond a critical overpotential. Thus, θ_H increases and H_2 oxidation reaction sustaining the current is no longer constrained by θ_{CO}. The anode overpotential, thus, drops quickly to a low value. This drop in the potential, however, recreates the situation where the rate of CO adsorption exceeds that of CO electrooxidation. Therefore, CO molecules begin to build up again on the catalyst surface and the electrode must again be polarized increasingly to a higher overpotential. Thus, the cycle repeats itself. The conditions for oscillatory state operation may change depending upon the cell temperature and composition of the reformate feed stream. The poisoning species in reformate may not necessarily be CO in order for oscillations to appear. Rather any species that blocks the catalyst surface at low overpotentials and can be electro-oxidized at high overpotentials could conceivably cause oscillatory behavior.

Self-organized potential oscillations occur at conditions far from thermodynamic equilibrium with the presence of appropriate feedback loops.[3] As discussed above, the dynamic instability is linked to the interplay of the electrode kinetics and the external electrical circuit trying to sustain a constant current. A negative differential resistance ($\partial V/\partial i < 0$), i.e., when the total current decreases with an increase of electrode potential, is a necessary feature for the existence of electrochemical instability, which has been shown to exist in the anode potential oscillations in this study.[12] The following processes have been identified as essential for the occurrence of these oscillations:[12] (1) a current carrying process (H electrooxidation, which depends upon the anode overpotenital); (2) a process responsible for the occurrence of the negative differential resistance (potential-dependent adsorption and desorption of OH); and (3) a potential-dependent process in which potential has a positive effect on the reaction rate (reactive removal of CO). The temporal evolution of the anode reaction system is quantitatively explained by the differential equations derived from charge as well as mass balance. By applying the linear

stability analysis, i.e., by the sign of the eigenvalues of the associated Jacobian matrix of the linearized equations governing the system, a Hopf bifurcation has been shown to exist in this system.

The oscillatory fuel cell voltage reflects the sustained effort for self-recovery on part of the catalyst surface in order to maintain a given current. The increased power output in the oscillatory state is evidently caused by the time-averaged cell voltage increase at a given current density. The increased average cell voltage is a result of the decreased average anode overpotential. It has been shown computationally and experimentally that under oscillatory state, the rise and fall of overpotential in a cycle is not symmetrical about the unstable steady-state value. The deviation of the minimum overpotential is larger than that of the maximum overpotential.[12] Furthermore, for a large fraction of the time in a cycle, the anode overpotential is at a lower value than that under a stable steady-state. Such a gain in the decrease in anode overpotential for a substantial fraction of the time in a cycle leads to the higher average cell voltage in the oscillatory state.

The increased power output in the oscillatory state is, as a matter of fact, consistent with the fact that the oscillations appear due to the effort by the system to maximize the entropy production rate σ_s.[9] In the fuel cell system, this is equal to current (reaction rate) times cell potential (which is proportional to the affinity of the reaction system).[13] The relation is shown by the following equation,

$$\sigma_s = \frac{1}{T} Ar = \frac{zF}{T} Vi$$

where σ_s is the entropy production rate, T is temperature, A is the affinity, r is the reaction rate, z is the number of electrons in the reaction, F is Faraday constant, V is cell voltage and i is the current. Thus, the rate of entropy production in a fuel cell is nothing but the rate of power production. We have shown that the phase angles of variables such as the surface coverage of CO, H and OH are different.[12] Phase lag among variables leads to different phase angle between the reaction rate (current) and affinity (voltage) of the system. This phase relation between affinity and reaction rate is another factor in determining the power output of a system.[7, 14]

There has been attempt to accelerate reaction rate or decrease the oxidation potential for the electro-oxidation of formic acid by forced oscillation, i.e., by superimposing a periodic potential[15] or current signal[16] with certain amplitude and frequency on the stable potential or voltage. It was found that in a certain range of frequency used, either the oxidation current is increased or the overpotential is decreased, implying an advantage of forced oscillatory operation over stable steady-state operation.[15-16] The gain in both reaction rate and efficiency has been demonstrated in biological reactions as well, where the biochemical reaction system exhibits autonomous oscillations.[7, 9] A perturbation to one of the reactants (i.e., oxygen influx) in the form of a sinusoidal wave was used instead of steady flux. It was found that several of the thermodynamic quantities were changed as compared to the undisturbed state. The phenomenon is believed to be due to resonance, which is a generic feature of oscillatory systems. Reaction rate enhancement in other chemical reaction systems has also been observed via forced concentration oscillations of reactants.[17] It was, thus, found that there is a significant improvement of the time-averaged production rate relative to optimal steady-state operation for the case of nonlinear kinetics, while for the case of linear kinetics there is no improvement.[17]

While advantages are reported for these forced oscillatory reactions, almost all of the examples demonstrated so far need an external oscillatory signal to force the reaction system into an oscillatory state. However, results reported here provide evidence that a system operating under an autonomous oscillatory condition also shows power output gains as compared to that at a stable steady-state under otherwise identical experimental conditions. Although the periodic forcing of the external parameters (e.g., reactant flow rates, current or cell voltage) may not be difficult in an energy conversion device such as fuel cell, cumbersome external control for periodic forcing is in general undesirable. Thus, our observation may be useful in managing power output for fuel cells, where the control of cell or stack current is not difficult. Although the periodic nature of voltage output would, in general, be undesirable, it is not a significant problem to condition this with modern electronic circuitry. Furthermore, the overall stack voltage may actually be less periodic, perhaps approaching the total average value due to the phase angle difference in cell voltage of the single oscillator (single cell) within a stack.

Raising the cell temperature can, undoubtedly, increase the power output of a fuel cell operating under a stable steady-state. However, the PEM fuel cell operating temperature can not usually exceed about 80-90 °C due to limitations imposed by the current polymer electrolyte membrane. Thus, utilizing the oscillatory kinetics may serve as an alternative approach to improving the power output (and thus managing CO poisoning) of a reformate-fed fuel cell. However, even in the oscillatory state operation, the power output is not comparable to that with pure hydrogen. Nevertheless, the present results provide evidence that operation under autonomous oscillatory conditions (due to the inherent nonlinear kinetics in electrode reactions) can indeed increase the power output as compared to that under a stable steady-state operation in an energy conversion device. This has been expected and hoped for by researchers working on nonlinear dynamics in electrochemical systems.[8]

6.5 Conclusions

A PEM fuel cell can be operated in an autonomous oscillatory state under constant current conditions when reformate is used as the anode feed. Compared to the stable steady-state operation, the time-averaged cell voltage, efficiencies, and power density are found to be higher under the oscillatory state. The increase in average cell voltage and power density is due to the decrease of the time-averaged anode overpotential under oscillatory conditions. There are relatively sharp bursts in the anode overpotential only periodically to rid the surface of the poisoning species. These observations may be useful for developing an operational strategy for improved management of power output in PEM fuel cells in the presence of CO.

References

1. G. Ertl, *Science*, **254**, 1750 (1991).
2. Y. J. Li, J. Oslonovitch, N. Mazouz, F. Plenge, K. Krischer, and G. Ertl, *Science*, **291**, 2395 (2001).
3. K. Krischer, In *Modern Aspects of Electrochemistry*; J. O'M Bockris, B. E. Conway, and R. E. White, Editors, Vol. 32, p. 1, Plenum Press, New York (1999).
4. J. L. Hudson, and T. T. Tsotsis, *Chem. Eng. Sci*., **49**, 1493 (1994).
5. M. T. M. Koper, *Adv. Chem. Phys*., **92**, 161 (1996).
6. P. Strasser, *Interface*, **9**, 46 (2000).
7. J. G. Lazar, and J. Ross, *Science*, **247**, 189 (1990).
8. P. Strasser, *Kinetic Oscillations and Spatiotemporal Self-Organization in Electrocatalytic Reactions*, *Ph.D. Thesis*, Freie Universitat Berlin, Berlin (1999).
9. J. G. Lazar, and J. Ross, *J. Chem. Phys*., **92**, 3579 (1990).
10. M. Schell, H. M. Schram, and J. Ross, *J. Chem. Phys*., **88**, 2730 (1988).
11. J. Zhang, and R. Datta, *J. Electrochem. Soc*., **149**, A1423 (2002).
12. J. Zhang, J. D. Fehribach, and R. Datta, *J. Electrochem. Soc*., **151***,* A689 *(2004)*.
13. I. Prigogine, *Introduction to Thermodynamics of Irreversible Processes*, p. 31, Intersciense Publishers, New York, (1961).
14. P. H. Richter, and J. Ross, *Science*, **211**, 715 (1981).
15. R. R. Adzic, K. I. Popov, and M. A. Pamic, *Electrochim. Acta*, **23**, 1191 (1978).
16. M. Schell, F. N. Albahadily, and J. Safar, *J. Electroanal. Chem*., **353**, 303 (1993).
17. J. Thullie, L. Chiao, and R. G. Rinker, *Chem. Eng. Sci*., **42**, 1095 (1987).

Chapter VII

Electrochemical Preferential Oxidation of CO in Reformate

In this chapter, an electrochemical preferential oxidation (ECPrOx) process, an alternative to the conventional preferential oxidation (PrOx) process, is developed to cleanse CO from a hydrogen rich gas mixture using a device similar in structure to the proton exchange membrane fuel cell. In this process, the selective CO electrooxidation is achieved at the anode by rendering the process electrochemical and by utilizing autonomous anode potential oscillations when operated at a constant low current density. The oscillation period and amplitude of the ECPrOx device adjust automatically to the CO levels in the feed stream so that a self-controlled autonomous potential pulsing is achieved with a low level of CO in the cleansed reformate. Some supplemental electrical power is produced from ECPrOx device while CO is removed from the reformate gas, without any H_2 or CO being wasted. The ECPrOx device can be operated at near room temperature, high anode pressure, atmospheric air breathing, and without external humidification. However, the operating conditions or the structure of ECPrOx are not optimized in this paper, but rather the feasibility of the concept is evaluated with a single cell unit. Contents of this chapter will be submitted to *J. Electrochem. Soc*..

7.1 Introduction

Proton exchange membrane (PEM) fuel cells have the potential to serve as the power systems for a new generation of "green" vehicles, as well as off-road power plants operating with increased efficiency and reduced emissions. A key issue limiting immediate fuel cell application, however, is that PEM fuel cells require pure hydrogen as the fuel. Since H_2 storage on-site or on-board vehicles is as yet impractical and its widespread availability is not likely for sometime, conventional fuels, e.g., natural gas,

gasoline or alcohols, must be reformed catalytically into H_2 at the point of usage.[1] The conventional reforming process produces substantial amounts of CO in addition to CO_2 and H_2. This is reduced via the water gas-shift (WGS) reaction. The exit gas from the low temperature shift (LTS) reactor following the high temperature shift (HTS) stage still contains roughly 5,000- 10,000 ppm (0.5 – 1%) CO, which can not be tolerated by PEM fuel cells. Thus, preferential oxidation (PrOx) reactors are used following the shift reactors to reduce CO to tolerable levels. The preferential oxidation (PrOx) reactor oxidizes CO into CO_2 typically over a Pt or other precious metal based catalyst by carefully bleeding small amounts of air or oxygen. This is able to reduce the CO level down to 50-100 ppm. Due to the limited selectivity, however, O_2 in excess of stoichiometry is required to reduce CO to low levels, which burns the hydrogen present in the reformate, thus reducing the overall efficiency.[2] The PrOx stage is also bulky and complex.

The success of the PrOx stage relies heavily on complex control of O_2 and temperature and on the high activity and selectivity of the catalyst in order to minimize the CO content in the effluent while keeping H_2 consumption at a low level. Much of the research on PrOx has focused on searching for better catalysts. Thus, Los Alamos National laboratory (LANL) has developed a PrOx catalyst and reaction system, which reportedly can achieve low concentrations of CO (10-20ppm) in a multistage PrOx reactor over a Pt/Al_2O_3 or Ru/Al_2O_3 catalyst.[3] A variety of catalytic materials were examined by Oh *et al*. in an integral flow reactor.[4] It was found that both Ru/Al_2O_3 and Rh/Al_2O_3 are very active in CO oxidation, achieving nearly complete CO conversion at temperatures as low as 100 °C (compared to ~200 °C required for Pt/Al_2O_3). Son *et al*.[3] found that Pt/Al_2O_3 catalyst pretreated with water could be operated over a broader temperature range (27-200 °C) than those prepared without such treatment. However, a reversible deactivation is caused by water adsorption at temperatures below 100 °C. Au/MnO_x has been tested for the selective oxidation of CO in simulated reformate as well.[5] The performance was found to be superior at 323-353 K, with a CO conversion of over 95% (i.e., less than 500 ppm in the outlet for a feed CO content of 1%). However, CO conversion dropped greatly for temperatures out of this range. Igarashi *et al*.[6] found that Pt-Ru supported on mordenite exhibited fairly high selectivity over a wide flow rate

range at 150 °C. Borup *et al.*[7] disclose in their patent that in the presence of an Ir-based supported catalyst, CO is selectively oxidized in the desired temperature range, preferably 210-260 °C. He *et al.*[8] reported CO selective oxidation in a reactor having a fuel cell type of configuration and under conditions similar to those in a fuel cell (60-80 ºC, high humidity). For the best catalyst tested (5% Ir/CoO_x-Al_2O_3/carbon), CO concentration in the effluent is found to be less than 100 ppm at 76 °C and 100% humidity (1% CO in the feed, at $O_2/CO \leq 2$).

A key variable determining selectivity in the PrOx reactor is temperature. Therefore, the CO selective oxidation reactor requires very careful cooling and temperature control, which is a major technical challenge. Thus, a two stage reactor with three heat exchangers to carefully control the temperatures of the process stream before, in between, and after the reactor was used by Vanderborgh *et al.*[9] Both of the O_2 streams to the reactors were predetermined and carefully controlled. Edwards *et al.*[10] report that the CO clean-up unit in the HotSpot® methanol processor uses several small and highly selective catalytic stages instead of one large catalyst bed.

Pilot scale CO preferential oxidation reactors have been successfully demonstrated. Thus, LANL has developed and tested a 50-kW catalyzed PrOx CO clean-up system.[11] A simulated methane partial oxidation reformate was used with an inlet CO concentration of 1%. The three–stage PrOx system consistently produced outlet CO concentrations below 50 ppm. Dudfield *et al.*[12] discribe a dual stage CO preferential oxidation reactor based upon catalyst coating of high surface area heat transfer technology. The catalyst used is Pt-Ru promoted by mixed transition metal oxide. Lee *et al.*[13] also demonstrated a PrOx reactor using Pt-Ru/Al_2O_3 as catalyst. The reactor adopted the dual stage design as well, with inter-stage cooling and controlled air injection. Under the optimum conditions, the CO was reduced from 1% to 20 ppm. It was also found that, for fast start-ups, the reactant temperature had to be at least 150 °C and the amount of air injected should be such that the O_2:CO molar ratio is ≥ 3. With these start-up procedures, it took about 3 minutes for the outlet CO concentration to fall below 20 ppm, experiencing a CO peak of about 2000 ppm.

Despite the fact that the PrOx technology is now universally adopted in fuel reformers, the process is, in fact, cumbersome, involving two or more stages with inter-

cooling and distributed air or water injection. The PrOx stage is bulky as well, being roughly 10-15% of the total size of the reformer plant. There is also a relatively long reactor warm-up period and large transient CO concentration during reactor start up. Recently, the idea of using electrochemistry for selective CO oxidation was proposed by Lakshmanan et al.,[2] based on the periodic use of an *external* power source. A proton-exchange membrane fuel cell was used as an electrochemical filter (EF) for the periodic selective oxidation of CO in H_2 with an external pulse potential control. At low potentials, the CO in reformate is allowed to adsorb on anode. Then the potential is increased to 0.6 – 1.0 V in order to oxidize it. While unlike in the PrOx process there is no net consumption of H_2, this reaction does represent very substantial *net power consumption*, since the device works like an electrochemical hydrogen pump.[14]

In this chapter, we present an entirely novel approach involving electrochemical preferential oxidation (ECPrOx) which can effectively remove CO from reformate gas.[15] In addition, this ECPrOx unit can simultaneously produce some supplementary power, which can be integrated into the fuel cell power plant. The design of ECPrOx is similar, but not identical, to the conventional PEM fuel cells and exploits the strong adsorption of CO at the anode along with the use of electric potential to selectively oxidize CO with air fed at the *cathode*. The necessary electric potential in our approach is supplied *not* by an external power source, but rather produced *in situ* by the potential difference established by O_2 reduction reaction and CO electro-oxidation as well as the hydrogen electro-oxidation reaction (HOR). The outlet CO is thus maintained at the desired level because the potential oscillates autonomously in an effort to maintain the desired current.[16] Experimental results that prove the feasibility of the concept of ECPrOx are presented for a single cell device. The effect of feed CO concentration, catalyst loading, operating temperature and pressure, and humidification are investigated.

7.2 Experimental

The basic construction of the electrochemical preferential oxidation (ECPrOx) unit is similar to a PEM fuel cell. A gas diffusion electrode loaded with 20% (w/o) Pt/C at a metal loading of 0.4 mg/cm^2, acquired from E-TEK, was used as the cathode, while 20% (w/o) PtRu/C at a 0.35 mg/cm^2 metal loading, or 40% (w/o) PtRu/C at a 0.7 mg/cm^2

metal loading were used as the anode. The electrodes were hot-pressed onto a Nafion® 117 proton-exchange membrane to form the membrane-electrode assembly (MEA) at 130 °C and under a pressure of 4000 lbs for about 2 minutes.

The MEA was then incorporated into a 5 cm^2 single cell from ElectroChem, Inc. (Woburn, MA), and tested in a test station with temperature, pressure, humidity and flow rate control. The graphite bipolar plate has serpentine flow channels. The ECPrOx unit was operated at the room temperature unless otherwise noted. The room temperature recorded in the laboratory varied between 25 and 30 °C. The anode and cathode gases were humidified in stainless steel bottles containing water at room temperature before introduction into the unit. The total pressure of both anode and cathode sides was maintained at 30 psig except in the experiments investigating the effect of pressure. The volumetric flow rates reported in this study are in units of standard (1 atm and 25 °C) cubic centimeters per min (sccm).

The current-voltage characteristics were recorded using a HP 6060B DC electronic load, interfaced with a PC using LabVIEW software (National Instruments, Austin, TX), with a data sampling rate of 0.226 s. The anode exit gas stream was monitored by a Model 200 IR CO/CO_2 gas analyzer (California Analytical Instruments, Orange, CA). The FP-AI-100 analog input module/FP-1000 network module (National Instruments, Austin, TX) was used to collect data from the gas analyzer using LabVIEW. Simulated reformate (from premixed gas cylinder) was introduced to the anode at a flow rate controlled by a mass flow controller. A variety of feeds was tested, namely, H_2/100 ppm CO, H_2/200 ppm CO (MG Industries, Morrisville, PA); H_2/1000 ppm CO (Spec Air, Auburn, ME); and H_2/24.1% CO_2/9380 ppm CO (AGA Gas, Maumee, OH). These premixed gases were used as anode feed, while oxygen was fed to the cathode.

7.3 Results and Discussions

7.3.1 Proof of Concept of ECPrOx

The electrochemical preferential oxidation (ECPrOx) is based on the recent advances in our fundamental understanding of CO electrooxidation and CO induced

potential oscillations in PEM fuel cells.[16-17] It has been found that when a PEM fuel cell is operated at a constant current density and the anode feed contains low concentration of CO, the fuel cell voltage oscillates at lower temperatures (< 80 °C). It is further observed that the potential oscillations adjust automatically according to the CO concentration in the feed stream. For Example, the cell voltage pattern when the anode feed is switched from H_2/200 ppm CO to H_2/1000 ppm CO is shown in Figure 7-1. It can be seen that with the introduction of higher concentration of CO in the anode feed, the oscillation period decreases, i.e., the oscillation becomes faster, which is predicted by our dynamic model.[17]

The mechanistic modeling of such potential oscillations has indicated that a significant amount of CO entering the anode is electrooxidized on the catalyst surface.[17] Such a prediction is further confirmed by our experimental observations. A typical result of the anode outlet CO concentration with the step change in anode inlet flow rate is shown in Figure 7-2. The anode feed is H_2 containing 200 ppm CO. The cell is operated at room temperature and a current density of 200 mA/cm^2. It can be seen that the exit CO concentration responds quickly and is very stable over time for different inlet flow rates. The CO concentration can be brought down to about 13 ppm at an inlet feed rate of 71.6 sccm, and below 2 ppm at 36.4 sccm for a feed containing 200 ppm CO. It is thus evident that the CO concentration in hydrogen can be reduced without resorting to an external power supply.

Based on the above experimental observations, thus, we propose the ECPrOx process for selectively removing CO from H_2 rich gas by utilizing the anode potential oscillations in a device with a structure similar to that of a fuel cell. A schematic of the proposed ECPrOx unit in the overall fuel processing system is shown in Figure 7-3. The ECPrOx unit has the same function as the conventional PrOx reactor. A CO sensor could be put in series with the ECPrOx exit stream to monitor the CO concentration, and possibly for control. A current control device is used to control the hydrogen consumption rate and the CO conversion. The supplemental power produced by the ECPrOx unit could be stored in a rechargeable battery or integrated directly into the fuel cell power plant. The ECPrOx unit can be built in the same modular structure as PEM fuel cells. In some cases, it may even be possible to replace the low temperature shift reactor with the ECPrOx unit.

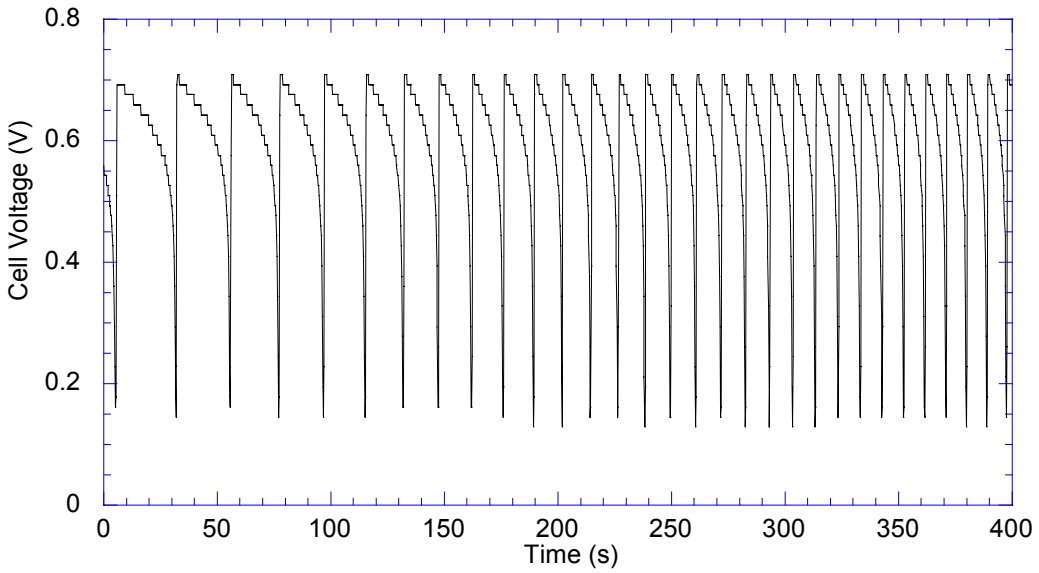

Figure 7-1. Cell voltage pattern for anode feed change from H_2/200 ppm CO to H_2/1000 ppm CO. Current density: 100 mA/cm^2; anode inlet flow rate: 60.1 sccm; room temperature; anode 0.7 mg/cm^2 PtRu.

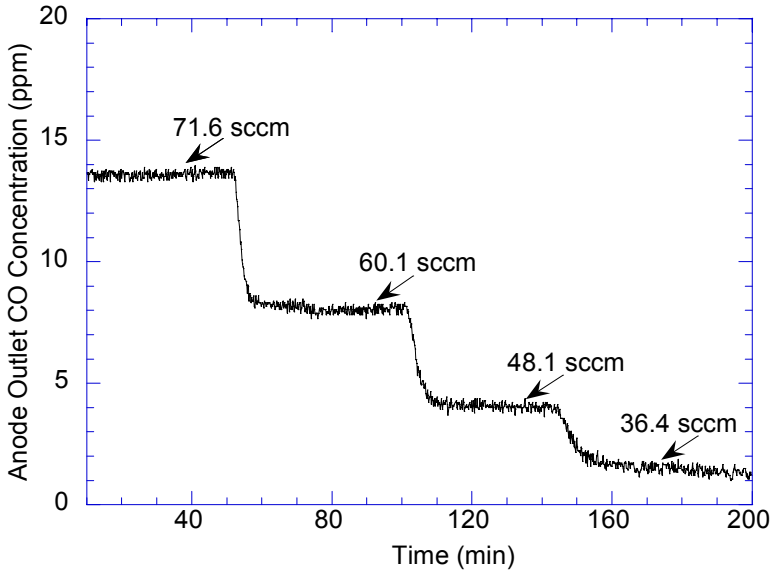

Figure 7-2. Anode outlet CO concentration at different inlet flow rates. Anode feed: H_2/200 ppm CO; current density: 200 mA/cm^2; room temperature; anode 0.35 mg/cm^2 PtRu.

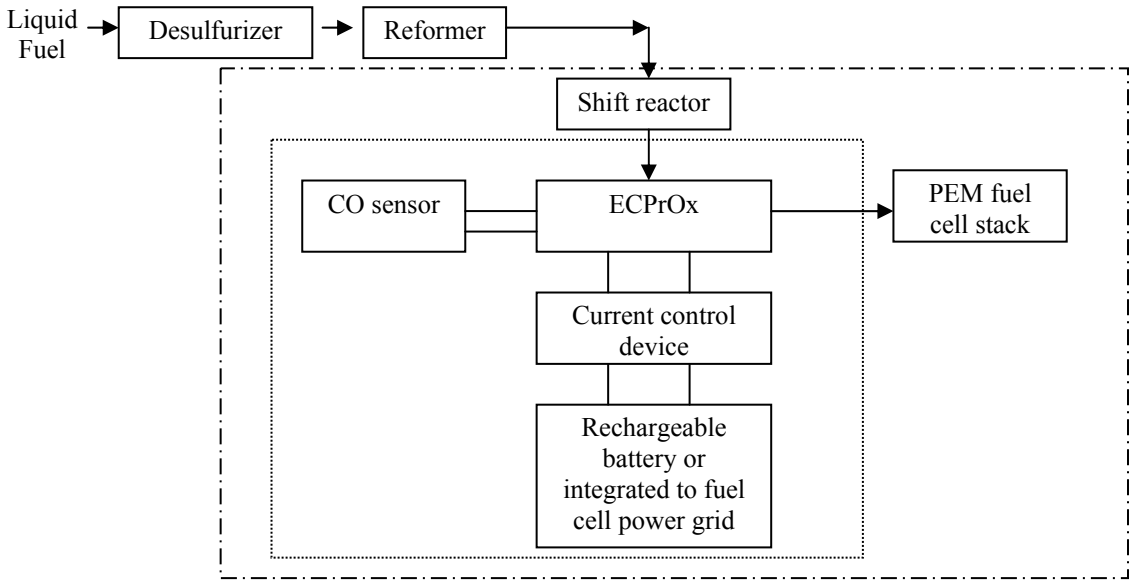

Figure 7-3. Schematic of Reformer/PEM Fuel Cell System with ECPrOx Unit.

7.3.2 Performance of ECPrOx at Different Feed CO Concentrations

Substantial hydrogen consumption is not desirable in the ECPrOx unit, although the H_2 consumed generates electrical power. In fact, there might be an optimal value of operating current in ECPrOx as far as the overall system efficiency is concerned. Hence, the preliminary results shown in this chapter are obtained at low but arbitrary current densities (less than 200 mA/cm^2), and without any consideration to the question of optimization of the overall system efficiency. Thus, the outlet CO concentration as a function of inlet flow rate is plotted in Figure 7-4a at various current densities for an anode feed containing 1000 ppm CO. It is seen that the CO concentration increases with the inlet flow rates at a given current density. Furthermore, the outlet CO concentration decreases with an increase of the current density at a given inlet flow rate. However, these differences in exit CO concentration become increasingly small for higher current densities.

Since a two-stage ECPrOx may be required depending upon inlet CO concentration and flow rate, experiments were conducted using higher feed CO concentrations as well. Thus, a feed gas of H_2/24.1% CO_2/0.938% CO was also used to simulate the reformate gas stream from the LTS reactor. The exit CO concentration for this feed as a function of inlet flow rate is plotted in Figure 7-4b, for an anode catalyst loading of 0.7 mg/cm^2 PtRu. It is seen that the CO concentration can be lowered from 9380 ppm to about 140 ppm for an inlet flow rate of 21.9 sccm, and to about 500 ppm at a flow rate of 55.6 sccm, and a current density of 150 mA/cm^2. In a two-stage EcPrOx, thus, the first stage might reduce the CO level from around 10,000 ppm to 500 ppm, while the second stage would reduce it to about 50 ppm.

It may be noticed that the trends observed in Figure 7-4b are different from that for the lower CO concentration shown in Figure 7-4a. This is due to transition of cell voltage between stationary and oscillatory states. We have found that the current density and flow rates are two key parameters that affect the onset of potential oscillations.[16] The effect of current density on the onset of potential oscillation was consistent with our previous observation, in that oscillations appeared at larger current densities for a given inlet flow rate. However, the onset of oscillations in terms of flow rate was opposite to

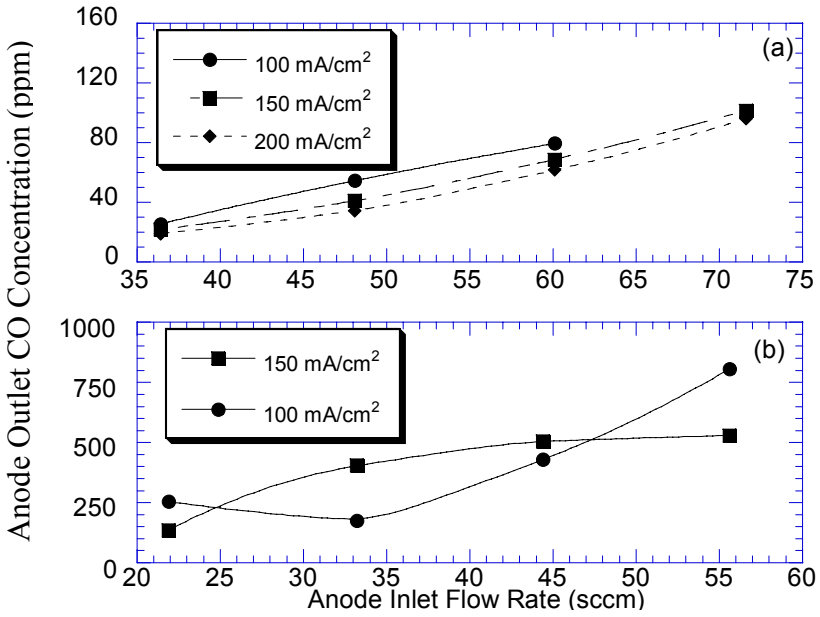

Figure 7-4. Anode outlet CO concentration as a function of inlet flow rates at various current densities. (a) Anode feed: H_2/1000 ppm CO; room temperature; anode 0.35 mg/cm^2 PtRu; (b) Anode feed: 75% H_2/24 % CO_2/9380 ppm CO; room temperature; anode 0.7 mg/cm^2 PtRu.

our earlier observations at the lower CO levels. Thus, the oscillations born at relatively smaller flow rates were suppressed when the flow rate was increased. For example, at a current density of 100 mA/cm^2, oscillations disappeared when the inlet flow rates exceeded 33.2 sccm, while at a current density of 150 mA/cm^2, the oscillations disappeared when the inlet flows was greater than 55.6 sccm. Due to the transition from an oscillatory state to a stationary one, the monotonic change in exit CO concentration with flow rates is not observed in Figure 4b for the current density of 100 mA/cm^2. The lower exit CO concentration at the stationary state is due to the fact that the cell voltage at stationary states is much lower than the time-averaged cell voltage at oscillatory states (i.e., the anode overpotential is higher at a stationary state than the time-averaged anode overpotential at oscillatory state).[18] The higher anode overpotential leads to a higher CO electrooxidation rate. However, for a given state of cell operation (either oscillatory or stationary), the exit CO concentration always increases with the inlet flow rates.

Due to the high concentration of CO_2 (24.1%) in the feed, there is the distinct possibility for the reverse water gas shift reaction to proceed on the anode catalyst as well. However, the reverse water gas shift reaction is not favored at low temperatures both kinetically and thermodynamically. We have previously measured the steady-state outlet CO concentration of fuel cell anode fed with H_2/20% CO_2 but without any CO, It was found that the CO concentration exiting the anode is only about 2-4 ppm when the fuel cell is operated at 80 °C, even though the calculated equilibrium CO concentration is over 100 ppm under these operating conditions. Furthermore, the CO concentration in the anode exit was found to decrease with a decrease of the fuel cell temperature. Therefore, the contribution of reverse water gas shift reaction to the CO concentration in the exit of ECPrOx unit is likely to be small even though there is a significant amount of CO_2 (> 20%) in the simulated reformate feed. Of course, the overpotential at anode promotes WGSR while constraining the reverse WGSR by virtue of the Butler-Volmer equation.

7.3.3 Supplemental Electrical Power

As has been mentioned in the previous section, no external electrical power source is needed for the ECPrOx. On the contrary, supplemental electrical power is

generated. In fact, it has been previously found by us that the power output of a PEM fuel cell operating under an oscillatory state is significantly higher than that at stationary state when the anode feed containing around 100 ppm CO.[18] Such enhanced power output was observed for higher CO concentration (e.g., 200 ppm and 1000 ppm CO) as well in the ECPrOx operation. A comparison of the supplemental power output under stationary and oscillatory states at the same experimental conditions is shown in Figure 7-5. It is seen in Figure 7-5a (for 200 ppm CO) that the maximum power density under steady state operation is about 47 mW/cm^2 at a current density of around 200 mA/cm^2. However, the power output under the oscillatory state is over 100 mW/cm^2, and has not yet peaked. Even when the anode feed contains 1000 ppm CO (Figure 7-5b), the power output under the oscillatory state does not fall appreciably even though the CO concentration in the feed has risen 5 folds. It can be further noticed that the power output at the oscillatory state does not change appreciably with inlet feed rates.

Thus, it is evident that the proposed ECPrOx process can effectively remove CO from reformate gas to produce clean hydrogen on the one hand, while also generating supplemental electrical power, which (at oscillatory state) is even higher than that at a stationary state at otherwise identical conditions. Although the power density is lower than that in fuel cell, such a characteristic of ECPrOx increases the overall energy efficiency of the reformer/fuel cell system.

7.3.4 Effect of Operating Temperature

Figure 7-6 shows the exit CO concentration at two different operating temperatures. In this experiment, the anode feed is hydrogen containing 100 ppm CO. It is seen that the exit CO increases with the cell temperature, exceeding 30 ppm for an inlet flow rate of 71.6 sccm at 55 °C. This indicates that lower temperature operation is preferable for ECPrOx to remove CO from the hydrogen rich gas stream. Similar results were obtained for the feed containing 9380 ppm CO representative of that in the first stage ECPrOx. At a current density of 140 mA/cm^2 and a flow rate of 44.4 sccm (catalyst loading 0.35 mg/cm^2), the exit CO concentration was 638 ppm at 35 °C, while the exit

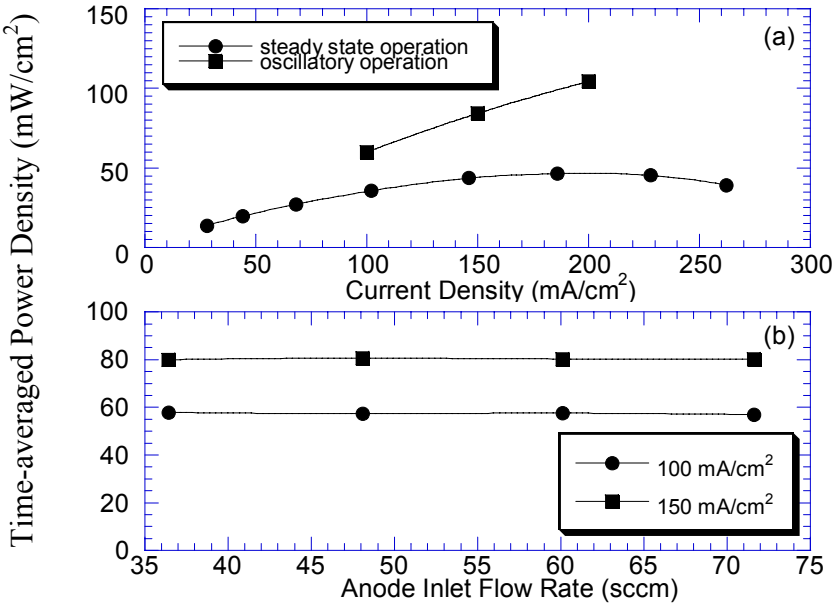

Figure 7-5. (a) Comparison of power outputs at stationary and oscillatory states. Anode feed H_2/200 ppm CO; anode inlet flow rate: 48.1 sccm; room temperature; anode 0.7 mg/cm^2 PtRu. (b) Effect of anode inlet flow rate on the time-averaged power density. Anode feed H_2/1000 ppm CO; room temperature; anode 0.7 mg/cm^2 PtRu.

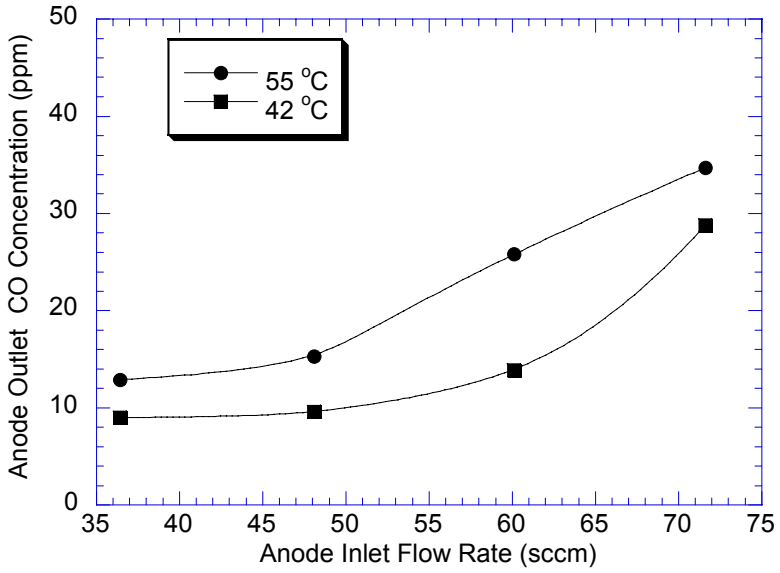

Figure 7-6. Effect of temperature on the outlet CO concentration. Anode feed H_2/108 ppm CO; current density: 300 mA/cm^2; anode 0.35 mg/cm^2 PtRu.

CO concentration was above 1000 ppm (over the detection range of the gas analyzer) when the unit was operated at 80 °C.

The kinetic and mechanistic study by Schubert *et al*.[19] showed that the selectivity of conventional CO preferential oxidation is determined by the steady-state surface coverage. Thus, there is a loss in selectivity with decreasing surface coverage of CO as CO partial pressure decreases. Similarly for ECPrOx, the CO surface coverage decreases at elevated temperatures and reduced CO partial pressures. The adsorption of CO on noble metal catalyst surface is an exothermic process, the enthalpy change being about -115 kJ/mol on Ru, and around -130 kJ/mol for Pt. The heat of adsorption decreases with an increase of surface coverage of CO, but is still about -45 kJ/mol at near saturation coverages.[20] Therefore, the majority of the experiments reported here were conducted at room temperature. This means that a heat exchanger would be required between the reformer and the ECPrOx to cool the reformate.

7.3.5 Effect of Operating Pressure

In order to study the influence of operating pressure on the performance of ECPrOx, the total pressure of both the anode and the cathode were lowered from 30 psig to 0 psig in a stepwise manner while the other experimental conditions remained fixed. The corresponding exit CO concentration as a function of inlet flow rate is shown in Figure 7-7a, for a feed containing 200 ppm CO with the unit operated at 100 mA/cm^2. It is clear that with the decrease of the operating pressure, there is a significant increase in the exit CO concentration. At a feed rate of 60.1 sccm, the CO concentration jumped from 10 ppm at 30 psig to 42 ppm at 0 psig. The increase in exit CO concentration becomes more significant as the total pressure approaches atmospheric pressure.

Since in the above experiment, the pressure of both electrode compartments was lowered simultaneously, further experiments were conducted to single out the effect of individual pressure change (Figure 7-7b). Thus, at an inlet flow rate of 71.6 sccm, the anode pressure was fixed at 0 psig while the cathode pressure was increased stepwise from 0 psig to 30 psig. The anode exit CO concentration remained unchanged (Figure 7-7b). However, when the cathode oxygen total pressure was fixed at 30 psig while the

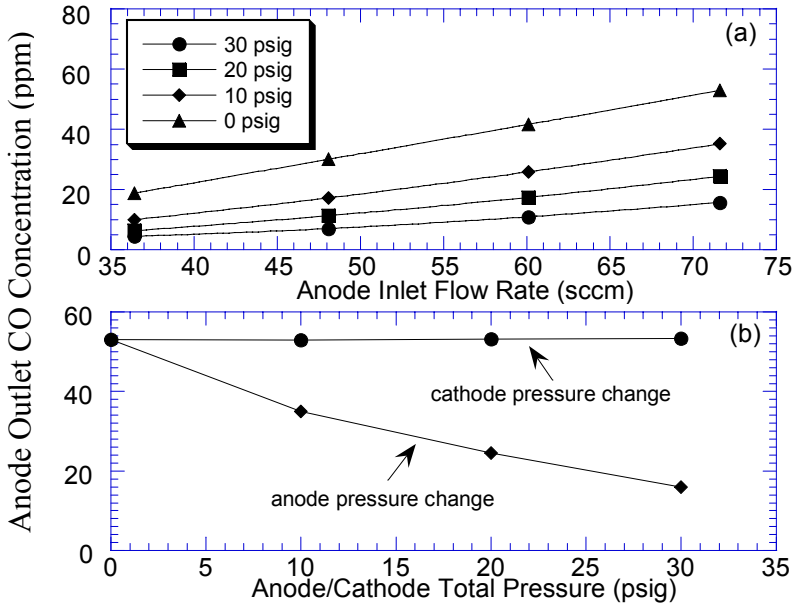

Figure 7-7. Effect of total pressures on the anode outlet CO concentration. (a) lowering the pressures of both electrodes (b) lowing the pressure of either electrode at an anode inlet flow rate: 71.6 sccm. Other conditions: Anode feed: H_2/200 ppm CO; current density: 100 mA/cm^2; room temperature; anode 0.7 mg/cm^2 PtRu.

anode total pressure was increased in the same manner as cathode, the exit CO concentration dropped in exactly the same manner as observed in Figure 7-7a. Therefore, it is evident that it is the anode pressure that is responsible for the change in exit CO concentration with varying operating pressures.

The same result was observed for a feed containing 9380 ppm CO. It is seen in Figure 7-8 that at a current density of 100 mA/cm^2 and at a feed rate of 44.4 sccm, the exit CO concentration decreases with an increase of the anode pressure. The CO concentration thus dropped from about 680 ppm at 10 psig to about 380 ppm at 30 psig.

A high anode total pressure (i.e., high CO partial pressure) is, thus, beneficial to the removal of CO from the gas stream. A high CO partial pressure leads to an increase in the CO adsorption rate, and a high CO surface coverage. Therefore, the CO electrooxidation rate increases. Although we had found in our previous work that O_2 permeating through the membrane from cathode also contributed partially to the CO removal in anode compartment,[21] the effect is apparently not significant for the thicker membrane (Nafion 117) used here for ECPrOx, especially for the high CO concentration and feed rates used in the present work. Therefore, contribution of any permeating oxygen from cathode to the removal of CO can be assumed to be negligible here. The above observation also indicates that the ECPrOx can be operated at low pressures, and with air at ambient pressure.

7.3.6 Effect of Catalyst Loading

The effect of catalyst loading is shown in Figure 7-9. A higher catalyst loading is beneficial in lowering the exit CO concentration. The improvement becomes more apparent at higher flow rates and at higher inlet CO concentrations typical of the first stage of the ECPrOx. At a flow rate of 71.6 sccm, the difference in exit CO concentration is about 5 ppm for the two different catalyst loadings investigated for a feed containing 200 ppm CO. However, as shown in Figure 7-9a, for a feed containing 1000 ppm CO, the difference is around 25 ppm.

The effect of catalyst loading for a feed containing 9380 ppm CO is shown in Figure 7-9b. In this figure, the exit CO concentrations are compared at a given inlet flow

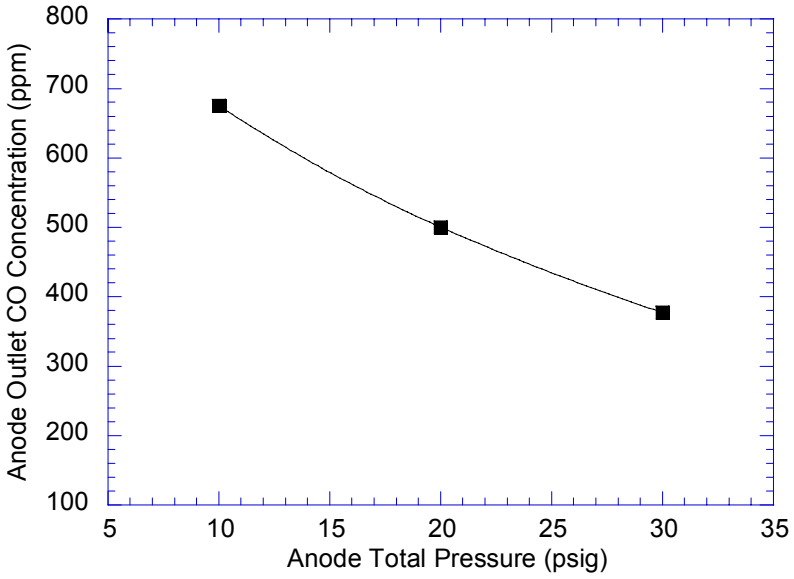

Figure 7-8. Effect of total pressures on the outlet CO concentration. Anode feed: 75% H_2/24 % CO_2/9380 ppm CO; anode inlet flow rate: 44.4 sccm; current density: 100 mA/cm^2; room temperature; anode 0.7 mg/cm^2 PtRu.

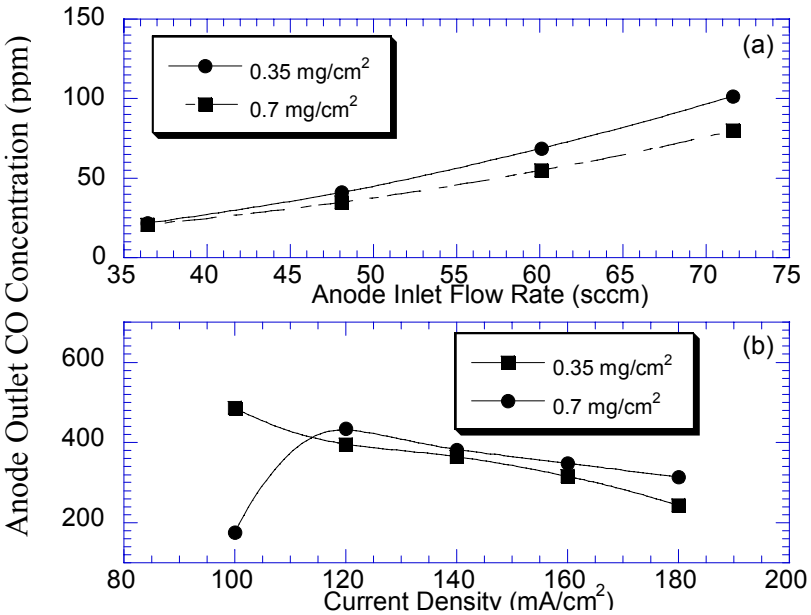

Figure 7-9. Effect of PtRu catalyst loading on the outlet CO concentration. (a) Anode feed: H_2/1000 ppm CO; current density: 150 mA/cm^2; room temperature. (b) Anode feed: 75% H_2/24 % CO_2/9380 ppm CO; anode inlet flow rate: 33.2 sccm; room temperature.

rate but at varying current density. It is seen that at a given inlet flow rate, the exit CO concentration decreases monotoniclly with the increase of operating current density for catalyst loading of 0.35 mg/cm^2. For this case, the cell voltage remained at a stationary state. However, the CO concentration experienced a large jump as current density increased from 100 to 120 mA/cm^2 for the case of the higher catalyst loading of 0.7 mg/cm^2. This sudden concentration change is due to the transition of the cell voltage from a stationary state to an oscillatory state as a result of increasing current density. At the upper branch (cell voltage in oscillatory state), however, the CO concentration decreased monotonically with increasing current density, and is in fact, somewhat higher than that at the lower catalyst loadings. It, thus, appears that the trends are similar although the performance depends upon whether the unit is in a steady or oscillatory state of operation. In the oscillatory state, the CO outlet content is higher but so is the supplemental power produced. For appropriate comparison of catalyst loading, the state of operation must be the same. Thus, e.g., for 100 mA/cm^2, the exit CO concentration for the lower catalyst loading is more than double as compared to that for the higher loading. Thus, higher catalyst loadings are desirable, although clearly there would be an optimum. Further, the supplemental power output increases as well at higher catalyst loadings in the anode. For example, at a current density of 150 mA/cm^2 and a feed containing 1000 ppm CO, the average power output is 43.5 mW/cm^2 for a catalyst loading of 0.35 mg/cm^2, while it is about 80 mW/cm^2 for an anode loading of 0.7 mg/cm^2.

7.3.7 Effect of Humidification

The exit CO concentration was also compared with and without humidification of the feed gases at room temperature and otherwise identical experimental conditions. Thus, the anode and cathode feed were introduced directly into the ECPrOx unit, with the humidifier bypassed, for an anode feed containing 200 ppm CO. It can be seen in Figure 7-10 that the exit CO concentrations are virtually identical. This result is not surprising because even in the case of humidification at room temperature, the water partial pressure is relatively small (0.032 atm, assuming a 100% relative humidity). Thus, for this case

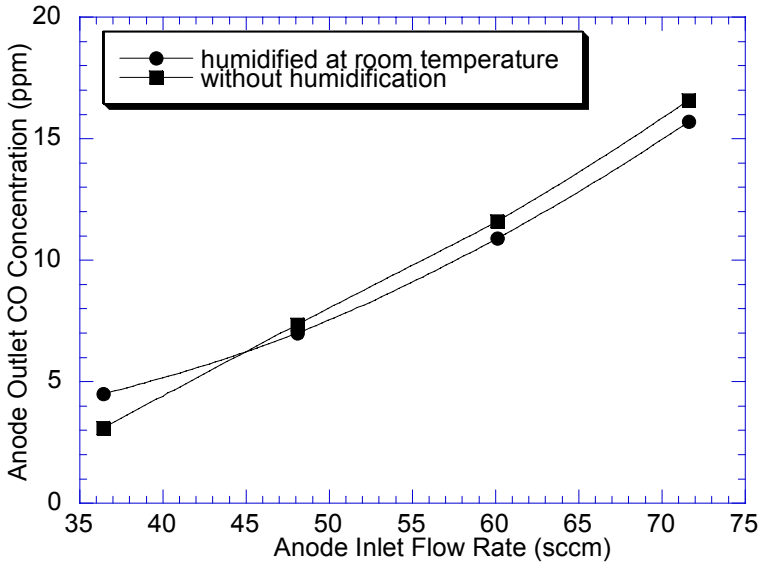

Figure 7-10. Effect of humidification on the outlet CO concentration. Anode feed: H_2/200 ppm CO; current density: 100 mA/cm^2; room temperature; anode 0.7 mg/cm^2 PtRu.

water produced by the electrochemical reaction at the cathode is more significant in terms of contribution to the hydration of the membrane.

In the operation of PEM fuel cell, membrane resistance may increase at the anode side at larger current densities due to the dehydration of membrane when insufficient water back diffusion occurs for a thicker membrane, as has been demonstrated by Buchi *et al*.[22] However, it has been shown by Slade *et al* [23]that for Nafion 115 membrane, the membrane conductivity does not change appreciably with current density up to about 1000 mA/cm^2, which is well above the current densities for ECPrOx in this work (100-200 mA/cm^2). Therefore, water transport due to any electro-osmotic drag can be counterbalanced by the back-diffusion of liquid water produced at the cathode membrane-electrode interface. Furthermore, membrane hydration is not a significant concern as high current densities is not a goal here. In fact, a drier membrane may be desirable since the goal is to provide the necessary anode overpotential for CO electrooxidation rather than high current densities. According to this logic, furthermore, thicker membranes may also be more desirable.

7.4 Further Discussion

7.4.1 Electrochemical Potential as an Additional Tool

PEM fuel cell is currently accepted as an efficient energy convertion device. When CO is present in the anode feed (using reformate as anode fuel), the fuel cell performance is seriously degraded. However, it has been shown in our previous work that there is finite CO electrooxidation in the fuel cell anode for both Pt and PtRu anode catalysts.[16,21] Thus, in the proposed ECPrOx, this is exploited by rendering the preferential oxidation of CO electrochemical so that electrode potential may be used as an additional tool to control the PrOx activity and selectivity. The conventional chemical processes utilize only thermal means for enhancing reaction rate on a given catalyst. Although temperature is an extremely effective tool for rate control, there are limitations of thermodynamics, selectivity, coking, catalyst sintering, and reactor material. In particular, frequently one runs into thermodynamic limitations at elevated temperatures

for exothermic reactions, so that enhanced activity and reduced equilibrium conversion must be balanced.

It so happens that, in addition to temperature, electrical potential is a particularly powerful tool for controlling the rate of a reaction for electrochemical and sometimes even for non electrochemical reactions. The reaction that occurs in ECPrOx at anode is, in fact, the electrochemical WGS, or EWGS, reaction

$$CO + H_2O \leftrightarrows CO_2 + 2H^+ + 2e^-$$

which could simply be viewed as the WGS reaction

$$CO + H_2O \leftrightarrows CO_2 + H_2$$

followed by the hydrogen oxidation reaction (HOR), i.e.,

$$H_2 \leftrightarrows 2H^+ + 2\ e^-$$

At the cathode, the normal oxygen reduction reaction (ORR) occurs, namely

$$2H^+ + 2\ e^- + 1/2O_2 \leftrightarrows H_2O$$

so that the overall reaction in ECPrOx is the same as in PrOx, i.e., simply the CO oxidation reaction

$$CO + 1/2O_2 \leftrightarrows CO_2$$

Thus, while the overall chemistry remains unchanged, by rendering the reactions electrochemical, the additional tool of potential available in ECPrOx can be effectively utilized. Furthermore, the thermodynamics is also improved by potential as explained by the Nernst equation.

7.4.2 Characterization of ECPrOx Unit

In order to characterize and compare the performance of ECPrOx unit with the conventional PrOx reactor, three quantities are defined.

The first is CO conversion, X_{CO}, which is defined similarly to that in the PrOx reactor, and evaluated by the CO concentration entering and exiting the ECPrOx unit,

$$X_{CO} = \frac{f_{in} x_{CO,in} - f_{out} x_{CO}}{f_{in} x_{CO,in}} \qquad [1]$$

where f_{in} and f_{out} are the total molar flow rates at inlet and outlet, respectively, and $x_{\mathrm{CO,in}}$ and x_{CO} are the CO mole fractions in the inlet and outlet gas stream.

In ECPrOx unit, a pre-determined (by the selected current density) amount of hydrogen is consumed to generate a current in order to polarize the anode. Meanwhile, CO electrooxidation contributes to the total Faradaic current drawn from the ECPrOx unit as well. Thus, the fraction of CO electro-oxidation current in the total Faradaic current, $\beta_{\mathrm{F}}^{\mathrm{CO}}$, is defined as

$$\beta_{\mathrm{F}}^{\mathrm{CO}} = \frac{i_{\mathrm{CO}}}{i_{\mathrm{CO}} + i_{\mathrm{H_2}}} = \frac{2Ff_{in}^{\mathrm{CO}} X_{\mathrm{CO}}}{I} \qquad [2]$$

where f_{in}^{CO} is the inlet molar flow rate of CO, F is Faraday constant, and I is the total current.

In principle, if the CO concentration is high enough, the ratio could approach one, i.e., almost all the Faradaic current and anode polarization is contributed from CO electro-oxidation. Then, CO may be viewed as a fuel instead of a poison.

The last factor to consider is the hydrogen recovery, defined as the ratio between the inlet and outlet hydrogen molar flow rate,

$$\varepsilon_{\mathrm{H_2}} = \frac{f_{out}^{\mathrm{H_2}}}{f_{in}^{\mathrm{H_2}}} = \frac{f_{in}^{\mathrm{H_2}} - I(1-\beta_{\mathrm{F}}^{\mathrm{CO}})/2F}{f_{in}^{\mathrm{H_2}}} \qquad [3]$$

Thus, the three characteristic quantities of the experimental results with 1000 ppm CO feed are illustrated in Figure 7-11 a-c. It can be seen in Figure 7-11a that the CO conversion decreases from 98% to 92% with the increase of inlet flow rate. This is due to the fact that the cell voltage does not change appreciably with inlet flow rate.

It is seen in Figure 7-11b that for an anode feed containing 1000 ppm CO, the CO contribution in the overall current is only about 0.6 to 2 %. The ratio of CO electrooxidation current in the total current increases with the inlet flow rates. Of Course, this ratio is higher as CO content of feed increases, as discussed below.

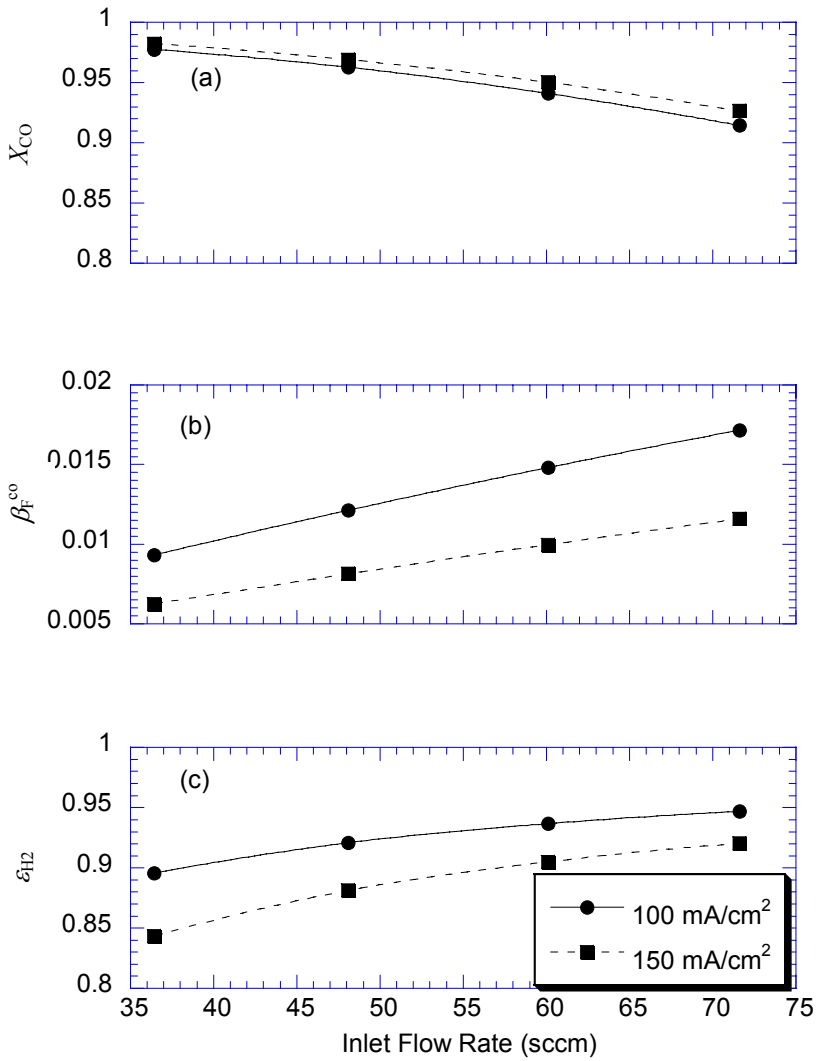

Figure 7-11. CO conversion (a), fraction of CO electrooxidation current (b), and hydrogen recovery (c) as a function of inlet flow rates at two current densities. Anode feed: H_2/1000 ppm CO; room temperature; anode 0.7 mg/cm^2 PtRu.

The recovery of hydrogen is predominantly determined by the operating current at a certain inlet flow rate. For a current density of 100 mA/cm^2, the hydrogen recovery is between 90 to 95% in the flow rates investigated. The recovery increases with the inlet flow rate for a given current density.

The CO conversion (Figure 7-12a) and CO contribution to the overall current (Figure 7-12b) are also compared at 100 mA/cm^2 and a flow rate of 36.4 sccm. The catalyst loading is 0.7 mg/cm^2. It can be seen from Figure 7-12a that the conversion of CO is nearly independent of the feed concentration. This is a very special feature of the ECPrOx Unit. It shows that this unit is self-regulated and naturally stable. The CO electrooxidation current increases with the CO concentration in the feed as shown in Figure 7-12b. It is seen that for a feed containing 9380 ppm CO, the contribution of CO electrooxidation has increased to almost 10 %, which is a substantial fraction of the total current drawn from the ECPrOx unit. Thus, CO can be viewed a fuel instead of poison.

Thus, we have shown that the ECPrOx can effectively remove CO from reformate gas while wasting no H_2 and producing a part of the power of the overall fuel cell power plant. Unlike conventional PrOx, no complex temperature or air flow control is required in order to attain desired activity and selectivity, especially for variable conditions such as those that might be encountered in automotive applications.

7.5 Conclusions

An electrochemical preferential oxidation (ECPrOx) process is proposed here for the selective oxidation of CO from H_2 rich reformate gas. This process exploits the strong adsorption of CO on the PtRu catalyst at low temperatures and the anode overpotential (in oscillatory state) to selectively electrooxidize CO over hydrogen. In addition to the cleansing of CO, supplemental electrical power is generated from the ECPrOx device. Thus, both hydrogen and CO are not wasted, but used to produce power. Room temperature and high anode pressure can facilitate CO adsorption, thus increasing the CO surface coverage and CO electrooxidation while lowering the CO concentration in the anode exit. The cathode total pressure is found to have no effect on the performance. Further, humidification is not necessary.

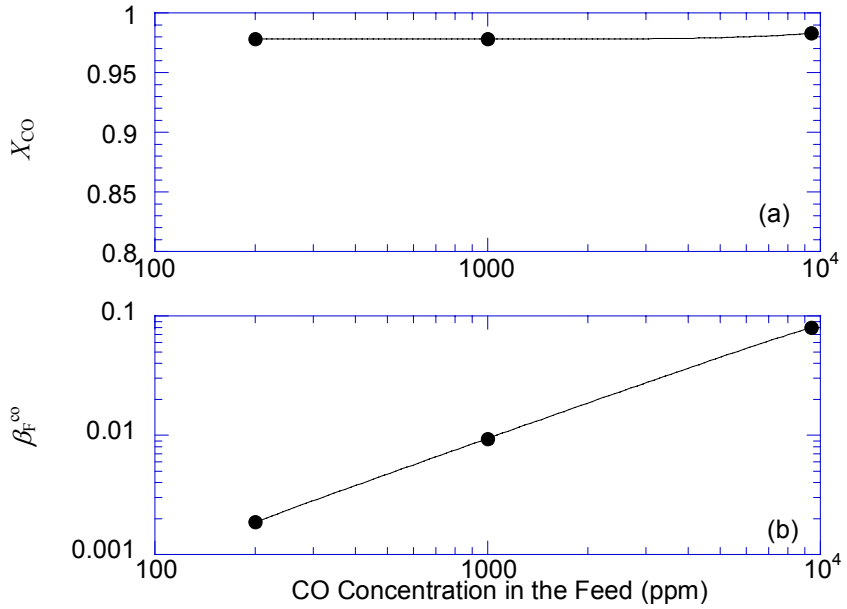

Figure 7-12. CO conversion (a) and fraction of CO electrooxidation current (b) at different CO concentrations. Anode inlet flow rate: 36.4 sccm; current density: 100 mA/cm^2; room temperature; anode 0.7 mg/cm^2 PtRu.

With further improvement and optimization, the ECPrOx technology may be a promising alternative to the conventional preferential oxidation of CO. It is also an interesting example of utilizing electrical potential besides temperature to enhance catalytic reaction. Moreover, the electrical potential used is not supplied from an external source but is generated *in-situ* and is in an autonomous oscillatory state.

Although the basic structure and construction of ECPrOx unit is similar to a PEM fuel cell in that the MEA consists of a PEM flanked on either side by an electrode, the design objective is completely different. The results presented in this paper simply demonstrate the feasibility of ECPrOx, without any effort to optimize the structure or operating conditions of the device. Of course, significant additional work is needed to optimize the design of the catalyst layer (e.g., more catalyst at anode, less at cathode), the catalyst used, as well as the operating conditions.

References

1. L. F. Brown, *Int. J. Hydrogen Energy*, **26**, 381 (2001)**.**
2. B. Lakshmanan, W. Huang, and J. W. Weidner, *Electrochem. Solid-State Lett*., **5**, A267 (2002).
3. I. H. Son, M. Shamsuzzoha, and A. M. Lane, *J. Catal*., **210**, 460 (2002).
4. S. H. Oh; and R. M. Sinkevitch, *J. Catal*., **142**, 254 (1993).
5. R. T. Sanchez, A. Ueda, K. Tanaka, and M. Haruta, *J. Catal*., **168**, 125 (1997).
6. H. Igarashi, H. Uchida, and M. Watanabe, *Studies in Surface Science and Catalysis*, **132**, 953 (2001).
7. R. L. Borup, G. W. Skala, M. A. Brundage, and W. J. LaBarge, U. S. Pat., 6,162,558 (2000).
8. C. Z. He, H. R. Kunz, and J. M. Fenton, *J. Electrochem. Soc*., **148**, A1116 (2001).
9. N. E. Vanderborgh, T. V. Nguyen, and J. Guante, U. S. Pat., 5,271,916 (1993).
10. N. Edwards, S. R. Ellis, J. C. Frost, S. E. Golunski, A. N. Keulen, N. G. Lindewald, and J. G. Reinkingh, *J. Power Sources*, **71**, 123 (1998).
11. S. G. Chalk, J. F. Miller, and F. W. Wagner, *J. of Power Sources*, **86**, 40 (2000).
12. C. D. Dudfield, R. Chen, and P. L. Adcock, *Inter. J. Hydro. Eng*. **26**, 763 (2001).
13. S. H. Lee, J. Han, and K. Y. Lee, *J. Power Sources*, **109**, 394 (2002).
14. B. Lakshmanan, and C. Karuppaiah, US patent application publication, U.S. 2002/0071977.
15. R. Datta, and J. X. Zhang, U. S. Provisional Application No.: 60/490,055 (2003).
16. J. X. Zhang, and R. Datta, *J. Electrochem. Soc*., **149**, A1423 (2002).
17. J. X. Zhang, J. D. Fehribach, and R. Datta,. *J. Electrochem. Soc*., **151**, A689 (2004).
18. J. X. Zhang, and R. Datta, *Electrochem. Solid-State Lett*., **7**, A37 (2004).
19. M. M. Schubert, M. J. Kahlich, H. A. Gasteiger, and R. J. Behm, *J. Power Sources*, **84**, 175 (1999).
20. N. M. Markovic, C. A. Lucas, B. N. Grgur, and P. N. Ross, *J. Phys. Chem. B*, **103**, 9616 (1999).
21. J. Zhang, T. Thampan, and R. Datta, *J. Electrochem. Soc.*, **149**, A765 (2002).
22. F. N. Buchi, and G. G. Scherer, *J. Electrochem. Soc.*, **148**, A183 (2001).

23. S. Slade, S. A. Campbell, T. R. Ralph, and F. C. Walsh, *J. Electrochem. Soc*., **149**, A1556 (2002).

Chapter VIII

Conclusions and Recommendations

The main objective of this work was to gain a basic understanding of the mechanisms of CO tolerance in proton exchange membrane fuel cells through a systematic investigation. The hope was that the knowledge so gained may be useful in designing novel operational strategies and better CO tolerant eletrocatalysts to improve the PEM fuel cell performance with reformate as anode feed. As a first step, thus, the mechanism and kinetics of standard PEM fuel cell catalysts, such as Pt and PtRu, were studied, under *in-situ* fuel cell conditions.

During the study of CO poisoning on PEM fuel cell performance with Pt anode catalyst, we found the dramatic influence of anode flow rate and cathode oxygen partial pressure. The results were explained on the basis of a CO inventory model. It is proved out there is finite CO electrooxidation on PEM fuel cell anode using Pt catalyst with H_2/CO as anode feed. As a result, anode overpotential and outlet CO concentration are a function of anode inlet flow rate at constant current density.

Motivated by the model predictions in chapter II, i.e., the outlet CO concentration in PEM fuel cell is a function of anode inlet flow rate at constant current density, experiments were conducted to monitor the anode outlet CO concentration by a CO gas analyzer. It was observed that the outlet CO concentration increases with anode inlet flow rate at a given current density for Pt catalyst, in agreement with the model predictions in chapter II. The CO outlet concentration with PtRu catalyst was found to depend upon the current density at a cell temperature of 80 °C. The anode outlet CO concentration was observed to decrease with the increase of anode inlet flow rate at low current densities, while at higher current densities, the outlet CO concentration followed a trend similar to that observed with Pt. The CO electrooxidation rate on Pt and PtRu was thus calculated using CO material balance on the anode side. The results indicate that the enhanced tolerance of PtRu catalyst is due to the dual mechanisms of reduced CO affinity (ligand effect) and enhanced CO electrooxidation rates (bifunctional effect), with either mechanism dominating depending upon the anode overpotential. This is the first *in-situ*

experimental results so far that prove that both mechanisms proposed in the literature in fact coexist.

In the investigation of H_2/CO electrooxidation mechanism on PtRu electrocatalysts, we found sustained potential oscillations in a PEM fuel cell operated under constant current densities. The oscillations are due to the coupling of the electrooxidation of H_2 and CO on the binary PtRu alloy surface. A surface reaction could be controlling the oscillations, likely the dissociation of H_2O or the electrooxidation of CO. A detailed anode dynamic model was given to explain the oscillatory phenomenon. A qualitative analysis also showed that a surface process may be controlling the potential oscillations, such as the dissociation of H_2O or the electrooxidation of CO. In order to further understand the mechanistic origin of the anode potential oscillation phenomenon, a detailed mathematical analysis was performed in chapter V on the kinetic model. It was found that the time-dependence of all the key surface species must be accounted for in order for the model to predict the oscillatory behavior, while the time-dependence of CO concentration in the anode chamber need not necessarily be considered. The bifurcation diagram of CO electrooxidation rate constant explained very well the effect of temperature on the oscillation pattern. The oscillator model is classified as a hidden negative differential resistance (HNDR) oscillator based on the dynamical response of the anodic current and surface species to a dynamic potential scan. The linear stability analysis indicated that the bifurcation experienced is a supercritical Hopf bifurcation

The periodic behavior in cell voltage during PEM fuel cell operation with feed containing CO was further found to be a practically useful approach in managing the fuel cell power output. It was observed that time-averaged cell voltage, cell efficiency and power density in an autonomous oscillatory state is higher than that in stable steady-state for a PEM fuel cell operating in the presence of CO in the anode feed reformate gas. The average power density under such an oscillatory state at 55 °C was found to be twice that under a stable steady-state. The average cell voltage and power density gain is due to the decrease of the time-averaged anode overpotential in the oscillatory state, as shown in the modeling analysis.

In addition to the enhanced power output, a second observation on the oscillation phenomenon prompted us to develop a novel way of CO cleansing, namely, the

electrochemical preferential oxidation (ECPrOx). We experimentally observed that the exit CO concentration from PEM fuel cell anode is significantly lower than the feed CO concentration when the fuel cell voltage is oscillating. In fact, a selective CO electrooxidation is achieved at the fuel cell anode by utilizing autonomous anode potential oscillations when operated at a constant current density. Thus, an ECPrOx process has been developed to cleanse CO from hydrogen rich gas mixture using a device similar to a proton exchange membrane fuel cell. The oscillation period and amplitude of the ECPrOx device adjust automatically to the CO levels in the feed stream so that a self-controlled autonomous potential pulsing is achieved. Moreover, supplemental electrical power is produced from ECPrOx device while CO is removed from the reformate gas, without H_2 or CO being wasted. The ECPrOx device can be operated at near room temperature, high anode pressure, with atmospheric air and without external humidification.

Based on the results accomplished so far, the following work is recommended as deserving further investigation.

Design and Optimization of Electrochemical Preferential Oxidation (ECPrOx) Process

Although the basic concept and feasibility of the ECPrOx have been fully demonstrated in chapter VII, the design and operating conditions are far from optimized. Significant additional work is needed to optimize the design of the catalyst layer, the gas diffusion layer, anode and cathode catalyst, polymer electrolyte membranes, as well as the operating conditions.

The structure and composition of conventional PEM fuel cell electrodes may not necessarily best serve the purpose of an ECPrOx device. For example, the catalyst loading in the anode and the cathode can be balanced according to the different requirements of anode and cathode reactions, *i.e.*, lower loading in the cathode and higher loading in the anode may be desirable and feasible. Anode catalyst with different Pt:Ru ratio other than 1:1 (atomic ratio) may be optimal for the anode reaction in ECPrOx. In addition, since the anode reaction is to promote the electrochemical CO oxidation rather than H_2 electrooxidation, the latter being the goal of a fuel cell, there may be other cheaper catalyst candidates for both anode and cathode which could perform similarly or

even better than PtRu alloy and Pt. As far as the electrolyte are concerned, alternative low cost PEMs other than Nafion may also be applicable. The Nafion® ionomer loading in the anode and cathode may be other parameters deserve considering in the design of ECPrOx device.

Since the ECPrOx device should be designed to be operated at low current density but high anode overpotential region, the operating conditions are less stringent than those in PEM fuel cells. The conditions that deserve to be considered include using low pressure oxygen or air at relatively low flow rates at unhumidified conditions. Such operation conditions will significantly lower the parasitic energy cost in compressing the cathode feed. As far as anode is concerned, even higher anode pressures than those employed by this work could be investigated, although it should be kept in mind that higher anode pressure will cause parasitic energy loss unless this is desirable in reformer. In addition, a newly made MEA in PEM fuel cell operation usually requires a conditioning step before the maximum performance is achieved. Since ECPrOx is operated at relatively low temperature, a pre-conditioning of the MEA before the operation of ECPrOx could be helpful in improving the performance in lowering the CO concentration.

The kinetic model developed in this work was reasonably well able to explain the oscillatory behavior of anode overpotential at given experimental conditions. It could be further utilized to predict the exit CO concentration at different flow rates and a variety of feed CO concentration in ECPrOx process. Preliminary results have shown that the model can describe the ECPrOx behavior at low feed CO concentration (108 ppm) for a 5 cm^2 electrode. However, the diffusion and adsorption of CO may be different when the CO concentration becomes higher (e.g., 1000 or 10,000 ppm). Thus, CO diffusion, adsorption, and reaction should be reconsidered for high CO concentration and large area electrode in the model.

Another desirable aspect about the model is that it may be used to predict reasonable design parameters. By changing the exchange current density, the roughness factor, anode capacitance *etc.* and predicting their effect on the exit CO concentration, it may be helpful in indicating a rational design of an ECPrOx device.

Study of CO Electrooxidation with Electrochemical Impedance Spectroscopy

It was discussed in chapter I that electrochemical impedance spectroscopy is a very powerful technique to study CO electrooxidation on metal and alloy catalyst surface. The processes occurring on the catalyst surface at different electrode potential can be identified. Thus, impedance spectroscopy could be used to get more detailed mechanistic information in the electrode reactions.

The 5 cm^2 single cell structure could be used in these experiments, with H_2/100 ppm CO fed to the anode side, and H_2 flowing in the cathode side acting as both a reference and counter electrode. Considering the fact that when H_2/100 ppm CO is used as anode feed, the total current will be over the measurement range of the potentialstat when the applied potential (or biased potential) is higher, an alternative way is to decrease the effective electrode size to 1 cm^2. The fuel cell impedance spectra could be recorded at different cell temperature, using Pt , PtRu and other alloys as anode catalyst. From the characteristics of the impedance spectra, the intermediate reaction steps could be identified.

Furthermore, impedance spectroscopy is also a very powerful tool in studying the system stability. The potential oscillation phenomenon has been observed and studied by the kinetic model analysis in chapter IV and V. However, it is almost certain that there must be other conditions where the PEM fuel cell will exhibit oscillatory system behavior. Thus, besides the model analysis, a practical diagnostic tool is also essential to predict the system dynamic behavior of a PEM fuel cell system. It has been found in other electrochemical systems that the change of the impedance pattern from the first and forth quadrant to the second and third quadrant usually hint the system will lose stability. Also the oscillation period may also be related to the frequency applied to the system during impedance measurement. Thus, the stability of PEM fuel cell system at any operation conditions (e.g., temperatures, anode feed types and concentrations, flow rates, current/voltage range, etc.) and some of its dynamic characteristics could be identified with impedance spectra in advance.

Prediction and Testing of CO Tolerant Electrocatalyst Candidates

Our basic approach in the rational design of the CO tolerant anode catalysts is the explicit recognition that not only the overall reaction but also the mechanism of CO tolerance in a fuel cell is simply the electro-chemical counterpart of the water-gas shift (WGS) reaction, or *electrochemical* WGS (EWGS). While in the WGS catalytic reaction, temperature is the key variable used to enhance the kinetics on a given catalyst (via the Arrhenius equation), in EWGS reaction, voltage is an additional tool available to enhance kinetics (via the Butler-Volmer equation):

$$\vec{k}_{\rho}^{\,*} = \vec{k}_{\rho,\Phi_0}^{\,*} \exp\left\{\frac{\beta_{\rho} \nu_{\rho e^-} F \eta}{RT}\right\}$$

where η is the overpotential. The eventual goal is to find a good low temperature WGS catalyst on which imposition of a small overpotential has a large enhancement in rate.

Catalyst candidates that are likely to present the best CO tolerance will act via both the "ligand" effect, i.e., CO affinity is reduced, as well as by the "bifunctional" effect, i.e., water is dissociated more readily on the alloy to promote the electrochemical water gas shift reaction of CO via adsorbed OH. Therefore, a feasible strategy is to look first for metals X for Pt-X alloys that would promote the ligand effect, and then compile a list of those that would promote the electrochemical water gas shift reaction. The final candidates would be those metals that are common on both these lists.

The alloying candidates that promote the ligand effect can be selected based on the recent *ab initio* density functional theory (DFT) calculations of Christofferson et al (ref. 51 of chapter I). These authors showed from first principles that the CO adsorption energy weakens directly as the *d*-band electron energy of Pt, as characterized by the *d*-band center, ε_d, reduces by virtue of alloying. They further provided the figure reproduced below that gives calculation results for the change in ε_d due to alloying of 3*d*, 4*d* and 5*d* metals.

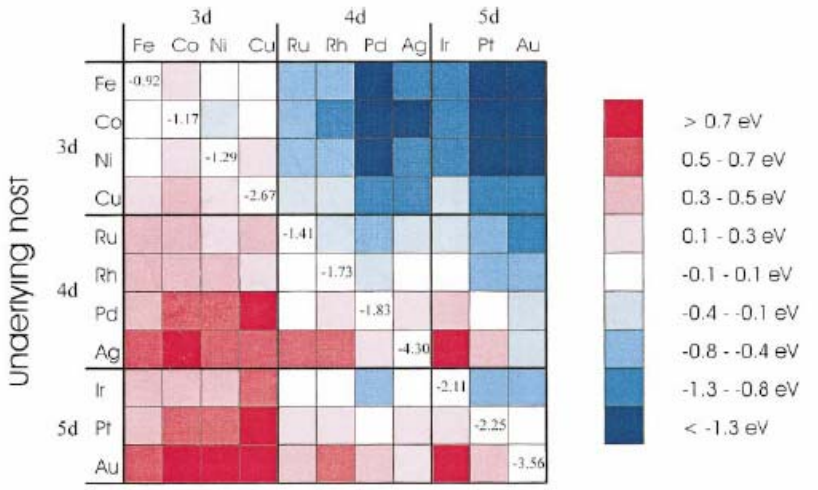

FIG. 4. Color-coded changes in the *d*-band centers for pseudo-morphic overlayers of transition metals on other transition metals. The calculations are based on fully self-consistent density functional calculations and are taken from Ref. (21).

Thus, those metals that lower the *d*-band energy of Pt (indicated by blue color in the figure above) would be suitable. These include the 3*d* non-precious metals considered, i.e., Cu, Ni, Co, and Fe in the order of increased effect in reducing CO affinity. Further, the 4*d*, 5*d* metals Rh, Ru, and Ir are indicated as suitable materials, although not to the same extent as the 3*d* metals. The explanation is that the alloying of the electron rich 5*d* metals (e.g., Pt) with electron poor metals (e.g., 3*d* metals) leads to a reduction in the electron density of the electron-rich metals. However, Christofferson et al. also found that the adsorbed hydrogen adsorption energy also unfortunately followed a similar trend, which would reduce the exchange-current density for the hydrogen-oxidation reaction (HOR), which is undesirable. In other words, alloying elements that are most effective in reducing the CO adsorption energy may not necessarily be the best candidates. Of course, the alloy composition would also determine the extent of actual change.

Next, in order to determine the propensity of an alloying metal for enhancing the electrochemical water gas shift reaction, the predicted energy of adsorption of OH (in Kcal/mol) can be utilized as given below for some metals of interest (ref. 31 in Chapter IV):

Cu	Ni	Pd	Pt	Rh	Ru	Ir	Fe
51.8	60.9	40	38.6	51	49.5	44.4	63.3

as well as the activation energy for $H_2O \rightarrow H + OH$ (in Kcal/mol):

Cu	Ni	Pd	Pt	Rh	Ru	Ir	Fe
17.6	14.2	18.2	18.8	16.1	14.3	18.7	12.0

These data show that 3*d* metals, namely, Cu, Ni and Fe (data for Co are not available yet) are effective alloying materials for formation of adsorbed OH from water. Furthermore, 4*d* metals Rh and Ru are effective as well, although not quite to the same extent. Thus, it is seen that the same metals that promote the "ligand" effect also promote the "bifunctional" effect. *Based on this preliminary analysis, thus, the list of alloying metals for Pt-X are X = Rh, Ru, Cu, Ni, Co, and Fe, in increasing order of effectiveness*. However, due to other considerations (e.g., effect on HOR, stability), the most effective co-catalysts may not be the optimum choice.

Of course, Pt-Ru is the leading current catalyst for imparting CO tolerance to anodes. However, there are few data available for the other candidates indicated. A very recent study (H. Igarashi, T. Fujino, Y. Zhu, H. Uchida, and M. Watanabe, *Phys. Chem. Chem. Phys*., **3**, 306, 2001) including some of these very alloying metals showed that Pt-Fe, Pt-Ni, Pt-Co, and Pt-Mo, all possessed a superior CO tolerance similar to Pt-Ru when tested at room temperature in an electrochemical cell. Furthermore, surprisingly these particular non-precious metals also had no problem with stability, although many other metals did. It was found that the alloy particles for these materials actually consisted of a Pt skin covering an underlayer of the alloy, presumably due to the dissolution of the non-precious metal atoms from the surface in the liquid acid electrolyte used. Nonetheless, the resulting structure remained highly effective in imparting CO tolerance while maintaining stability.

In other words, these particular alloying elements have the ability to modify the Pt electronic property in order to lower its affinity for CO, while at the same time, enhancing the nucleation of oxygen containing species such as OH at relatively lower anode overpotentials so that CO electro-oxidation via electrochemical water gas shift reaction can be enhanced. It is further noteworthy that these metals, namely Cu, Ru, Ni,

Co, and Fe are all excellent WGS catalysts in the order of increasing temperature of reaction. Thus, Cu and Ru are excellent low temperature shift (LTS) catalysts, Ni and Co are intermediate WGS catalysts, and Fe is the commercial high temperature shift (HTS) catalyst. The above analysis indicates that they should also be good candidates for electrochemical water gas shift reaction catalysis and improved CO tolerance. These metals have not so far been extensively investigated directly in fuel cells and may deserve further research effort.

CO Poisoning of PEM Fuel Cell by Reverse Water Gas Shift Reaction

In addition to the poisoning of the electrocatalyst by CO present directly in the reformate gas, the catalyst is also poisoned by CO_2 in the reformate gas, which can be up to 25% of the gas mixture depending the reforming reaction. The performance degradation caused by CO_2 has not received much attention in the literature, possibly due to the fact that the poisoning effect is not as severe as that of CO.

It has already been known in the literature that CO_2 has some modest poisoning effect on Pt anode catalyst. The effect is more severe than that caused by hydrogen dilution only. It has been anticipated that this may be due to the reverse water gas shift reaction, but direct evidence and systematic study is still missing.

Based on the results shown in previous chapters, the electrooxidation of CO on PEM fuel cell anode is essentially an electrochemical counterpart of water gas shift reaction. Thus, it may be interesting to experimentally confirm if the reverse electrochemical water gas shift reaction exist at PEM fuel cell operating conditions with an anode feed of H_2/CO_2. The on-line CO analyzing technique described in chapter III will be extremely useful to for this system. A preliminary result is shown in Figure 8-1. It is seen that there is indeed CO formation in the anode when the anode feed is H_2/20% CO_2. However, the observed CO concentration is much lower than that of the thermodynamic equilibrium CO concentration. From such research efforts, the mechanism of CO poisoning by the reverse water gas shift reaction could be explored. For instance, the effect of electrode potential on the equilibrium of the electrochemical water gas shift reaction may be investigated.

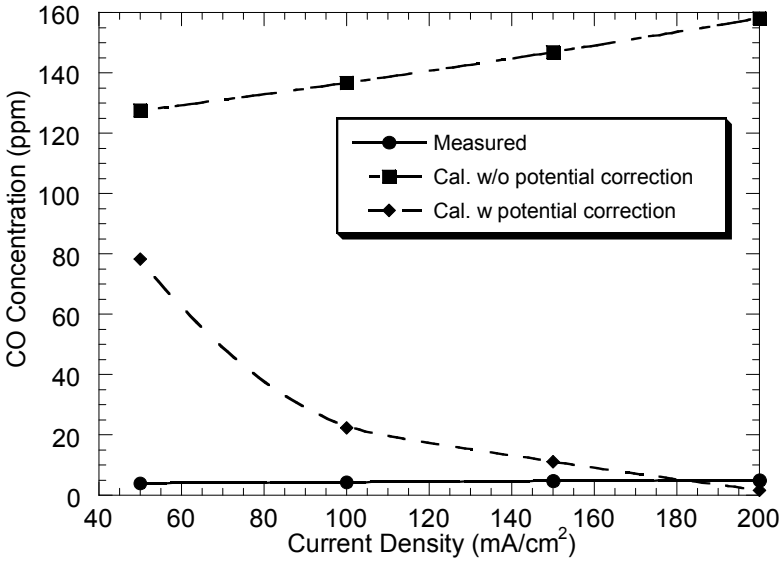

Figure 8-1. CO concentration in PEM fuel cell with 0.4 mg/cm^2 Pt/C anode catalyst due to reverse WGSR. Experimental result for 60 °C; 100% humidity, anode feed containing 20% CO_2 are compared with the thermodynamic equilibrium CO concentration with and without considering the effect of anode overpotential.